SAIMM
JOURNAL OF THE SOUTHERN AFRICAN INSTITUTE OF MINING AND METALLURGY
FOUNDED 1894
VOLUME 119 NO. 5 MAY 2019

# We aren't afraid to get our hands dirty,

# because when it comes down to it...

**MINING STUDIES**

**ON-SITE TECHNICAL SERVICES**

**CPR/ITR**

# WE DO MINING

We service the industry's demand for independent technical mining advisory for studies and public reports as well as capacity building and knowledge transfer. Let our expert team members advise you every step of the way, across the mining value chain - from bankable feasibility studies to competent persons reports, to onsite expertise and training. Ukwazi follows sound and proven technical and project management principles, based on relevant experience, a solid track record and industry best practice.

UKWAZI
advisory

## OFFICE BEARERS AND COUNCIL FOR THE 2018/2019 SESSION

***Honorary President***

Mxolisi Mgojo
President, Minerals Council South Africa

***Honorary Vice Presidents***

Gwede Mantashe
Minister of Mineral Resources, South Africa

Rob Davies
Minister of Trade and Industry, South Africa

Mmamoloko Kubayi-Ngubane
Minister of Science and Technology, South Africa

***President***

A.S. Macfarlane

***President Elect***

M.I. Mthenjane

***Senior Vice President***

Z. Botha

***Junior Vice President***

V.G. Duke

***Incoming Junior Vice President***

I.J. Geldenhuys

***Immediate Past President***

S. Ndlovu

***Co-opted to Office Bearers***

R.T. Jones

***Honorary Treasurer***

V.G. Duke

***Ordinary Members on Council***

I.J. Geldenhuys
C.C. Holtzhausen
W.C. Joughin
G.R. Lane
E. Matinde
H. Musiyarira
G. Njowa
S.M Rupprecht
N. Singh
A.G. Smith
M.H. Solomon
D. Tudor
A.T. van Zyl
E.J. Walls

***Past Presidents Serving on Council***

N.A. Barcza
R.D. Beck
J.R. Dixon
M. Dworzanowski
H.E. James
R.T. Jones
G.V.R. Landman
C. Musingwini
J.L. Porter
S.J. Ramokgopa
M.H. Rogers
D.A.J. Ross-Watt
G.L. Smith
W.H. van Niekerk
R.P.H. Willis

G.R. Lane–TPC Mining Chairperson
Z. Botha–TPC Metallurgy Chairperson

K.M. Letsoalo–YPC Chairperson
G. Dabula–YPC Vice Chairperson

***Branch Chairpersons***

| | |
|---|---|
| Botswana | Vacant |
| DRC | S. Maleba |
| Johannesburg | D.F. Jensen |
| Namibia | N.M. Namate |
| Northern Cape | F.C. Nieuwenhuys |
| Pretoria | R.J. Mostert |
| Western Cape | L.S. Bbosa |
| Zambia | D. Muma |
| Zimbabwe | C. Sadomba |
| Zululand | C.W. Mienie |

## PAST PRESIDENTS

*Deceased

* W. Bettel (1894–1895)
* A.F. Crosse (1895–1896)
* W.R. Feldtmann (1896–1897)
* C. Butters (1897–1898)
* J. Loevy (1898–1899)
* J.R. Williams (1899–1903)
* S.H. Pearce (1903–1904)
* W.A. Caldecott (1904–1905)
* W. Cullen (1905–1906)
* E.H. Johnson (1906–1907)
* J. Yates (1907–1908)
* R.G. Bevington (1908–1909)
* A. McA. Johnston (1909–1910)
* J. Moir (1910–1911)
* C.B. Saner (1911–1912)
* W.R. Dowling (1912–1913)
* A. Richardson (1913–1914)
* G.H. Stanley (1914–1915)
* J.E. Thomas (1915–1916)
* J.A. Wilkinson (1916–1917)
* G. Hildick-Smith (1917–1918)
* H.S. Meyer (1918–1919)
* J. Gray (1919–1920)
* J. Chilton (1920–1921)
* F. Wartenweiler (1921–1922)
* G.A. Watermeyer (1922–1923)
* F.W. Watson (1923–1924)
* C.J. Gray (1924–1925)
* H.A. White (1925–1926)
* H.R. Adam (1926–1927)
* Sir Robert Kotze (1927–1928)
* J.A. Woodburn (1928–1929)
* H. Pirow (1929–1930)
* J. Henderson (1930–1931)
* A. King (1931–1932)
* V. Nimmo-Dewar (1932–1933)
* P.N. Lategan (1933–1934)
* E.C. Ranson (1934–1935)
* R.A. Flugge-De-Smidt (1935–1936)
* T.K. Prentice (1936–1937)
* R.S.G. Stokes (1937–1938)
* P.E. Hall (1938–1939)
* E.H.A. Joseph (1939–1940)
* J.H. Dobson (1940–1941)
* Theo Meyer (1941–1942)
* John V. Muller (1942–1943)
* C. Biccard Jeppe (1943–1944)
* P.J. Louis Bok (1944–1945)
* J.T. McIntyre (1945–1946)
* M. Falcon (1946–1947)
* A. Clemens (1947–1948)
* F.G. Hill (1948–1949)
* O.A.E. Jackson (1949–1950)
* W.E. Gooday (1950–1951)
* C.J. Irving (1951–1952)
* D.D. Stitt (1952–1953)
* M.C.G. Meyer (1953–1954)
* L.A. Bushell (1954–1955)
* H. Britten (1955–1956)
* Wm. Bleloch (1956–1957)
* H. Simon (1957–1958)
* M. Barcza (1958–1959)
* R.J. Adamson (1959–1960)
* W.S. Findlay (1960–1961)
* D.G. Maxwell (1961–1962)
* J. de V. Lambrechts (1962–1963)
* J.F. Reid (1963–1964)
* D.M. Jamieson (1964–1965)
* H.E. Cross (1965–1966)
* D. Gordon Jones (1966–1967)
* P. Lambooy (1967–1968)
* R.C.J. Goode (1968–1969)
* J.K.E. Douglas (1969–1970)
* V.C. Robinson (1970–1971)
* D.D. Howat (1971–1972)
* J.P. Hugo (1972–1973)
* P.W.J. van Rensburg (1973–1974)
* R.P. Plewman (1974–1975)
* R.E. Robinson (1975–1976)
* M.D.G. Salamon (1976–1977)
* P.A. Von Wielligh (1977–1978)
* M.G. Atmore (1978–1979)
* D.A. Viljoen (1979–1980)
* P.R. Jochens (1980–1981)
G.Y. Nisbet (1981–1982)
A.N. Brown (1982–1983)
* R.P. King (1983–1984)
J.D. Austin (1984–1985)
H.E. James (1985–1986)
H. Wagner (1986–1987)
* B.C. Alberts (1987–1988)
* C.E. Fivaz (1988–1989)
* O.K.H. Steffen (1989–1990)
* H.G. Mosenthal (1990–1991)
R.D. Beck (1991–1992)
* J.P. Hoffman (1992–1993)
* H. Scott-Russell (1993–1994)
J.A. Cruise (1994–1995)
D.A.J. Ross-Watt (1995–1996)
N.A. Barcza (1996–1997)
* R.P. Mohring (1997–1998)
J.R. Dixon (1998–1999)
M.H. Rogers (1999–2000)
L.A. Cramer (2000–2001)
* A.A.B. Douglas (2001–2002)
S.J. Ramokgopa (2002-2003)
T.R. Stacey (2003–2004)
F.M.G. Egerton (2004–2005)
W.H. van Niekerk (2005–2006)
R.P.H. Willis (2006–2007)
R.G.B. Pickering (2007–2008)
A.M. Garbers-Craig (2008–2009)
J.C. Ngoma (2009–2010)
G.V.R. Landman (2010–2011)
J.N. van der Merwe (2011–2012)
G.L. Smith (2012–2013)
M. Dworzanowski (2013–2014)
J.L. Porter (2014–2015)
R.T. Jones (2015–2016)
C. Musingwini (2016–2017)
S. Ndlovu (2017–2018)

**Honorary Legal Advisers**
Scop Incorporated

**Auditors**
Genesis Chartered Accountants

**Secretaries**
The Southern African Institute of Mining and Metallurgy
Fifth Floor, Minerals Council South Africa
5 Hollard Street, Johannesburg 2001 • P.O. Box 61127, Marshalltown 2107
Telephone (011) 834-1273/7 • Fax (011) 838-5923 or (011) 833-8156
E-mail: journal@saimm.co.za

**Typeset and Published by**
The Southern African Institute of Mining and Metallurgy
P.O. Box 61127
Marshalltown 2107
Telephone (011) 834-1273/7
Fax (011) 838-5923
E-mail: journal@saimm.co.za

**Printed by**
Camera Press, Johannesburg

**Advertising Representative**
Barbara Spence
Avenue Advertising
Telephone (011) 463-7940
E-mail: barbara@avenue.co.za

**ISSN 2225-6253 (print)**
**ISSN 2411-9717 (online)**



SAIMM
JOURNAL OF THE SOUTHERN AFRICAN INSTITUTE OF MINING AND METALLURGY
VOLUME 119 NO. 5 MAY 2019

# Contents



## PAPERS OF GENERAL INTEREST






# The changing landscape of elements being mined and beneficiated leading up to and beyond 2020, and what this could mean to sub-equatorial Africa and globally

The exploitation of minerals and metals over the centuries has been driven by many factors, including perceived value due to rarity and functionality in applications such as adornment, coinage, military and domestic uses, as well as in construction and manufacturing of products our forebears (and some of us) could probably never have dreamt of. This revolution has impacted our everyday lives, but we are also facing some of the unintended consequences, such as climate change.

There is an almost logarithmic relationship between the level of concentration of the elements in the upper crust of the Earth and the value or price, as well as the quantities produced and the demand. The relationship was characterized for many years by gold at the top of the list, but with other precious metals of the platinum group being added as they became identified and exploited during the past couple of centuries. However, with the advent of advanced materials, high-tech electronics, and battery (EV) technologies and developments in related industries, numerous additional ultra-low concentration and rare earth elements have begun to challenge, and could possibly in some cases even supersede, some of the precious metals.

There are also two much less scarce elements of interest that are conspicuous by their lying above the average trend line, namely magnesium and titanium. Both are reasonably abundant and occur at concentration levels of up to 40% and 50% as the carbonate and oxide respectively. However the cost of producing these metals is relatively high due to the energy-intensive processes required. This has contributed to them being used perhaps less than they could be. A number of technology improvements have been proposed, but none have been scaled up so far, including Mintek's Thermal Magnesium Process (MTMP), which was operated on a pilot scale at close to atmospheric pressure instead of a vacuum. However the biggest impact on magnesium production in the past 25 years has been the manner in which the informal Chinese economy has apparently enabled the main reducing agent, ferrosilicon (FeSi), to be supplied at almost half the price of that in most other regions. This has contributed to China producing up to 80% of the global magnesium supply of close to 1 Mt/a and has brought this ultra-light metal (density 1.7 t/m$^3$) closer to the trend line referred to above.

While the use of magnesium in the transportation industries, including aerospace, offers reductions in fuel-based $CO_2$ emissions in the longer term, its production from dolomite and FeSi does have an ongoing negative impact. The main question is whether this current economy of low-priced FeSi and the use of dolomite is a sustainable approach. Current magnesium prices in China are around US$2–2.50 per kilogram, but realistically prices should be closer to double this if production costs in China are normalized to compare with other regions. The uncertainty in this matter is probably impacting on growth potential, and this situation is unfortunate due to the positive effects of magnesium's strength and lightness on fuel and energy saving, even when compared with aluminium (density 2.7 t/m$^3$). A better approach to the production of magnesium is almost certainly needed.

Furthermore, there is also a close relationship between magnesium and titanium, since magnesium is the reducing agent for converting $TiCl_4$ into titanium metal. Although Mg is recycled by electrolysis of the $MgCl_2$ formed and the Cl produced is recycled to reductively chlorinate the $TiO_2$ to $TiCl_4$, a lower Mg price would lower that of Ti too as some of the recycled Mg needs to be replaced to make up losses. However, an increase in the magnesium price would also impact that of titanium, as would the price of an important alloying element such as vanadium were it to increase as a result of the potential demand for use in a new generation of high-power storage batteries.

There are large resources of magnesium in the equatorial region of Africa, where the Congo River could potentially provide up to 500 GW of electrical energy from hydropower. Previous studies have considered the distribution of over 300 GW in the Southern African region, which could resolve the well-known current power supply issues. The magnesium in Central Africa is contained in significant carnallite deposits that are being evaluated for potash production, and could also in principle produce up to a million tons of magnesium per year. Investment in these mega projects, together with the promotion of the increased use of lightweight elements and those that result in high-strength lighter components being manufactured, can significantly reduce emissions of greenhouse gases. Surely these are some of the considerations that need to be worked on, together with renewable and energy-efficient solutions, as a top priority for the sustainability of the planet.

The development of new projects is driven by many of the above considerations, and as expected, exploration activities increase at times of higher prices due to increased demand. However the lead time to finding new deposits and improving the delineation of existing ones often takes many years, by which time markets have usually changed. The junior resources companies and the funding of their activities play an important role in providing a source of new projects, due

to the somewhat different risk profile they often have compared with the larger, more established and, understandably, more conservative, companies. However the juniors often face challenges in procuring the necessary funding based on what is usually a limited balance sheet. This, along with other factors, can result in projects stalling or sometimes even being abandoned or sold off for very little return. The production of co-and by-products such as Cu, Ni, and Co, Ni and Pd, and Pt and Pd can also impact these element balances, especially where they co-exist in the minerals being mined.

Nevertheless, at the end of the day a sufficient number of projects have to succeed out of a given investor's or group of investors' portfolios to justify their overall objectives of making a high enough return from the successful projects to more than justify the relatively higher risks and offset the failures. Even major mining companies have experienced costly technical and operational setbacks in the development and implementation of new projects in several cases for reasons that could, especially in hindsight, have been avoided. A stronger focus on the lessons learned (or sometimes not learned) is a theme that the SAIMM could consider for conferences and even schools, so that current and future generations can benefit from the learning curve.

Changes in demand for metals driven by developments in technology can also impact existing mining and processing operations, as well as longer-term exploration and the targeting of new project implementation. The relatively recent shift towards the use of palladium over platinum in autocatalysts (this has also occurred previously) is a case in point, with more far-sighted and flexible producers being able to better exploit the opportunity this type of change creates. The directions that need to be taken often come from a better understanding of changes in the downstream uses and related developments in advanced technologies.

There is also strong competition for funding from other industries, including natural resources. For example, the permitting of cannabis in several countries, has stimulated significant investment in this industry and potentially reduced that in mining projects to some extent.

Increasing pressure from environmentalists, and especially those concerned about climate change, is also having an impact, and it is yet to be seen whether this affects production more or less than that it does demand. These uncertainties contribute to the future challenges that our industry faces, and we need to work harder and smarter to address them with resources that are becoming increasingly scarce. However, on a more positive note there is enormous potential for regional and global cooperation to make a valuable contribution to lowering the impact on the environment by changing the dynamics in the production of many of the metals needed for sustainable growth, with the benefits of a major reduction in $CO_2$ emissions over the next ten years.

Figures 1 and 2 show the main elements in the Earth's crust as well as the relationship between abundance and the market prices. These are mostly based on data from 2018, or estimated where the data was not available or uncertain, and the information should be validated if any possible use is to be made of it. Magnesium, titanium, and potassium referred to above all feature among the top nine major crustal constituents.
These relationships, while well known over many years, have been studied further and reported in a number of publications, some of which are shown below.

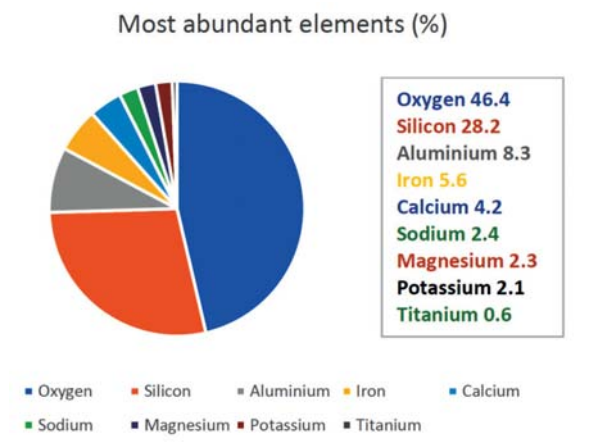


**Figure 1—The proportions of the main elements in the Earth's crust**

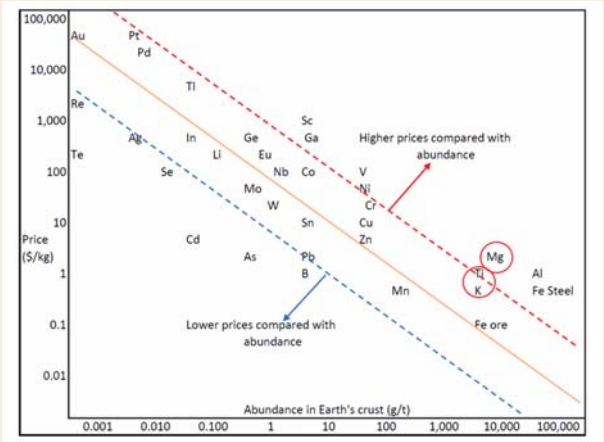


**Figure 2—Indicative prices compared with abundance in the Earth's crust for selected elements**

## References


Jaffe, R., Price, J., Hitzman, M., and Slakey, F. 2011. Energy-critical elements for sustainable development, *Physics & Society*, vol. 40, no. 3. https://www.aps.org/units/fps/newsletters/201107/jaffe.cfm

Hurd, A.J., Kelley, R.L., Eggert, R.G., and Lee, M-H. 2012. Energy-critical elements for sustainable development. *MRS Bulletin*, vol. 37, no. 4. https://www.researchgate.net/publication/259420442_Energy-critical_elements_for_sustainable_development


**N.A. Barcza**

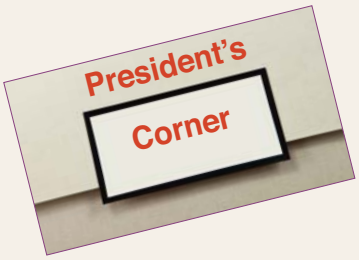


# Trying to demystify Industrial Revolution 4.0.

There is much excitement in the air around 'Industrial Revolution 4.0' amongst information systems experts and data scientists, while on the other hand there is a fear of an impending tsunami of new technology which, if you don't ride on the crest of the wave, will leave a trail of destruction of conventional wisdom and systems, leaving the conventionalists behind in its wake.

Often, remarks are made about the 'inevitability' of Industrial Revolution 4.0, and the need to 'embrace it', by commentators and organizations that do not fully understand what it is, or what the real implications may be.

To create the mystique of this revolution, a new language has been developed which is baffling and incomprehensible to the uninitiated, talking about the Internet of Things, artificial intelligence, big data, cloud computing, blockchain, interoperability, and motes.

So, how do we demystify this in our world of mining, in order to ensure we are not swept aside, left behind, or abandoned as an industry populated by Luddites?

From Wikipedia, 'Industry 4.0 is a name given to the current trend of automation and data exchange in manufacturing technologies. It includes cyber-physical systems, the Internet of things, cloud computing and cognitive computing.'

This mouthful of cyber parlance merely indicates that Industrial Revolution 4.0 is about data, and how we use that data in improving the efficiency and cost of production, not only in manufacturing but in all sectors, including mining.

We have had data for many years. In a paper in the Association of Mine Managers from 1937 (MacNiven and Roberts: *Underground mule haulage*, Association of Mine Managers of South Africa, 1937) a study was done on measuring the productivity of underground mules, which were used as the primary source of power for what in those days passed for 'mechanized' haulage. Measurements included factors like food consumption, living conditions, temperatures, speed of walking *etc*. Less easy to quantify was the temperament of the animals. Of course, in those days, in order to analyse this data, it first had to be captured manually.

The difference between those days and today lies in the amount of data that is available, how it is collected and transmitted, and how it is analysed, as in all cases this is done automatically and remotely. This trend has progressed as the industry transitioned from the first industrial revolution (mechanization, water power, and steam power), to the second revolution (mass production, assembly line, and electricity), to the third (computers and automation), and to the fourth, based on cyber-physical systems.

Thus, the first issue to demystify is that this is not a sudden event, but rather a transition that we have been party to for quite a long time. Let us consider how this data has been collected in mining, by taking two examples. Firstly, mine survey data has typically been collected through measurement and recording, taking place whenever the surveyor is present to conduct such measurements. This data then gets translated through spreadsheets, and eventually finds its way to a reporting system, which typically reports at month end. It is then compared to other measurements which have been taken by other people (such as the shift supervisor), and because these were collated differently, these reconciliations are usually difficult. Secondly, mine ventilation data within a fire detection system is collected by a system which automatically triggers an alarm when a particular monitor underground detects smoke. What then happens depends on the reaction of a control room operator, who needs to make a decision. Often, the calibre of the person having to make the decision is such that perhaps the wrong decision is made, or the matter is elevated to a higher-level decision-maker, which causes a delay (which could be critical).

The two instances described here are completely unconnected, and one has no impact on the other. This may or may not be important, but if, for example, there is a communication system to people in the mine workings that automatically alerts them that there is smoke in the mine, evacuation could happen immediately.

Thus, a transition that is fundamentally important to understand is the interoperability of data systems, or in layman's terms how the data systems should be connected to each other.

Data monitoring has been very fertile ground for system salespeople, and has, in most cases, been blind to the interoperability issues, with the result that mines end up with a plethora of independent systems that do not talk to each other. This has resulted in the need for layers of data collation and interpretation, which allow a flow across systems and between layers, so that signals are sent to the right places for the right decisions to be made.

This gives rise to the '*Internet of Mining Things*', wherein, in a modernized mine, a complete map is required, or architecture, that defines what data needs to be collected, how it is to be collected, how it is transmitted, how it is integrated, and how it is analysed. Thus, given the level of data that can be collected, management needs to define what decisions it needs to make and at what level, and how frequently these decisions need to be made. Given that just about everything can be measured in real time, the amount of data available becomes excessive, and may become too much for it to be transmitted through to, say, a central control room, especially if it includes video data.

So, serious thought needs to be given to defining what data is required for production monitoring and control, and health and safety, and for what purpose. For a highly mechanized mine, this would be closer to real-time data on positioning, performance, and condition monitoring on machines, leading to the possibility of autonomous operations. On the other hand, for a multi-stope, conventional gold mine, the need may be for real-time health and safety monitoring, but for accurate end-of-shift reporting of mining production.

All of the above tends to put the focus of Revolution 4.0 on data and information. However, mining is a physical business, which is a complex system, and which has a clearly defined value chain. This implies that the focus for modernization of the mining industry needs to be on a balanced combination of people, processes, and technologies, and not an over-emphasis on one aspect in particular.

In terms of technologies, this includes not only focus on information technologies, but also on 'hard technologies' such as drill rigs, haulage systems, and rapid development systems, as well as improved comminution and metallurgical circuits, to deliver improved results. Indeed, various surveys of global mining companies on their view of modernization seem to indicate that these companies wish to concentrate on reduced dilution through in-pit or in-mine recovery processes, decreased environmental footprints, decreased energy costs, decreased water usage, appropriate automation, and condition monitoring for improved efficiency. These issues are all process issues, involving technologies and people, and are issues that are aimed at significant bottom line improvement for the industry.

While the issue of automation is high on the agenda of international mining operations, especially those in remote areas where labour is scarce, in the South African context it is relatively low on the agenda of conventional mining operations because of the possible socio-economic impacts as well as the complexity of the multi-stope operations. Instead, what is appropriate is the enhancement of operations, through providing solutions to operators and supervisors which make their work easier, safer, and healthier. This is where semi-remote operations, artificial intelligence, and augmented reality become the necessary focus areas, coupled with appropriate mechanization and real-time monitoring and control.

Augmented reality offers the opportunity for operators to conduct their work with immediate support for decision-making. For example, a poor ground condition that requires immediate corrective action can be dealt with immediately, through the operator having assistance from technical support *via* the augmented reality monitors that he or she can don. This then solves the problem of a long delay and production interruption while the matter is escalated to the right decision-making level.

Similarly, arduous and repetitive work can be done using artificial intelligence, applied through semi-remote operations, where the fatigue element and the need for the operator to work in an unsafe or unhealthy environment are removed. This then allows the operator to become more autonomous him/herself, by being able to think about the operation and the risks within it, and being involved in more satisfying work.

The Minerals Council states that 'Modernisation is not simply mechanisation and/or gradual implementation of new technology. It is not the replacement of people with machines. It is not a euphemism for job losses.

'It is a process of transition of the mining industry of yesteryear and today to that of tomorrow.'

The application of Industrial Revolution 4.0 to the mining value chain has some profound impacts, and is clearly a part of the modernization thrust.

First, because the value chain now becomes data-enabled, this implies that people throughout the value chain are themselves data-enabled. This has an impact on the requisite organizational structure in terms of the levels and points at which decisions are made, in real time.

Second, increased levels of modernization require more real-time control, which impacts on the point within the organization where critical decisions are made, and the skills required to make those decisions.

Third, implementation of augmented reality and artificial intelligence frees up operator time, for these operators to conduct higher skill work. This will require the definition of the skills required for these people.

The impacts of Industrial Revolution 4.0 upon people cannot be over-emphasised. This is in terms of the technologies which they will be required to work with and operate, and the requisite skills to operate in this environment. This applies equally to operators, supervisors, and management, and infers that skills, syllabi, and learning materials need to be changed for this new environment as it unfolds. It also implies that strong support in terms of engineering and data science is required.

Since so much emphasis has to be placed on people during the transition to Industrial Revolution 4.0, it is very clear that the people affected must be involved in the process of transition. This involvement needs to include both organized labour and the immediate communities. The importance of these dialogues lies in understanding what the concerns and expectations of these constituencies are, and how they can be accommodated in the transition. Clearly, in terms of tracking of people, for example, there are sensitivities that organized labour has concerns about, whereas tracking in terms of knowing where people are in an emergency and being able to communicate with them is of importance to all stakeholders. Other concerns relating to invasion of privacy and health monitoring data also needs to be addressed to the satisfaction of all parties.

Frequently, statements are made implying that Industrial Revolution 4.0 and automation will not lead to job losses. However, from a labour or community point of view, these statements need to be proven through joint, collaborative investigation and impact assessment.

The transition to Industrial Revolution 4.0 and modernization of our industry is therefore not something to be afraid of. Instead, it should be embraced as a means to keep our mines open, and to open new ones. This transition must be holistic and must involve all stakeholders.

The Institute is holding an increasing number of events around these issues, as exemplified by the New Technology in Mining conference in June. This will be followed by various other events to tackle specific issues. It is perhaps indicative of the focus on technology rather than people that the vast majority of abstracts for the conference received thus far are based on specific technology developments. Thus it is important that the people-centric approach advocated above becomes an equal, if not greater component of these discussions, dialogues, and debates.

**A.S. Macfarlane**
*President, SAIMM*


# Metal recovery from $TiCl_4$ slurry by evaporation and acid leaching

**X. Xiang[1], X. Wang[2], W. Xia[1], and J. Yin[1]**

**Affiliation:**
[1]School of Metallurgical and Materials Engineering, Central South University, Changsha, China.
[2]School of Metallurgy and Environment, Chongqing University of Science and Technology, Chongqing, China.

**Correspondence to:**
X. Xiang

**Email:**
xxycsu@163.com

**Dates:**
Received: 5 Apr. 2018
Revised: 12 Jul. 2018
Accepted: 29 Oct. 2018
Published: April 2019

**How to cite:**
Xiang, X., Wang, X., Xia, W., and Yin, J.
Metal recovery from $TiCl_4$ slurry by evaporation and acid leaching.
The Southern African Insitute of Mining and Metallurgy

DOI ID:
http://dx.doi.org/10.17159/2411-9717/85-192-1/2019

ORCiD ID:
X. Xiang
https://orchid.org/0000-0002-7080-7980

## Synopsis

**$TiCl_4$ slurry containing valuable metals is an unavoidable by-product of the titanium ore chlorination process. The recovery of these valuable metals, which include titanium, niobium, tantalum, and aluminum, is an urgent issue to tackle in the titanium industry. The results of this investigation show that the valuable metallic elements can be recovered from the slurry by evaporation in a sealed container and leaching with dilute hydrochloric acid. After evaporation at 200°C for 60 minutes, nearly 99% of the titanium was recovered in the form of $TiCl_4$, which was formed by the reaction of the $TiO_2$ in the slurry with $AlCl_3$. After evaporation, metals like niobium, aluminum, and tantalum remained in the residue. By leaching with 2.1 mol/L HCl at a L/S ratio of 6:1 mL/g at 80°C for 60 minutes, the soluble metals, such as aluminum, iron, and copper were all removed from the residue, and the niobium and tantalum were further enriched in the leach residue. A concentrate containing 53.40 wt% Nb and 5.57 wt% Ta was obtained by washing the leach residue with dilute aqueous ammonia under stirring. A potential waste water purifying agent containing 263.75 g/L $AlCl_3$ was produced by purifying the leaching solution with $Al(OH)_3$ and modified polyacrylamide.**

**Keywords**
**$TiCl_4$ slurry, niobium, recovery, evaporation,leaching.**

## Introdution

Titanium tetrachloride ($TiCl_4$) is an important intermediate in titanium metallurgy that is widely used in the production of titania and titanium sponge (Akhtar, Xiong, and Pratsinis, 1991). In conventional titanium metallurgical processes, high-titanium materials such as synthetic rutile and high-titanium slag are reacted with chlorine to produce $TiCl_4$ in a fluidized-bed furnace. Accompanying elements, such as Al, Nb, and Fe also react with chlorine to form chlorides, which are mixed with gaseous $TiCl_4$ (Anderson, 1917). In the condensation process, gaseous $TiCl_4$ is refrigerated and high-boiling-point chlorides are precipitated in the liquid $TiCl_4$ to form a slurry containing 50~60 wt% $TiCl_4$ (Wang, Xiang, and Wang, 2012).

Various methods have been proposed to recover $TiCl_4$ from the slurry, including microwave heating and spray drying (Wang, Xiang, and Wang, 2012, Wang *et al.*, 2010a). To date, the only way to recover the $TiCl_4$ is to return the slurry to the fluidized-bed furnace. However, this causes fluctuations in the temperature in the furnace, resulting in incomplete reaction between titanium-rich materials and chlorine. Therefore, the slurry is often rinsed with water and neutralized by adding lime, which caused serious environmental pollution and wastes a valuable resource (Roy, Bhatt, and Rajagopal, 2003).

The $TiCl_4$ slurry contains considerable quantities of niobium (Wang *et al.*, 2012), which is one of the accompanying elements in titanium ore. Niobium is a rare metal that is widely used in steel, electronics, and other high-tech industries (Miller, 1959a; He, Liu, and Zhang, 1998). In nature, niobium is often associated with titanium, tantalum, the rare earth elements, and tin (Gupta and Suri, 1994; Miller, 1959b), and is usually recovered by hydrometallurgical methods such as decomposing tantalum-niobium concentrate with hydrofluoric acid (El-Hussaini, 2001; Gupta and Suri, 1994; Wang *et al.*, 2010) and leaching niobium from low-grade niobium materials with concentrated KOH solution (Zhou, Zheng, and Zhang, 2005; Wang *et al.*, 2009a; Zhou *et al.*, 2005b). These methods cannot be used to recover niobium from the slurry because of the high content of $TiCl_4$. However, the niobium can be easily recovered from the slurry by leaching after the $TiCl_4$ has been removed by evaporation (Fran, 1978).

The objective of this study is to transform the slurry from a waste material into a valuable resource and reduce pollution. The methods employed include evaporation of the slurry in a sealed container and leaching of the residue with dilute hydrochloric acid.

## Experimental

### *Materials and analysis*

All the chemical reagents used in this study were analytical grade, and deionized water was used. The $TiCl_4$ slurry was obtained from Zunyi Titanium Industry Co. Ltd. Its chemical composition is listed in Table I. It was found that about 80% of the titanium existed as $TiCl_4$ in the slurry, which was confirmed by washing the slurry with $CCl_4$.

The contents of titanium, aluminum, niobium *etc*. were measured by inductively coupled plasma atomic emission spectroscopy (ICP-AES) using a PS-6 Plasma Spectrovac, Baird (USA). Samples analysed for niobium were dissolved in hydrofluoric acid and hydrochloric acid (Lima and Conte, 2003; Lu and Makishima, 2007; Yang and Pin, 2002). The X-ray diffraction (XRD) patterns were recorded on a Rigaku Miniflex diffractometer with Cu K  X-ray radiation at 35 kV and 20 mA.

### *Experimental procedure*

Table I shows that the contents of titanium, aluminum, and niobium are much higher than those of other metallic elements in the slurry. Hence, the experimental work focused on the recovery of titanium, niobium, and aluminum. The experimental procedure was performed as shown in Figure 1. First, $TiCl_4$ was recovered from the slurry by evaporation and condensation. The residue was then leached with dilute hydrochloric acid to remove the aluminium and enrich the niobium content. The leach residue was washed with ammonia solution and filtered to recover a niobium concentrate. The leaching solution was purified to produce an $AlCl_3$ solution, which could be used as a purifying agent in waste water treatment.

Figure 2 is a schematic of the experimental set-up for $TiCl_4$ recovery from the slurry. During the operating process, the slurry (25 g each test) was added into a 50 ml stopper flask which was heated by an oil bath. $TiCl_4$ in the slurry was volatilized from the flask and condensed in the forced-water condenser with a vortex tube. The liquid $TiCl_4$ was collected in a calibrated measuring cylinder. After evaporation for the required time, the residue was removed and weighed.

The leaching experiments were conducted in a 300 ml glass flask, which was heated by a water bath. After the required contact time, the suspension was vacuum-filtered. The leach residue was washed with ammonia solution while stirring to remove residual chlorine, then dried and analysed for niobium and other elements.

### *Experimental fundamentals*

From Table I, it can be seen that the slurry was mainly composed of chlorine, titanium, aluminum, and niobium. Most of the titanium in the slurry was in the forms of $TiCl_4$ and $TiO_2$ (Wang, Xiang, and Wang2012). During evaporation, $TiCl_4$ was preferentially vaporized from the slurry as its boiling point is lower than that of other chlorides such as $AlCl_3$, $NbCl_5$, and $FeCl_3$ (Dean, 1985; Lide, 1991). During evaporation, complex chemical reactions can take place in the slurry (Den, 2010), expressed as follows:

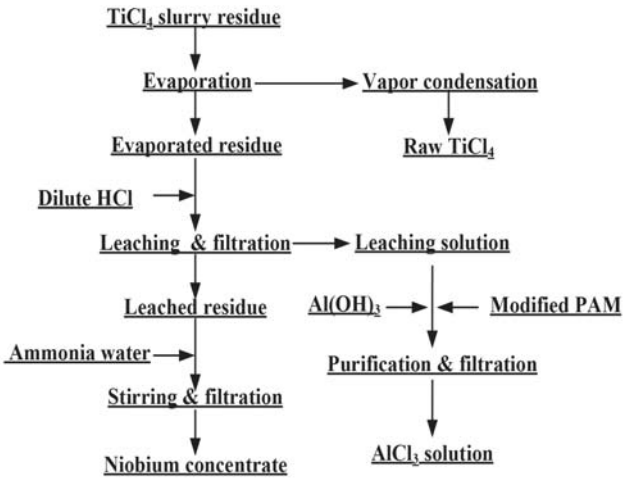


**Figure 1—Schematic flow sheet of metal recovery from $TiCl_4$ slurry residue**

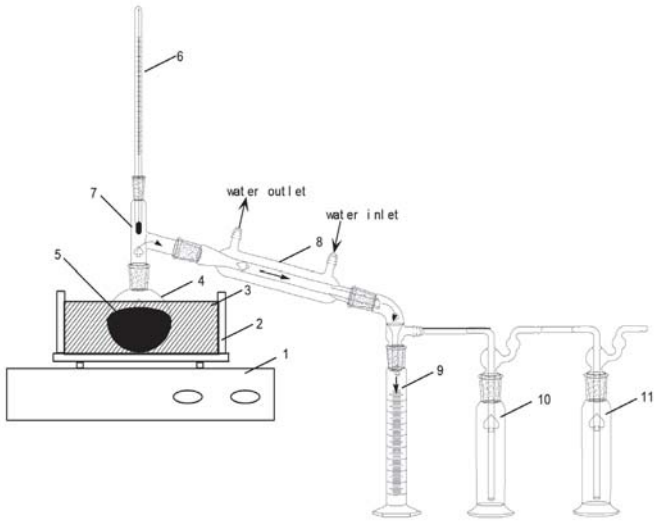


**Figure 2—Schematic pf the experimental set-up for $TiCl_4$ recovery from $TiCl_4$ slurry residue: (1) shaker, (2) heating tape, (3) oil bath, (4) distillation flask, (5) slurry, (6) heat indicator, (7) still head, (8) condenser, (9) measuring cylinder, (10) filtering flask with dried NaOH, (11) filtering flask with silica gel desiccant**

*Table I*

**Composition of the $TiCl_4$ slurry and products (wt%)**

| Material | O | Al | Cl | Ti | Nb | Fe | Cu | Ta | Zr |
|---|---|---|---|---|---|---|---|---|---|
| $TiCl_4$ slurry | 10.36 | 7.68 | 61.63 | 17.41 | 2.23 | 0.10 | 0.33 | 0.23 | 0.22 |
| Evaporation residue | 41.26 | 25.93 | 21.32 | 0.79 | 7.71 | 0.32 | 1.01 | 0.79 | 0.75 |
| Leache residue | 49.87 | 1.59 | 8.01 | 1.75 | 30.49 | 0.08 | 0.14 | 3.18 | 2.95 |
| Nb concentrate | 28.14 | 2.95 | 0.82 | 3.60 | 53.40 | 0.14 | 0.23 | 5.57 | 5.18 |

$$TiO_2 + 2AlCl_3 \rightarrow 2AlOCl + TiCl_4 \quad [1]$$

$$3TiO_2 + 4AlCl_3 \rightarrow = 2Al_2O_3 + 3TiCl_4 \quad [2]$$

$$TiO_2 + 4AlOCl \rightarrow 2Al_2O_3 + TiCl_4 \quad [3]$$

$$Nb_2O_5 + 5AlCl_3 \rightarrow 5AlOCl + 2NbCl_5 \quad [4]$$

$$A1Cl_3 + NbOCl_3 \rightarrow NbCl_5 + AlOCl \quad [5]$$

The free energy changes of reactions [1]–[5] at 200°C are listed in Table II. As seen, the reactions can occur when the slurry is heated to 200°C. Although the free energy changes are different, the reactions are not selective as they take place not in solution but in the slurry. Therefore the $TiO_2$ in the slurry can transform into $TiCl_4$, which then vaporizes. Hence, by controlling the evaporation temperature, titanium can be effectively separated and recovered from the slurry. Subsequently, aluminum, iron. and copper remaining in the residue can be easily leached with dilute hydrochloric acid, while the niobium, zirconium, and tantalum are insoluble in dilute acid (Dean, 1985; Zhu and Cheng, 2011; Gibalo, 1970). After washing with ammonia solution, chloride remaining in the leached residue is almost completely removed. Therefore, the niobium contained in the slurry can be effectively enriched by using the process shown in Figure 1.

## Results and discussion

### $TiCl_4$ slurry evaporation

#### Effect of evaporation temperature

Figure 3 shows the effect of temperature on the evaporation of titanium, niobium, and aluminium from the slurry over 60 minutes of heating. It was found experimentally that only when the temperature was increased to 145°C could liquid $TiCl_4$ be observed in the condenser, because the temperature difference between the oil bath and the still head outlet was about 25°C. In order to avoid the evaporation of high-boiling-point chlorides, the test temperature was changed from 150°C to 220°C. As can be seen, the evaporation of titanium increased considerably as the temperature increased from 150 to 164°C, and then increased very slowly in the range of 164–220°C. After evaporation at 164°C for 60 minutes, 3.5% of the titanium remained in the residue, decreasing to 1.5% when the temperature was raised to 200°C. This can be attributed to the reaction between $TiO_2$ and gaseous $AlCl_3$, because the sublimation temperature of $AlCl_3$ is 178°C (Dean, 1985).

Figure 3 shows that the evaporation of titanium reached up to 98.5% at 200°C, whilc the evaporations of niobium and aluminum were 0.1% and 13.27% respectively. With further increases in temperature, the evaporation of titanium remained constant, while the evaporation of niobium and aluminum increased quickly, which might be due to the evaporation of $AlCl_3$ and $NbCl_5$. Table III gives the vapour pressures of chlorides at different temperatures (Dean, 1985). As can be seen, the vapour pressure of $AlCl_3$ and $NbCl_5$ increases with increasing temperature, and the vapour pressures of $AlCl_3$ and $NbCl_5$ are higher than those of $TaCl_5$ and $ZrCl_4$ at temperatures below 200°C. However, it is interesting to see that the evaporation of $AlCl_3$ is lower than expected, which may be due to the inhibitory effect of $TiO_2$ and $Nb_2O_5$. Therefore, to separate and recover $TiCl_4$ from the slurry, the evaporation temperature should not exceed 200°C.

#### Effect of evaporation time

Figure 4 shows the effect of varying evaporation time from 5 to 40 minutes on the evaporation of titanium at different temperatures. It can be seen that the evaporation of titanium was fast initially, and then gradually slowed as evaporation neared completion. The times needed for evaporation at temperatures 220°C, 200°C, 180°C, and 160°C were 25, 30, 35, and 40 minutes respectively, which indicates that the lower the evaporation temperature and the less the amount of $TiCl_4$ remaining in the slurry, the more difficult the evaporation of titanium from the residue. From Figures 3 and 4, it can be determined that the recovery of titanium from the slurry should be carried out in the temperature range of 180–200°C for more than 35 minutes.

The residue obtained by evaporating the slurry at 200°C for 60 minutes (see Table I) was used for niobium recovery experiments. As can be seen from Table I, after evaporation, the content of titanium decreased from 17.41 wt% to 0.79 wt% while the contents of aluminum, niobium, zirconium, tantalum,

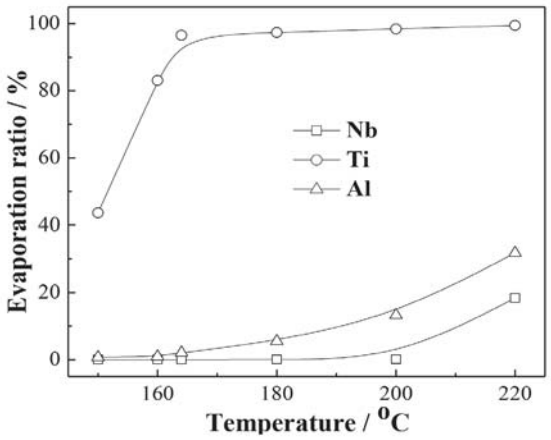


**Figure 3—Effect of temperature on titanium evaporation**

Table II

**Free energy changes for reactions [1]–[5] at 200°C (kJ/mol)**

| Reaction | [1] | [2] | [3] | [4] | [5] |
|---|---|---|---|---|---|
| $\Delta G$ | –134.41 | –317.58 | –48.76 | –264.85 | –12.69 |

*Table III*

**Vapour pressure of chlorides at different temperatures (kPa)**

| Temperature (°C) | 150 | 160 | 180 | 200 | 220 |
|---|---|---|---|---|---|
| $AlCl_3$ | 14.62 | 31.25 | 127.33 | — | — |
| $NbCl_5$ | 6.51 | 9.29 | 18.02 | 33.10 | 57.79 |
| $TaCl_5$ | 6.06 | 8.81 | 17.68 | 33.48 | 60.19 |
| $ZrCl_4$ | 1.28 | 1.97 | 4.41 | 9.22 | 18.14 |

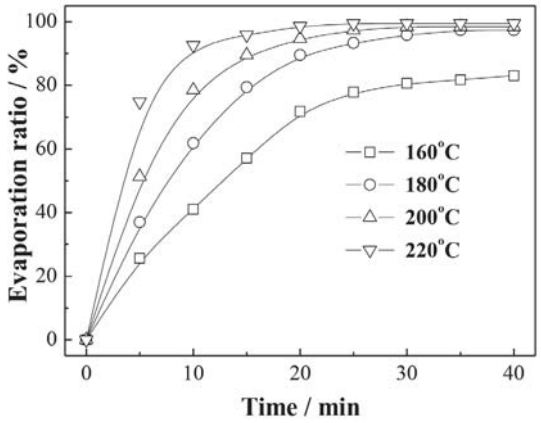


**Figure 4—Effect of time on titanium evaporation at different temperatures**

copper, and iron all increased proportionally. Compared with a titanium content of 29.6 wt% in the residue obtained by spray drying with argon at about 250°C (Wang *et al.*, 2012), it can be seen that evaporation in a closed container is an effective method of recovering titanium from the slurry. During the evaporation process, 66.7 wt% of the slurry evaporated to form a yellowish distillate with a $TiCl_4$ content of 97.5%, together with some impurities such as $AlCl_3$, $NbCl_5$, and $FeCl_3$. Therefore, the distillate represents a crude titanium tetrachloride and could be used to produce pigment or titanium sponge after purification (Den, 2010). Figure 5 shows the XRD pattern of the residue from evaporation. As seen from Figure 5 and Table I, the high-boiling-point chlorides and oxides all remained in the residue, indicating that the most appropriate method of separating and recovering titanium from $TiCl_4$ slurry is to evaporate the slurry in a closed container at 200°C for 60 minutes.

### *Leaching of the evaporation residue*

It can be seen from Table I that the metallic elements contained in the evaporation residue can be divided into two types – those that are soluble in dilute hydrochloric acid, which include aluminum, copper, and iron, and those that are insoluble, including niobium, zirconium, and tantalum (Dean, 1985). The content of aluminum in the residue is much higher than that of copper and iron. Therefore, this paper focuses on the separation of aluminum and niobium.

### *Effect of acid concentration*

The effect of acid concentration on the separation of aluminum and niobium was tested at 30°C at a liquid-to-solid ratio of 6:1 mL/g and leaching time of 120 minutes. Figure 6 shows that the acid concentration was an important factor in the separation. The leaching ratio of aluminum increased with increasing acid concentration, with more than 97% of the aluminum being leached when the acid concentration increased to 2.1 mol/L. A further increase in acid concentration had little effect. The remaining aluminum might be occluded by the leach residue. The leaching ratio of niobium was nearly zero at an acid concentration below 1.7 mol/L, and increased quickly at acid concentrations over 2.1 mol/L. This could be attributed to the dissolution of niobium oxides at high acid concentrations (El-Hussaini and Mahdy, 2002), and the possible reaction is given in Equation [6]. Therefore, to separate aluminum from niobium, the preferred hydrochloric acid concentration was determined to be 2.1 mol/L.

$$NbO(OH)_3(s) + H^+(aq) \rightarrow Nb_2^+(aq) + 2H_2O \quad [6]$$

### *Effect of temperature*

The effect of temperature on the leaching of the residue from evaporation is illustrated in Figure 7. The experiments were performed with liquid-to-solid ratio of 6:1 mL/g, and a leaching time of 120 minutes in 2.1 mol/L HCl. As can be seen from Figure 7, the effect of temperature on aluminum leaching was slight, while the effect on niobium leaching was more pronounced. As the temperature was increased from 30°C to 70°C, leaching of niobium decreased slowly, which might be attributed to hydrolysis of niobium in the leaching solution. Only 1.28% of the niobium was leached at 70°C, and further increase of temperature had little effect. Therefore, keeping the leaching temperature over 70°C is propitious for the enrichment of niobium.

### *Effect of time*

Figure 8 shows the results obtained by varying the leaching time from 5 to 120 minutes at 80°C with a liquid-to-solid ratio of 6:1 mL/g in 2.1 mol/L HCl. As can be seen, 95% of the aluminum

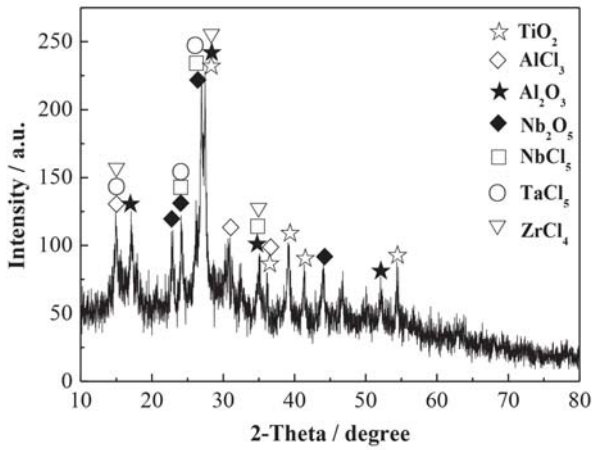


**Figure 5—XRD pattern of the residue from evaporation**

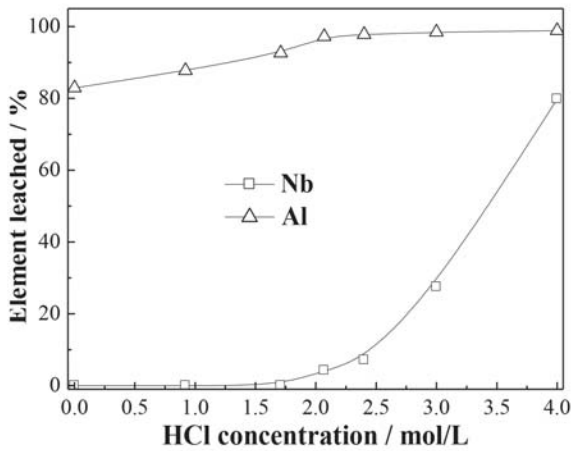


**Figure 6—Effect of acid concentration on the leaching of Al and Nb from the evaporation residue**

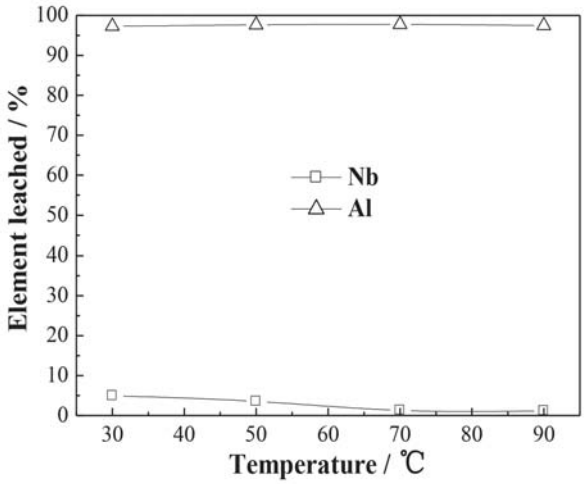


Figure 7—Effect of temperature on the leaching of Al and Nb from the evaporation residue

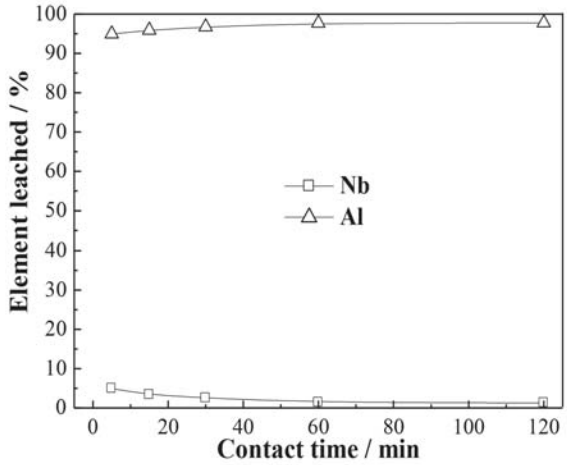


Figure 8—Effect of time on the leaching of Al and Nb from the evaporation residue

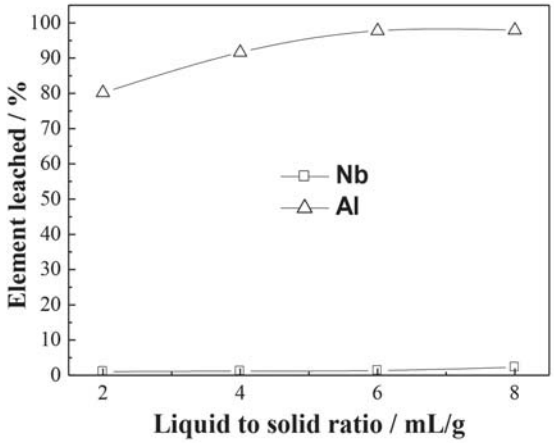


Figure 9—Effect of liquid-to-solid ratio on the leaching of Al and Nb from evaporation residue

was leached within 5 minutes, while only 5% of the niobium was leached. During the experiment, it was found that once the residue was added into the hydrochloric acid solution under stirring, the solid became suspended in the solution and the amount decreased appreciably. This indicated that aluminum contained in the evaporation residue dissolved easily in dilute hydrochloric acid. As the leaching time increased, the leaching ratio of aluminum increased slowly, while the leaching ratio of niobium decreased markedly. With a leaching time of 60 minutes, the leaching ratio of aluminum increased to 97.67%, while that of niobium decreased to 1.39%. The leaching ratio of niobium remained almost constant with further increases in leaching time. As aluminum was leached, the acidity of the leaching solution decreased rapidly, which caused the hydrolysis precipitate of niobium to dissolve in the solution. Therefore, a contact time of 60 minutes was selected for the following experiments.

### *Effect of liquid-to-solid ratio*

The effect of liquid-to-solid (L/S) ratio was examined in 2.1 mol/L HCl at 80°C for 60 minutes. The results are presented in Figure 9. As can be seen, the leaching ratio of aluminum increased from 80.16% to 97.73% when the L/S ratio increased from 2:1 to 6:1 mL/g, and then remained constant. However, the leaching ratio of niobium remained almost constant as the L/S ratio increase from 2:1 to 6:1 mL/g. At a L/S ratio over 6:1 mL/g, the leaching ratio of niobium increased markedly. Therefore, a L/S ratio of 6:1 mL/g was considered appropriate in this work.

The compositions of the leached residue and leaching solution are listed in Table I and Table IV respectively, obtained by treating the evaporation esidue with a L/S ratio of 6:1 mL/g in 2.1 mol/L HCl at 80°C for 60 minutes. As can be seen, aluminum, iron, and copper were almost completely leached from the evaporation residue, while the leaching of chlorine was only about 85%. This indicated that the leached residue might contain oxychlorides (Rodrigues and Silva, 2010; Guo and Wang, 2009). In order to remove the residual chlorine, the leached residue was washed with 2 mol/L aqueous ammonia at a L/S ratio of 4:1 mL/g under stirring at room temperature for 30 minutes and then filtered. After drying at 115°C for 24 hours, a niobium concentrate with the composition listed in Table I was obtained. Table I shows that after evaporation of the $TiCl_4$ slurry in a closed container, leaching of the residue with dilute HCl, and washing with dilute ammonia, the niobium, tantalum, and zirconium contents in the slurry were enriched dramatically. Although the content of Nb was 53.40 wt% in the concentrate, which is equivalent to 76.39 wt% of $Nb_2O_5$, it was found that the niobium in the concentrate was amorphous. Figure 10 shows the XRD pattern of the niobium concentrate roasted at 600°C for 4 hours. As seen, the $Nb_2O_5$ changed from amorphous to crystalline

*Table IV*

**Compositions of leaching solution before and after purification**

| Constituent | Al (g/L) | Ti (mg/L) | Nb (mg/L) | Fe (mg/L) | Cu (mg/L) | Ta (mg/L) | Zr (mg/L) | $H^+$ (mol/L) |
|---|---|---|---|---|---|---|---|---|
| Before purification | 41.87 | 588 | 146 | 481 | 1568 | 116 | 248 | 1.39 |
| After purification | 53.37 | 2.7 | 1.2 | 3.6 | 5.3 | 1.5 | 1.1 | pH=3.6 |

after roasting. It can also be seen from Table I that the $Nb_2O_5$ plus $Ta_2O_5$ content can reach up to 83.19wt% in the Nb concentrate. Therefore, this is a high-quality raw material for extracting niobium and tantalum by hydrofluoric acid decomposition and solvent extraction (El-Hussaini, 2001; Gupta and Suri, 1994; Guo and Wang, 2009).

### *Purification of leaching solution*

Table IV shows that the leaching solution contains aluminum, iron, copper, titanium, niobium, zirconium, and tantalum. To recover aluminum, the impurities should be removed from the solution. The pH of the solution was adjusted to 3.5 by adding 36 g of $Al(OH)_3$ to 1000 mL of leaching solution, which caused Fe, Ti, Zr, Nb, and Ta to precipitate. Subsequently, modified polyacrylamide (PAM) was added to remove Cu and other trace heavy metals before filtration (Li *et al.*, 2010). The composition of the purified solution after filtration is listed in Table IV. The purified solution contained 263.75 g/L $AlCl_3$, which can be used as a purifying agent for waste water (Zhao *et al.*, 2009).

## Conclusions

Experiments confirmed that the valuable metals in $TiCl_4$ slurry can be recovered by evaporation and acid leaching. In this process, $TiCl_4$, niobium concentrate, and $AlCl_3$ solution were obtained separately. More than 98% of the titanium was recovered from the slurry by evaporation at 200°C for 60 minutes. The residue was leached with 2.1 mol/L HCl at a L/S ratio of 6:1 at 80°C for 60 minutes, then washed with 2 mol/L aqueous ammonia at a L/S ratio of 4:1 mL/g under stirring at room temperature for 30 minutes. After filtration, a niobium concentrate containing 53.40 wt% Nb and 5.57 wt% Ta was obtained. The leaching solution was purified by adding $Al(OH)_3$ and modified polyacrylamide, and a solution containing 263.75 g/L $AlCl_3$ was produced. Future work will focus on testing the performance of the purified leaching solution during wastewater treatment.

## Acknowledgements

The authors would like to thank the National Natural Science Foundation of China (No. 51604055 and No. 51674057) and the Chongqing Research Program of Basic Research and Frontier Technology (cstc2016jcyjA0645) for their financial support of this work.

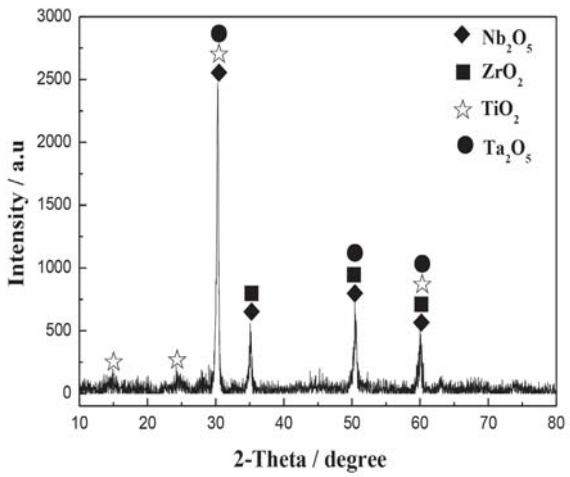


**Figure 10—XRD pattern of the roasted niobium concentrate**

## References

Akhtar, M.K., Xiong, Y., and Pratsinis, S.E. 1991. Vapor synthesis of titania powder by titanium tetrachloride oxidation. *Journal of Aerosol Science*, vol. 22, suppl. 1. pp. S35–S38.

Anderson, R.J. 1917. The metallurgy of titanium. *Journal of the Franklin Institute*, vol. 184, no. 4. pp. 469–508.

Dean, J.A. 1985. Lange's Chemistry Handbook. 13th edn. McGraw-Hill, New York.

Den, G.Z. 2010. The Metallurgy of Titanium. Metallurgical Industry Press, Beijing [in Chinese].

El-Hussaini, O.M. 2001. Extraction of niobium and tantalum from nitrate and sulfate media by using MIBK. *Mineral Processing and Extractive Metallurgy Review*, vol. 22. pp. 633–650.

El-Hussaini, O.M., and Mahdy, M.A. 2002. Sulfuric acid leaching of Kab Amiri niobium-tantalum bearing minerals, Central Eastern Desert, Egypt. *Hydrometallurgy*, vol. 64. pp. 219–229.

Frank, P. 1978. Metal extraction process. US patent, 4100252.

Gibalo, I.M. 1970. Analytical Chemistry of Niobium and Tantalum. Ann Arbor Humphery Science Publishers, Ann Arbor, Michigan.

Guo, Q.W. and Wang Z.X. The Metallurgy of Niobium and Tantalum. Metallurgical Industry Press, Beijing [in Chinese].

Gupta, C.K. and Suri, A.K. Extractive Metallurgy of Niobium. CRC Press, London.

He, C., Liu, Z., and Zhang, H. 1998 Treatment of fluorine-containing waste gas from hydrometallurgy of tantalum and niobium ore. *Nonferrous Metal*, vol. 4. pp. 141–142 [in Chinese].

Li, F.T., Jiang, J.Q., Wu, S.J., and Zhang, B.R. 2010. Preparation and performance of a high purity poly-aluminum chloride. *Chemical Engineering Journal*, vol. 156. pp. 64–69.

Lide, D.R. 1991. Handbook of Chemistry and Physics. CRC Press, Boca Raton, Florida.

Lima, B.B. and Conte, R.A. 2003. Analysis of nickel-niobium alloys by inductively coupled plasma optical emission spectrometry. *Talanta*, vol. 59. pp. 89–93.

Lu, Y.H. and Makishima, A. 2007. Coprecipitation of Ti, Mo, Sn and Sb with fluorides and application to determination of B, Ti, Zr, Nb, Mo, Sn, Sb, Hf and Ta by ICP-MS. *Chemical Geology*, vol. 236. pp. 13–26.

Miller, G.L. 1959a . Metallurgy of the Rarer Metals-6, Tantalum and Niobium. Butterworths Scientific Publications, London. Chapter 4.

Miller, G.L. 1959b. Tantalum and Niobium. Butterworths Scientific Publications, London.

Rodrigues, L.A. and Silva, M.L.C.P. 2010. Thermodynamic and kinetic investigations of phosphate adsorption onto hydrous niobium oxide prepared by homogeneous solution method. *Desalination*, vol. 263. pp. 29–35.

Roy, P.K., Bhatt, A., and Rajagopal, C. 2003. Quantitative risk assessment for accidental release of titanium tetrachloride in a titanium sponge production plant. *Journal of Hazardous Materials A*, vol. 102. pp. 167–186.

Wang, W.H., Zheng, S.L., Xu, H.B., and Zhang, Y. 2009a. Leaching of niobium and tantalum from a low-grade ore using a KOH roast–water leach system, *Hydrometallurgy*, vol. 98. pp. 219–223.

Wang, X.W., Zhang, L.P., Shang, G.H., Zhang, G.Q., Yuan, J.W., and Gong, S.C. 2009b. Processing copper-vanadium precipitate formed from crude $TiCl_4$ in titania and titanium sponge production. *Hydrometallurgy*, vol. 99, no. 3-4. pp. 259–262.

Wang, X.W., Tian, J.Q., Wang, M.Y., Guo, R.L., Peng, J., and Luo, L. 2010a. The method used to dry the slurry formed in raw titanium tetrachloride. Chinese patent, CN102092783A.

Wang, N., Gu, H.N., Jiang, Y., Fu, Y.H., and Tian, Y.J. 2010b. Study on niobium-tantalum resources in waste from the process of refining titanium tetrachloride by copper wires. *Science Technology and Engineering*, vol. 10, no. 31. pp. 7728–7730 [in Chinese].

Wang, X.W., Xiang, X.Y., and Wang, M.Y. 2012. The method used to separate and recover titanium and niobium from the slurry formed in raw titanium tetrachloride. Chinese patent 201210259878.8.

Wang, X.W., Wang M.Y., Xiang X.Y., Gong S C., and Zhao, Y.R. 2012. Recovery of $TiCl_4$ from precipitation slime by spray drying. *Titanium Industry Progress*, vol. 29, no. 5. pp. 36–38.

Yang, X.J. and Pin, C. 2002. Determination of niobium, tantalum, zirconium and hafnium in geological materials by extraction chromatography and inductively coupled plasma mass spectrometry. *Analytica Chimica Acta*, vol. 458. pp. 375–386.

Zhao, H.Z., Liu, C., Xu, Y., and Ni, J.R. 2009. High-concentration poly-aluminum chloride: Preparation and effects of the Al concentration on the distribution and transformation of Al species. *Chemical Engineering Journal*, vol. 155. pp. 528–533.

Zhou, H.M., Zheng, S.L., and Zhang, Y. 2005. Leaching of a low-grade niobium–tantalum ore by highly concentrated caustic potash solution. *Hydrometallurgy*, vol. 80. pp. 83–89.

Zhou, H.M., Zheng, S L., Zhang, Y., and Yi, D.Q. 2005. A kinetic study of the leaching of a low-grade niobium–tantalum ore by concentrated KOH solution. *Hydrometallurgy*, vol. 80. pp. 170–178.

Zhu, Z.W. and Cheng, C.Y. 2011. Solvent extraction technology for the separation and purification of niobium and tantalum: A review. *Hydrometallurgy*, vol. 107. pp. 1–12. ◆


# An evaluation framework for virtual reality safety training systems in the South African mining industry

**E.A. van Wyk[1] and M.R. de Villiers[2]**

**Affiliation:**
[1]Faculty of ICT, Tshwane University of Technology, South Africa.
[2]School of Computing, University of South Africa.

**Correspondence to:**
E.A. van Wyk

**Email:**
vanwykea@tut.ac.za

**Dates:**
Received: 7 Mar. 2018
Revised: 26 Sept. 2018
Accepted: 29 Oct. 2018
Published: May 2019

**How to cite:**
Van Wyk, E.A., and De Villiers, M.R.
An evaluation framework for virtual reality safety training systems in the South African mining industry
The Southern African Insitute of Mining and Metallurgy

DOI ID:
http://dx.doi.org/10.17159/2411-9717/53/2019

ORCiD ID:
E.A. van Wyk
https://orchid.org/0000-0002-0436-2741

M.R. de Villiers
https://orchid.org/0000-0002-9849-6723

**Synopsis**

**Mining companies strive to increase and maintain production, while simultaneously remaining competitive in the global economy. Furthermore, they must ensure workers' safety and maintain good safety records. The use of virtual reality (VR) facilitates the development of tools and systems for various purposes that can improve knowledge and understanding of the work environment. VR is a rapidly growing technology that uses the ever-increasing power of computing to simulate real-world and imaginary environments and situations with a high degree of realism and interaction. The availability of 3D modelling tools and simulation programming engines that work effectively with a mid-range desktop PC and standard 3D graphics card, make VR technology viable and attractive for mainstream training applications. The design, development, and implementation of interactive VR training systems is proposed as an innovative approach to augment safety training. However, in order to assess the impact of such VR training systems it is of particular importance to determine the effectiveness of the design of such systems. This article proposes an evaluation framework for this vital purpose. This framework comprises criteria to assess VR training systems, specifically relating to usability, instructional design, VR systems design, and mining industry context-specific aspects. Although the framework was developed as an evaluation tool to assess effectiveness of the design of such systems, it can equally well be used as a set of design principles to inform the design of VR training systems for mining.**

**Keywords**
**virtual reality, mine safety training, design-based research, evaluation framework.**

## Introduction

Mining in South Africa has been the main driving force behind the history and development of Africa's richest and most advanced economy (Coka, 2012). The South African mining industry is frequently criticised for its poor safety record and high fatality rate (Stoddard and Skweyiya, 2016). Inadequate or insufficient training is often cited as a root cause of accidents (Van Wyk and De Villiers, 2009; Tichon and Burgess-Limerick, 2011). Virtual reality (VR) is a rapidly growing technology that utilizes the ever-increasing power of computing to simulate real-world and imaginary environments and situations with a high degree of realism and interaction (Webber-Youngman and Van Wyk, 2013). VR is currently being used or investigated as a training solution in a variety of industries. VR technology has developed rapidly and costs have fallen to levels where it can now be considered for mainstream training applications. The availability of 3D modelling tools and simulation programming engines that work effectively with a mid-range desktop PC and a standard 3D graphics card, make VR even more attractive to mine training centres (Van Wyk and De Villiers, 2009).

The design, development, and implementation of interactive VR training systems is proposed as an innovative approach to augment safety training. However, in order to assess the impact of such VR training systems it is of particular importance to determine the effectiveness of the design of such systems. An approach is therefore required that evaluates the appropriateness and effectiveness of the VR systems design within the context of mine safety training. This article proposes an evaluation framework for this vital purpose.

Current evaluation frameworks are limited because they are either confined to evaluation of a specific type of virtual environment or they focus on a particular aspect of such environments. Hence this article reports on four cycles within a design-based research process, which led to the implementation of two interactive desktop VR safety training systems and the generation of an evaluation framework for evaluating such systems. Due to the increase of VR training in the mining sector and other industrial domains, the evaluation framework makes an important contribution in evaluating the effectiveness of training systems. Moreover, the framework can be applied not only to evaluate such systems, but its criteria can also serve as design aids.

# An evaluation framework for virtual reality safety training systems in the SA mining industry

## Background

Current mining training relies mainly on repetitive classroom-style learning with some instruction situated in a physical mock-up of an underground workplace, followed by on-the-job training. But under classroom conditions, workers do not make safety decisions under the same situations of stress and pressure they experience underground. Depending on the stress levels of the real working situation, the decisions taken in the authentic underground workplace may differ significantly from those taken under more relaxed circumstances in the classroom. To enhance the effectiveness of training, a training design is required that simulates threats as closely as possible (Van Wyk, 2015).

VR-based training tools can provide realistic simulations of such threats. Using VR, trainees can experience simulated working conditions in a virtual environment, yet without being subjected to the risks associated with the real environment. VR is currently being used and investigated in training solutions for a variety of fields, such as the military, medical, power generation, and aircraft industries (Van Wyk and Prinsloo, 2015). VR has features that are well suited to training for the mining environment and, in particular, for hazard recognition and associated remedial safety action. The most relevant features are: the facility to expose trainees to simulated hazardous situations without putting them in actual danger; the ability to present simulated hazardous situations more frequently than they are encountered in the real world; the simulation of situations that have not previously occurred, but which could be encountered in the workplace; and showing the possible consequences of actions taken by trainees.

## Virtual reality

VR technology is evolving rapidly, and it would be risky to define VR in terms of specific devices that might fall out of favour in the short term (La Valle, 2017). In general, VR refers to a technology where a user interacts with a three-dimensional computer-simulated environment that is perceived as comparable to real-world objects and events. As computer hardware and software improve and technology is frequently updated, the ease with which interactive simulations can be developed and deployed has improved considerably and lower-cost, high-quality development tools have become available. Based on the level of immersion, one can distinguish between three categories of VR system.

### *Immersive VR systems*

Immersive systems are the most technically advanced. The user is essentially isolated from the outside world and fully enveloped within a computer-generated environment. Immersive VR systems require users to wear a head-mounted display (HMD) unit that presents an image directly in front of each eye and magnifies it to fill a wide field of view. This creates the impression of actually being inside an environment, rather than observing a screen (Daden, 2016). The view is based on computer-generated images that react to the position and orientation of the user's head. HMD technology has certain disadvantages, including encumbrance due to wearing a headset with cables, a sense of isolation when viewing the virtual world while not knowing what is happening around you in the real world, high cost, and occasional simulator sickness and disorientation (Rogers, Sharp, and Preece, 2011; Stone and Knight, 2012). Various approaches to HMDs are emerging:

- The *integrated approach* uses a headset with all displays and functionality built in, while a computer generates the graphics. Examples are Oculus Rift, HTC Vive, and Sony Morpheus.
- The *smartphone approach* uses a smartphone as the display, processor. and movement detector. The phone resides within a holder with lenses, such as the Google Cardboard or Samsung Gear.
- Google is currently developing a standalone VR headset, called Daydream, that will not require a separate computer, smartphone, or cables (Google, 2017).

### *Semi-immersive VR systems*

In semi-immersive VR systems, computer-generated images are displayed on large screens by stereo projection and are viewed via special stereo eyewear. Interaction with onscreen menus occurs via a remote keypad, while other input is handled by devices such as 3D controllers or joysticks.

The use of multiple projection-based systems can result in substantial cost, which can run in the order of millions of rands, but high-resolution images can be produced. The configuration in which the user is surrounded by projection screens is sometimes referred to as a CAVE (cave automatic virtual environment). A CAVE creates the illusion of immersion by projecting high-resolution stereo images on the walls and floor of a room-sized cube. Several persons wearing lightweight stereo glasses can enter and walk freely inside the CAVE (Van Wyk, 2015). Although their fixed display position and limited display area restrict the user's range of interactions, projected VR systems have the advantage that the user is not constrained within a headset and can communicate freely with other participants.

### *Desktop VR systems*

Since not all applications require immersion to the extent described in the above categories, more affordable, non-immersive VR systems provide practical alternatives. An important feature of VR is the provision of a sense of actual presence in the simulated environment. Presence refers to the subjective experience of 'being' in the computer-generated environment, rather than in the actual real-world environment. In desktop VR systems the user remains visually aware of the real world, but can also observe the virtual world on a high-resolution monitor. In comparison to immersive systems, desktop VR provides a lower level of presence, but the lower capital cost of hardware, software, and peripherals make desktop VR systems an attractive and realistic substitute. Desktop systems utilize standard computer hardware. Input devices include a keyboard, mouse, 3D controller, joystick, and track pad or voice to interact with and manipulate the virtual environment. The sense of subjective immersion in desktop VR systems can be enhanced through stereoscopic glasses, which provide three-dimensional depth.

The boundaries between these types of VR systems are not clear-cut. The creative use of display and audio peripherals in desktop or semi-immersive systems can promote a sense of presence as experienced in immersive systems, even without the ability to fully control the virtual environment.

## Virtual reality and mine training

Mining in the 21st century is a high-technology industry. Mining companies strive to increase and maintain production,

while simultaneously remaining competitive within the global economy. Importantly, they should ensure workers' safety and maintain a good safety record, aiming towards zero harm. VR offers opportunities to develop tools and systems for a variety of purposes that can improve knowledge and understanding of the work environment. VR systems for the mining industry have been developed for mine planning and design, use of equipment, and training applications.

A primary objective of developing VR systems for mining is to allow personnel to practise and experience situations, activities, and processes that are encountered in the day-to-day operations at a mining site. Using VR, customized simulations of mine layouts and comprehensive virtual environments can be set up, allowing users to move around the virtual mine and take decisions. The consequences of both correct and incorrect decisions can be immediately fed back to trainees, giving them the opportunity to learn from their mistakes. VR also allows trainees to experience conditions that would be difficult or impossible to re-create in the real world. VR simulations can provide a wide range of possible training scenarios without incurring the high costs and risks to personnel and equipment (Van Wyk and Prinsloo, 2015). Moreover, VR is ideal for training workers who perform tasks in dangerous or hazardous environments. Trainees can practise procedures in a risk-free virtual situation, while being exposed to 'life-threatening' scenarios in a safe and controlled situation (Webber-Youngman, 2014).

## Literature review

Different types of VR training systems have already been developed for the mining industry. and will be discussed in detail in the sections to follow.

### *Incident reconstruction simulations*

Mining incidents are unfortunately a regular occurrence, due to the inherently hazardous nature of mining. With the aim of preventing recurrences, VR can be used to simulate the circumstances relating to previous serious incidents. Such incident reconstruction simulations help to emphasise the significance of unsafe acts and to promote a strong safety culture. They enable the workers to understand how and why an incident happened, how it could have been prevented, and how injuries or fatalities could have been avoided. Simulating a range of incident scenarios on a computer screen and viewing them from multiple angles enables investigators and workers to understand the underlying causes of an incident (STS3D, 2017). Continuous employee education and training, with the aim of establishing a strong safety culture in the industry, is a major factor in preventing fatal and non-fatal mining incidents (Schafrik, Karmis, and Agioutantis, 2003). VR training can play a meaningful role in the transfer of this knowledge (Webber-Youngman and Van Wyk, 2011).

### *Hazard awareness*

As previously stated, VR applications for training in hazard awareness enhance traditional training methods without unnecessarily exposing trainees to actual hazardous situations. Various systems have been developed that focus on simulating hazards relating to specific machinery or particular situations in the workplace, *e.g.* conveyor belts (Lucas, Thabet, and Worlikar, 2007) and trackless mobile machines (STS, 2013). Orr, Mallet, and Margolis (2009) developed a VR system for enhanced fire escape training for mine workers. VR technology has also been used to simulate hazards relating to the underground ventilation system (Ji-zu *et al.*, 2009).

### *Training related to mining equipment*

Many global mining equipment manufacturers have developed simulators of their more advanced equipment. Sandvik and Atlas Copco have drilling simulators, while Bucyrus International introduced simulation training for electric mining shovels (Chadwick, 2009). Caterpillar and Volvo supply simulators of their heavy machinery, including wheel loaders and excavators. These simulators feature state-of-the-art software with advanced 3D graphics to reproduce the operational movements of the real machines (CAT, 2014; Oryx, 2014).

### *Evaluation of VR training systems*

Tsiatsos, Andreas, and Pomportsis (2010:67) point out the *'need for a detailed theoretical framework for VR-based learning environments that could guide future development'*. They propose a framework for a specific category of collaborative virtual environments, which entail group work in a single immersive environment. This evaluation approach is not appropriate to the present study, as it relates to individualized desktop VR training.

Hanna, Nader, and Richards (2014) propose an evaluation framework for VR, but this similarly focuses on collaborative virtual environments, which are outside the scope of this study. Earlier frameworks include the work by Bowman, Koller, and Hodges (1998), who presented a framework for the analysis and evaluation of travel techniques in immersive virtual environments. This system, however, is limited to viewpoint motion control techniques. Bowman, Gabbard, and Hix (2002) overviewed usability evaluation of virtual environments, but focused on issues that differentiate evaluation of virtual environments from evaluation of traditional user interfaces. Gang, Jun, and Yingzhen (2006) proposed an evaluation framework for evaluating virtual geographic environments, but this framework evaluates only three aspects, namely the reality portrayed, immersion, and usability of such environments.

To summarize, existing evaluation frameworks are limited. They are either designed to evaluate a specific type of virtual environment or they focus on a restricted aspect of such environments. This research addresses the gap in tools for evaluating desktop VR training systems for the mining industry. This is done through a framework that investigates the design and development of such systems meticulously and comprehensively from the perspectives of instructional design, usability, and VR systems design, situated in the context of mining. These varying perspectives are integrated into a single framework, providing a multi-faceted evaluation approach.

## Research methodology

The underlying research paradigm of this study is design research, which is currently a maturing research methodology within a number of disciplines. Two streams exist within design research:

- *Design science research* (DSR) in the discipline of information systems
- *Design-based research* (DBR) in the domain of educational technology.

DBR was selected for this study because of its cyclic nature of

design, evaluation, and redesign, and its mandatory production of both theory and actual solutions in real-life contexts, in this case, the context of VR training systems for the mining industry.

The iterative research process is depicted in the DBR model shown in Figure 1. Each cycle comprises various steps (Van Wyk and De Villiers, 2016):

- Analyse the problem in context: An authentic problem is identified in a complex environment. Literature is reviewed to examine the problem and identify appropriate theory. Researchers and practitioners collaborate in analysing the problem and establishing research goals.
- Design the solution: Influenced by contextual limitations and the complexity of real-world interactions and settings, an initial design is proposed to address the problem.
- Develop the solution: A prototype is developed that serves the research purpose. Development is informed by existing design principles and technological innovations.
- Evaluate in practice: The artefact is tested in an authentic setting. Data is collected and analysed to answer the research questions and to construct principles or theory.
- Reflection, leading to dual outcomes:
  - Practical real-world contribution – As reflection occurs upon the data, the solution is enhanced. New designs can be developed, implemented, and improved, leading to an ongoing subcycle of design-reflection-design.
  - Theoretical contribution – Design principles should be continuously and cumulatively documented in order to be transferable and utilized by others in similar settings.

Figure 1 shows the process flow from problem to solution, where each blue oval represents an occurrence of the DBR cycle. The red blocks indicate actions, and the green blocks indicate the artefacts or theory deliverables that are the outcomes of the DBR process.

## Development and results

The first steps in the design research process were the development and trial-in-practice of two VR safety training systems. They required theoretical evaluation and refinement. This confirmed the lack of a suitable tool for evaluating VR for safety training systems, therefore a framework to address this gap was synthesised from the literature. The two VR training systems were then evaluated using the evaluation framework. This process served the purpose of identifying their inadequacies and also tested the evaluation framework itself in a design research process. After this practical application, the evaluation framework was formally and finally evaluated in a meta-evaluation. The next subsections describe the iterative evaluate-and-improve DBR process.

### *DBR cycle 1*

The research process commenced by defining the real-world problem. More than 100 workers die annually in the South African mining industry and thousands are injured (Webber-Youngman and Van Wyk, 2013). An aim of this study was to propose, model, prototype, and evaluate two novel electronic training interventions to improve the safety of mineworkers. These e-learning (also termed e-training) systems were implemented at a South African mine, using VR technology to simulate underground conditions and potential hazards, and to supplement conventional classroom training.

First, a desktop VR training prototype, *Look, Stop and Fix (LSF)*, was designed and developed based on the problem analysis and literature reviews. This prototype simulated the underground working areas, incorporating potential hazards. Mineworkers had to spot the hazards, identify them correctly, and indicate appropriate actions to be followed in response to each hazard. Incorrect identification of a hazard or failure to indicate

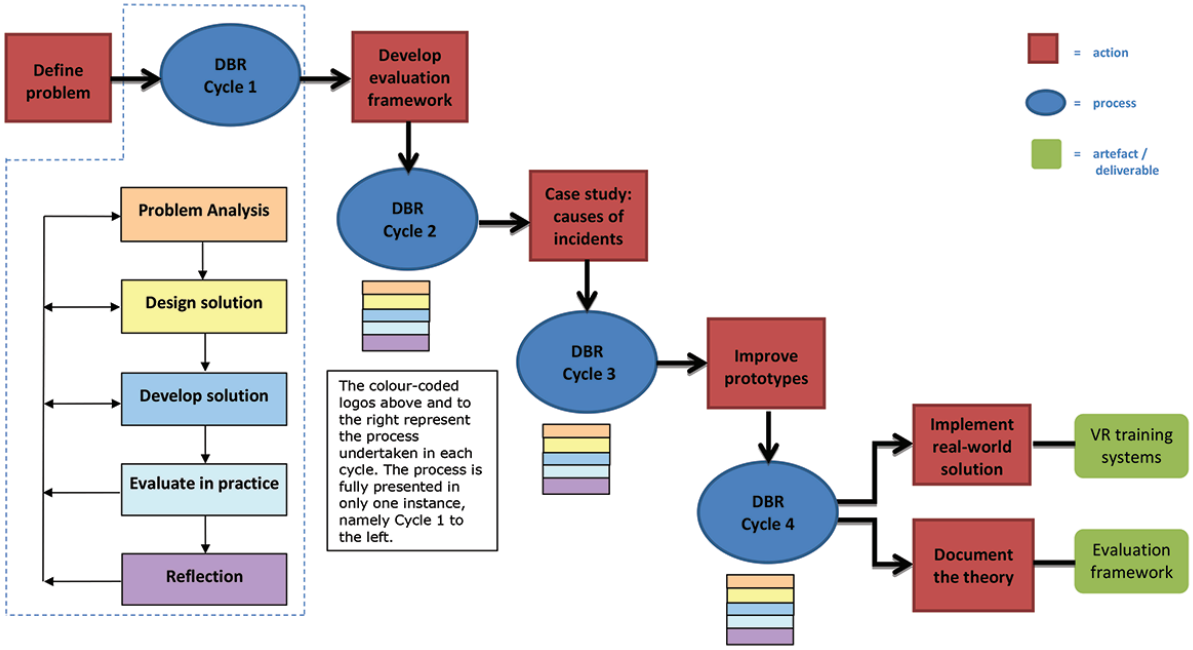


Figure 1—Research process flow diagram

the correct action to deal with it prompted an animation. This showed the possible consequences of ignoring it or responding incorrectly. The LSF prototype was evaluated in practice by user surveys at a large platinum mine, which resulted in several design problems that needed attention being identified.

### *Evaluation framework and DBR cycle 2*

Following cycle 1, a formal evaluation framework called the *Desktop Virtual Reality Evaluation Framework (DEVREF)* and a set of criteria were developed for evaluating desktop VR training applications. This was done by means of heuristic evaluation by experts. During cycle 2, the design of *LSF* was refined and further evaluated using *DEVREF.* This cycle included several internal DBR subcycles to determine inadequacies and problems in *LSF* and led to an improved version of *LSF*.

### *Case study and DBR cycle 3*

Upon reflection, the mine indicated that the *LSF* prototype, which focuses on generic hazards, should be expanded to focus on major causes of incidents. A case study was done to identify such causes. This culminated in DBR cycle 3 in the design and development of a new geological conditions prototype called *Interactive Simulated Geological Conditions (ISGC)*. In the *ISGC* prototype, trainees had to identify 21 different geological conditions occurring in that particular mine. They also had to specify the associated risks and controls for each condition. *ISGC* animations show possible consequences of ignoring or incorrectly addressing the geological conditions. *DEVREF* was then used to evaluate *ISGC* and problematic issues were identified and addressed:

- ➤ Some trainees struggled with orientation in the virtual environment and it was decided to add orientation labels.
- ➤ Additional visual learning material was required to better explain some of the geological conditions.
- ➤ Scenes containing combinations of more than one geological hazard, as is practically experienced underground, were added to the system.

### *Improvement of evaluation framework and DBR cycle 4*

In the process of evaluating the *LSF* and *ISGC* prototypes, inadequacies emerged in the *DEVREF* evaluation framework itself. To fix these, modifications were made to some criteria and additional evaluation statements were added to the framework to address important aspects not fully covered. After improving the prototypes, a further DBR cycle (cycle 4) was applied to improve *DEVREF* itself, so as to strengthen future evaluations. To evaluate the appropriateness and effectiveness of the evaluation framework, a meta-evaluation was undertaken. This process is discussed in the section *Evaluating the evaluation framework.* The findings of this process were used to enhance *DEVREF* and its functionality.

### *Outcomes of the DBR process*

Figure 1 indicates the outcomes resulting from the processes. In line with design-based research, there are dual outcomes involving a *practical* real-world solution in the form of novel desktop VR training systems and a *theoretical* contribution which is the evaluation framework, *DEVREF*, for evaluating desktop VR training systems.

### *DEVREF - a synthesised framework for heuristic evaluation of VR training applications*

As stated above, the DBR process had dual outcomes: the production of real-world innovative products and the development of theory. The practical outcome – the desktop VR training systems, *LSF* for hazards recognition and *ISGC* for geological conditions, evolved from prototypes to products, becoming real-world training systems currently in use at various mines (Van Wyk and De Villiers, 2014). The focus of this article, however, is the theoretical contribution made by the new evaluation framework, *DEVREF*.

Various factors determine the theoretical foundations for investigating e-learning applications. No single paradigm is appropriate for all situations, since domain, context, and content must all be considered (De Villiers, 2005). To find an appropriate approach, technological issues, educational theories, and usability should be taken into account. Costabile *et al.* (2005) advise that evaluation of educational systems should investigate pedagogical effectiveness and usability aspects. When integrating usability into learning, usability features that support the achievement of educational goals should be addressed (Rogers, Sharp, and Preece, 2011).

Ardito *et al.*, (2006), advocate that specific custom-designed guidelines should be provided for the evaluation of e-learning, rather than using sets of general criteria. In response, this study synthesises a new set of guidelines and a single, integrated evaluation framework, specifically customized to evaluate interactive desktop VR training systems for safety in the mining industry. Therefore, the design and development of such systems are investigated meticulously and comprehensively from four different perspectives, integrated into a single framework, namely *DEVREF*, as presented in Table I. *DEVREF* provides a multi-faceted approach, with four categories of heuristics (performance criteria) extracted from an extensive in-depth study of the literature:

- Category 1: Instructional design – heuristics related to pedagogical effectiveness, learning theories, and multimedia learning design.
- Category 2: General usability – interface design, navigation and interaction, and heuristics that support the goals of usability.
- Category 3: Virtual reality system design – heuristics specific to the design of VR systems.
- Category 4: Mining-specific heuristics – heuristics relating to the context and content of the application domain.

## Evaluating the evaluation framework

The findings of the prototype evaluations indicated some inadequacies in *DEVREF* and a meta-evaluation was done to strengthen it. No standard meta-evaluation checklist was appropriate for evaluating *DEVREF,* due to its innovative and extensive nature. A custom-built instrument was therefore developed to evaluate both (i) the criteria that comprise the *DEVREF* evaluation framework and (ii) the methodology employed in the evaluation. The meta-evaluation was a systematic review conducted by six experts in various aspects, four of them being double experts who had expertise in more than one of the *DEVREF* categories. Each category was evaluated separately.

The meta-evaluation instrument was designed in the context of evaluating desktop VR training systems. The challenge was determining appropriate criteria for evaluating the merit of evaluation frameworks themselves. First, criteria were selected from the literature by acknowledged experts within *DEVREF's*

four categories. The selected criteria were consolidated into a set of evaluation statements, which resulted in the first part of the meta-evaluation questionnaire used to evaluate the DEVREF evaluation criteria. The second part was used to evaluate the evaluation method employed, in this case heuristic evaluation. This questionnaire was used as the instrument in the meta-evaluation, and the participating expert evaluators were the same evaluators who had conducted the heuristic evaluations of the prototype VR training programs.

The meta-evaluation was done six months after the heuristic evaluation of the second prototype, ISGC. Each expert evaluator was approached individually, the purpose and procedure of the process was explained, and a copy of the *DEVREF* framework was provided for reference during their meta-evaluation.

The findings of the meta-evaluation clearly indicated that evaluating the evaluation framework itself was a meaningful exercise and that it achieved its aim of determining whether the evaluation statements in *DEVREF* cover all the pertinent considerations. Using the feedback received from the experts, *DEVREF* was further enhanced by incorporating six new evaluation statements and rephrasing two others. The framework in Table I is the final improved version of *DEVREF.*

*Table I*

**Improved heuristic evaluation framework for desktop VR training applications**

| | Heuristic | References |
|---|---|---|
| | **Category 1: Instructional design** | |
| 1 | **Clear goals, objectives, or outcomes:** | |
| | The training program makes it clear to the learner what is to be accomplished and what will be gained from its use. | McLoughlin, in Edmundson (2003); |
| | There are clear goals, objectives, or outcomes for the training. | Ardito *et al.* (2004). |
| | Clear goals, objectives, or outcomes are communicated at the beginning of the training program. | |
| | The outcomes are measurable. | |
| 2 | **Instructional assessment:** | |
| | The program provides assessment opportunities that are aligned with the objectives or outcomes. | Patel *et al.* (2006). |
| | The assessment opportunities will serve to enhance trainees' performance and knowledge. | |
| 3 | **Feedback to user responses:** | |
| | The training program provides trainees with constructive and supportive feedback on their performance | Alessi and Trollip (2001); |
| | The feedback is relevant to the training content. | Vrasidas (2004); |
| | The feedback informs the trainee regarding his level of achievement in the training program. | Munoz and Chalegre (2012). |
| | The feedback indicates incorrect responses and provides information on the correct responses. | |
| 4 | **Motivation and creativity:** | |
| | The system supports intrinsic motivation by providing challenges to trainees | Vrasidas (2004); |
| | The system provides encouragement when errors are made | Ssemugabi and de Villiers (2007); |
| | The program captures the trainee's attention early and retains it throughout. | Magner *et al.* (2013); |
| | This training program increases trainees' confidence by providing them with reasonable opportunities to accomplish the objectives successfully. | Mayer (2014). |
| | The program engages trainees by its relevant content. | |
| | The program engages trainees by its interactivity. | |
| | The program has a captivating storyline. | |
| 5 | **Differences between individual users:** | |
| | The system takes account of linguistic and cultural differences by allowing trainees to select between different languages. | Rogers, Sharp, and Preece (2011); |
| | In terms of content, the system caters for both novice and knowledgeable trainees. | Lau *et al.* (2014). |
| | The system caters for trainees with different levels of computer experience. | |
| 6 | **Reduction of extraneous processing in working memory:** | |
| | The training program effectively uses signalling to highlight essential issues (*e.g.* restating important points, using headings for important points, or stressing them in audio mode). | Sweller, Ayres, and Kaluga (2011); Morrison, Dorn, and Guzdial (2014); |
| | Redundancy is avoided *i.e.* unnecessary information is not presented. | Mason, Cooper, and Wilks (2015). |
| | Redundancy and overload are avoided by not reiterating the same material in multiple modes (*e.g.* the program presents information using pictures and spoken words, rather than in pictures, spoken words, and printed words). | |
| 7 | **Fostering of germane cognitive load (germane cognitive load is the load devoted to the processing, construction, and automation of schemas):** | |
| | The training program supports the formation of mental schema by explaining where new knowledge fits into the bigger picture. | Ardito et al. (2004); |
| | The system encourages encoding of the training content in long-term memory by presenting questions after each learning segment. | Sweller, Ayres, and Kaluga (2011); |
| | Scaffolding support is provided (in the form of hints, prompts, and feedback) to help trainees achieve training goals. | Teräs and Herrington (2014). |
| | The program presents narration in a colloquial conversational style. | |
| | The training program prompts trainees to link concrete example information for each problem category to more abstract information. | |
| 8 | **Appropriate intrinsic cognitive load:** | |
| | Working through the training program does not cause trainees to split their attention between multiple sources of visual information. | Sweller, Ayres, and Kaluga (2011); |
| | The program enhances retention by presenting information in learner-paced segments, rather than as a continuous presentation. | Munoz and Chalegre (2012); |
| | The system effectively supports dual channel processing of simultaneous visual and verbal material. | Lau *et al.* (2014). |

*Table I*

**Improved heuristic evaluation framework for desktop VR training applications**

| | Heuristic | References |
|---|---|---|
| | **Category 2: General Usability** | |
| 1 | **Functionality:**<br>The interface provides the level of functionality the user requires to complete a task.<br>The interface provides adequate back-button functionality to return to a previous screen.<br>Icons, labels, and symbols are intuitive and meaningful to trainees, bearing in mind the level of trainee context and experience.<br>Objects are designed with attributes that support affordance. | Adebesin, Kotze, and Gelderblom (2010);<br>Hvannberg, Halldórsdóttir, and Rudinsky (2012). |
| 2 | **User guidance:**<br>The interface provides clear indications of what the next required action will be.<br>Help for operating the program is accessible at any time.<br>Trainees receive clear instructions on how to use the training program.<br>Guidance to solve problems is given in the form of examples, diagrams, videos, or photographs.<br>Help for operating the program is appropriate. | Adebesin *et al.* (2010);<br>Guimarães and Martins (2014);<br>Lau *et al.* (2014). |
| 3 | **Consistency:**<br>There is consistency in the sequence of actions taken in similar situations.<br>There is consistency in the use of images, prompts, screens, menus, colours, fonts, and layouts.<br>Objects, options, and permissible actions are visible so that users do not have to remember instructions.<br>Different screens that have similar operations use similar elements for achieving similar tasks. | Adebesin *et al.* (2010); Olsen (2010);<br>Hvannberg *et al.* (2012);<br>Munoz and Chalegre (2012);<br>Guimarães and Martins (2014). |
| 4 | **Error correction:**<br>Error messages are expressed in plain language.<br>Learners are provided with the necessary help to recover from cognitive errors.<br>Error messages indicate precisely what the problem is and give simple, constructive, specific instructions for recovery. | Adebesin *et al.* (2010);<br>Guimarães and Martins (2014). |
| 5 | **System status:**<br>The training program keeps the trainee informed about what is going on through constructive, appropriate, and timely feedback.<br>For every action taken by the trainee, there is a visual or audio response by the training program so that learners can see and understand the results of their actions.<br>The program responds to actions initiated by the user and there are no surprise actions from the system's side. | Rogers, Sharp, and Preece (2011);<br>Rusu (2011);<br>Guimarães and Martins (2014). |
| 6 | **Error prevention:**<br>The training program is designed in such a way that the learner cannot easily make serious errors.<br>When the learner makes an error, the system responds with an error message.<br>Trainees can recognize situations where errors occur due to the way they provided input, and not due to incorrect content in their response.<br>The system is robust and reliable throughout. | Rusu *et al.* (2011);<br>Munoz and Chalegre (2012). |
| 7 | **Aesthetics:**<br>The screens are pleasing to look at.<br>The buttons and selections are of a size that is adequately viewable.<br>The text is of a size that is adequately viewable.<br>There is not too much content or information on the screens. | Magner *et al.* (2013);<br>Guimarães and Martins (2014). |
| 8 | **Interactivity:**<br>The training program uses clear and simple terminology that supports trainees in understanding how to interact with the system.<br>The program provides interactions that support trainees in learning the necessary content.<br>Working through the program requires regular trainee interactivity to maintain attention and facilitate comprehension. | Schofield (2014);<br>Lau *et al.* (2014);<br>Mason, Cooper, and Wilks (2015). |
| | **Category 3: Virtual reality system design** | |
| 1 | **User control:**<br>The user is able to interact with, or control, the virtual environment in a natural manner.<br>Responses from the environment to the participant's control actions and movements are perceived as immediate or close-to-immediate.<br>The system permits easy reversal of actions.<br>Trainees are able to exit the system at any time they need to do so. | Rebelo and Noriega (2012);<br>Guimarães and Martins (2014);<br>Lau *et al.* (2014). |
| 2 | **Multimodal system output/feedback:**<br>The effect of the trainee's actions on objects in the virtual environment is immediately visible and conforms to the laws of physics and the trainee's perceptual expectations.<br>The visual representation of the virtual world maps to the trainee's normal perception of that environment.<br>Distortions are not noticeable in visual images<br>Audio is integrated seamlessly into user task activity.<br>Audio information is meaningful and timely.<br>The system provides appropriate haptic output. | Lau *et al.* (2014);<br>Schofield (2014). |

*Table I*

**Improved heuristic evaluation framework for desktop VR training applications**

| | Heuristic | References |
|---|---|---|
| | **Category 3: Virtual reality system design** | |
| 3 | **Presence:** | |
| | Users feel as if they are part of the virtual environment and not isolated from it. | Rebelo and Noriega (2012); |
| | The virtual environment experience is consistent with similar real-world experiences. | Su *et al.* (2013). |
| 4 | **Orientation:** | |
| | Users find it easy to maintain knowledge (or 'awareness') of their location while moving through the virtual environment. | Munoz and Chalegre (2012); |
| | The virtual environment includes appropriate spatial labels and landmarks to assist user orientation. | Rebelo and Noriega (2012). |
| | It is clear to the user how to exit the virtual environment | |
| 5 | **Navigation:** | |
| | Users easily move and reposition themselves in virtual environment. | Alessi and Trollip (2001); |
| | Ways of navigation are consistent throughout the system. | Munoz and Chalegre (2012); |
| | Logical barriers are used in areas where physical barriers are absent, but to which users should not be granted access. | Su *et al.* (2013). |
| | Users can relocate using a terrain map. | |
| 6 | **Object interaction – selection and manipulation:** | |
| | Input devices are easy to use and easy to control. | Munoz and Chalegre (2012); |
| | Object interactions are designed realistically to reproduce real-world interaction. | Rebelo and Noriega (2012). |
| | The system provides the ability to rotate 3D objects and increase levels of detail when necessary for task performance. | |
| 7 | **Fidelity:** | |
| | The simulations in the system are accurate | Collins (2012); |
| | The objects in the virtual environment move in a natural manner. | Schofield (2014). |
| | The virtual environment displays adequate levels of realism. | |
| | High-fidelity graphics are used where required. | |
| 8 | **Various user modes:** | |
| | The system provides various user-guidance modes, *e.g.* Free mode, Presentation mode, Guided mode, and Discovery mode. | Arendarski, Termath, and Mecking |
| | The system provides shortcuts to frequent users. | (2008); Bennett *et al.* (2010). |
| | **Category 4: Mining-specific criteria** | |
| 1 | **Authentic tasks:** | |
| | The training system supports particular work practices in the context of their natural environment. | Vrasidas (2004); |
| | The system is customized according to learner-specific needs and the relevance of the curriculum. | Ssemugabi and de Villiers (2007); |
| | The program includes tasks applicable to the actual job context of the trainee. | Teräs and Herrington (2014). |
| 2 | **Appropriate reference materials:** | |
| | The system includes additional reference materials, providing information to trainees on standard operating procedures used in the application domain. | Alessi and Trollip (2001); |
| | The reference materials included in the system are relevant to the problem scenarios. | Mason, Cooper, and Wilks (2015). |
| | The reference materials are at a level appropriate to the trainees. | |
| 3 | **Comprehensive scope of the system:** | |
| | The learning material in the program covers all the vital aspects relating to the topics being addressed. | Experience of the researcher |
| | The training also covers possible consequences of trainees not applying the learning material correctly in their workplace. | |
| 4 | **Adaptive design:** | |
| | The design of the training system is adaptive to changes in site practices. | Experience of the researcher; |
| | The system refers to the latest current standard operating procedures. | Rusu *et al.* (2011); |
| | The system randomizes assessment details such as questions and multiple-choice answers when presenting assessment opportunities. | Su *et al.* (2013). |
| 5 | **Relevant subject matter:** | |
| | The subject matter matches the goals and objectives of the training. | Alessi and Trollip (2001); |
| | The subject matter is presented in an appropriate content structure. | Rogers, Sharp, and Preece (2011). |
| | The information provided in the program is accurate. | |
| | The system 'speaks the trainee's language' by using terms, phrases, symbols, and concepts familiar to the trainee and common to the application domain. | |
| | The level of language use, in terms of grammar and style, is applicable to the target audience. | |
| 6 | **Trainee preparedness:** | |
| | Trainees are shown how to use the software prior to doing the training programme. | Hollender *et al.* (2010). |
| | PC literacy pre-training is available to trainees not comfortable with using computers for training. | |

*Table I*

**Improved heuristic evaluation framework for desktop VR training applications**

| | Heuristic | References |
|---|---|---|
| | **Category 4: Mining-specific criteria** | |
| 7 | **Appropriate record-keeping:**<br>The system maintains student records and assessment results.<br>The system monitors and displays student progress.<br>The system ensures legal compliance in the application domain by capturing detailed individual performance data. | Vrasidas (2004). |
| 8 | **Understandable and meaningful symbolic representation:**<br>Symbols, icons, and terminology used to represent concepts and objects are used consistently throughout the program.<br>Symbols, icons and terminology used are intuitive within the context of the task.<br>Metaphors used correspond to real-world objects or concepts. | Oviatt (2006);<br>Rogers, Sharp. and Preece. (2011). |

## Discussion and recommendations

DEVREF, developed and evaluated in this research, applies specifically to desktop VR. The reasons for using desktop technology instead of immersive technology are as follows.

- Desktop VR systems run smoothly on standard desktop PCs, using input devices such as a keyboard and mouse. At most, an additional graphics card with onboard memory may be required for effective delivery.
- The lower capital cost of hardware, software, and peripherals makes desktop VR systems an attractive and realistic alternative.
- The general low literacy level of employees in the mining industry exacerbates the problem of safety training. By starting with desktop VR, such training can be introduced gradually.
- The application of immersive systems is usually highly individualized since each trainee requires separate equipment to interact with the system. The high cost of such equipment makes it infeasible to train high numbers of trainees simultaneously. This study aims at augmenting safety training of the underground mining workforce, hence the focus is on proposing solutions that can cater for large numbers. A non-immersive training solution is therefore more viable and attractive at this stage.

The training material in the *LSF* and *ISGC* prototypes covered generic and geological hazards. The same design principles can be applied to evaluate other learning content, for example, generic induction, site-specific induction, equipment operation, drilling and blasting, loading and hauling, and various mining methods. As immersive training becomes more feasible over time, DEVREF can be extended to cover semi-immersive or immersive VR training systems. This can be done by adapting criteria or adding additional criteria.

## Conclusion

VR offers innovative and versatile possibilities in training and holds potential to increase productivity and improve safety awareness, hence the number of VR applications in the industry is increasing. Due to the novelty of the technology for the local mining industry and the availability and growing acceptance of desktop computer training, the evaluation framework, DEVREF, was developed specifically for desktop VR training systems. Furthermore, DEVREF was meta-evaluated in the DBR process to improve it and strengthen its validity. Because of the feasibility and acceptance of this non-immersive technology, desktop VR training systems are already in use at several mine training sites throughout South Africa and it is envisaged that they will be used at many more sites in the foreseeable future. This ensures the viability and future use of the framework in evaluation.

Although DEVREF is presented as an evaluation framework, its criteria also relate closely to design aspects. Consequently the framework can serve two valuable theoretical purposes.

- In its primary purpose, it can be applied as an evaluation tool comprising criteria/heuristics to assess the effectiveness of existing interactive desktop VR training systems with regard to their usability, instructional design, VR systems design, and mining context-specific aspects.
- Since design principles are implicitly incorporated in the framework, DEVREF can also be used as a set of design principles to inform the design of new VR training systems.

To date, interactive training systems resulting from prototype systems described in this article have been implemented at fifteen training centres at various mines and smelting plants throughout South Africa. These training sites are committed to further development of VR training systems, and DEVREF can play a significant role in the effective design and evaluation thereof.

## References


Adebesin, F., Kotze, P., and Gelderblom, H. 2010. The complementary role of two evaluation methods in the usability and accessibility evaluation of a non-standard system. *Proceedings of the Annual Research Conference of the South African Institute of Computer Scientists and Information Technologists (SAICSIT 2010)*.

Alessi, S.M. and Trollip, S.R. 2001. Multimedia for Learning: Methods and Development. 3rd edn. Allyn and Bacon, Boston, MA.

Ardito, C., Costabile, M.F., De Marsico, M., Lanzilotti, R., Levialdi, S., Plantamura, P., Roselli, T., Rossano, V., and Tersigni, M. 2004. Towards guidelines for usability of e-learning applications. *User-centered Interaction Paradigms for Universal Access in the Information Society - 8th ERCIM Workshop on User Interfaces for All 2004*. Springer-Verlag, Berlin. pp. 185–202.

Ardito, C., Costabile, M.F., De Marsico, M., Lanzilotti, R., Levialdi, S., Roselli, T., and Rossano, V. 2006. An approach to usability evaluation of e-learning applications. *Information Society*, vol. 4, no. 3. pp. 270–283.

Arendarski, B., Termath, W., and Mecking, P. 2008. Maintenance of complex machines in electric power systems using virtual reality techniques. *Proceedings of the 2008 IEEE International Symposium on Electrical Insulation (ISEI) 2008*. Vancouver. IEEE, New York. https://ieeexplore.ieee.org/iel5/4544566/4570258/04570378.pdf

Bennett, L., Stothard, P., and Kehoe, J. 2010. Evaluating the effectiveness of virtual reality learning in a mining context. *SimTecT 2010 Conference Proceedings*. Leigh, D.E. (ed.). Simulation Industry Association of Australia, Brisbane.

Bowman, D.A., Gabbard, J.L. and Hix, D. 2002. A survey of usability evaluation in virtual environments: Classification and comparison of methods. *Presence: Teleoperators and Virtual Environments*, vol. 11, no. 4. pp. 404–424.

Bowman. D.A., Koller, D., and Hodges, L.F. 1998. A methodology for the evaluation of travel techniques for immersive virtual environments. *Virtual Reality*, vol. 3, no. 2. pp. 120–131.

Chadwick, J. 2009. Simulators and virtual training. *International Mining*, September 2009. http://www.infomine.com/publications/docs/InternationalMining/Chadwick2009s.pdf [accessed 22 April 2010].

Collins, C. 2012. Should virtual environments be realistic? *Hypergrid Business Magazine*, May 2012 http://www.hypergridbusiness.com/2012/05/should-virtualenvironments-be-realistic/ [accessed 16 January 2015].

Costabile, M.F., De Marsico, M., Lanzilotti, R., Plantamura, V.L., and Roselli, T. 2005. On the usability evaluation of e-learning applications. *Proceedings of the 38th Hawaii International Conference on System Science*, 2005, IEEE Computer Society, Washington. pp. 1–10.

Daden, 2016. Virtual reality without the hype. https://www.daden.co.uk/downloads/Virtual%20Reality%20-%20Without%20the%20Hype%20v1.pdf [accessed 10 October 2017].

De Villiers, M.R. 2005. e-Learning artefacts: Are they based on learning theory? *Alternation*, vol. 12, no. 1b. pp. 345-371.

Edmundson, A. 2003. Decreasing cultural disparity in educational ICTs: Tools and recommendations. *Turkish Online Journal of Distance Education*, vol. 4, no. 3. http://tojde.anadolu.edu.tr/tojde11/articles/edmundson.htm. [accessed 12 July 2009].

Gang, W., Jun, G. and Yingzhen, L. 2006. The construction of evaluation framework for virtual geographic environment. *Proceedings of the 16th International Conference on Artificial Reality and Telexistence, ICT '06* IEEE, New York. pp. 20–25.

Google, 2017. Introducing Daydream standalone VR headsets. https://vr.google.com/daydream/standalonevr/ [accessed 15 October 2017].

Guimarães, M.D.P., and Martins, V.F. 2014. A checklist to evaluate augmented reality applications. Proceedings of the XVI *Symposium on Virtual and Augmented Reality*, 2014. IEEE, New York. pp. 45–52.

Hanna, N. and Richards, D. 2014. Evaluation framework for 3D collaborative virtual environments (the CORE). *Proceedings of the Pacific Asia Conference on Information Systems*. Paper 284. Association for Information Systems. http://elibrary.aisnet.org/Default.aspx?url=https://aisel.aisnet.org/cgi/viewcontent.cgi?article=1104&context=pacis2014

Hollender, N., Hofmann, C., Deneke, M., and Schmitz, B. 2010. Integrating cognitive load theory and concepts of human–computer interaction. *Computers in Human Behavior*, vol. 26. pp. 1278–1288.

Hvannberg, E.T., Halldórsdóttir, G., and Rudinsky, J. 2012. Exploitation of Heuristics for Virtual Environments. *Proceedings of the 7th Nordic Conference on Human-Computer Interaction: Making Sense Through Design*. Association for Computing Machinery, New York. pp. 308–317.

Ji-zu, L., Li-mei, A., Jin-yun, W., and Xiao-li, Y. 2009. Research on simulation of safety behavior in coal mines based on the 3D and VIRTOOLS technologies. ICCSIT 2009: *Proceedings of the 2nd IEEE International Conference on Computer Science and Information Technology*. IEEE, New York. pp. 477–480.

La Valle, S.M. 2017. Virtual Reality. http://vr.cs.uiuc.edu/ [accessed 12 October 2017].

Lau, R.W.H., Yen, N.Y., Li, F., and Wah, B. 2014. Recent development in multimedia e-learning technologies. *World Wide Web Journal*, vol. 17, no. 2. pp. 189–198.

Lucas, J., Thabet, W., and Worlikar, P. 2007. Using virtual reality (VR) to improve conveyor belt safety in surface mining. ITC Digital Library. http://itc.scix.net/cgi-bin/works/Show?w78_2007_42 [accessed: 10 June 2009].

Magner, U.I.E., Schwonke, R., Aleven, V., Popescu, O., and Renkl, A. 2013. Triggering situational interest by decorative illustrations both fosters and hinders learning in computer-based learning environments. *Learning and Instruction*, vol. 29. pp. 141–152.

Mason, R., Cooper, G., and Wilks, B. 2015. Using cognitive load theory to select an environment for teaching mobile apps development. *Proceedings of the Seventeenth Australasian Computing Education Conference ACE2015*, Sydney, Australia, January 2015. Australian Computer Society. https://epubs.scu.edu.au/cgi/viewcontent.cgi?article=1664&context=bus_tourism_pubs

Mayer, R.E. 2014. Incorporating motivation into multimedia learning. Learning and Instruction, vol. 29. pp. 171–173.

Morrison, B.B., Dorn, B., and Guzdial, M. 2014. Measuring cognitive load in introductory CS: Adaptation of an instrument. *Proceedings of the Tenth International Conference on Computing Education Research (ICER2014)*, Glasgow, Scotland. Association for Computing Machinery, New York. pp. 131–138

Munoz, R. and Chalegre, V. 2012. Defining virtual worlds usability heuristics. *Proceedings of the Ninth International Conference on Information Technology: New Generations (ITNG)*, Las Vegas, 2012. IEEE, New York. pp. 690–695.

Olsen, D.R. 2010. Building interactive systems: Principles for human-computer interaction. Course Technology, Cengage Learning. Boston, MA.

Orr, T.J., Mallet, L.G., and Margolis, K.A. 2009. Enhanced fire escape training for mine workers using virtual reality simulation. *Mining Engineering*, vol. 61, no. 11. pp. 41–44.

Oryx, 2014. Oryx launches Volvo simulators. http://www.miningmagazine.com/technology/simulation/ [accessed: 10 January 2015].

Oviatt, S. 2006. Human-centered design meets cognitive load theory: Designing interfaces that help people think. *Proceedings of the 14th Annual ACM International Conference on Multimedia*. pp. 871–880. Association for Computing Machinery, New York.

Patel, H., Stefani, O., Sharples, S., Hoffmann, H., Karaseitanidi, I., and Amditis, A. 2006. Human centred design of 3-D interaction devices to control virtual environments. *International Journal of Human-Computer Studies*, vo. 64, no. 3. pp. 207–220.

Rogers, Y., Sharp, H., and Preece, J. 2011. Interaction Design – Beyond Human-Computer Interaction. 3rd edn. Wiley, Chichester, UK.

Rusu, C., Muñoz, R., Roncagliolo, S., Rudloff, S., Rusu, V., and Figueroa, A. 2011. Usability Heuristics for Virtual Worlds. Proceedings of AFIN 2011: the *Third International Conference on Advances in Future Internet*, -Nice, France. 21-27 August 2011. Curran Associates, Red Hook, NY. pp. 16–19.

Schafrik, S.J., Karmis, M., and Agioutantis, Z. 2003. Methodology of incident recreation using virtual reality. *Proceedings of the SME Annual Meeting, Cincinnati, Ohio*, February 2003. Society for Mining, Metallurgy & Exploration, Littleton, CO.

Schofield, D. 2014. A virtual education: Guidelines for using games technology. *Journal of Information Technology Education: Innovations in Practice*, vol. 13. pp. 25–43.

Ssemugabi, S. and de Villiers, M.R. 2007. Usability and learning: A framework for evaluation of web-based e-learning applications. *Proceedings of Ed-Media 2007: World Conference on Educational Multimedia, Hypermedia & Telecommunications*, Vancouver, Canada, 25 June 2007. Association for the Advancement of Computing in Education. Waynesville, NC. http://hdl.handle.net/10500/13207

Stoddard, E. and Skweyiya, S. 2016. SA mine deaths rise after years of improving safety/ https://www.iol.co.za/business-report/economy/sa-mine-deaths-rise-after-years-of-improving-safety-2063416 accessed 26 November 2017].

Stone, R.J. and Knight, J.F. 2012. 3D Displays: A Human-Centred Review. BAE Systems, Yeovil, Somerset, UK: https://www.birmingham.ac.uk/Documents/college-eps/eece/research/bob-stone/HFI-DTC-publication-3D-displays.pdf

STS3D, 2017. Accident reconstruction. http://sts3d.co.za/_workplace-safety/. [accessed 10 October 2017].

Su, K., Wang, H., Wu, Y. and Kuo, N. 2013. The interface design and usability evaluation of interactive virtual reality navigation system. *Applied Mechanics and Materials*, vol. 302. pp. 635–639.

Sweller, J., Ayres, P., and Kalyuga, S. 2011. Cognitive Load Theory. Springer, New York.

Teräs, H. and Herrington, J. 2014. Neither the frying pan nor the fire: In search of a balanced authentic e-learning design through an educational design research process. *International Review of Research in Open and Distance Learning*, vol. 15, no. 2. http://www.irrodl.org/index.php/irrodl/article/view/1705/2835

Tichon, J. and Burgess-Limerick, R. 2011. A review of virtual reality as a medium for safety related training in mining. *Journal of Health and Safety Research and Practice*, vol. 3, no. 1. http://burgess-limerick.com/download/a54.pdf

Tsiatsos, T., Andreas, K., and Pomportsis, A. 2010. Evaluation framework for collaborative educational virtual environments. *Educational Technology and Society*, vol. 13, no. 2. pp. 65–77.

Van Wyk, E.A. 2015. An evaluation framework for virtual reality safety training systems in the South African mining industry. PhD thesis, University of South Africa.

Van Wyk, E.A. and de Villiers, M.R. 2009. Virtual reality training applications for the mining industry. *Proceedings of the ACM Afrigraph Conference 2009*, Pretoria. Association for Computing Machinery, New York. http://hdl.handle.net/10500/13155

Van Wyk, E.A. and de Villiers, M.R. 2014. Applying design-based research for developing virtual reality training in the South African mining industry. *Proceedings of SAICSIT 2014, Annual Research Conference of the South African Institute of Computer Scientists and Information Technologists*. Pretoria. pp. 70–81.

Van Wyk, E.A. and de Villiers, M.R. 2016. Applying educational design research to virtual reality safety training in mines. *Proceedings of ECRM 2016: the 15th European Conference on Research Methodology for Business and Management Studies*. Kingston University, London, UK, 9-10 June 2016. Academic Conferences and Publishing International Limited.

Van Wyk, E.A. and Prinsloo, M.W. 2015. Applying virtual reality to prevent repeat incidents. *Proceedings of Virtual Reality and Spatial Information Applications in the Mining Industry*, University of Pretoria, July 2015. Southern African Institute of Mining and Metallurgy, Johannesburg.

Vrasidas, C. 2004. Issues of pedagogy and design in e-learning systems. *Proceedings of the 2004 ACM Symposium on Applied Computing*, Cyprus, March 2004. Association for Computing Machinery, New York. http://dl.acm.org/citation.cfm?id=968086

Webber-Youngman, R.C. 2014. Students need to become 'imagineers', academic urges. *Mining Weekly*. http://www.miningweekly.com/article/students-need-to-become-imagineers-academic-urges-2014-09-16 [accessed: 9 January 2015].

Webber-Youngman, R.C.W. and Van Wyk, E.A. 2013. Incident reconstruction simulations-potential impact on the prevention of future mine incidents. *Journal of the Southern African Institute of Mining and Metallurgy*, vol. 113, no. 6. pp. 519–528. ◆


# Field validation of estimated primary fragment size distributions in a block cave mine

**S. Annavarapu**[1]

**Affiliation:**
[1]Master Geotech Services Pvt LTD, Nagpur, India.

**Correspondence to:**
S. Annavarapu

**Email:**
mgsrikant@gmail.com

**Dates:**
Received: 16 July 2016
Revised: 10 June 2018
Accepted: 29 Oct. 2018
Published: May 2019

**How to cite:**
Annavarapu, S.
Field validation of estimated primary fragment size distributions in a block cave mine.
The Southern African Insitute of Mining and Metallurgy

DOI ID:
http://dx.doi.org/10.17159/2411-9717/16/287/2019

ORCiD ID:
S. Annavarapu
https://orchid.org/0000-0001-6054-4104

## Synopsis

**Fragment size distributions play an important part in the design and planning of block cave mining operations. Though several methods have been proposed for estimating fragment size distributions in advance of mining, the calibration of these estimating procedures to field measurements has been a challenge. The Block Size Estimator (BSE) program was developed for providing an assessment of primary fragmentation expected in a block cave mine using drill-core piece length data and joint characteristics from the exploration and geotechnical evaluation programmes. In order to validate the results from the BSE program, the drill-core piece length data and the joint characteristics in different rock types from the DOZ block cave mine in Indonesia were used to help generate fragment size distributions in different areas of the mine. The predicted fragment size distributions were compared with the fragmentation observed at the drawpoints during operation of the mine.**

**This paper presents the details of the validation of the fragment size estimates by the BSE program using fragment size distribution data from the drawpoints at the extraction level at the DOZ block cave mine, and the challenges encountered in developing reasonable correlations between the estimated and measured fragment size distributions.**

**Keywords**
**block caving, fragmentation, size distribution, rock mass characteristics, modelling.**

## Introduction

The assessment of fragmentation is an important aspect of the design and planning of the block cave mining method, and forms an integral part of the design of the excavations at the extraction level and the selection of material handling systems for transporting the ore to the processing stations. Secondary blasting requirements can also be estimated based on the fragment size distributions developed for the block cave (Laubscher, 1994).

Several methods of estimating fragment size distributions in block cave mines have been developed based on joint set parameters estimated from structural data from oriented core drilling campaigns and mapping of available excavations and outcrops. The BCF program (Esterhuizen, 1999) estimates the fragmentation using a combination of empirical, analytical, and rational methods to model the behaviour of materials during the primary and secondary fragmentation processes. The program JKFrag uses advanced tessellation of joint traces to create rock blocks and then generate fragment size distributions (Brown, 2002). Nickson, Coulson and Hussey (2000) presented the details of processing of the geotechnical data from the Mont Porphyre project, including an assessment of block sizes from the data collected on the core logging sheet. The distance between natural fractures was used to create distributions of block lengths, and a distribution of potential block sizes was estimated assuming that the blocks had equal dimensions in all directions. The results agreed closely with the results of the BCF program. Hadjigeorgiou, Grennon, and Nickson (2002) demonstrated the use of oriented borehole data to provide characteristic block size distributions for a mining project using a software package called Stereoblock, which generates a three-dimensional joint network for a given volume and calculates the volumes of blocks created by the intersections of these joints, simulated as circular planes. The distributions of joint orientation and joint spacing generated from statistical analysis of the oriented core data are used for the creation of the Stereoblock model. The diameter of the circular planes representing the joints is determined based on the mean and standard deviation of the joint trace length obtained from scan-line mapping.

Of these approaches, the BCF program has found the greatest acceptance in the block cave sector and has been used extensively for developing fragment size distributions from the scoping study stage (with limited geotechnical data) to the operational stage (with available observations for back-analyses).

However, Butcher and Thin (2007) reported that '... the model ore blocks are generated independently of the jointing statistics.' The fragmentation results from the BCF program are often too coarse because the effects of block formation due to stress-induced joint extension, and stress-induced failure of rock bridges between joints are not considered.

The availability of structural data from different parts of a block cave mine is often limited by the extent of the geotechnical programme in general and the core orientation programme in particular. The cost and time associated with these programmes, especially in the early stages of exploration of the orebody, makes it difficult to assign significant resources to them. However, the larger number of exploration holes from which core piece length data is available makes a case for developing an algorithm for using this data for estimating fragment size distributions within the block cave. With this motivation, the Block Size Estimator (BSE) program was developed for estimating the block size distribution using core piece length to generate *in-situ* and primary fragmentation estimates for block cave operations (Srikant, 2013).

Validating the fragment size estimates produced by the various available programs through calibration against field observations is essential for the development of confidence in the prediction of fragment size distributions. Although drawpoint fragmentation estimation using photographic methods, comparative charts, and size assessment has been undertaken at many mines (Srikant, 2004; Brown, 2007) a major problem in such validation studies is that the programs develop estimates of *in-situ* or primary fragmentation and use empirical approaches or expert systems for estimating the secondary fragmentation at different heights of draw. The validation is therefore for the complete system of *in-situ* block size estimation followed by the simulation of the process of comminution within the draw column (Moss, 2012).

Recent studies at Ridgeway Deeps and Cadia East mines in Australia (Brunton, Lett, and Thornhill, 2017) compared the fragment size distribution predicted using the BCF software with the observed fragment size distribution generated by analysis of photographs of the drawpoints using the SPLIT Desktop system. The authors concluded that BCF predictions matched relatively well to the measured coarser component of the fragmentation distribution (top size and $P_{80}$), but for the finer component of the fragmentation distribution ($P_{50}$ and $P_{20}$), the BCF predictions were significantly coarser than the measured values.

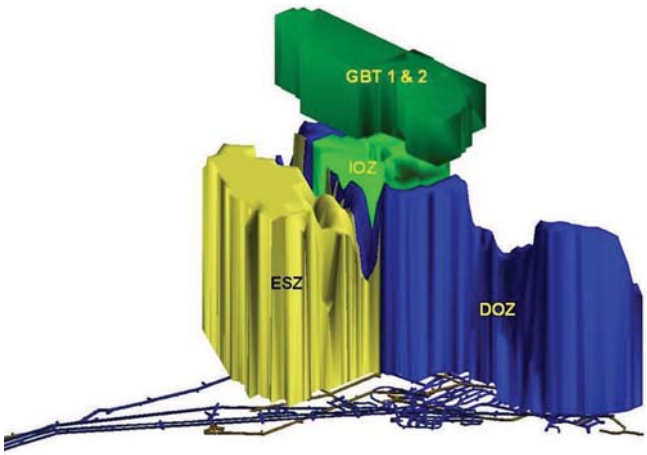


**Figure 1—Mines in the East Ertsberg skarn system (after Widijanto, Arsana, and Srikant, 2006)**

Since the only observations that can be used to calibrate the primary fragmentation estimates are at the drawpoints at the extraction level of the block caves, it is difficult to correlate the primary fragment size distributions estimated by the program with field observations. The fragments observed at the drawpoints can be expected to be finer than the primary fragments since they would have been subjected to comminution forces within the draw column. However, limited breakdown of the rock fragments is expected within the first 50 m of draw from the drawpoints and the fragment size distributions may be closer to the primary fragmentation.

The observations of fragmentation at the drawpoints in a block cave mine in Indonesia during the period from 2004 to 2007 were used to validate the outputs from the BSE program. The mines of the Ertsberg District, in the province of West Papua in Indonesia, are operated by PT Freeport Indonesia (PTFI). The Deep Ore Zone (DOZ) mine is a copper-gold deposit found on the northeast flank of the Ertsberg diorite and lies within the Ertsberg District of Papua Indonesia. The DOZ mine is essentially the third lift of the block cave operations that have exploited the East Ertsberg skarn system (Figure 1), and benefits from experience gained while mining the previous block caves in the same skarn system. The mine is laid out for LHD mining using 6.1 $m^3$ and 8.4 $m^3$ capacity LHDs at the extraction level, from where the broken rock is transferred through grizzlies feeding 55 t low-profile dump trucks which direct-dump into a gyratory crusher with a 1.37-m wide feed opening size (Barber, Thomas, and Casten, 2000).

Four major rock types are mined in the DOZ – Ertsberg diorite, forsterite skarn, magnetite skarn, and DOZ breccia. Fragmentation characteristics for these rock types vary from fine (in the DOZ breccia) to coarse (in the diorite). The fragment size distributions for the DOZ block cave were estimated by the BSE program using the drill-core piece length data from different zones in the DOZ block cave and the joint set characteristics of the different rock types. The estimated fragment size distributions show significant correlation to the observed fragmentation at the drawpoints in similar rock conditions for the first 50 me of draw.

## Estimating fragment size distributions

The BSE program requires the drill-core piece lengths, core piece orientation, and the joint set characteristics (joint set dip, dip direction, and spacing) to generate the fragment size distributions. At the DOZ mine, several campaigns of geotechnical drilling resulted in the development of a large data-set with good core piece length data. Drill-hole survey data was also available for many of the drill-holes, which could be used to generate the orientation of each ore piece. Joint set characteristics were available for different rock types from campaigns of geological and geotechnical mapping of underground excavations in different rock types.

### *Drill-core piece length data*

During several campaigns of drilling at the DOZ mine, geotechnical and geological data was collected and stored in a comprehensive database. The collected data included information that could be used to develop drill-core piece length data. From each drill run, the data collected included the length of the drill

*Table I*

**Joint set characteristics for forsterite and diorite rock types in the DOZ block cave**

| Rock type | Set no. | Mean dip | Std dev. dip | Mean DDR | Std dev. DDR | Mean spacing (m) | Std dev. spacing (m) |
|---|---|---|---|---|---|---|---|
| **Diorite** | 1 | 53 | 20 | 273 | 20 | 0.18 | 0.23 |
| | 2 | 36 | 20 | 144 | 20 | 0.15 | 0.22 |
| | 3 | 37 | 20 | 15 | 20 | 0.28 | 0.34 |
| | 4 | 79 | 20 | 146 | 20 | 0.27 | 0.34 |
| **Forsterite** | 1 | 43 | 20 | 39 | 20 | 0.12 | 0.15 |
| | 2 | 82 | 20 | 156 | 20 | 0.34 | 0.46 |
| | 3 | 51 | 20 | 311 | 20 | 0.34 | 0.46 |

run (*Len_run*), the core diameter (*Dia*), the cumulative length of recovered core (*Len_Rec*), the cumulative length of whole core pieces longer than twice the core diameter (*Len_RQD*), the cumulative length of broken core (*Len_br*), the length of the longest piece of whole (non-broken) core (*Len_lp*), the number of whole core pieces (*Num_pc*), the cumulative length of pieces that are longer than or equal to 0.4 m length (*Len_0.4*), the cumulative length of pieces that are longer than or equal to 0.2 m length (*Len_0.2*), and the cumulative length of pieces that are 1.0 cm in size (*Len_0.01*). Drill-hole geotechnical data for the DOZ mine was sorted into a series of size ranges and the cumulative lengths of logged core pieces with lengths that fall within each bin size were tallied.

For each drill run within the data-set, the downhole survey data was used to calculate the azimuth and plunge of the drill run and this information was assigned to each core piece within the drill run. The enhanced data-set now contained drill-core piece lengths and orientation data for each core piece. The drill-hole data was then sorted by location and rock type so that the predicted fragmentation could be compared with that observed at the drawpoints. The footprint of the DOZ block cave was split into three-panel wide sections, and all the drill-hole intercepts within each section lying within the expected column height for the panels in the section were accumulated and sorted by rock type. The resulting data-set for each rock type and panel within the first 50 m of the block cave was then used for developing the primary fragment size distributions for each of the sections.

### *Joint set characteristics for different rock types*

The joint set characteristics used in the BSE model for the diorite and forsterite skarn rock types were generated from analysis of oriented core drilling and from mapping in the available drifts at the extraction and undercut levels in the DOZ block cave (Table I).

### *The Block Size Estimator program*

The development of the primary fragment size distribution for block cave mining from drill core data requires the estimation of three-dimensional volumetric fragment sizes from one-dimensional drill-core piece lengths. The basic premise of the BSE program is that each core piece represents an *in-situ* block intersected by the drill-hole. The block is created using three almost orthogonal joint sets. Adjacent joints within the same joint set are expected to have similar orientations and rock blocks can, therefore, be expected to be parallelepipeds in shape. The volume of the parallelepiped is estimated based on the length of the drill-core piece and the orientation of the drill-hole with respect to the sides of the parallelepiped.

The conversion of the one-dimensional drill-hole data into a three-dimensional block volume is undertaken based on trigonometry concepts using the core piece length ($l$), drill-hole azimuth ($\theta$) and drill-hole plunge ($\phi$) along with the dip direction (DDR), dip (DIP), and spacing (s) of joint set data. The BSE computer program was developed based on the concepts presented in Srikant and Nicholas (2004), as shown in Figure 2.

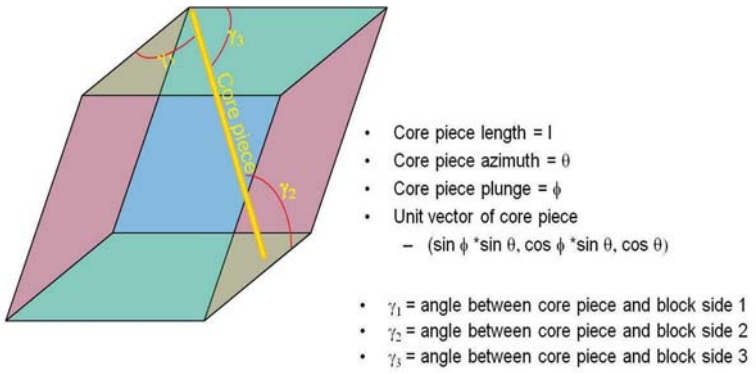


**Figure 2—Core piece and unit rock block**

*Table II*

**Distribution of drill-hole data in DOZ east**

| Panels | | Forsterite | Forsterite magnetite | Magnetite | Diorite |
|---|---|---|---|---|---|
| P15-17 | Drilled metres | 199.80 | 529.15 | 125.00 | 138.25 |
| | Drill records | 71 | 186 | 41 | 50 |
| P18-20 | Drilled metres | 394.40 | 162.00 | 118.25 | 11.30 |
| | Drill records | 136 | 56 | 48 | 6 |
| P21-27 | Drilled metres | 800.20 | 406.70 | 67.60 | 800.20 |
| | Drill records | 282 | 147 | 32 | 65 |

### *Primary fragmentation estimates in the DOZ*

The primary fragment size distributions were estimated for the DOZ mine based on the geotechnical drilling data available from the different sectors of the DOZ. However, most of the drawpoint fragmentation observations during the period of data collection were from the east side of the block cave (panels 13–27), so only the relevant data was analysed. Table II shows the number of drill-core data records available in each zone by rock type. Since some of the zones within the footprint of the DOZ block cave had sparse data within the lower 50 m of the draw column, the data from these zones was not used to estimate fragment size distributions in that zone. In order to avoid poorly distributed data, zones with less than 30 drill-core records were not analysed for fragment size distribution.

The overall primary fragmentation estimates generated by the BSE model for the DOZ mine for the forsterite skarn and the diorite rock types are shown in Figure 3.

### *Problems with estimating fines*

The estimation of fragment sizes from drill-hole data requires the conversion of one-dimensional piece length data to three-dimensional block size information. In the BSE program, each core piece from the drill-hole was assumed to represent a rock fragment and average aspect ratios were used to generate a volume-weighted block size distribution. Wellman *et al.* (2012) studied the impact of this assumption on the distribution of block sizes and concluded that the use of the volume-weighted or length-weighted, or some intermediate weighting factor to represent the distribution of block sizes, is key in representing the distribution of expected block sizes, as shown in Figure 4.

The development of an appropriate model for estimating fragment size distributions within a region using drill-hole data is essentially a sampling problem. One- and two-dimensional data-sets are used to estimate the appropriate three-dimensional size distribution. Although the BSE model can help convert even small core pieces to small block volumes, the percentage of fines generated by the smallest pieces was observed to be very small. The smallest core piece length used in the computation of rock fragment volumes was 0.005 m (5 mm), which can be converted to a block volume of 0.0000125 $m^3$ (125 $mm^3$), which is still significantly larger than the fines observed at the drawpoints. In order to better represent fines in the primary

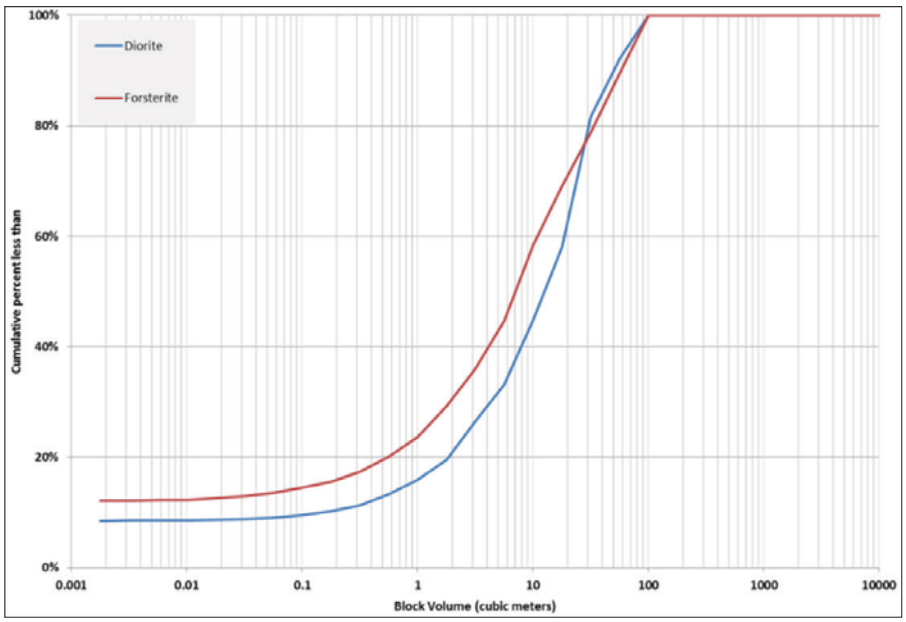


**Figure 3—Primary fragmentation estimates for forsterite and diorite rock types in the DOZ block cave**

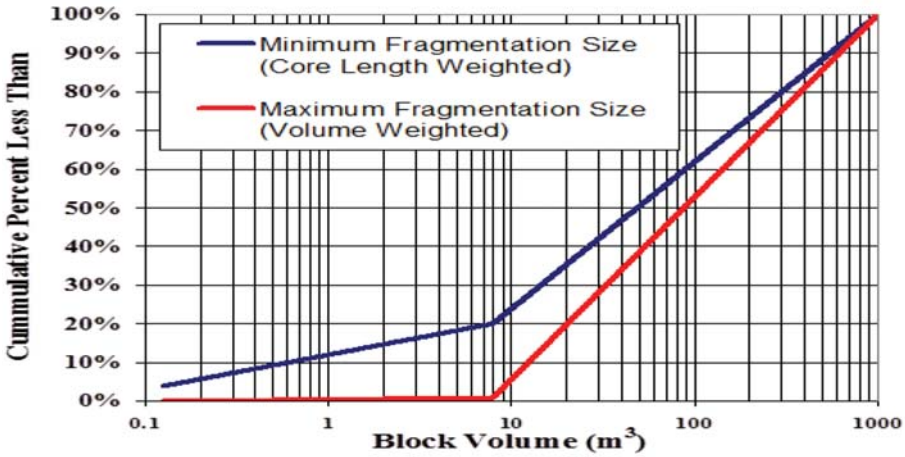


**Figure 4—Effect of sample weighting assumption on fragment size estimation (after Wellman *et al*., 2012)**

fragmentation estimates from the BSE model, the percentage of fines is estimated to be equal to the percentage of the drill-hole that can be correlated to fines (*Len_br* + *Len_run* – *Len_rec*). This formulation was included in the BSE model to help generate fines in the primary fragmentation estimates.

### Drawpoint mapping

Measuring fragmentation at the drawpoints of a block cave mine is a very difficult task and current methods of mapping yield estimates of the actual fragmentation. Field measurements have been conducted at the Tongkuangyu copper mine (Aimin and Yongxue, 2000), but such techniques are not practical in a high-production mines with large equipment and low manpower. Mapping of the fragmentation at the drawpoints at the DOZ block cave was undertaken in several campaigns to help correlate the predicted and observed fragmentation (Srikant, Nicholas, and Rachmad, 2004). Drawpoint fragmentation data from the DOZ mine was also collected by students from the Institut Teknologi, Bandung (ITB) in Indonesia (Lukito, 2005; Sinaga, 2005). Recognizing that observers can more readily assess block side lengths rather than block volumes in a drawpoint, the procedure relied on estimates of block side lengths as illustrated in Table III, which shows a partially completed drawpoint fragmentation log.

The material size distribution is divided into five categories: fines, small block, intermediate block, large block, and oversize. The first three categories represent the material size that could pass through a 1 × 1 m grizzly. The large blocks category represents the material that could be handled by the LHDs without any size reduction. The oversize category represents the material that requires either secondary blasting at the drawpoint or hang-up blasting. The dimensions of the largest block were also recorded to help assess average aspect ratios for the different rock types.

The observer counts the number of intermediate blocks (0.5 m to 1 m side length) and large blocks (1 m to 2 m side length) and multiplies the numbers with proportional area-based percentages, 2% for each intermediate block and 5% for each large block. The percentages of oversize and fines were estimated, while the small blocks category was calculated to make up the rest. The draw height information for each drawpoint, which was important for the analysis, was collected through the Cave Management System (CMS), a monthly-planning interface between the long-term block cave planning software and the daily production planning systems at the DOZ block cave (Samosir, Brannon, and Diering, 2004). Rock type information was collected through routine geological mapping at the drawpoints. Several rock types are normally observed at each drawpoint, and the percentage of occurrence of the different rock types was recorded. For the purposes of this study, the most dominant rock type was assigned to the drawpoint.

In many cases, fines were observed to cover several small and medium boulders at the drawpoint and thus the percentage

*Table III*

**Partially completed drawpoint fragmentation log**

| PT FREEPORT INDONESIA – drawpoint fragmentation log | | | | | | | | | |
|---|---|---|---|---|---|---|---|---|---|
| Logged by: | Srikant Annavarapu | | | | Area | DOZ Panel 19 | | Date: | 10/12/2005 |
| Drawpoint No. | Hang-up (Y N) | Condition Rating (1 – 5) | Fines % <5 cm Estimate % | Small blocks 5–50 cm | Intermediate 50 cm – 1 m Count X2% | Large Blocks 1 m – 2 m Count x 5% | Oversize >2 m Estimate # | Max Block L x W (m) | Notes |
| P19-DP12E | N | 3 | 20 | 20 | 12 x 2 = 24 | 4 x 5 = 20 | 10 | 2.1 x 1.5 | |
| P19-DP12W | N | 1 | 60 | 24 | 8 x 2 = 16 | 0 | 0 | 0.8 x 0.6 | |
| P19-DP138 | N | 4 | 20 | 17 | 4 x 2 = 8 | 7 x 5 = 35 | 20 | 2.4 x 1.8 | |

*Table IV*

**Observed aspect ratios of blocks in the DOZ mine**

| Rock type | Length to width (K1) | Length to height (K2) |
|---|---|---|
| Forsterite | 1.31 | 1.46 |
| Forsterite-magnetite | 1.15 | 1.45 |
| Magnetite | 1.32 | 1.45 |
| Diorite | 1.10 | 1.45 |

of fines recorded during drawpoint fragmentation mapping was found to be high (Srikant, 2006). This is particularly true in the first 10 m of draw, where there is a high possibility of the large primary fragments being covered by the fine material resulting from the undercut and/or drawbell blasts.

The drawpoint mapping method described above was easy to implement in the DOZ mine, but cannot be used as an accurate measure of fragment size distributions at the drawpoints. The measurements are known to be quite subjective, but a large data-set was available for calibration of fragment size distributions estimated using the BSE program. While several attempts were made to measure drawpoint fragmentation using analysis of photographs taken at the drawpoints in the DOZ mine, the procedures required environments relatively free of dust and moisture and were difficult to establish as a routine. The measurements by Lukito and Sinaga are of value since they were conducted by the same persons over several weeks.

Visual estimates of drawpoint fragmentation can potentially be used to calibrate the results of fragmentation analyses. However, correlation of the estimates with observations proved to be a challenge since the fragmentation estimates were reported as volumetric estimates by convention, and the drawpoint mapping procedures developed for the DOZ evaluated the fragmentation observed at the drawpoints as linear measures. Table IV shows the average aspect ratios observed at the drawpoints for the different rock types in the DOZ mine. These observed aspect ratios for the two rock types were used for converting the linear fragment size estimates from drawpoint mapping to volumetric estimates.

## Comparison of observed and predicted primary fragmentation

Primary fragment size distributions were developed from the block volumes generated by the BSE models using drill-hole core piece lengths from the lower 50 m in the draw column at the DOZ mine. The distributions from each zone were compared to the fragment size distributions observed at the drawpoints in the same zone with draw heights up to 50 m. The linear dimensions in the drawpoint fragmentation mapping form were converted to volumes using the values in Table V, which are based on the aspect ratios of the blocks in the forsterite and the diorite. Drawpoints in the DOZ mine are 4.5 m wide and 4.5 m high and the total volume of rock in the drawpoint was estimated to be 65 $m^3$ using an angle of repose of 35 degrees. The dimensions of the largest block observed in the drawpoint were used to estimate the volume of the largest block. The fragment size distribution was adjusted accordingly to account for the volume of the largest block observed in the drawpoint.

*Table V*

**Converting side lengths to volumes in drawpoint mapping**

| Fragment side length (m) | Estimated fragment volume ($m^3$) | |
|---|---|---|
| | Forsterite | Diorite |
| 0.005 | 1.25E-07 | 1.25E-07 |
| 0.1 | 0.01913 | 0.01595 |
| 0.5 | 0.23908 | 0.19938 |
| 1.0 | 1.9126 | 1.5950 |
| 2.0 | 15.30 | 12.76 |

More than 3800 observations of fragment size distributions at the drawpoints in the DOZ were reported by Srikant (2006) and Sinaga (2005). The observations were sorted by rock type, panel, and draw height. Though 8091 m of drill-core data records are available from the lower 50 m of the DOZ mine along with 580 drawpoint fragmentation records, only eight zones could be used for calibrating the BSE model against primary fragmentation observations. These zones are shown in Table VI.

### *Forsterite skarn*

A total of 143 drawpoint observations were recorded in the forsterite rock type for draw heights less than 50 m. Of these, 49 observations were from drawpoints in panels 18–20 and 94 were from drawpoints in panels 21–27. The predicted and observed primary fragment size distributions for these panel groups within the forsterite rock type are shown in Figure 5 and show a reasonable correlation, though the predicted fragmentation is slightly coarser than the observed fragment size distribution. A significant reason for this difference could be the fact that large boulders are often obscured by fines.

### *Diorite*

A total of 28 drawpoint observations were recorded in the diorite rock type for draw heights less than 50 m. Of these, three observations were from drawpoints in panels 12–14, 13 were from drawpoints in panels 15–17, and 12 observations were from drawpoints in panels 21–27. The predicted and observed fragment size distributions for these panel groups within the diorite rock type are shown in Figure 9. Unlike in the forsterite rock type, there is a significant difference between the observed and predicted fragment size distributions with the predicted fragment size distribution being coarser by an order

*Table VI*

**Data available for calibration of the BSE program**

| Panels | | Forsterite | Diorite |
|---|---|---|---|
| P15-17 | Drilled metres | 199.80 | 138.25 |
| | Drawpoint observations | 4 | 13 |
| P18-20 | Drilled metres | 394.40 | 11.30 |
| | Drawpoint observations | 49 | - |
| P21-27 | Drilled metres | 800.20 | 800.20 |
| | Drawpoint observations | 94 | 12 |

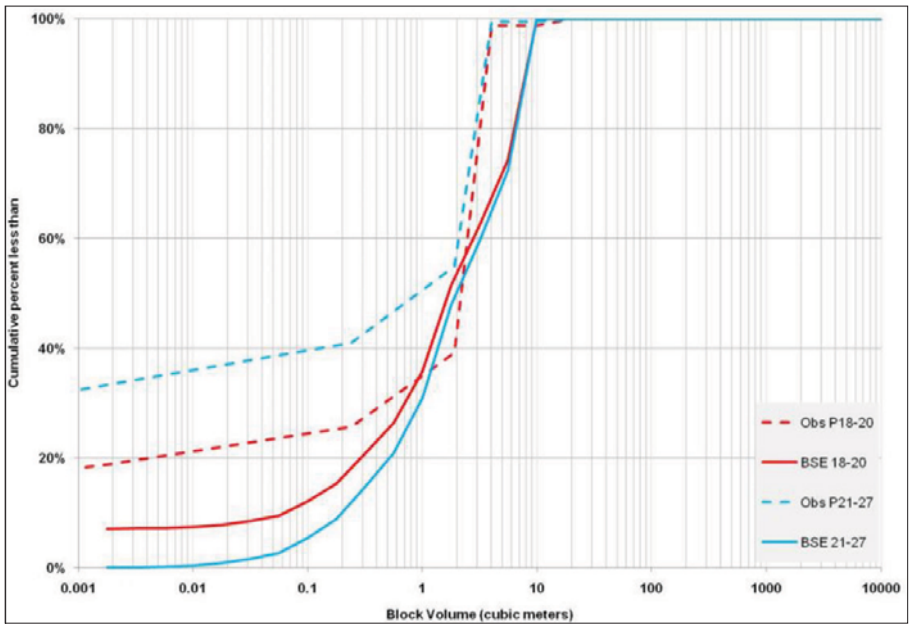


Figure 5—Comparison of predicted and observed fragmentation in forsterite

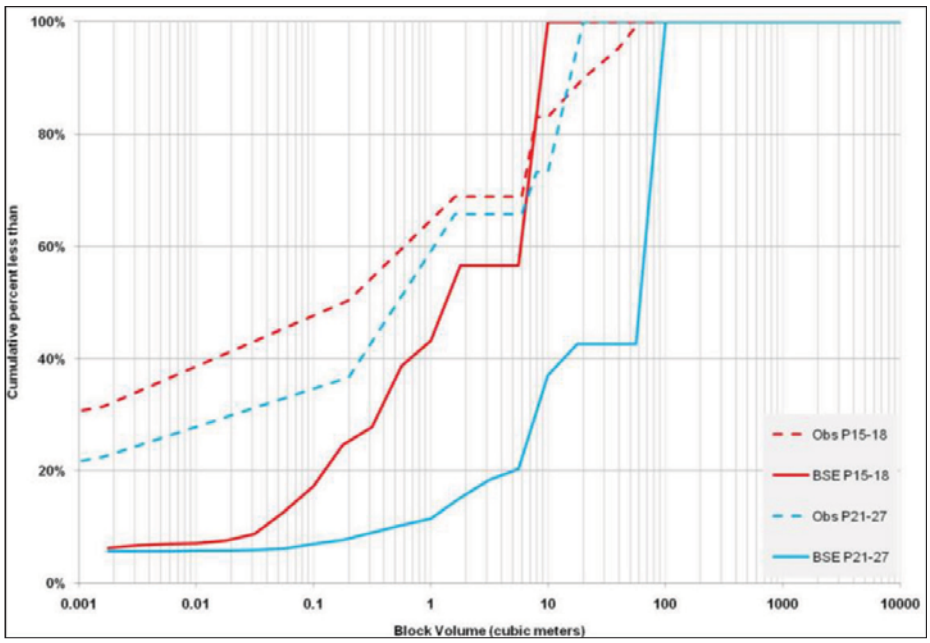


Figure 6—Comparison of predicted and observed fragmentation in diorite

of magnitude. An examination of the fragment sizes generated by the BSE model shows that there are two blocks with volumes greater than 100 $m^3$. These blocks have resulted from core piece lengths greater than 3 m and the higher aspect ratios in the diorite rock type.

## Conclusions

The BSE program was developed to estimate primary fragment size distributions using drill-core data, especially for block cave operations. The program uses drill-core data, which is generally available from most parts of the areas to be mined, from the initial stages of discovery of the deposit to mine development, along with joint set information so that the estimates can reflect the variability of fragmentation within the orebody. The BSE program helps the mine engineering group to evaluate fragmentation and plan mine facilities prior to construction of the mine.

Success in the estimation of primary fragmentation at the extraction level in a block cave is limited by the large number of unknowns about the rock mass and about the processes of comminution within the draw column. The characteristics of the jointed rock mass can only be estimated based on data generated

from geotechnical drilling, and the spatial relationships of these characteristics are less understood than those of mineral compositions and assay values. The density of geotechnical data is also often very low and there is, therefore, less confidence in the extrapolation of the data to areas where there has been no drilling or even in the interpolation of data between adjacent drill-holes.

Drawpoint fragmentation mapping information can be a very useful tool in the calibration of procedures for estimating fragmentation. However, such mapping was found to be time-consuming and required a geological or geotechnical technician to interrupt operations while taking measurements of fragmentation at the drawpoints. The analysis of scaled photographs of fragmentation at the drawpoints can help reduce the time taken to obtain the information from the field and also reduce the subjectivity involved in mapping fragmentation at the drawpoints, but the lighting conditions at the drawpoints and the presence of dust and moisture in the underground environment made it difficult to take quality photographs that can be analysed using programs such as SPLIT Desktop to develop fragment size distributions. While Zamora (2006) developed a system to quickly take scaled photographs at the drawpoints in El Teniente, reducing the interruption of mucking operations at the extraction level, the use of the camera system to take scaled photographs at the drawpoint in the DOZ was not successful due to the moisture and dust levels at the drawpoints.

A campaign of drawpoint fragmentation assessment using photographs from the drawpoints was initiated in 2006 and the data was analyzed by Lukito (2005) using the SPLIT Desktop software. Though the data was collected over a period of 3 months, adequate correlations could not be drawn between the cave height and the fragment size distributions. Most of the problems were related to the covering of boulders with fines, which caused an under-estimation of the larger blocks at the drawpoint.

In this study, the BSE model was calibrated against the limited number of drawpoint fragmentation mapping observations from the DOZ block cave collected during the period 2004 to 2007. The use of a larger database of fragment size distributions from different mines in different rock types is recommended to help improve calibration of the BSE model. In addition, efforts must be undertaken to better understand the processes of comminution within the draw column.

## Acknowledgements

This paper is based on the study conducted by the author as part of his PhD dissertation and was undertaken at the DOZ mine with the approval of the management of PT Freeport Indonesia. The author gratefully acknowledges the assistance and guidance of David Nicholas of Call & Nicholas, Inc., David Flint, George MacDonald, and Tim Casten and Chuck Brannon of Freeport McMoRan during the course of this study. The guidance of Mary Poulton, John Kemeny, and Sean Dessureault at the University of Arizona is also acknowledged.

## References

Aimin, Z. and Yongxue, S. 2000. Application of block caving system in the Tongkuangyu Copper Mine. *Proceedings of MassMin 2000.* Chitombo, G. (ed). Australasian Institute of Mining and Metallurgy, Melbourne, Australia. pp. 325–331.

Barber, J., Thomas L., and Casten, T. 2000. Freeport Indonesia's Deep Ore Zone Mine. *Proceedings of MassMin 2000.* Chitombo, G. (ed). Australasian Institute of Mining and Metallurgy, Melbourne, Australia. pp. 289–294.

Brown, E.T. 2007. Block Cave Geomechanics. 2nd edn.. JKMRC, University of Quensland, Australia.

Brunton, I., Lett, J., and Thornhill, T. 2016. Fragmentation prediction and assessment at the Ridgeway Deeps and Cadia East block cave operations. *Proceedings of the Seventh International Conference and Exhibition on Mass Mining (MassMin 2016).* Australasian Institute of Mining and Metallurgy, Melbourne. pp 151–159.

Butcher, R.J. and Thin, I.G.T. 2007. The inputs and choices for predicting fragmentation in block cave projects. *Proceedings of the 1st International Symposium on Block and Sub-level Caving,* Cape Town. Southern African Institute of Mining and Metallurgy, Johanesburg, South Africa. pp. 35–49.

Esterhuizen, G.S. 1999, BCF Version 3.0 – A program to predict block cave fragmentation - Technical reference and user's guide. Society for Mining, Metallurgy & Exploration, Littleton, Colorado.

Hadjigeorgiou, J., Grennon, M., and Nickson, S. 2002. In situ block size distributions from borehole data: a case study. *Transactions of the Society for Mining, Metallurgy and Exploration,* vol. 312. pp. 20–27.

Laubscher, D.H. 1994. Cave mining – the state of the art. *Journal of the South African Institute of Mining and Metallurgy,* vol. 94, no. 10. pp. 279–292.

Lukito, H.A. 2005. Analysis of secondary fragmentation size distribution in DOZ block cave mine, PT Freeport Indonesia. B. Mining Report. Institut Teknologi Bandung, Bandung, Indonesia.

Moss, A. 2012. Caving: The need to measure. *Proceedings of the 2nd Mining Innovation Conference,* Sydney, Australia. Australasian Institute of Mining and Metallurgy, Melbourne. pp. 3–4. .

Nickson, S., Coulson, A., and Hussey, J. 2000. Noranda's approach to evaluating a competent deposit for caving. *Proceesings of MassMin 2000,* Brisbane. Australasian Institute of Mining and Metallurgy, Melbourne. pp. 367–383.

Samosir, E., Brannon, C., and Diering, T. 2004. Implementation of cave management system (CMS) tools at the Freeport DOZ Mine. *Proceedings of MassMin 2004.* Karzulovic, A. and Alfaro, M.A. (eds). Instituto de Ingenieros de Chile, Santiago, Chile. pp. 513–518.

Sinaga, H.N. 2005. Analyze efficiency explosive and secondary blasting cost based on HOD and rock type dominant. B. Mining Report. Insitut Teknologi Bandung, Bandung, Indonesia.

Srikant, A., and Nicholas, D.E. 2004. Assessment of primary fragmentation from drill core data. *Proceedings of MassMin 2004.* Karzulovic, A. and Alfaro, M.A. (eds). Instituto de Ingenieros de Chile, Santiago, Chile. pp. 55–58.

Srikant, A., Nicholas, D.E., and Rachmad, L. 2004. Visual estimation of fragment size distributions in the DOZ block cave. *Proceedings of MassMin 2004.* Karzulovic, A. and Alfaro, M.A. (eds). Instituto de Ingenieros de Chile, Santiago, Chile. pp. 286–290.

Srikant, A. 2006. Fragment size estimation and measurement in the DOZ block cave. *Mining Engineering,* vol. 58, no. 10. pp. 43–47.

Srikant, A. 2013. Estimating primary fragment size distributions from drill core data. PhD dissertation, University of Arizona, Tucson, AZ.

Widijanto, E., Arsana, N., and Srikant, A. 2006. Geotechnical challenges in the DOZ block cave mine. *Rock Mechanics in Underground Construction: Proceedings of the 4th Asian Rock Mechanics Symposium.* Leung, C.F. and Zhou, Y.X. (eds). World Scientific, Singapore. p. 210.

Wellman, E.C., Annavarapu, S., Pratt, R.W., and Nicholas, D.E. 2012. Prediction of fragmentation - an update of the Core2Frag program. *Proceedings of MassMin 2012.* Sudbury, Ontario. Canadian Institute of Mining, Metallurgy and Petroleum, Montreal.

Zamora, A. V. 2006. Persoanl communication. ◆


# Optimization of iron ore blending in the COREX shaft furnace

**X. Liu[1], C. Liu[2], B. Wang[2], and F. Ye[2]**

**Affiliation:**
[1]Engineering Training Center, Wuhan University of Science and Technology, China.
[2]The State Key Laboratory of Refractories and Metallurgy, Wuhan University of Science and Technology, China.

**Correspondence to:**
C. Liu

**Email:**
liuchengsong@wust.edu.cn

**Dates:**
Received: 22 Jan. 2018
Revised: 10 Oct. 2018
Accepted: 24 Oct. 2018
Published: May 2019

**How to cite:**
Liu, X., Liu, C., Wang, B., and Ye, F.
Optimization of iron ore blending in the COREX shaft furnace.
The Southern African Insitute of Mining and Metallurgy

DOI ID:
http://dx.doi.org/10.17159/2411-9717/18/018/2019

ORCiD ID:
X. Liu
https://orchid.org/0000-0002-0015-5630
C. Liu
https://orchid.org/0000-0002-0271-693X
B. Wang
https://orchid.org/0000-0002-2987-7127
F. Ye
https://orchid.org/0000-0001-8521-4451

## Synopsis

**To extend the variety of lump ores that are used in the COREX shaft furnace and to optimize iron ore blending, the original evaluation method for iron ores that was proposed by Voestalpine AG has been improved. Physicochemical and metallurgical properties of iron ores, including Sishen lump ore and CVRD pellets, which are currently used in the COREX process, and three other lump ores, were assessed and compared. Ore matching principles were proposed and five optimized iron ore blending schemes designed and verified by laboratory experiments to prove the effectiveness of the improved evaluation method. The replacement of Sishen lump ore by the alternative L2 and L3 lump ores without varying the proportion of CVRD pellets could improve the degree of reduction and rate of metallization, and decrease the bonding index. Based on the results of laboratory test work and industrial- trials, an ore blending scheme of 60% CVRD, 20% L2, and 20% L3 is recommended for use in the COREX process.**

**Keywords**
**COREX, iron ores, metallurgical properties, blending optimization.**

## Introduction

In recent years, problems such as environmental pollution and a shortage of coke and coal resources for blast-furnace ironmaking have become increasingly apparent. Based on sustainable developments in the iron- and steelmaking industries, the environmentally friendly COREX smelting-reduction process with low energy consumption was developed and introduced (Zhou and Du, 2013; Song, Lv, and Yin, 2015; Xu *et al.*, 2016; Kurunov, 2010). The evaluation system for lump ore that was proposed by Voestalpine AG recommends that only Sishen lump ore from South Africa be used in the COREX process, because of the stringent physicochemical and metallurgical property requirements. This situation significantly hampers improvements to the technical and economic aspects of the COREX ironmaking process, especially in China (Eberle, Siuka, and Bohm, 2006). No theoretical or technical basis has been provided for the evaluation system, and the assessment approach for iron ores also presents problems that need to be discussed and resolved.

The COREX process consists of two reactors: the prereduction shaft furnace and the melting gasifier as shown in Figure 1 (Wu *et al.*, 2017). Pellets and lump ores which are charged to the prereduction shaft should have a good reducibility and metallization with a low degradation index (Li *et al.*, 2016; Wu *et al.*, 2011; Kumar *et al.*, 2009; Kang, Gupta, and Sahajwalla, 2007). The properties and microstructure of the iron ore pellets which are required to achieve a high productivity and a lower fuel rate in the COREX process have been investigated (Umadevi *et al.*, 2011). Some efforts have also been made to investigate the behaviour of lump ores in the COREX shaft furnace, including the disintegration characteristics and the reduction degradation (Umadevi *et al.*, 2011; Zhou *et al.*, 2015; Xu *et al.*, 2013; Li, Feng, and Zou, 2013; Hou *et al.*, 2014). However, few studies have focused on the optimization of ore blending for partial or total substitution of the expensive Sishen lump ore by other, cheaper lump ores to reduce the production cost. The technology for the utilization of blended lump ores in the COREX process is still in its early development stages (Zhou *et al.*, 2017; You *et al.*, 2017).

In this work, the original evaluation system for iron ores that was proposed by Voestalpine AG was modified and improved to approach the actual requirements for the production of hot metal in the COREX process. The properties of Sishen lump ore, CVRD pellets, and three alternative lump ores, including chemical compositions, size distribution, amount of adhesive powder, thermal cracking properties, reducibility, and reduction degradation and bonding properties, were investigated and compared. Ore

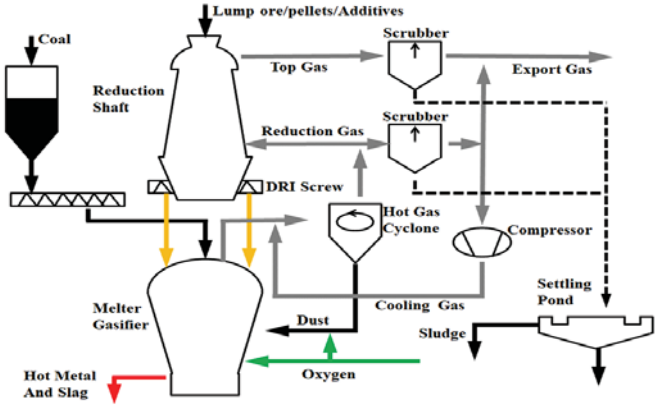


**Figure 1—Schematic diagram of the COREX process (Wu *et al.*, 2017)**

blending principles are proposed and discussed based on the above physicochemical and metallurgical property results. Five schemes of iron ore blending were designed and verified by laboratory experiments. Finally, the industrial feasibility of the optimal blending scheme was verified through the COREX production practice.

## Proposal for the improved evaluation of iron ores

### *Supplementary evaluation system*

The original evaluation system as developed by Voestalpine AG targeted the physicochemical characteristics and static reduction properties of iron ores. The former include the chemical composition, size distribution, and bulk density, whereas the latter comprise the reduction degree, reduction degradation, and bonding properties at high temperature. However, according to previous work (Wu *et al.*, 2011), a significant low-temperature reduction degradation of iron ore occurred in experiments and during production, which affected the furnace's smooth operation. Thus it was necessary to incorporate the low-temperature reduction degradation of iron ore into the evaluation system. In addition, because of thermal stress, thermal cracking probably occurs in the iron ores, especially lump ores, which reduces burden permeability and causes an uneven distribution of gas flow and a low degree of metallization. A measurement of the thermal cracking index should also be taken into account when assessing the properties of iron ores that are used in the COREX process. In addition, in the COREX production process, the large-size lump ores in the charge will gradually break down to small particles and powder due to thermal cracking and low-temperature reduction degradation during heating. However, before the lump ores are charged into the reduction shaft furnace, a certain amount of original ore powder, which is generated during mining and transportation due to interparticle impact and abrasion, adheres to the lump surfaces. The original ore powder will be charged into the reduction shaft furnace along with the lump ores and affect the permeability of the burden. Therefore, in order to comprehensively and accurately evaluate the properties of the lump ores, the inclusion of adhesive powder with an equivalent diameter below 1.0 mm is proposed in this study. The amount of adhesive powder was also measured and analysed, and will be further elaborated on later.

### *Modification of measurement approaches*

#### *Experimental temperature*

In original measurements of the static loading reduction of iron ores, the highest experimental temperature was set at 1073 K, lower than the actual gas temperature, which was in the range 1073–1173 K at the furnace inlet during practical COREX production. In this study, the highest experimental temperature in the modified measurement approach was increased to 1123 K to study the behaviour of iron ores in the shaft furnace more practicably.

#### *Temperature curve*

During the COREX ironmaking process, the heating and reducing durations at the high temperature are approximately 3 hours and 2 hours, respectively. The original measurement for the static loading reduction of iron ores as proposed by Voestalpine AG requires only 1 hour for the iron ore sample to be heated from room temperature to the highest temperature, with the sample being maintained at that temperature for 5 hours. The temperature curve for the reduction test in this study was modified according to the practical parameters. Initially, the temperature was increased by 5 K/min from room temperature to 1123 K, and then maintained for 2 hours. The cooling rate was about 4 K/min after power off.

#### *Gas flow rate*

In the original measurement for the static loading reduction of iron ores, the gas flow rate per kilogram of iron ore was 6.7 L/min, compared with 20 L/min during COREX ironmaking production. Therefore, the gas flow rate in the experiments was increased to 20 L/min per kilogram of iron ore to simulate production in the revised measurement approach.

The comparison of the current and desired parameters in the reduction test is summarized in Table I.

## Physicochemical characteristics of iron ores used in the experiments

### *Chemical composition*

Sishen lump ore and CVRD pellets were used initially in the COREX shaft furnaces in China. Alternative lump ores L1, L2, and L3 were imported from Brazil, Australia, and South Africa respectively. The dominant phase in the iron ores was haematite. The chemical compositions of the iron ore samples, measured by X-ray fluorescence spectrometry, are shown in Table II.

### *Size distribution*

The particle size distributions and average sizes of the iron ore samples are shown in Table III. The CVRD pellets exhibited a narrower particle size distribution and a lower average size, which is beneficial for burden permeability and reduction efficiency. Sishen lump ore had a moderate size-distribution

*Table I*

**Comparison of the current and desired parameters in the reduction test**

| Parameter | Current value | Desired value |
|---|---|---|
| Highest experimental temperature | 1073 K | 1123 K |
| Heating time | 1 h | Approx. 3 h |
| Reduction time | 5 h | 2 h |
| Gas flow rate | 6.7 L/min | 20 L/min |

*Table II*

**Chemical composition of iron ore samples (wt%)**

| Sample | Fe (total) | CaO | $SiO_2$ | $Al_2O_3$ | $TiO_2$ | P | S | $K_2O$ | $Na_2O$ | LOI |
|---|---|---|---|---|---|---|---|---|---|---|
| L1 | 65.79 | 0.07 | 2.88 | 1.57 | 0.08 | 0.063 | 0.006 | 0.010 | 0.002 | 1.71 |
| L2 | 64.58 | 0.08 | 3.20 | 1.48 | 0.05 | 0.074 | 0.011 | 0.014 | 0.005 | 2.66 |
| L3 | 65.24 | 0.06 | 3.39 | 1.47 | 0.07 | 0.019 | 0.021 | 0.180 | 0.029 | 0.48 |
| Sishen | 65.94 | 0.07 | 3.22 | 0.76 | 0.03 | 0.041 | 0.018 | 0.050 | 0.003 | 0.61 |
| CVRD | 65.73 | 2.65 | 2.37 | 0.80 | 0.04 | 0.039 | 0.006 | 0.019 | 0.024 | 0.08 |

*Table III*

**Particle size distributions of iron ore samples (wt%)**

| Size fraction | L1 | L2 | L3 | Sishen | CVRD |
|---|---|---|---|---|---|
| >31.5 mm | 5.01 | 39.55 | 0 | 0 | 0 |
| 25–31.5mm | 14.33 | 30.03 | 47.88 | 5.23 | 0 |
| 20–25 mm | 14.89 | 20.5 | 38.55 | 27.84 | 0 |
| 16–20 mm | 33.23 | 7.04 | 12.35 | 35.21 | 20 |
| 12.5–1 6mm | 19.90 | 2.88 | 1.22 | 20.03 | 66.83 |
| 10–12.5 mm | 12.64 | 0 | 0 | 9.13 | 13.17 |
| 8–10 mm | 0 | 0 | 0 | 1.54 | 0 |
| 6.3–8 mm | 0 | 0 | 0 | 1.12 | 0 |
| <6.3 mm | 0 | 0 | 0 | 0 | 0 |

uniformity and average size, whereas L1 lump ore had a relatively broad particle size distribution and a higher average size. For L2 and L3 lump ores, the particle size distributions were better than those of L1 and the Sishen lump ores. Iron ores are probably crushed into powder or small particles during production in the COREX prereduction shaft furnace because of the high pressure, so the larger average sizes of L2 and L3 benefited production.

### *Amount of adhesive powder*

As indicated before, in the processes of mining and transportation, some ore powder is generated and adheres to the surface of lump ores, which would probably affect the gas flow distribution, burden permeability, and the degree of reduction and metallization rate during COREX production. The amount of adhesive powder was calculated from the weight difference of the iron ore samples before and after brushing. Firstly, 1 kg portions of the original iron ore samples containing all size fractions were prepared and dried in a box furnace at 373 ± 5 K for 12 hours. The samples were then brushed with water, screened at a mesh size of 1 × 1 mm, dried again at 373 ± 5 K for 12 hours, and weighed. The proportion of adhesive powder (PAP) was obtained by Equation [1].

$$PAP = \frac{W_0 - W_1}{W_0} \times 100\% \quad [1]$$

where $W_0$ is the mass of the original iron ore sample after drying, and $W_1$ is the mass of sample (>1 mm) after brushing and drying.

This process was repeated for three times to obtain the average value. The results are shown in Table IV.

## Metallurgical properties of iron ores for experiments

### *Experimental procedures*

### *Thermal cracking*

The thermal cracking propensity of the iron ores was measured by a thermal impact method according to ISO 8371:2007 (ISO, 2017). The lump ore samples were crushed and sieved to a grain size of 20–25 mm before use, whereas a size of 12.5–16 mm was selected for the CVRD pellet experiments, which were conducted by using the static loading reduction equipment in Figure 2. The adhesive powder on the particles was brushed off with water, and then the large-size iron ores were dried in an oven at 373 ± 5 K for 12 hours. The reactor tube was heated from room temperature to 773 K, 873 K, 973 K, and 1073 K, respectively. Then, the samples were placed into a tube with a $N_2$ gas flow of 15 L/min. After a 30-minute holding time, the heating and $N_2$ gas flow were interrupted to cool the samples to room temperature.

To study the thermal cracking properties of the iron ore samples, the decrepitation indices $DI_{-10}$, $DI_{-6.3}$, and $DI_{-3.15}$ were calculated by using the following equations (ISO, 2017):

$$DI_{-10} = \frac{W_1}{W_0} \times 100\% \quad [2]$$

$$DI_{-6.3} = \frac{W_2}{W_0} \times 100\% \quad [3]$$

$$DI_{-3.15} = \frac{W_3}{W_0} \times 100\% \quad [4]$$

*Table IV*

**Proportions of adhesive powder in the iron ore samples**

| Sample | L1 | L2 | L3 | Sishen | CVRD |
|---|---|---|---|---|---|
| PAP (wt%) | 8.11 | 5.02 | 0.52 | 4.13 | 1.91 |

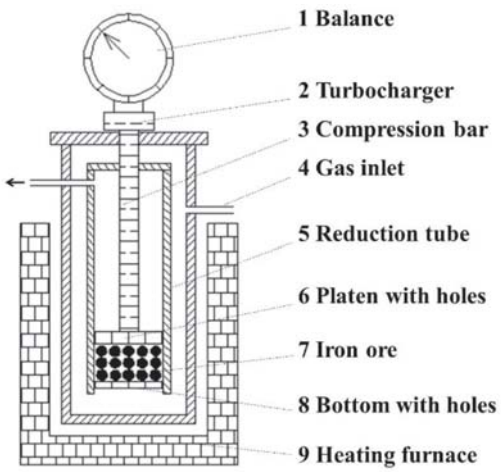


**Figure 2—Diagram of static loading reduction equipment**

where $W_0$ is the mass of the iron ore samples after heating at 773 K, 873 K, 973 K, and 1073 K, and $W_1$, $W_2$, and $W_3$ are the masses of particles that are smaller than 10 mm, 6.3 mm, and 3.15 mm, respectively.

### *Reducibility and reduction degradation*

In the improved evaluation system for iron ores, as was done in the reduction test (Qiu *et al.*, 2017, Li *et al.*, 2016; Standardization Administration of the PR China, 2017, 2016; Li, 2008; Wu, Xu, and Zhang, 2008), lump ore samples were heated from room temperature to 1123 K under $N_2$ gas at a flow rate of 3 L/min. Reducing gas with a composition of 68% CO, 9% $CO_2$, and 23% $H_2$ was injected into the tube and the samples were reduced for 2 hours. After the reduction, the gas was changed to $N_2$ to cool the samples to room temperature. Reduction test procedures in the improved evaluation system are shown in Figure 3. Based on the standard GB/T13241-2017 (Standarization Administration of the PR China, 2017), the reduction products were weighed to calculate the reduction degree $R$ and metallization rate $M$ as follows (Standardization Administration of the People's Republic of China, 2017):

$$R = \frac{m_0 - m_R - m_{LOI}}{m_0 \times \left[0.43 \times \left(w_{(Fe)} - 0.11 \times w_{(FeO)}\right)\right]} \times 10^4 \quad [5]$$

$$M = 100 - \frac{1.5}{1.05}(100 - R) \quad [6]$$

where $m_0$ and $m_R$ represent the initial mass of the iron ore sample before and after reduction at room temperature, respectively, $m_{LOI}$ represents the loss on ignition, $w_{(Fe)}$ indicates the total iron content in the sample, and $w_{(FeO)}$ indicates the FeO content, which was obtained from the ferrous iron content as calculated from Equation [7]. The mass of $Fe^{2+}$ was measured by the method proposed in the national standard GB/T 6730.8-2016 (Standardization Administration of the PR China, 2016).

$$w_{(FeO)} = \frac{56 + 16}{56} \cdot w(Fe^{2+}) = 1.286 \cdot w(Fe^{2+}) \quad [7]$$

The procedures for the reduction degradation test were similar to those for the reduction test, except that the experimental temperature was 823 K and the composition of the reducing gas was 46% CO, 36% $CO_2$, and 18% $H_2$. After cooling to room temperature under $N_2$ gas, the samples were tested in a tumbling drum (130 mm diameter, 800 mm height) at a rotation speed of 30 r/min for 30 minutes. The samples were then sieved at 6.3 mm, 3.15 mm, and 0.5 mm mesh to determine the particle size distribution.

### *Bonding property*

The procedures for the bonding property test were similar to those of the reduction test, except for an applied load of 0.1 MPa (Li, 2008; Wu, Xu, and Zhang, 2008). In this experiment, the degree of reduction and volume shrinkage were measured, which are important for determining the bonding characteristics of the iron ore. The bonding index SI was used as an indicator of the bonding property of iron ores as calculated from the following equation:

$$SI = \frac{m_1}{m_R} \times 100\% \quad [8]$$

where $m_R$ represents the sample mass after reduction, and $m_1$ is the mass of particles that are larger than 12.5 mm after the drum test.

The volume shrinkage $VI_E$ was determined from the height of the burden before and after reduction, as shown in the following equation (Li, 2008; Wu, Xu, and Zhang, 2008):

$$VI_E = \frac{h_0 - h_E}{h_0} \times 100\% \quad [9]$$

where $h_0$ and $h_E$ represent the height of the burden before and after reduction, respectively.

### *Results*

Figure 4 shows the experimental results for the thermal cracking property of the iron ore samples. No thermal cracking occurred in the CVRD pellets at the experimental temperatures because of their low degree of hydration during induration. With an increase in temperature, the thermal cracking indices, including $DI_{-10}$, $DI_{-6.3}$, and $DI_{-3.15}$ showed an upward tendency for all lump ores. Compared with Sishen lump ore, L1 and L2 lump ores were considered to have higher thermal cracking indices according to the experimental results at various temperatures, especially the L2 lump ore, whereas the thermal cracking indices of the L3 lump ore were lower.

Figure 5 shows the degree of reduction and metallization rate of the samples after the reduction test at 1123 K. The degree of reduction and metallization rate of the CVRD pellets reached 91% and 87%, respectively, which were higher than the values for all the lump ores. The results indicate that the reduction degrees and metallization rates of the alternative lump ores L1, L2, and L3 were superior to, or at least similar to, those of Sishen lump ore in the improved reduction test at 1123 K. A probable explanation for this is that the mineral phases and pore structure affect the reduction properties of the iron ores. In this study, the dominant

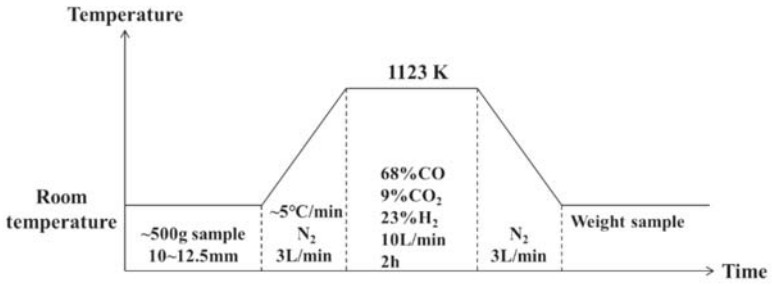


**Figure 3—Reduction test procedures in the improved evaluation system**

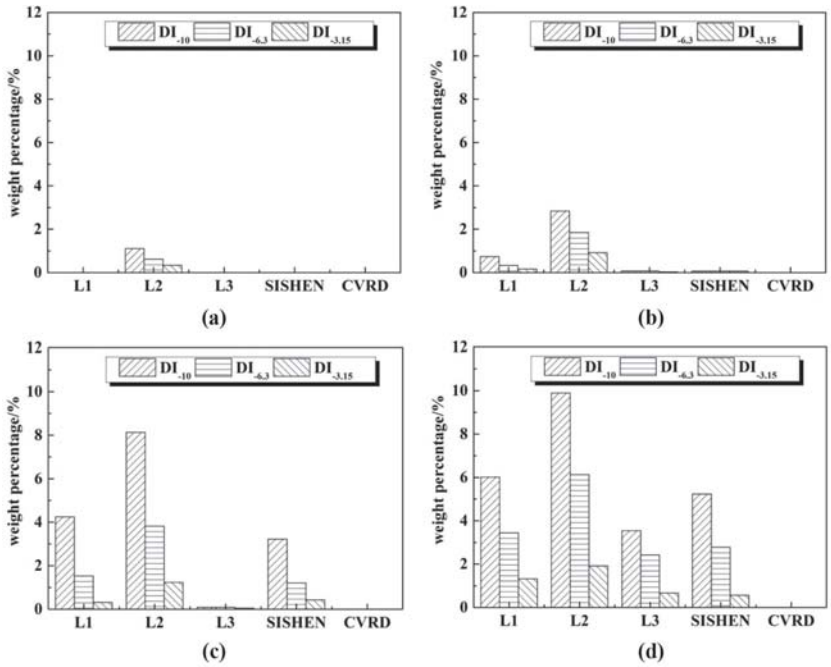


Figure 4—Thermal cracking test results: (a) 773 K, (b) 873 K, (c) 973 K, (d) 1073 K

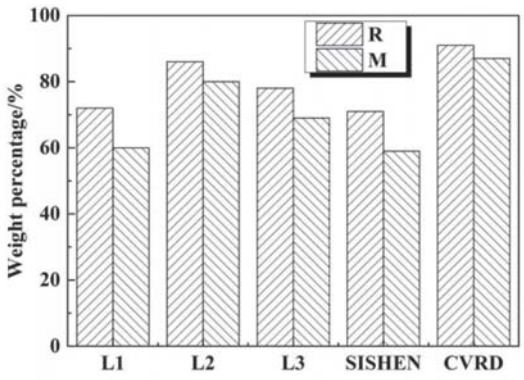


Figure 5—Reduction degree and metallization rate of iron ores at 1123 K

phase in all the iron ores was haematite. Actually, with the increase in the amount of open pores in the ores, the reducing gas can permeate the particles more easily and the interfacial areas between the ore and reducing gas increases, which could promote the reduction reactions and improve the reduction degree and metallization rate of the ores (Wu *et al.*, 2011). Based on the results shown in Figure 5, it is suggested that the apparent porosities of L1, L2, and L3 lump ores are higher than that of Sishen lump ore, but lower than that of CVRD pellets.

Figure 6 shows the degree of reduction and reduction degradation behaviour of the iron ore samples at 823 K. After reduction, L2 lump ore has the highest mass ratio of particles smaller than 0.5 mm and smaller than 3.15 mm, which means that the degradation behaviour of L2 lump ore was the most severe. The $RDI_{-0.5}$ of the L1 and L3 lump ores was close to that of the Sishen lump ore. The CVRD pellets had a higher $RDI_{-0.5}$, despite the $RDI_{-3.15}$ being lower. Previous work has shown that the basic reason for the reduction degradation of iron ore is that, during the reduction of $Fe_2O_3$ at low temperature (673–873 K), the transformation of haematite to magnetite causes crystal lattice deformation and an increase in internal stress, which contributes to the degradation of the ore Wu *et al.*, 2017).

Figure 7 shows the bonding index, volume shrinkage, and degree of reduction of iron ore samples after the bonding property test. A marked bonding propensity would impair the reduction. In general, as shown in Figure 7, Sishen lump ore has the highest bonding index among all the samples. The bonding indices of the L2 lump ore and the CVRD pellets were lower than those of the L1 and L3 lump ores. L1, L2, and L3 lump ores exhibited a better bonding performance than the Sishen lump ore.

The bonding index correlated positively with the reduction degree and volume shrinkage of the lump ores For the CVRD pellets, although the reduction degree was high with a large amount of metallic iron, the spherical shape and low volume shrinkage resulted in a point contact with a small bonding area and low bonding strength. Contact between the particles is also a critical factor in the bonding behaviour of iron ores.

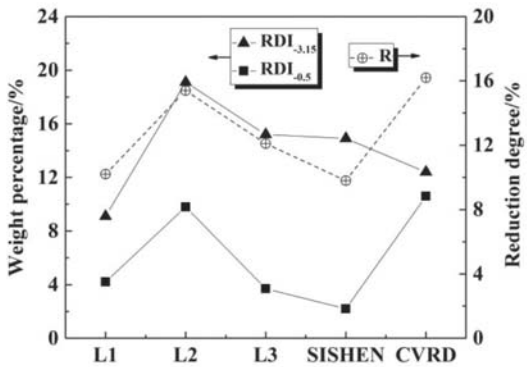


Figure 6—Reduction degree and reduction degradation index of iron ores at 823 K

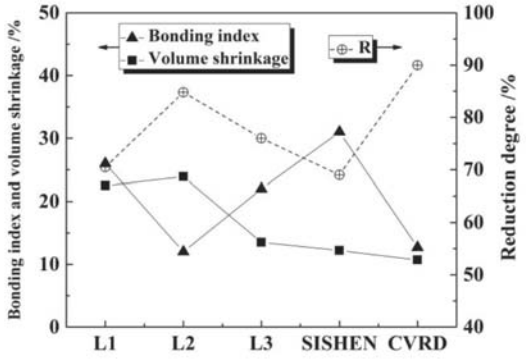


**Figure 7—Bonding index, volume shrinkage, and reduction degree of iron ores at 1123 K**

## Optimization of iron ore blending in the COREX shaft furnace

### *Substitutability of the alternative lump ores*

The substitutability of the alternative lump ores was assessed by comparing the physicochemical and metallurgical properties of the Sishen lump ore and lump ores L1, L2, and L3 using the improved evaluation method.

Compared with the Sishen lump ore, the total Fe, S, and $K_2O$ contents of the L1 lump ore were 0.15%, 0.012%, and 0.04% lower, respectively, whereas the P content and loss on ignition (LOI) were higher by 0.022% and 1.1%, respectively. After brushing, cleaning, and drying, the proportion of adhesive powder in the L1 lump ore was 3.98% higher than that in the Sishen lump ore. The L1 lump ore size distribution was broader. The thermal cracking at different temperatures, the reduction degree, and the metallization rate at 1123 K of the L1 lump ore were very similar to those of the Sishen lump ore, although its $RDI_{-3.15}$ and bonding index at 823 K were lower by 3.3% and 5%, respectively. In general, little difference was found between the Sishen and L1 lump ores in terms of physicochemical properties, thermal cracking propensity, and reduction and reduction degradation behaviour, although the higher bonding index of the L1 lump should be taken into consideration.

The total Fe, S, and $K_2O$ contents of the L2 lump ore were lower than those of the Sishen lump ore by 1.36%, 0.007%, and 0.036%, respectively, whereas the P, $Na_2O$, and LOI were higher by 0.033%, 0.002%, and 2.05%, respectively. The proportion of adhesive powder in the L2 lump ore was also higher than that in the Sishen lump ore by 0.89%. The size distribution of the L2 lump ore was relatively narrow and its average particle size was almost twice that of the Sishen lump ore. As regards drum strength, the $DI_{-10}$, $DI_{-6.3}$, and $DI_{-3.15}$ of L2 lump ore at 1073 K were 9.89%, 6.13%, and 1.92%; higher than the Sishen lump ore by 4.66%, 3.35%, and 1.36%, respectively. However, at 1123 K, the degree of reduction and metallization rate of L2 lump ore were higher than the values for Sishen lump ore by 15% and 21%. The bonding index of L2 lump ore was only 12%, compared with 31% for the Sishen lump ore. So, although the physicochemical properties, thermal cracking propensity, and reduction degradation behaviour of the L2 lump ore were inferior to Sishen lump ore, due to its excellent reduction and bonding properties, L2 lump ore could probably substitute for Sishen lump ore in the COREX ironmaking process. However, the amount of adhesive powder in the L2 lump ore needs to be determined carefully to maintain a smooth COREX operation.

For L3 lump ore, the total Fe, P, and LOI were lower than for the Sishen lump ore by 0.7%, 0.022%, and 0.13%, respectively, whereas the S, $K_2O$, and $Na_2O$ contents were higher by 0.003%, 0.13% and 0.026%, respectively. The proportion of adhesive powder in the L3 lump ore was 0.52% lower than that of the Sishen lump ore. The size distribution of the L3 lump ore was also relatively narrow and the average size was 6.43%. larger than that of the Sishen lump ore As mentioned previously, the thermal cracking indices of the L3 lump ore were the lowest among the four lump ores at various temperatures. The reduction degree and metallization rate of the L3 lump ore at 1123 K ore were similar to those of the Sishen lump ore, as well as the reduction degradation at 823 K. The bonding index of the L3 lump ore was lower than that of Sishen lump ore by 9%. So, L3 lump ore is also a reasonable choice for replacing Sishen lump ore in the COREX ironmaking process. However, the excess alkali in L3 lump ore should be avoided.

A rating system was established by using points to comprehensively evaluate the physicochemical and metallurgical properties of Sishen lump ore, CVRD pellets, and L1, L2, and L3 lump ores to study the substitutability. Due to space limitations, only some rating examples are shown in Table V. Besides the points, the weights for the physicochemical properties, thermal cracking propensity, reducibility and reduction degradation, and bonding property are also different, and were artificially set at 15%, 15%, 45%, and 25%, respectively. A higher point rating represents better comprehensive properties of the iron ore. Evaluation points for the L1, L2, L3, Sishen, and CVRD ores are shown in Figure 8. The comprehensive evaluation scores of the L1, L2, and L3 lump ores were all higher than that of Sishen lump ore, which indicated their substitutability. This was validated in the subsequent industrial experiments. CVRD pellets present the highest evaluation score of 4.24, as shown in Figure 8.

*Table V*

**Examples in the rating system to evaluate the physicochemical and metallurgical properties of the iron ores**

| Physicochemical properties (wt%) | | | | | | Metallurgical properties | | |
|---|---|---|---|---|---|---|---|---|
| Point | Fe total | P | S | $K_2O$ | $Na_2O$ | $DI_{-6.3}$ at 873 K | Bonding index at 1123 K | R at 1123 K |
| 0 | <62 | >0.08 | >0.05 | >0.18 | >0.04 | >3% | | |
| 1 | 62–65 | 0.05–0.08 | 0.03–0.05 | 0.10–0.18 | 0.02–0.04 | 2–3% | | |
| 2 | >65 | <0.05 | <0.03 | 0.03–0.10 | <0.02 | 1–2% | 25–35% | 50–60% |
| 3 | | | | <0.03 | | 0–1% | 15–25% | 60–70% |
| 4 | | | | | | | 5–15% | 70–80% |
| 5 | | | | | | | <5% | 80–90% |
| 6 | | | | | | | 0 | >90% |

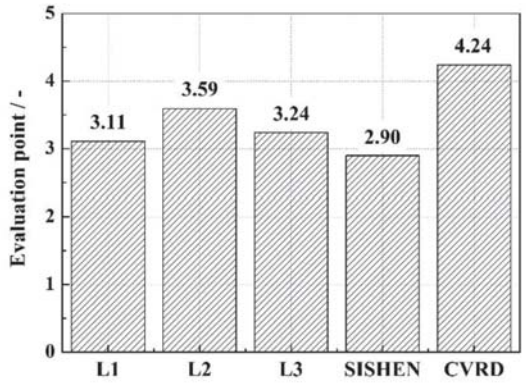


Figure 8—Evaluation scores for the iron ores

### *Schemes for iron ore blending and simulated industrial experiments*

To improve the reduction performance, inhibit the bonding behaviour of the lump ores, and control the production cost, based on the physicochemical and metallurgical properties of the iron ores in this study, five alternative schemes for optimizing the iron ore blend have been proposed and tested in COREX production experiments. The degree of reduction, metallization rate, and bonding index were measured to evaluate these blending schemes. The experimental procedures are shown in Figure 9. The ore blending schemes are shown in Table VI.

The experimental results are shown in Table VII. Compared with the original scheme, the degree of reduction, metallization rate, and bonding performance of schemes I, II and III were improved, whereas the degree of reduction and metallization rate of schemes IV and V decreased. The improved bonding behaviour was due to the decrease in the proportion CVRD pellets to 50%. The reduction degrees for schemes I, II, and III were higher than 90% and the metallization rates were higher than 85%, with scheme III the highest. However, the bonding index of scheme III was low. Sishen lump ore could therefore be totally replaced by a blend of L2 and L3 lump ores, as shown in scheme III. The defects of a single variety of iron ore and a high bonding index can be overcome by optimized iron-ore blending. The results confirm the effectiveness of the improved evaluation method for iron ores.

### *Industrial verification of iron ore blending scheme*

Due to the high metallization rate and low bonding index, blending scheme III was selected to conduct an industrial experiment to verify its effectiveness in COREX production. In order to maintain steady production without sudden changes to the burden structure, the proportion of blended L2 and L3 lump ores (in a 1:1 ratio) was increased progressively. Thus in the industrial trials, 20 and 40 mass% of Sishen lump ore were replaced by the L2 and L3 blend. The experiment results, including metallization rate and hydraulic pressure in the discharge equipment, for one month of production for original the scheme (60% CVRD, 40% Sishen), scheme A (60% CVRD, 20% Sishen, 20% blended L2 and L3), and scheme B (60% CVRD, 40% blended L2 and L3) are compared in Figure 10. It is shown that as the proportion of blended L2 and L3 increased from zero to 20% to 40%, the average metallization rate rose from 61.8% to 65.7% to 73.5%, indicating the improvement in productivity.

*Table VI*

**Ore blending schemes for the simulated COREX production experiments**

| Scheme | Original | I | II | III | IV | V |
|---|---|---|---|---|---|---|
| CVRD | 60% | 60% | 60% | 60% | 50% | 50% |
| Sishen | 40% | 20% | - | - | - | - |
| L1 | - | - | 20% | - | 30% | - |
| L2 | - | - | - | 20% | - | 30% |
| L3 | - | 20% | 20% | 20% | 20% | 20% |

*Table VII*

**Results for the simulated COREX production experiments**

| Scheme | Reduction degree (%) | Metallization rate (%) | Bonding index (%) |
|---|---|---|---|
| Original | 89.2 | 84.6 | 7.2 |
| I | 90.1 | 85.8 | 6.5 |
| II | 90.2 | 85.9 | 6.1 |
| III | 92.8 | 89.8 | 5.1 |
| IV | 82.5 | 75.0 | 5.6 |
| V | 85.4 | 79.1 | 4.9 |

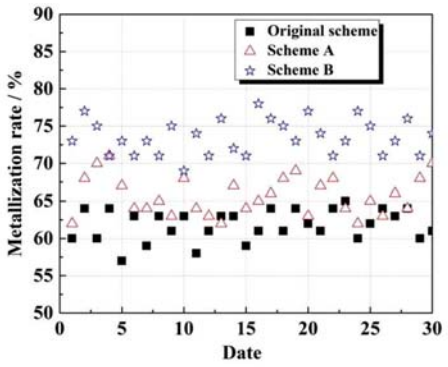


Figure 10—Metallization rates of iron ores in industrial production

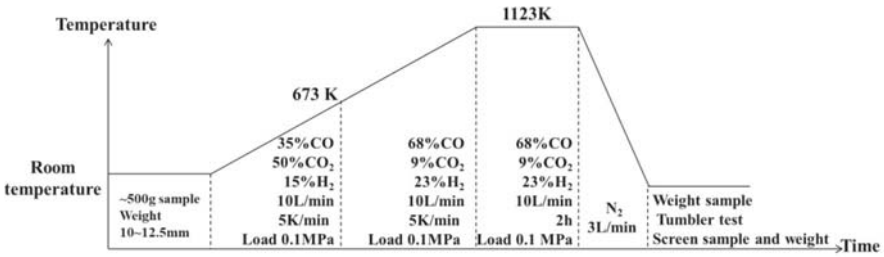


Figure 9—Procedures for simulated COREX production experiments

*Table VIII*

**Hydraulic pressure of screw equipment in the industrial experiment**

| Scheme | Hydraulic pressure of screw (MPa) | | | | | | | |
|---|---|---|---|---|---|---|---|---|
| | 1 | 2 | 3 | 4 | 5 | 6 | 7 | 8 |
| Original scheme | 3.11 | 2.75 | 2.66 | 3.10 | 3.33 | 2.76 | 2.70 | 2.97 |
| Scheme A | 2.87 | 2.71 | 2.80 | 3.07 | 2.69 | 2.55 | 2.49 | 2.71 |
| Scheme B | 2.75 | 2.60 | 2.60 | 2.65 | 2.40 | 2.39 | 2.28 | 2.54 |

Generally, the screw load in the lower part of the shaft furnace increases with the gradual bonding of the burden (Li *et al.*, 2013; Hou *et al.*, 2014). The average hydraulic pressure of each screw for one month in this study is shown in Table VIII. The hydraulic pressure decreased as the proportion of blended L2 and L3 increased, indicating that the bonding behaviour was inhibited, which benefited smooth production and reduced the amount of clean-up required. Both the production efficiency and safety were greatly improved. The laboratory and industrial experiments proved that blended L2 and L3 lump ores could effectively replace Sishen lump ore, which accounted for 40% of the burden weight, and be used in combination with CVRD pellets in COREX production.

## Conclusions

- In line with the conditions of industrial-scale COREX production, the highest experimental temperature, reduction time, and gas flow rate in the original evaluation system were modified to 1073–1173 K, 2 hours for reduction,, and 20 L/min per kilogram of iron ore, respectively. The amount of adhesive ore powder, low-temperature reduction degradation, and the thermal cracking propensity were included in the evaluation system.
- Thermal cracking indices $DI_{-10}$, $DI_{-6.3}$, and $DI_{-3.15}$ of all lump ores increased with increasing experimental temperature, with those of the L3 lump ore being the lowest at various temperatures.
- The reducibility and bonding behaviour of all the alternative lump ores were better than or similar to those of Sishen lump ore. The $RDI_{-3.15}$ of L1 was markedly lower, and the $RDI_{-3.15}$ of L3 was similar to that of Sishen lump ore. The $RDI_{-0.5}$ and $RDI_{-3.15}$ of L2 were higher than those of the Sishen lump ore, whereas the bonding behaviour of L2 was much better than that of the Sishen lump ore.
- Based on a comprehensive consideration of the three alternative lump ores, five new schemes for iron ore blending were tested under conditions simulating industrial-scale production. The results showed that the reducibility and bonding behaviour of blending ore could be improved by substituting Sishen ore with an alternative lump ore, especially by a blend of L2 and L3, without altering the proportion of CVRD pellets. The substitutability of the new lump ore blend and the effectiveness of the improved evaluation method for iron ores in the COREX process were verified in an industrial test.
- Compared with the original blending scheme, the metallization rate and the bonding behaviour were improved with increasing proportions of blended L2 and L3 lump ore from zero to 20% and 40% in the industrial trials.

## Acknowledgements

This work was supported by the National Natural Science Foundation of China under Grant nos. 51604201 and 51774217, and the scholarship from China Scholarship Council (CSC) under the Grant CSC no. 201708420228. We also thank Liwen Bianji, Edanz Group China (www.liwenbianji.cn/ac) for editing the English text of a draft of this manuscript.

## References

Eberle, A., Siuka, D., and Bohm, C. 2006. New Corex C-3000 plant for Baosteel and status of the Corex technology. *Stahl Und Eisen*, vol. 126, no. 3. pp. 31–39.

Hou, Q.F., Samman, M., Li, J., and Yu, A.B. 2014. Modeling the gas-solid flow in the reduction shaft of COREX. *ISIJ International*, vol. 54, no. 8. pp. 1772–1780.

International Organization for Standardization (ISO). 2017. ISO 8371-2007. Iron ores for blast furnace feedstocks - Determination of the decrepitation index. Geneva.

Kang, T., Gupta, S., and Sahajwalla, V. 2007. Characterizing swelling behaviour of iron oxides during solid state reduction for COREX application and their implications on fines generation. *ISIJ International*, vol. 47, no. 11. pp. 1590–1598.

Kumar, P.P., Barman, S.C., Reddy, B.M., and Sekhar, V.R. 2009. Raw materials for Corex and their influence on furnace performance. *Ironmaking &. Steelmaking*, vol. 36, no. 2. pp. 87–90.

Kurunov, I.F. 2010. The direct production of iron and alternatives to the blast furnace in iron metallurgy for the 21st century. *Metallurgist*, vol. 54, no. 5-6. pp. 335–342.

Li, H.F., Zhou, H., Zhang, T., You, Y., Zou, Z.S., and Xu, W.R. 2016. Influence of screw design on burden descending velocity and particle segregation in COREX shaft furnace. *Journal of Iron and Steel Research International*, vol. 23, no. 6. pp. 516–524.

Li, Q., Feng, M.X., and Zou, Z.S. 2013. Validation and calibration approach for discrete element simulation of burden charging in pre-reduction shaft furnace of COREX process. *ISIJ International*, vol. 53, no. 8. pp. 1365–1371.

Li, W.G. 2008. Operation status quo and technology problems of COREX-3000. *Proceedings of the Baosteel Biennial Academic Conference 2008, Bac.* pp. A-75-83.

Qiu, Z.L., Luo, Z.G., Zhou, H., Chen, R., Wang, F., and Zou, Z.S. 2017. Effect of screw casing structure on descending of burdens in COREX shaft furnace. *Journal of Iron and Steel Research International,* vol. 24, no. 1. pp. 18–26.

Song, H., Lv, X.P., and Yin, X.P. 2015. Analysis of sponge iron carburization behavior in COREX pre-reduction shaft furnace. *Research on Iron & Steel*, vol. 43, no. 5. pp. 9–11.

Standardization Administration of the People's Republic of China. 2017. GB/T13241-2017, Iron ores - Determination of reducibility.

Standardization Administration of the People's Republic of China. 2016. GB/T 6730.8-2016, Iron ores - Determination of iron (II) content - Potassium dichromate titrimetric method.

Umadevi, T., Kumar, P., Lobo, F.N., Prabhu, M., Mahapatra, P.C., and Ranjan, M. 2011. Influence of pellet basicity (CaO/SiO2) on iron ore pellet properties and microstructure. *ISIJ International*, vol. 51, no. 1. pp. 14–20.

Wu, S.L., Xu, H.F., and Zhang, Q. 2008. Study on the characteristics in shaft furnace of Corex-3000 process. *Proceedings of the Baosteel Biennial Academic Conference 2008*, A-102-107.

Wu, S.L., Wang, L.X., Kou, M.Y., Wang, Y.J., and Zhang, J.C. 2017. Analysis of operational parameters affecting the sulfur content in hot metal of the COREX process. *Metallurgical and Materials Transactions B*, vol. 48, no. 1. pp. 276–285.

*Wu, S.L., Liu, X.Q., Zhou, Q., Xu, J., and Liu, C.S.* 2011. Low temperature reduction degradation characteristics of sinter, pellet and lump ore. *Journal of Iron and Steel Research International*, vol. 18, no. 8. pp. 20–24.

Xu, J., Wu, S.L., Kou, M.Y., and Du, K.P. 2013. Numerical analysis of the characteristics inside pre-reduction shaft furnace and its operation parameters optimization by using a three-dimensional full scale mathematical model. *ISIJ International*, vol. 53, no. 4. pp. 576–582.

Xu, R.S., Zhang, J.L., Wang, G.W., Zuo, H.B., Li, P.C., Wang, H.Y., Lin, H., and Liu, S.Y. 2016. Isothermal kinetic analysis on fast pyrolysis of lump coal used in COREX process. *Journal of Thermal Analysis and Calorimetry*, vol. 123, no. 1. pp. s773–783.

You, Y., Luo, Z.G., Hou, Q.F., Li, H.F., Zhou, H., Chen, R., and Zou, Z.S. 2017. Experimental study of burden distribution in the COREX melter gasifier. *Steel Research International*, vol. 88, no. 12. https://onlinelibrary.wiley.com/doi/epdf/10.1002/srin.201700025.

Zhou, H., Wu, S.L., Kou, M.Y., Tang, B., Cheng, H.C., Zhang, Y.L., and Shen, Y.S. 2017. Solid flow in a shaft furnace in smelting reduction process under circumferential imbalance conditions. *Steel Research International*, vol. 88, no. 12. https://onlinelibrary.wiley.com/doi/epdf/10.1002/srin.201700212

Zhou, H., Luo, Z.G., Zou, Z.S., Zhang, T., and You, Y. 2015. Experimental study on burden descending behavior in COREX shaft furnace with AGD beams. *Steel Research International*, vol. 86, no. 9. pp. 1073–1081.

Zhou, X.L. and Du, Z.N. 2013. The introduction of COREX process development. *Advances in Materials Research*, no. 774-776. pp. 1430–1433. ◆

# PGM recovery from a pregnant leach solution using solvent extraction and cloud point extraction: a preliminary comparison

**L. Makua[1,2], K. Langa[1,2], C. Saguru[1,2], and S. Ndlovu[1,2]**

**Affiliation:**
[1]School of Chemical and Metallurgical Engineering, University of the Witwatersrand, South Africa.
[2]DST/NRF SARChI: Hydrometallurgy and Sustainable Development; University of the Witwatersrand, South Africa.

**Correspondence to:**
C. Saguru

**Email:**
tatendasaguruc@gmail.com

**Dates:**
Received: 24 Jun. 2018
Accepted: 3 Oct. 2018
Published: May 2019

**How to cite:**
Makua, L., Langa, K., Saguru, C., and Ndlovu, S.
PGM recovery from a pregnant leach solution using solvent extraction and cloud point extraction: a preliminary comparison.
The Southern African Insitute of Mining and Metallurgy

DOI ID:
http://dx.doi.org/10.17159/2411-9717/17/484/2019

ORCiD ID:
C. Saguru
https://orchid.org/0000-0002-6014-2495

## Synopsis

**Global demand for the three platinum group metals (PGMs) Pt, Pd, and Rh has been steadily growing due to their widespread use in emission control, industrial catalysis, and numerous other applications. The primary supply of PGMs is currently the mining industry. However, legislative, operational, and environmental challenges faced by many mining operations result in erratic supply patterns and deficits for these three metals. Naturally, recycling scrap material to recover Pt, Pd, and Rh has therefore aroused research interest in the scientific and engineering communities. Given that the majority of the global demand for these three metals is driven by emission control devices, autocatalytic converters are therefore a significant source of already processed and beneficiated PGMs for recycling.**

**Although pyrometallurgical processes dominate the recycling industry, hydrometallurgical processes may offer certain advantages, chief among these being lower emissions and reduced energy consumption. In this investigation, scrap converter material was leached in acidic chloride media and the leach liquor subjected to solvent extraction and cloud point extraction (CPE) to recover the PGMs. The recoveries for Pt and Pd using Alamine 308® dissolved in kerosene with decanol as a modifier were 95% and 81%, respectively. The maximum recoveries using CPE after complexation with 2-mercaptobenzothiazole (2-MBT) in the presence of Triton X-100 and tin (II) chloride dihydrate as a reductant were 97% for Pd, 96% for Pt, and 91% for Rh. This demonstrates that CPE, although relatively new, may have some potential as a breakthrough PGM recovery technology.**

**Keywords**
**platinum group metals, recycling, hydrometallurgy, chloride leaching, solvent extraction, cloud point extraction.**

## Introduction

Platinum group metals (PGMs) have found a wide variety of applications in different industries due to their chemical, catalytic, and physical properties. PGMs are essential in automobile emission abatement, petroleum refining, and the pharmaceutical and electrical industries (Carabias-Martınez *et al.*, 2000). However, the abundance of PGMs in the Earth's crust is low and their primary sources are fast depleting (Crundwell *et al.*, 2011).

The high demand for PGMs, together with social, economic, environmental, and political aspects related to their production, has led to concerns about their future supply. This has resulted in renewed interest in recycling end-of-life material. PGM supply from recycling has doubled over the last decade, and currently contributes 22% to global supply (Johnson Matthey, 2016). This is in part due to the environmental, social, and operational challenges associated with mining of PGMs. For example, labour unrest, energy cuts, declining commodity prices, and declining ore grades have collectively made the mining landscape economically challenging (KPMG, 2015). On the other hand, the high content of PGMs in secondary sources makes their recovery from the increasing quantities of waste products important from a resource conservation viewpoint. Moreover, PGMs obtained through recycling have been demonstrated to have a 1% environmental cost from a life-cycle perspective, whereas PGMs obtained from mining contribute the remaining 99% of environmental cost (Bossi and Gediga, 2017). Sustainable resource recovery and the economic incentive of recycling have therefore been major drivers to justify investment in PGM recycling. The autocatalytic converter industry accounts for about 70% of the global consumption of these metals (Johnson Matthey, 2016) and therefore recycling spent converters has become a major source of Pt, Pd, and Rh (Figure 1).

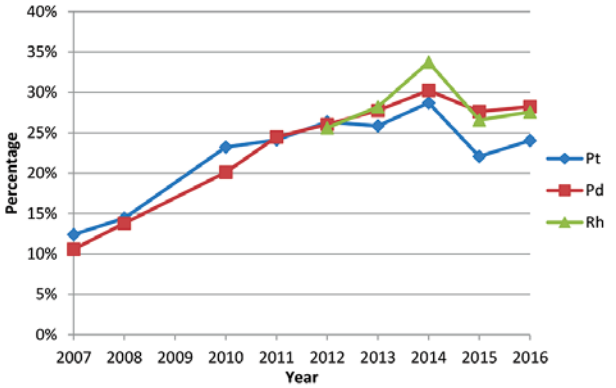


**Figure 1—Contribution of PGM recycling to global supply from 2007 to 2016 (Johnson Matthey, 2016)**

In the light of all these considerations, there have been concerted efforts to develop more efficient and more sustainable processes for the recovery of PGMs from secondary sources. Iodide complexation was investigated by Zanjani and Baghalha, (2009), and cyanide complexation by Chen and Huang, (2006) for leaching Pt, Pd, and Rh. Saguru and Ndlovu (2017) developed a leaching process for catalytic converters using acidic chloride media, which attained recoveries of 15%, 78%, and 86% for Rh, Pt, and Pd respectively.

Solvent extraction (Nguyen, Kumar, and Lee, 2016, Nguyen, Sonu, and Lee, 2016, Gandhi *et al.*, 2015), ion exchange resin technology, classical precipitation (Crundwell *et al.*, 2011) and more recently, cloud point extraction (CPE) (Suoranta *et al.*, 2015) have been investigated for PGM recovery from chloride leach liquors. CPE has been used for the analytical determination of metals at low concentration, and due to the nature of the chemicals used, has been touted as a more environmentally friendly option. It was intended in this study to investigate the potential for recovering Pt, Pd, and Rh from a leach solution using CPE and then compare it to the more mature solvent extraction technology.

Solvent extraction (SX) refers to the distribution of a species between two liquid phases based on differences in solvation energies or relative affinities for the species. SX is a mature technology in the metal extraction industry, which nonetheless still has some operational demerits. The use of volatile solvents creates unsafe working conditions, and extractants are often expensive, translating to high operating expenditure. The technology has, however, been in the industry for over 50 years, and is well understood. Newer alternatives over the years have included ion exchange resins (Nikoloski and Ang, 2014), molecular recognition technologies (Izatt *et al.*, 2015), and more recently CPE (Suoranta *et al.*, 2015).

CPE is a technique used to preconcentrate and separate many different elements in biological and chemical systems. Much of the development and applications have dealt with the extraction and preconcentration of inorganic solutes. CPE has recently attracted a lot of attention, mainly because it is premised on 'green' sustainable chemistry.

CPE generally involves the following steps; forming neutral compounds of analytes with a chelating agent, extraction of these hydrophobic compounds to micelles formed by adding a surfactant, and separation of the surfactant-rich and aqueous phases by heating the system above its cloud point temperature (Hayes, 1993). The technique has been employed by analytical chemists as a preconcentration step in sample preparation for trace element analysis. Suoranta *et al.*, (2015) used CPE to extract PGMs from a leach solution after microwave-assisted leaching. The underlying principles of CPE in the extraction of PGMs from leach solutions were reviewed by the authors. It was concluded that the efficiency of the CPE method depends on the pH of the solution, surfactant and complexing agent, hydrochloric acid concentration, and the presence of a reducing agent.

It was therefore the purpose of this research to conduct a preliminary comparison of using Alamine 308® in kerosene for SX with CPE using 2-mercaptobenzothiazole (2-MBT) in the presence of Triton X-100 and tin (II) chloride dihydrate. The underlying chemistry for both extraction schemes is presented in the following section.

### *Chemistry of PGM solvent extraction*

Nguyen, Kumar, and Lee (2016) illustrated the potential for using tri-iso-octylamine (Alamine 308) to recover Pt (IV), Pd (II), and Rh (III) from a synthetic acidic chloride solution. We sought to investigate the performance of tri-iso-octylamine in a real leach solution. Tri-iso-octylamine is a tertiary amine with three alkyl ($-C_8H_{17}$) groups surrounding a single nitrogen atom. Metal extraction using tri-iso-octylamine occurs via protonation and anion exchange. Consequently, tri-iso-octylamine will only extract PGMs from acidic solutions. In the presence of an acid solution, for example in HCl, the basic N atom in the amine structure reacts with the excess protons and forms an amine salt according to Equation [1].

$$[R_3N]_{(org)} + HCl_{aq} \leftrightarrow R_3NH^+Cl^-_{(org)} \quad [1]$$

When this organic intermediary salt is in the vicinity of Pt-chloro anions, it exchanges its $Cl^-$ anion for the $PtCl_62^-$ anion group:

$$2R_3NH^+Cl^-_{(org)} + PtCl_6{}^{2-}_{(aq)} \leftrightarrow (R_3NH^+)_2PtCl_6{}^{2-}_{(org)} + 2Cl^-_{(aq)} \quad [2]$$

The required anion is thereby extracted into the organic phase.

### *Chemistry of PGM extraction using cloud point extraction*

The mechanisms CPE are complex and not yet fully understood (Yu *et al.*, 2010). However, in essence CPE involves the transfer of a surfactant from one liquid phase to another by heating the system above its cloud point temperature (CPT). The surfactant molecules form micelles at their critical micelle concentration (CMC). On increasing the temperature of the solution, the micelles are dehydrated and therefore accumulate (Yu *et al.*, 2010). This results in the phase separation of the solution into a surfactant-micelle-rich phase and a surfactant-poor phase (aqueous phase). The surfactant concentration and temperature are manipulated to extract solutes into the micelle phase (Streat, 1999). Consequently, metal ions can be preconcentrated and/or separated from an aqueous solution using CPE.

## Experimental methodology

The experimental work consisted of two parts, the solvent extraction experiments and the CPE experiments. A leach solution was obtained following the work conducted by Saguru and Ndlovu, (2017), in which an autocatalytic converter was crushed, ground, homogenized, and leached in an acidic chloride medium. The leach solution used for the extraction experiments assayed 22 ppm Pt, 408 ppm Pd, and 11 ppm Rh.

### *Solvent extraction experiments*

Pt and Pd were co-extracted using Alamine 308 dissolved in kerosene with a 5% v/v n-decanol modifier following the method of Nguyen, Kumar, and Lee (2016). Based on preliminary experiments, it was determined that an acidification procedure was necessary prior to extraction, and as such HCl was used to acidify the pregnant leach solution. In these acidification experiments, 15 mL of the pregnant leach solution was added to 5 mL of hydrochloric acid at five different concentrations. The acidified solutions were then individually mixed with 20 mL of 0.1 M organic Alamine 308 in kerosene and shaken on a reciprocal shaker for 30 minutes at 300 r/min and room temperature. After shaking, the two layers were allowed to settle and separate into an organic and an aqueous phase. The aqueous phase was submitted for analysis and the percentage extraction calculated using mass balances.

Once the acidification concentration that produced a maximum extraction was determined, 750 mL of the pregnant leach liquor was mixed with 250 mL of acid at the chosen concentration to form a bulk solution for subsequent extraction experiments. In the second round of solvent extraction experiments, 20 mL of the acidified aqueous PGM solution was added to 20 mL of the organic solution at different concentrations, mixed for 30 minutes using a reciprocating shaker at 300 r/min, and allowed to settle. The two phases were separated by decanting and the aqueous phase sent for analysis, with percentage extraction calculated by mass balances. All experiments were duplicated.

### *Cloud point extraction experiments*

Solutions of 10% m/v Triton X-100, 10% m/v tin (II) chloride in 6 M hydrochloric acid, 4 M NaOH, and 0.5 M ammonium hydroxide were prepared by dissolution in distilled water following the method of Suoranta *et al.* (2015). To the ammonium hydroxide solution, 1% m/v 2-mercaptobenzotiazole (2-MBT) was added to prepare the stock 2-MBT solution.

20 mL of pregnant leach solution was first diluted using water (the dilution ratio varied between 1 and 33) and then pipetted into 50 mL centrifuge tubes. 2 mL of the previously prepared Triton X-100 solution and 1 mL of 2-MBT solution were added to the centrifuge tubes and the solutions allowed to stand for 15 minutes, after which 1.5 mL of the prepared tin (II) chloride solution was added. The open centrifuge tubes were then placed in a thermostat-controlled water bath at 90°C. The solutions were heated in the water bath for 25 minutes and then held at 90°C for 120 minutes. A refrigerator set at 8°C was used to cool the solutions for 30 minutes, followed by further cooling in a freezer set to –10°C for 15 minutes. The aqueous phase was then separated from the surfactant-rich phase by decanting, and sent for analysis.

In this set of experiments, the dilution factor and starting pH were varied to obtain an optimum dilution ratio and pH. Once these were established, the additions of Triton X-100 (0.25 mL to 2 mL), 2-MBT (0.5 mL to 3 mL), equilibration temperature (70°C to 95°C) and incubation time (30 minutes to 130 minutes) were varied to identify their effects on PGM extraction efficiency. All experiments were duplicated.

## Results and discussion

### *Solvent extraction results*

#### *Effect of HCl concentration on PGM recovery*

The effect of HCl concentration on PGM extraction is presented in Figure 2.

The extraction of Pt and Pd is directly correlated to the amount of excess $H^+$ ions available to protonate the amine complex. As such, it was expected that increasing the HCl concentration would result in an increase in Pt and Pd co-extraction into the organic phase.

Increasing HCl concentration is also expected to increase the proportion of non-hydrated PGM chloro-complexes in the pregnant leach solution. Hydrated PGM chloro-complexes are chloro-complexes in which one or more of the chloride ions have been substituted by a hydroxide ion. The amount of hydrated PGM chloro-complexes increases with increasing pH of solution. Hydrated PGM chloro-complexes are hydrophilic – *i.e.* they attract more water molecules around each hydrated chloro-complex. This increases the solvation layer of the complex, which translates to fewer coulombic interactions between the protonated amine complex and the negative PGM chloro-complex. The decreased strength of attraction reduces the efficiency of extraction of the hydrated PGM chloro-complex into the organic phase. Decreasing the pH, by adding concentrated HCl, was therefore expected to reduce the proportion of hydrated PGM chloro-complexes, which increased PGM extraction as illustrated in Figure 2. An HCl concentration of 5 M, with an acidification volume ratio of PGM aqueous solution to acid of 3:1 was then chosen for the subsequent organic extractant concentration experiments.

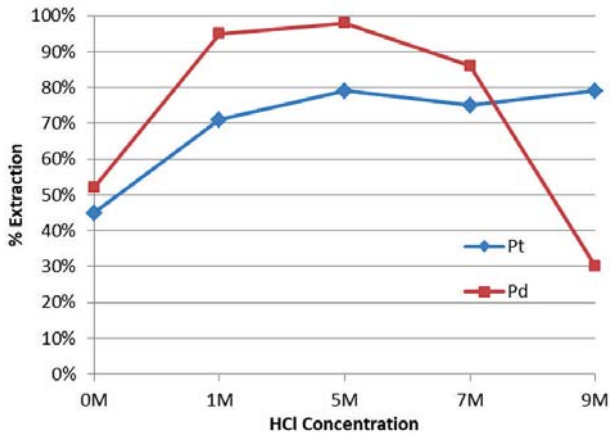


**Figure 2—Effect of [HCl] on PGM extraction ([Alamine 308] = 0.01 M in kerosene, 5% v/v decanol, 30 minutes' shaking time at 300 r/min, 1:1 O/A volume ratio)**

### *Effect of Alamine 308 concentration on PGM recovery*

An increase in the extractant concentration resulted in an increase in PGM extraction, peaking at 0.1 M concentration as shown in Figure 3. For all organic acid concentrations, it was also observed that Pt extraction was consistently higher than Pd extraction, which is in agreement with results obtained by Nguyen, Kumar, and Lee (2016). The $PdCl_4^{2-}$ ion has a higher charge density than $PtCl_6^{2-}$. It is therefore highly polarizing and attracts water molecules. This increases its solvation layer and reduces the strength of attraction between the $PdCl_4^{2-}$ anion and the slightly positive end of the protonated amine, much like how hydration reduces attraction as explained in the previous section. This therefore reduces the degree of extraction of the Pd chloro-complex into the organic phase, compared to the Pt chloro-complex.

## *Cloud point extraction results*

### *Effect of dilution ratio*

CPE has previously been applied for analytical purposes in low concentration ranges. In order to apply the technique to PGM leach liquor, a dilution factor had to be established. From Figure 4, it can be observed that the recovery increases with an increase in dilution factor. At a dilution factor of unity, the recoveries were not quantitative. The concentrations of the analytes were too high and therefore most of the analytes could not successfully be extracted and entrapped in the micelles. PGM extraction peaked at a dilution factor of seven, as illustrated in Figure 4, and this dilution factor was used for the rest of the tests.

### *Effect of pH*

The pH is a critical parameter for the complexation of metal ions and the coacervation of the micelles (Bezerra, Arruda, and Ferreira, 2005). Figure 5 shows the effect of pH on the recovery of PGMs.

The effect of pH was investigated in the range 2–8. At a pH of 2, the recoveries for all the PGMs were below 45%. The recoveries increased with increasing pH value, with recoveries around

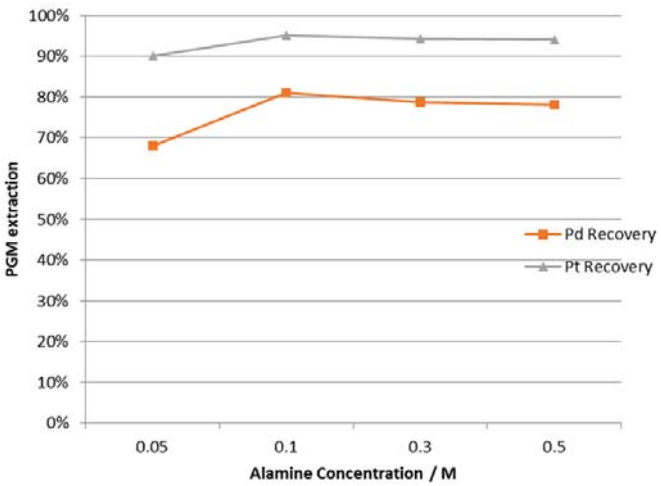


**Figure 3—Effect of [Alamine 308] on PGM extraction (dissolved in kerosene with 5% v/v decanol, 30 minutes' shaking time at 300 r/min, 1:1 O/A volume ratio)**

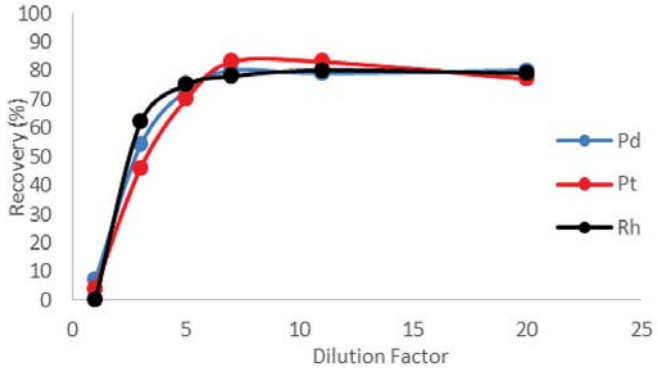


**Figure 4—Effect of dilution factor on PGM extraction**

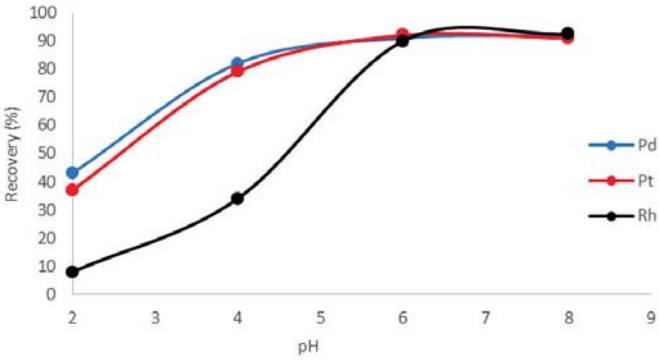


**Figure 5—Effect of pH on PGM extraction**

90% for all PGMs at pH 6. There was no significant change in recoveries with a further increase in pH .

The pH of the solution affects the overall charges of the PGM-chloro complexes and therefore affects the formation of metal complexes. The optimal pH range matches the range most favourable for complex formation, but should still be lower than the pH range for precipitation of the metals. The low recoveries at acidic conditions are due to the fact that complexation is weak under acidic conditions. Under acidic conditions, the metal ions compete with hydrogen ions for binding with the complexing agent, therefore resulting in lower recoveries. At lower pH values the micelles are also easily destroyed, reducing the system's entrapping capability. The pH was set to 6 for the rest of the tests.

### *Effect of amount of surfactant*

Triton X-100 was chosen as the surfactant because of its commercial availability, stability, low toxicity, low cost, and low cloud point temperature. Figure 6 shows the effect of Triton X-100 dosage on the PGM recoveries. At a dosage of 0.25 mL, recoveries were below 50%. An increase in surfactant dosage resulted in an increase in recoveries until a dosage of 1 mL, after which the recoveries remained constant despite increasing surfactant dosage. High recoveries above 80% were achieved at a dosage range of 1–2 mL. The low recoveries at a low dosage of 0.25 mL were due to the surfactant concentration being too low to form an adequate number of micelles with an adequate aggregation number to entrap the hydrophobic metal complexes quantitatively. With increasing surfactant concentration, the aggregation number of the formed micelles

increased, which resulted in an increase in recoveries until a dosage of 1 mL, where the micelles were able to successfully entrap most of the complexes. A further increase in surfactant dosage resulted in no significant change in the recoveries. The for surfactant dosage was therefore set to 1 mL.

### *Effect of amount of 2-MBT complexing agent on PGM extraction*

2-MBT was chosen as the complexing agent because it produces sufficiently hydrophobic complexes with PGM-chloro complexes and it is selective for the PGMs. The complexing agent dosage was investigated in the range 0.25–3 mL. From Figure 7, it can be observed that the recovery of the complexes increases with an increase in complexing agent dosage. Above a dosage of 1 mL the recoveries remained constant. The low recoveries at a low dosage of 0.25 mL were due to insufficient complexing agent for reaction with all the PGMs. Above a dosage of 1 mL, the recoveries remained constant because the complexing agent was now in excess. Initially, the recoveries of rhodium were very low compared to the other PGMs. This is probably due to the fact that rhodium is very inert and the probability of it reacting with a very small amount of the complexing agent is low. The amount of complexing agent was therefore set to 1 mL.

### *Effect of equilibration temperature and incubation time*

It is desirable to employ the lowest possible equilibration temperature and shortest incubation time from a process economics and productivity viewpoint. From Figure 8 it can be observed that the recoveries increase with an increase in equilibration temperature up to 90°C, and decrease above 90°C. Below 90°C, the system has not reached its cloud point temperature, which is why recoveries are lower. Temperature is the driving force for phase separation. When the system is below its cloud point temperature the phase separation between the bulk aqueous phase and the surfactant-rich phase is incomplete, and therefore some of the complexes are still in the aqueous phase. At 90°C the system is above its cloud point temperature, which explains the maximum recoveries achieved. Above 90°C the recoveries begin to decrease due to the decomposition of the metal complexes at temperatures higher than the cloud point temperature. The optimum equilibration temperature was therefore set to 90°C.

Figure 9 show that an increase in incubation time resulted in an increase in recoveries. At an incubation time of 30 minutes the recoveries were very low. The maximum recoveries were achieved after 120 minutes. The gravitational settling of the micelles with the attainment of cloud point temperature to form a surfactant-rich phase depends on the time for complete phase separation. The optimum incubation time was chosen as 120 minutes.

The optimum parameters found in each test conducted were combined and tested again in a duplicate experiment which attained recoveries of 97% for Pd, 96% for Pt, and 91%, for Rh.

### ***Comparison between solvent extraction and cloud point extraction, and recommendations for further test work***

CPE has been used substantively in analytical test work. Recently, due to its environmental competitiveness, it has been

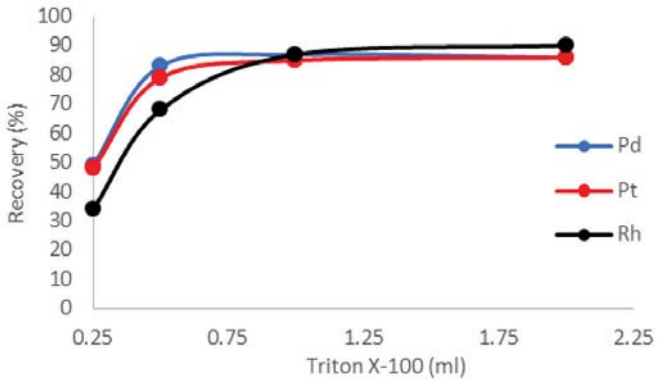


Figure 6—Effect of amount of surfactant on PGM extraction

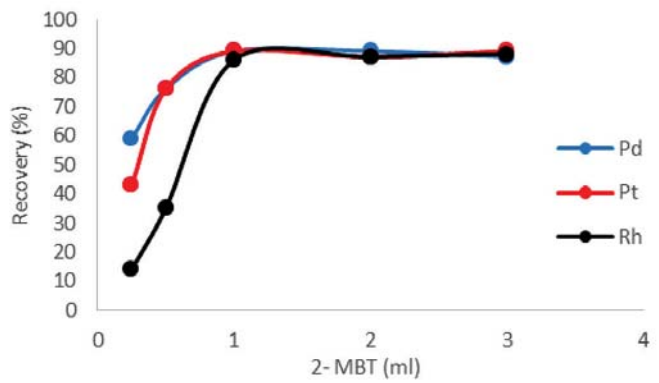


Figure 7—Effect of amount of 2-MBT on PGM extraction

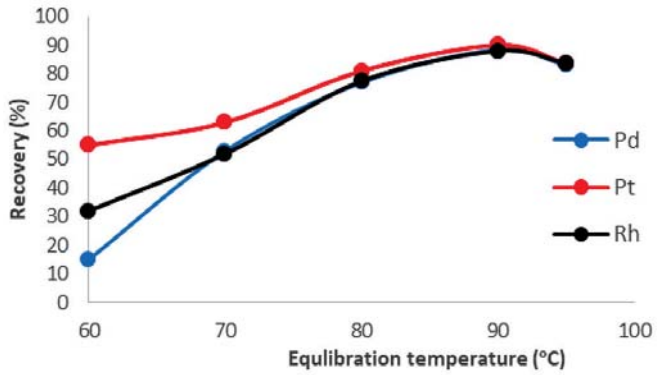


Figure 8—Effect of equilibration temperature on PGM extraction.

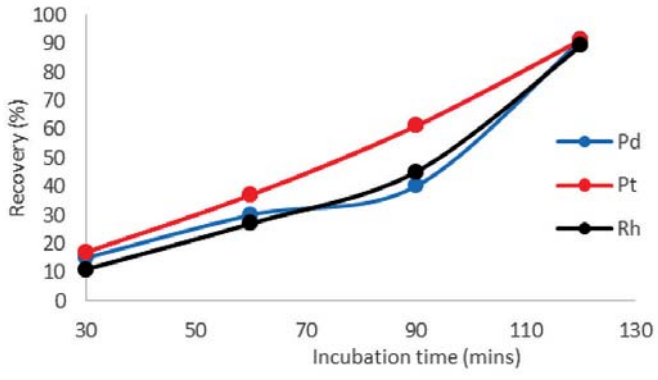


Figure 9—Effect of incubation time on PGM extraction

shown to be a viable contender for PGM extraction, at least, at the bench scale. In this work, high recoveries were obtained using both CPE and solvent extraction. However, with CPE all the PGMs were extracted in a single step – which may or may not be an advantage. The advantage is that for operations that are in the middle of the value chain, CPE could be used to extract all PGMs into one phase before collective precipitation. The crude precipitate would then be sold to operations that are at the end of the value chain for final metal separation. However, metal stripping tests have not yet been conducted; therefore the selective separation of the metals is not well understood. In contrast, solvent extraction technologies are well understood. For example, it is known that Pt and Pd could be selectively stripped from the Alamine 308 organic solution using HCl and thiourea (Nguyen, Kumar, and Lee, 2016). In order for more comprehensive comparisons to be conducted, not only between CPE and solvent extraction, but also between CPE and any other recovery technology, there will be a need for comprehensive studies into the science and engineering of CPE.

For this preliminary study, the methodology of changing one factor at a time was employed, which is rather limited in terms of statistical robustness of the results. We therefore suggest the use of response surface methodology for statistical design in further test work. This research was aimed at providing an insight on the performance of this relatively new technology in a real leach solution for PGM extraction.

It was also established that CPE works best at low PGM concentrations, and therefore concentrated solutions may require dilution. Although this study was limited to the recovery of PGMs from an autocatalytic converter leach solution, CPE could be investigated for application on other low-concentration solutions, such as tailings solution streams. It is also imperative to investigate the extent of entrainment of other metal solutions before CPE can be seriously considered in the PGM extraction industry.

It is therefore recommended that further test work be conducted on CPE for PGM extraction, with the ultimate goal of comparing it against mature technologies like solvent extraction through piloting, cost-benefit analyses, and process costing. This work has illustrated that CPE could be a potential technology for recovery of PGMs.

## Conclusions

Cloud point extraction using Triton X-100 as a surfactant and 2-mercaptobenzothiazole as the complexing agent was successfully used to extract PGMs from leach solutions. Although the results indicate that the CPE technique is feasible, much more work is required to compare CPE with existing extraction methods. CPE offers an attractive alternative to conventional extraction methods by reducing the consumption of, and exposure to, the solvents, disposal cost, and increasing environmental sustainability. CPE offers several advantages over conventional solvent extraction, ion exchange, and precipitation processes, including simplicity, safety, low cost, high concentration factors, and high recovery and selectivity.

## Acknowledgements

The authors wish to acknowledge the National Research Fund and Department of Science and Technology, South Africa for funding this research work.

## References

Bezerra, M. de A., Arruda, M.A.Z., and Ferreira, S.L.C. 2005. Cloud point extraction as a procedure of separation and pre concentration for metal determination using spectroanalytical techniques: A review. *Applied Spectroscopy Reviews*, vol. 40. pp. 269–299. https://doi.org/10.1080/05704920500230880

Bossi, T. and Gediga, J. 2017. The environmental profile of platinum group metals. *Johnson Matthey Technology Review*, vol. 61. p. 111. https://doi.org/doi:10.1595/205651317x694713

Carabias-Martinez, R., Rodriguez-Gonzalo, E., Moreno-Cordero, B., Perez-Pavon, J., Garcia-Pinto, C., and Fernandez Laespada, E. 2000. Surfactant cloud point extraction and preconcentration of organic compounds prior to chromatography and capillary electrophoresis. *Journal of Chromatography*, vol. A 902. pp. 251–265.

Chen, J. and Huang, K. 2006. A new technique for extraction of platinum group metals by pressure cyanidation. *Hydrometallurgy*, vol. 82. pp. 164–171. https://doi.org/10.1016/j.hydromet.2006.03.041

Crundwell, F.K., Moats, M.S., Ramachandran, V., Robinson, T.G., and Davenport, W.G. 2011. Extractive Metallurgy of Nickel, Cobalt and Platinum-group Materials. Elsevier, Amsterdam, Boston.

Hayes, P.C. 1993. Process Principles in Minerals and Materials Production. Hayes Publishing, Brisbane, Australia.

Izatt, R.M., Izatt, S.R., Izatt, N.E., Krakowiak, K.E., Bruening, R.L., and Navarro, L. 2015. Industrial applications of molecular recognition technology to separations of platinum group metals and selective removal of metal impurities from process streams. *Green Chemistry*, vol. 17. pp. 2236–2245. https://doi.org/10.1039/C4GC02188F

Johnson M. 2016. PGM market report May 2016, Supply and demand in 2015.

KPMG. 2015. Commodity insights bulletin (Insight). KPMG.

Nguyen, T.H., Kumar, B.N., Lee, and M.S. 2016. Selective recovery of Fe(III), Pd(II), Pt(IV), Rh(III) and Ce(III) from simulated leach liquors of spent automobile catalyst by solvent extraction and cementation. *Korean Journal of Chemical Engineering*, vol. 33. pp. 2684–2690. https://doi.org/10.1007/s11814-016-0123-5

Nguyen, T.H., Sonu, C.H., and Lee, M.S. 2016. Separation of Pt(IV), Pd(II), Rh(III) and Ir(IV) from concentrated hydrochloric acid solutions by solvent extraction. *Hydrometallurgy*, vol. 164. pp. 71–77. https://doi.org/10.1016/j.hydromet.2016.05.014

Nikoloski, A.N. and Ang, K.-L. 2014. Review of the application of ion exchange resins for the recovery of platinum-group metals from hydrochloric acid solutions. *Mineral Processing and Extractive Metallurgy Review*, vol. 35. pp. 369–389. https://doi.org/10.1080/08827508.2013.764875

Rajiv Gandhi, M., Yamada, M., Kondo, Y., Shibayama, A., and Hamada, F. 2015. Selective extraction of Pd(II) ions from automotive catalyst residue in $Cl^-$ media by O-thiocarbamoyl-functionalized thiacalix[n]arenes. *Hydrometallurgy*, vol. 151. pp. 133–140. https://doi.org/10.1016/j.hydromet.2014.11.017

Saguru, C. and Ndlovu, S. 2017. Preliminary study on PGM leaching from used autocatalytic convertors using $AlCl_3$ and HOCl. *Proceedings of the European Metallurgical Conference 2017. Production and Recycling of Non-Ferrous Metals: Saving Resources for a Sustainable Future*, GDMB, Leipzig, Germany. pp. 55–70.

Suoranta, T., Zugazua, O., Niemelä, M., and Perämäki, P. 2015. Recovery of palladium, platinum, rhodium and ruthenium from catalyst materials using microwave-assisted leaching and cloud point extraction. *Hydrometallurgy*, vol. 154. pp. 56–62. https://doi.org/10.1016/j.hydromet.2015.03.014

Yu, F., Xi, C., He, Z., and Chen, L. 2010. Development of cloud point extraction for simultaneous extraction and determination of platinum and palladium using inductively coupled plasma optical emission spectrometry in platinum-palladium spent catalysts. *Analytical Letters*, vol. 43. pp. 972–982. https://doi.org/10.1080/00032710903491112

Zanjani, A. and Baghalha, M. 2009. Factors affecting platinum extraction from used reforming catalysts in iodine solutions at temperatures up to 95°C. *Hydrometallurgy*, vol. 97. pp. 119–125. https://doi.org/10.1016/j.hydromet.2009.02.001 ◆


# Rock properties and machine parameters evaluation at Rössing Uranium Mine for optimum drill performance

**B. Adebayo[1,2] and J.G.M. Mukoya[1]**

**Affiliation:**
[1]Department of Mining and Metallurgical Engineering, University of Namibia.
[2]Department of Mining Engineering, Federal University of Technology, Akure.

**Correspondence to:**
B. Adebayo

**Email:**
baayoakinola@googlemail.com

**Dates:**
Received: 2 May 2017
Revised: 19 May 2018
Accepted: 6 Aug. 2018
Published: May 2019

**How to cite:**
Abebayo, B. and Mukoya, J.G.M. Rock properties and machine parameters evaluation at Rössing Uranium Mine for optimum drill performance.
The Southern African Insitute of Mining and Metallurgy

DOI ID:
http://dx.doi.org/10.17159/2411-9717/17/155/2019

ORCiD ID:
B. Abebayo
https://orchid.org/0000-0001-8954-5768

## Synopsis

**This work was carried out to determine the influence of rock properties and drilling machine parameters on the penetration rate at the SJ pit of Rössing Uranium Mine, Namibia. Rock properties (uniaxial compressive strength, tensile strength, and modulus of elasticity) of samples collected were determined in the laboratory. Drilling experiments were conducted in which feed pressure, air pressure, rotary speed, weight on the bit, and torque were varied to measure their effect on the penetration rate. The uniaxial compressive strength varied from 90–180 MPa for layered marble-quartzite and banded gneiss. Increases in feed pressure, weight on the bit, and rotary speed beyond the optimum level led to a decrease in penetration rate and caused the drill bit to 'stall'. Results of the study revealed that penetration rate increases with an increase in the feed pressure and air pressure. After reaching a maximum value, the penetration rate begins to decrease despite increasing feed pressure. A very high torque causes the drill bit to stall, since the feed pressure is too high and the air pressure is not sufficient to remove the cuttings from blast-hole at maxium bailing velocities. The average penetration rate varied from 19 to 45 m/h for phase 2 of the pit, and from 17 to 68 m/h for phase 3. The optimum drilling machine parameters obtained in phase 2 and phase 3 were slightly lower than those currently being used at the mine. The trials of the optimum machine parameters will assist in reducing the cost of drilling, which varied from N$29.48 to N$36.31 per metre for the tricone bit.**

**Keywords**
**rotary drilling, machine parameters, rock properties, penetration rate.**

## Introduction

Drilling and blasting contribute most to the operational cost in opencast mining and have the potential to influence the cost of downstream operations (Aipanda, 2011). The drillability of rocks depends not only on the rock properties, but also on the drilling tools and operational variables. In rotary drilling, rotational speed, thrust, and flushing are the operational variables, and are known as the controllable parameters. Rock properties and geological conditions are the uncontrollable parameters. Although, many attempts have been made to correlate drillability with rock properties, the rock characteristics affecting rotary drilling have not been entirely defined (Hartman, 1962; Kahraman, Bilgin, and Feridunoglu, 2003). The drill bit is forced into a rock surface from the rotary power head, hence creating stresses and cracks at the bit-rock interface. The performance of a particular bit in any formation is dependent on the properties of the rock and drill operating parameters (Adebayo and Akande, 2015).

The response to this stress field depends on the rock type and loading system. Kahraman, Bilgin, and Feridunoglu (2003) discovered that around the contact of the button with the rock a new state of stress is initiated. Around the contact four important destruction mechanisms can be distinguished: under the bit button a crushed zone of fine rock powder is formed (impact); starting from the crushed powder zone, radial cracks are developed (induced tensile stress); when the stress in the rock is high enough, larger fragments of the rock can be sheared off between the button grooves (shear stress) (Ozdemir, 1977). The penetration rate is considered as one of the primary factors that affect drilling costs and hence it must be given prior consideration when planning for the optimization of a drilling operation. The subject of the penetration rate has been extensively analysed from both the theoretical and the experimental standpoints with the objective of maximizing penetration rate and improving operating efficiencies (Lummus, 1969).

Clark and Shafto (1987) presented theoretical bit torque relationships derived by testing many types of rocks with coring and non-coring bits. They found that the penetration rate increases with torque and a critical value of torque exist, below which penetration does not occur. Increasing the fluid flow rate also results in an increase in the differential pressure (Garnier and Lingen, 1959). However, a drill has an optimum weight-on-bit (WOB) for maximum penetration which corresponds to proper indentation at

the bit-rock interface. The optimum WOB also depends on the other optimal drilling conditions (Clark 1979). An increase in the bit rotary speed results in greater wear on the bit and may even cause chattering, micro-chipping, and cracking of the cutting indenters or teeth of the bit. The rotational speed may be restricted by the stability of the rig and the drill rods (Clark 1979).

The function of thrust in rotary-percussive drilling is to ensure that the percussion energy is transmitted to the rock. The relationship between thrust and penetration rate has been studied by Sinkala (1989) and Pearse (1985), who found that penetration rate increases with thrust until a peak penetration rate value is reached. The researchers suggested that as the thrust increases further the penetration rate will drop until the drill finally stalls. In addition, at low thrust the bit will not be in constant contact with the bottom of the hole. Low thrust results in free rotation of the bit and poor chip formation, and at higher thrust the torque required for bit rotation increases and sometimes reduces (Sinkala 1989). Excessive feed pressure in jointed rock causes rods to jam in weak rocks. The bit action cannot break the rock sufficiently for chip removal by the flushing medium, which results in a low penetration rate (Tandanand and Unger, 1975). The amount of reflected stress energy will depend on the rock properties and the magnitude of applied feed force. The feed force causes the bit to move back in contact with the rock before the next piston blow occurs (Jiao, 1989). An increase in air pressure improves the cleaning of the hole, and this consequently leads to a higher penetration rate. High loading forces may be due to excessive feed force, hardness of the rock, and improper cleaning of the hole; however, high torque will affect the machine performance (Nguyen 2011).

The majority of drill rig operators do not take into account the effect of adjusting drilling machine parameters in softer and harder rock formations. This leads to excessive bit wear, reduced penetration rate, breaking of roller cones and deck bushes, and straining of the rods and stabilizers. Therefore, there will be an increase in the drilling costs due to the reduction in the life of the drill consumables coupled with the longer time needed for drilling a blast-hole. The objectives of this paper are to determine the properties (strength parameters and Young's modulus) of selected rocks; measure machine parameters (air pressure, rotational speed, feed pressure, torque, weight on the bit); evaluate the penetration rates; and determine optimum machine parameter for improved drill performance.

## Description of the study area

Rössing Uranium is located 70 km inland from the coastal town of Swakopmund in the Erongo region of Namibia, and 12 km from Arandis (Rössing Uranium, 2013) as shown in Figure 1.

## Materials and methods

### *Determination of point load strength index*

Point load strength was determined following the standard method suggested by ISRM using Equation [1] (ISRM, 1989).

$$I_S = \frac{P}{D^2} \quad [1]$$

where $P$ is the load exerted on the sample (kN), and $D$ is the diameter of the sample (mm).

### *Determination of uniaxial compressive strength*

The uniaxial compressive strength test was carried out in accordance with the standard method suggested by ISRM (1989). The uniaxial compressive strength was determined using Equation [2].

$$UCS\ (MPa) = \frac{P}{A} \quad [2]$$

where UCS is the uniaxial compressive strength, $P$ is the peak load (kN), and $A$ is the cross-sectional area of the sample (mm). In cases where core length constrained $L/D$ values to less than 2, the UCS values were corrected by applying Equation [3].

$$\sigma_{c2} = \frac{8\sigma_c}{7+\frac{2D}{L}} \quad [3]$$

where $\sigma_c$ is the uncorrected measured UCS (MPa), $D$ is the specimen diameter (mm), $L$ is the specimen length (mm), and $\sigma_{c2}$ is the corrected UCS (MPa) of the specimen.

### *Determination of tensile strength*

The tensile strength of the samples was determined using Equation [4] (Jimeno, Jimeno, and Francisco, 1995).

$$TS\ (MPa) = \frac{0.636P}{D^2} \quad [4]$$

where $P$ is the load exerted on the sample (kN) and $D$ is the diameter of the sample (mm)

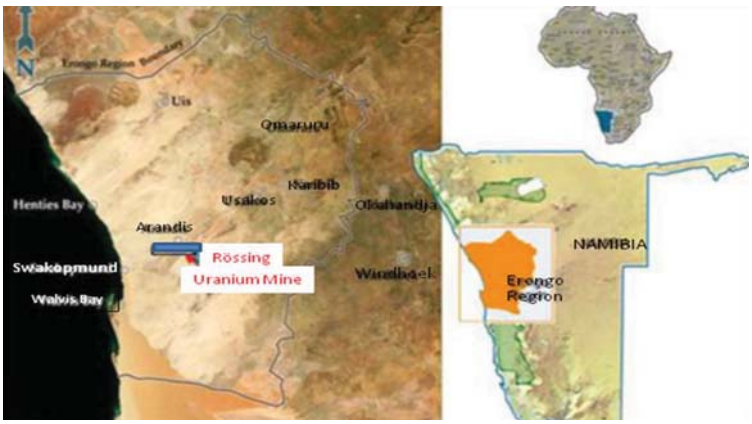


Figure 1—Location of Rössing Uranium Mine in the Namib Desert, Erongo Region, Namibia (after Abraham, 2009)

### *Determination of Young's modulus*

The modulus of elasticity or Young's modulus, $E$ (GPa), is the ratio of stress to corresponding strain. The relationship between UCS and Young's modulus expressed in Equation [5] (Horsrud, (2001) was used to determine the Young's modulus of the rock.

$$UCS = 7.22E^{0.712} \quad [5]$$

where UCS is the uniaxial compressive strength (MPa) and $E$ is Young's modulus (GPa).

### *Determination of weight on bit*

Weight on the bit was estimated using the expression in Equation [6], and the dead load is expressed in Equation [7].

$$\text{Weight on the bit (kg)} = \text{Feed Pressure} + \text{Dead Load} \quad [6]$$

$$\text{Dead Load} = \text{The Weight of Rotary head} + \text{The Weight of drilling rods} + \text{weight of the couplings} \quad [7]$$

### *Measurement of drilling machine parameters*

The Pit Viper rig is a rotary drilling machine with a tricone bit 311 mm in diameter for drilling vertical holes in the rock. The machine parameters (air pressure, rotational speed, feed pressure) were recorded in phase 2 and phase 3 of the pit while the machine was drilling blast-holes 311 mm in diameter with a bench height of 15 m. Phase 2 and phase 3 refer to selected sections of the pit – phase 2 consists of lower banded gneiss and phase 3 consists of the upper marble and layers of marble and quartzite.

## Results and discussion

### *Analysis of strength parameters and Young's modulus for the rocks*

Table I presents strength parameters and Young's modulus for phase 2 and 3 of the pit. The uniaxial compressive strength varied from 89.8 MPa for the interlayered marble and quartzite to 180.3 MPa for the lower banded gneiss. Point load strength index varied from 10.5–30.9 MPa, tensile strength from 16.10-5 MPa, and Young's modulus from 38.1–90.6 GPa.

### *Effect of rock properties on the penetration rates in phase 2 and phase 3*

Figure 2 presents a plot of point load strength index *versus* average penetration rate of the bits. A power relationship exists between the average penetration rate and point load strength index, with a coefficient of correlation $R^2 = 0.72$. This means that a modest correlation exists, as shown in Figure 2, and the penetration rate will be faster in the weaker rocks. The net penetration rate varied from 47 to 29 m/h.

*Table I*

**Strength parameters and Young's modulus for phase 2 and phase 3**

| Rock type | Uniaxial compressive strength (MPa) | Point load hardness (MPa) | Tensile strength (MPa) | Young's modulus (GPa) |
|---|---|---|---|---|
| Lower banded gneiss | 180.3 | 20.9 | 31.5 | 90.6 |
| Upper marble unit | 104.3 | 12.1 | 18.2 | 55.9 |
| Interlayered marble and quartzite | 89.8 | 10.5 | 16.1 | 38.1 |

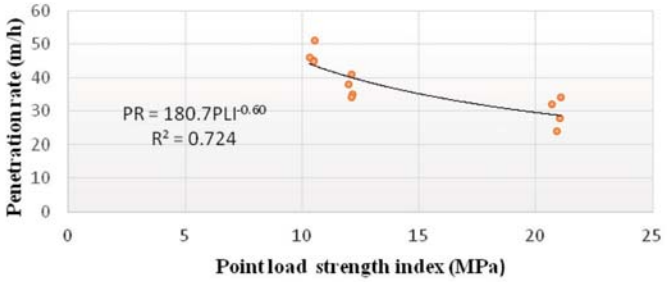


Figure 2—Point load strength index *versus* penetration rate

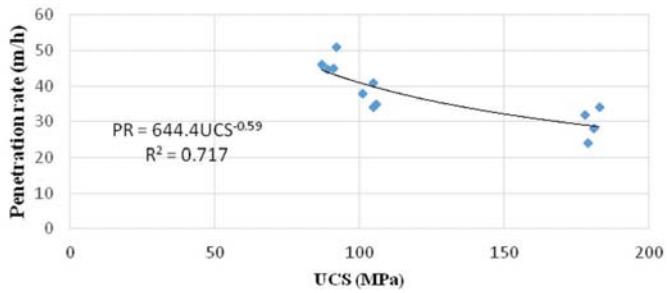


Figure 3—Uniaxial compressive strength *versus* penetration rate

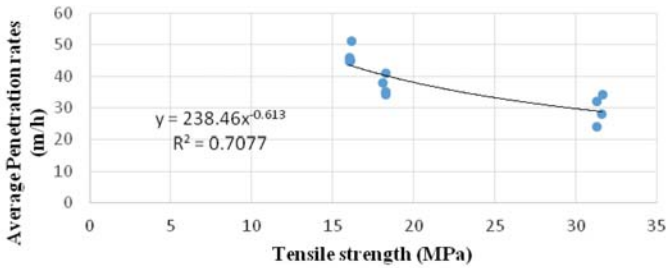


Figure 4—Tensile strength *versus* penetration rate

Figure 3 presents a plot of uniaxial compressive strength against the average penetration rate. A power relationship exists between average penetration rate and uniaxial compressive strength, with coefficient of correlation R = 0.71. This means that a modest correlation exists between the two variables, and the stronger rocks will be penetrated more slowly. It was observed that as the compressive strength of the rock increases, the penetration rate decreases.

Figure 4 presents a plot of tensile strength against the average penetration rate of the bits. A power relationship exists between the average penetration rate and tensile strength with a coefficient of correlation $R^2 = 0.70$. This indicates a modest correlation, and rock with a lower tensile strength will be drilled faster. The tensile strength varied from 16 to 31 MPa, and net penetration rate varied from 47 to 29 m/h.

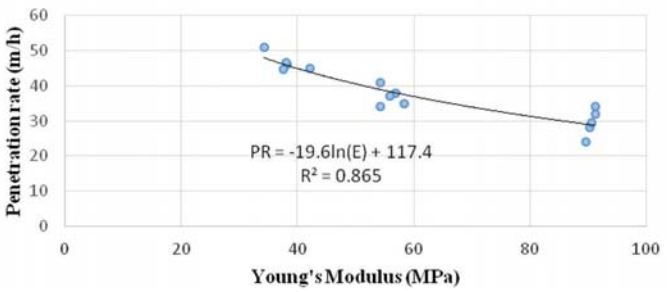


Figure 5—Young's modulus *versus* penetration rate

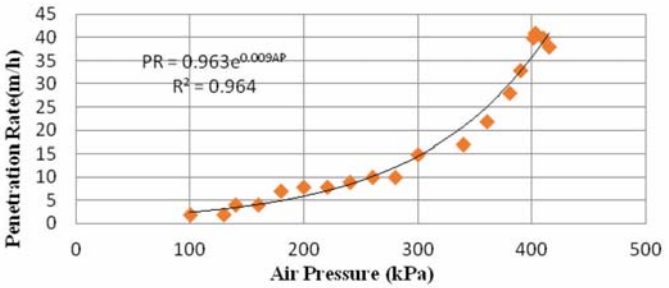


Figure 6—Air pressure *versus* penetration rate in phase 2

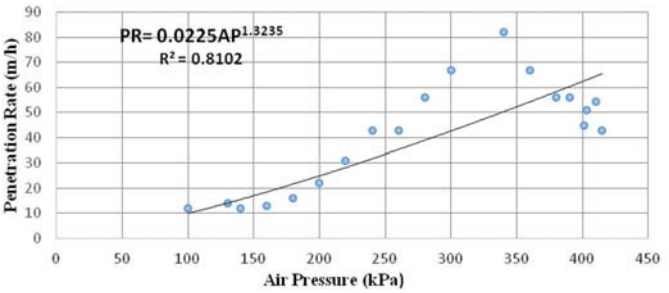


Figure 7—Air pressure *versus* penetration rate in phase 3

Figure 5 presents a plot of Young's modulus against the average penetration rate. A logarithmic relation exists, with a coefficient of correlation $R^2 = 0.865$, indicating a good correlation. The more rigid rock drill more slowly.

### *Optimum drilling parameters for phase 2 and phase 3 of the pit*

Figures 6 and 7 present the plots of air pressure against the penetration rate in phase 2 and phase 3 of the pit. The penetration rate increases with increasing air pressure until a peak value is reached, and then drops suddenly. However, 96% of the points for phase 2 and 81% for phase 3 fit into the equation of best exponential and power curves of fitness, respectively. Optimum air pressure value was observed to be 390 kPa with a corresponding penetration rate of 41 m/h in phase 2, and 330 kPa with an optimum penetration rate of 81 m/h in phase 3.

Figures 8 and 9 present the plots of rotation speed against penetration rate for phases 2 and 3 of the pit. Penetration rate is almost constant at 24 m/h at rotary speeds of between10 r/min and 62 r/min for phase 2, and almost constant at 8 m/h between rotary speeds of 10 r/min and 62 r/min for phase 3. A further increase in rotary speed from 63 to 79 r/min and 63 to 83 r/min caused a rapid increase in the penetration rates from 24 to 45 m/h and 9 to 73 m/h for phase 2 and phase 3 respectively. Then it started to drop again, to 39 m/h at a rotary speed of between 80 and 84 r/min for phase 2, and 47 m/h at 83 to 85 r/min for phase 3. More importantly, 79.9% of the points for phase 2 and 71% for phase 3 fit into the equation of the best exponential curve of fitness. The highest penetration rates of 36 to 45 m/h were attained at a rotational speed between 73 and 89 r/min

Figures 10 and 11 present the plots of feed pressure against penetration rate for phases 2 and 3. It can be seen that as the feed pressure increases, the penetration rate for both phases also increases until it reaches a peak value, after which it remains constant. The optimum feed pressure was 330 kN for phase 2, with a corresponding optimum penetration rate of 44 m/h, and 300 kN for phase 3, with a corresponding optimum penetration rate of 66 m/h. In addition, 96.8% and 97.6% of the points fit in the equation of best polynomial curves for phases 2 and 3 respectively.

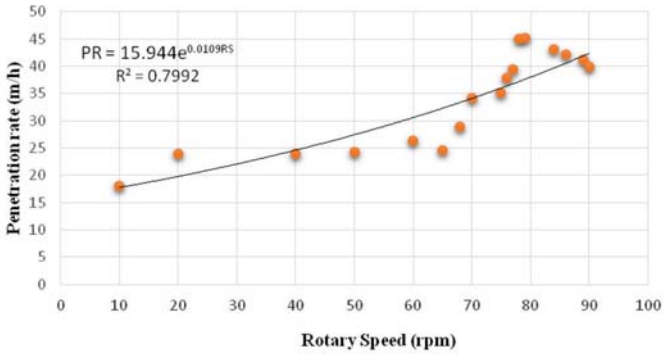


Figure 8—Rotary speed *versus* penetration rate for phase 2

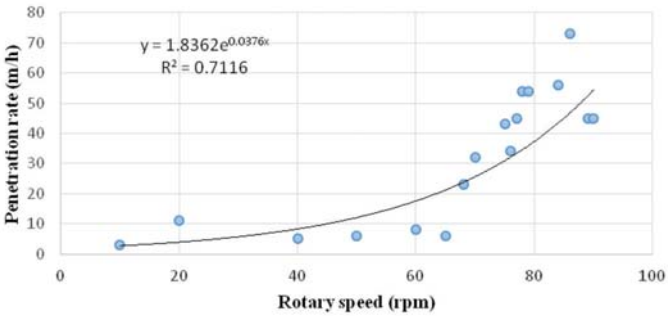


Figure 9—Rotary speed *versus* penetration rate for phase 3

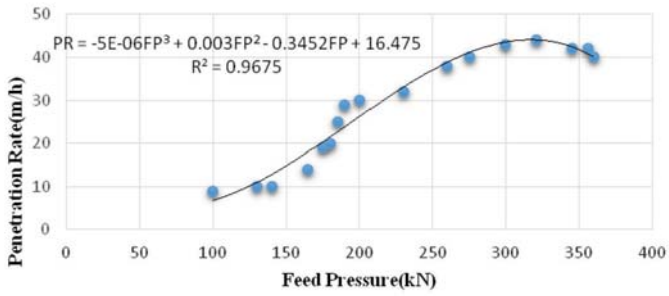


Figure 10—Feed pressure *versus* penetration rate for phase 2

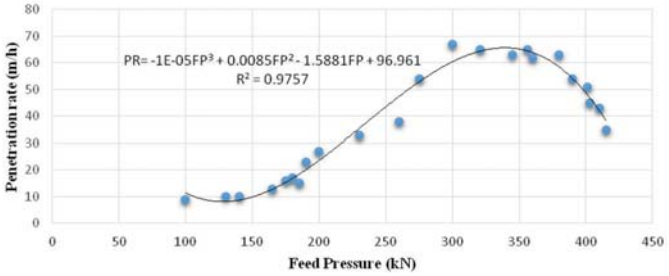


Figure 11—Feed pressure *versus* penetration rate for phase 3

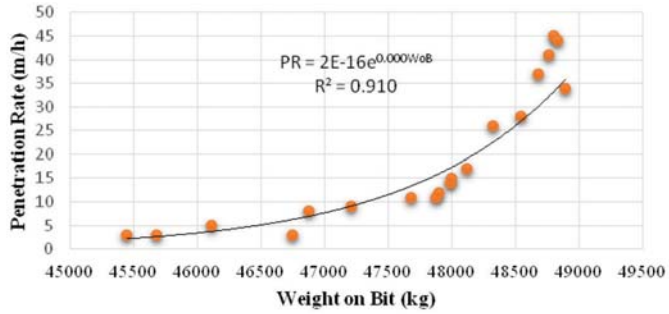


Figure 12—Weight on bit *versus* penetration rate for phase 2

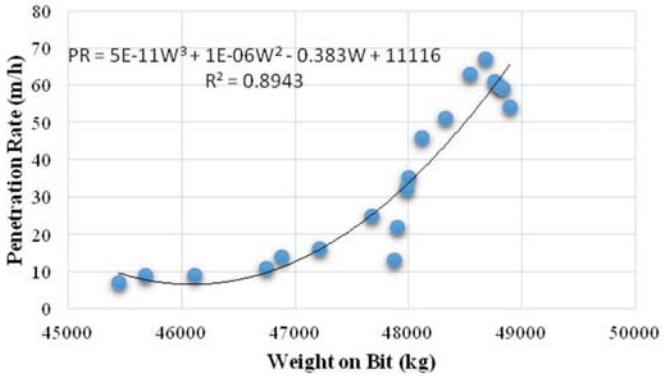


Figure 13—Weight on bit *versus* penetration rate for phase 3

Figures 12 and 13 present the plots of weight on the bit against penetration rate. At between 45 400 and 46 800 kg force the penetration rate was hovering between 4 and 5 m/h for phase 2, and 8 to 11 m/h for phase 3. Increasing the weight from 47 900 to 48 850 kg force for phase 2 resulted in a rapid increase in the penetration rate from 10 to 45 m/h, and for phase 3 an increase from 47 200 to 48 700 kg force on the bit increased the penetration rate from 17 to 68 m/h. The optimum weight on the bit was recorded as 48 700 kg force for phase 2 and 48 600 kg for phase 3 for an optimum penetration rate of 69 m/h. Furthermore, 91.0% of the points for phase 2 and 88.0% for phase 3 fit the equation of best exponential and polynomial curves of fitness.

## Statistical modelling

### *Tricone bit performance*

Table II shows the performance of the tricone bits tracked from January to May 2015 before the optimum machine parameters had been determined. The table also shows the actual metres drilled, number of bits drawn and, most importantly the drilling cost per metre. Drilling cost varied from N$37.90 per metre in February to N$107.20 per metre in April.

*Table II*

**Tricone bit performance from January to May 2015**

| Month | Actual metres for the drill rigs | Bits drawn | Cost per bit (N$) | Total costs (N$) | Cost per metre (N$/m) | Phase |
|---|---|---|---|---|---|---|
| Jan | 12 896.4 | 7 | 70 000 | 490 000 | 38.00 | Phase 3 |
| Feb | 12 927.6 | 7 | 70 000 | 490 000 | 37.90 | Phase 3 |
| Mar | 15 179.0 | 9 | 70 000 | 630 000 | 41.50 | Phase 2 |
| Apr | 9 135.0 | 14 | 70 000 | 980 000 | 107.20 | Phase 2 |
| May | 18 453.0 | 13 | 70 000 | 910 000 | 49.31 | Phase 2 |

*Table III*

**Tricone bit performance from September to October 2015**

| Month | Actual metres for the drill rigs | Bits drawn | Cost per bit (N$) | Total costs (N$) | Cost per metre (N$/m) | Phase |
|---|---|---|---|---|---|---|
| Sep | 14 245 | 6 | 70 000 | 420 000 | 29.48 | Phase 3 |
| Oct | 15 421 | 8 | 70 000 | 560 000 | 36.31 | Phase 2 |

*Table IV*

**Drill pipe performance from January to May 2015**

| Month | Actual metres for the drill rigs | Drill pipes drawn | Cost per pipe (N$) | Total costs (N$) | Cost per metre (N$) | Phase |
|---|---|---|---|---|---|---|
| Jan | 12 896.4 | 2 | 100 000 | 200 000 | 15.51 | Phase 3 |
| Feb | 12 927.6 | 1 | 100 000 | 100 000 | 7.74 | Phase 3 |
| Mar | 15 179.0 | 6 | 100 000 | 600 000 | 39.53 | Phase 2 |
| Apr | 9 135.0 | 3 | 100 000 | 300 000 | 32.84 | Phase 2 |
| May | 18 453.0 | 3 | 100 000 | 300 000 | 16.26 | Phase 2 |

### *Tricone bit performance using new optimum machine parameters*

Table III shows the performance of the tricone bits that was recorded when the new optimum drilling machine parameters were tested in the field from September to October 2015.

### *Drill pipe performance*

Table IV shows the performance of the drill pipes tracked from January to May 2015. The table shows the actual metres drilled before the drill pipes were changed, the number of drill pipes drawn, and the drilling cost per metre. The drilling cost varied from N$7.74 per metre in February to N$39.53 per metre in March

### *Drill pipe performance using new optimum machine parameters*

Table V shows the performance of the drill pipes that was

*Table V*

**Drill pipes performance from September to October 2015**

| Month | Actual metres for the drill rigs | Drill pipes drawn | Cost per drill pipe (N$) | Total costs (N$) | Cost per metre (N$/m) | Phase |
|---|---|---|---|---|---|---|
| Sep | 14 245 | 2 | 100 000 | 200 000 | 14.04 | Phase 3 |
| Oct | 15 421 | 2 | 100 000 | | | Phase 2 |

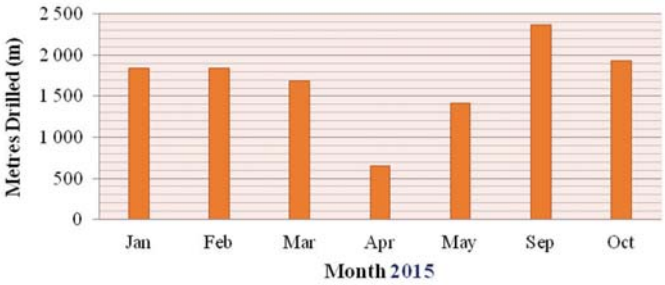


**Figure 14—Production metres drilled by tricone bits**

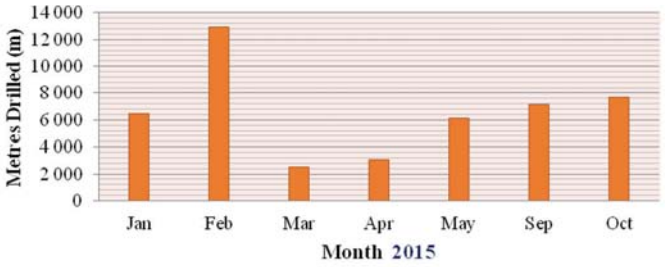


**Figure 15—Production metres drilled by drill pipe**

recorded when the new drilling machine parameters were tested in the field from September to October 2015.

Figures 14 and 15 present production metres drilled by tricone bit and drill pipe respectively. All the blast-holes drilled from January to May were shorter than the holes drilled in September and October when the new optimum machine parameters were tested. This indicates that the optimum machine parameters improved the drilling performance in phases 2 and 3 of the pit.

## Conclusion

The performance of the Pit Viper drill rig at Rössing Uranium Mine, Namibia was evaluated. The rock properties determined and the drilling machine parameters were correlated to obtain regression models to be used for predicting the penetration and the drilling rate. The uniaxial compressive strength, Young's modulus, and the tensile strength were all higher in phase 2 than in phase 3. It was observed that the optimum drilling parameters obtained were slightly lower than those used by the drill operators.

The optimum machine parameters in phase 2 are rotary speed 78 r/min, air pressure 400 kPa, and feed pressure 330 kN. The mine currently uses a rotary speed of 75 r/min, air pressure of 400 kPa, and feed pressure of 350 kN in phase 2. The optimum machine parameters in phase 3 are rotary speed 82 r/min, air pressure 330 kPa, and feed pressure 300 kN. The mine currently use a rotary speed of 84 r/min, air pressure of 350 kPa, and feed pressure of 300 kN in phase 3.

The trial of the new optimum machine parameters revealed that there is a reduction in the cost of drilling per metre, which varied from N$29.48 to N$36. 31 per metre for tricone bits using the new machine parameters, and N$7.74 to N$39.5 per metre for drill pipes as compared to N$37.90 to N$ 107.20 per metre for tricone bits and N$12.97 to N$14.04 per metre for drill pipe with the standard parameters.

## Acknowledgements

We acknowledge the administration and technical personnel of Rössing Uranium Mine, Namibia for providing an enabling environment for acquisition of data for this work. Also, Mr Wulff-Dieter Wieland is acknowledged for his assistance during data collection at the mine.

## References

Adebayo, B. and Akande, J.M. 2015. Analysis of button bit wear and performance of down-the-hole hammer drill. *Ghana Mining Journal*, vol.15, no. 2. pp. 36–41.

Abraham. I.M. 2009. Geology and spatial distribution of uranium mineralisation in SK anomaly area, Rössing, area Namibia, MSc thesis, University of the Witwaterstrand, Johanesburg, South Africa. 180 pp.

Aipanda, T. 2011. Personal communication facing challenges head-on. Rössing Uranium Mine, Report of Stakeholders. Swakopmund. 15 pp.

Clark, I.E. and Shafto, G.R. 1987. Core drilling with Syndax 3 PDC. *Industrial Diamond Review*, vol. 47, no. 521. pp. 169–173.

Garnier, A.J. and Lingen, N.H.V. 1959. Phenomena affecting drilling rate at depth. *Journal of Petroleum Technology, Transactions of AIME*, vol. 217. pp. 232–239.

Hartman, H.L. 1962. Crater geometry relations in percussive drilling – single blos studies. *Mine Quarry Engineering*, vol. 28. pp. 530–536.

Horsrud, P. 2001. Estimating mechanical properties of shale from empirical correlations. *SPE Drill*, no. 16. pp. 68–73.

ISRM. 1989. Rock characterization testing on monitoring. *ISRM Suggested Methods*. Brown, E.T. (ed.). Pergamon Press, Oxford. p. 211.

Jiao, D. 1989. Analysis of variables affecting the performance of a hydraulic rotary percussive drill. PhD thesis, University of Newcastle-on- Tyne, UK.

Jimeno, C.L., Jimeno, E.L. and Francisco, J.A. 1995. Drilling and Blasting of Rock. Balkema, Rotterdam.

Kahraman, S., Bilgin, C., and Feridunoglu, C. 2003. Dominant rock properties affecting penetration rate of percussive drills. *International Journal of Rock Mechanics and Mining Sciences*, vol. 40, no. 2. pp. 711–723

Lummus, J.L. 1969. Factors to be considered in drilling optimization. *Journal of Canadian Petroleum*, vol. 8, no. 4. pp. 138–147.

Nguyen, V.G. 2011. The effect of weight on bit on dogleg severity of the wellbore. *Scientific-Technical Journal of Mining and Geology*, vol. 34. pp. 16–19.

Ozdemir L., Miller, R., and Wang, F.D. 1977. Mechanical tunnel boring, prediction and machine design. Annual report, CSM APR 73-07776-A03. Transportation Research Board. 250 pp.

Pearse, G. 1985. Hydraulic rock drills. *Mining Magazine*. pp. 220-231.

Rössing Uranium. 2013. History and location of Rössing. https://www.rossing.com/history.htm [accessed 17 November 2018].

Sinkala, T. 1989. Hole deviations in percussion drilling and control measures. PhD thesis, Luleå University of Technology, Sweden.

Tandanand, S. and Unger H.F. 1975. Drillability determination – A drillability index of percussive drills. *RI* 8073. US Bureau of Mines. pp. 47–52.

Warren, T.M. 1984 Factors affecting torque for roller bits. *Journal of Petroleum Technology*. pp. 1500–1508. ◆


# Comparison of the efficiency of plaster stemming and drill cuttings stemming by numerical simulation

**H. Cevizci**[1]

**Affiliation:**
[1]Suleyman Demirel University, Engineering Faculty, Mining Engineering Department, Turkey.

**Correspondence to:**
H. Cevizci

**Email:**
halimcevizci@sdu.edu.tr

**Dates:**
Received: 29 Mar. 2018
Revised: 29 Sep. 2018
Accepted: 29 Oct. 2018
Published: April 2018

**How to cite:**
Cevizci, H.
Comparison of the efficiency of plaster stemming and drill cuttings stemming by numerical simulation.
The Southern African Insitute of Mining and Metallurgy

DOI ID:
http://dx.doi.org/10.17159/2411-9717/18/068/2019

ORCiD ID:
H. Cevizci
https://orchid.org/0000-0003-4016-5136

## Synopsis

**Numerical simulation of the plaster stemming method (PSM) was performed and compared with the conventional drill cuttings stemming method (DCSM). Many earlier *in situ* tests have proved that PSM can use the blast energy more efficiently than DCSM. Despite PSM generating more blast vibrations, it has advantages over DCSM such as better fragmentation and lower cost per unit volume of rock blasted. In this study, numerical simulation with Autodyn software using a 2D tool was employed to prove the efficiency of plaster stemming by comparing parameters such as pressure, Y-velocity, Y-force, internal energy, acceleration-Y, and compression. For example, the maximum pressure attained at the top of explosive column was 7 395 MPa for DCSM whereas it was as high as 11 945 MPa for PSM. Most of the computed parameters were significantly higher in PSM than those obtained for DCSM. This paper is the first study elucidating the efficiency of PSM by numerical simulation. It is concluded that PSM can save substantial amounts of money and effort.**

**Keywords**
**blasting, stemming, plaster, drill cuttings, numerical simulation, Autodyn.**

## Introduction

The stemming of blast-hole collars in surface mines with an inert material redirects blasting energy to the rock more efficiently, thus the blast-induced energy is utilized more effectively in breaking rock. With proper stemming, the gases should not escape due to loose stemming material. More efficient stemming with better confinement therefore increases the blast fragmentation. In addition, the distance of scatter is increased, giving rise to a looser rock pile that can be more easily loaded and transported. In order to improve the performance of a blast, stemming is used to help maintain the gas pressure over time (Konya and Konya, 2018). Proper stemming has been shown to increase the explosive efficiency by over 41% (Snelling and Hall, 1912).

The most common stemming material in open pits and quarries is drill cuttings because of their ready availability at blast sites and the drill cuttings stemming method (DCSM) is a low-cost method. However, it has a major disadvantage in that dry drill cuttings eject very easily from blast-holes during an explosion, thus a great percentage of the blast energy is wasted and lost to the atmosphere. Cevizci (2012, 2014, 2013, 2017) studied blasting parameters in open pits and obtained better results with the plaster stemming method (PSM) in many limestone, basalt, and clay quarries. Moulding plaster is preferred for stemming because of the fast hardening time of 25–30 minutes.

Plaster stemming confines blast-induced pressure, therefore a shorter stemming column provides the same effect as a longer column of drill cuttings. Hence more explosive can be used per drill-hole. Cevizci and Ozkahraman (2012) pointed out that generally, as the stemming column increases, more large fragments are produced, which cause loading and hauling problems and increase costs. Also, increased utilization of hole length reduces specific drilling costs due to the increased burden and spacing distances. The biggest cost item in blasting operations is blast-hole drilling. Another advantage of PSM is better fragmentation, with more cracks induced within the rocks.

Many studies of the stemming effect have been carried out by numerical simulation. Park and Jeon (2010) investigated vibration reduction in tunnelling by air deck stemming, by means of numerical and experimental studies. The numerical and experimental results agreed well. Fiserova (2006) compared numerical modelling and experimental results and found good agreement. In addition, numerical studies are cost-effective and easier to set up and run than experiments. To date, many studies have been done to investigate the accuracy of numerical simulations and experiments.

# Comparison of the efficiency of plaster stemming and drill cuttings stemming by numerical simulation

### *A plaster stemming trial and blast-induced vibrations*

Cevizci (2012) carried out tests comparing plaster stemming and drill cuttings stemming, each method being used on a single row of seven holes 89 mm in diameter. The stemming length was 1.5 m and 58.7 kg ANFO with 1.25 kg primer was used in the case of the DCSM. A stemming length of 1 m and 61.3 kg ANFO with 1.25 kg primer was used for the PSM. Nonel caps with 42 ms delay were used at the surface, and 500 ms delay at the hole bottom. Vibration levels were measured 88 m away from the blast-holes. PSM achieved better fragmentation and lower cost per unit volume. However, blast-induced vibration was considerably increased. Of course, such an increase can be detrimental to equipment, pit slope stability, and general safety. However, the measured values were under the legal threshold values.

For the DCSM trial (Cevizci, 2015), peak particle velocity (PPV) was 12.0 mm/s. The components of vibration were transverse PPV 6.22 mm/s at 14 Hz, vertical PPV 11.9 mm/s at 19 Hz, longitudinal PPV 9.78 mm/s at 23 Hz. For the plaster stemming trial, PPV was 17.8 mm/s. The components of vibration were transverse PPV 12.8 mm/s at 13 Hz, vertical PPV 8.76 mm/s at 21 Hz, and longitudinal PPV 17.8 mm/s at 14 Hz. The vertical component of vibration was lower and the frequency was higher, which constitutes an advantage for PSM, but the longitudinal and transverse components were higher and frequencies were lower, which is disadvantageous. However, the measured values were under the safety limits despite the short measuring distance.

### Numerical simulation of drill cuttings and plaster stemming methods

In this study, numerical simulation with Autodyn 2D axial symmetry was performed. Two rock types with different strengths and a constitutive model were used for the simulation. Blasting can be numerically described by a general system of differential equations such as the laws of conservation of mass, momentum, energy, and a supplementary equation. In order to solve these equations, finite difference, finite volume, and finite element numerical techniques have been developed (Oran and Boris, 2001; Toro, 1997; Zukas, 2004; Benson,1992).

In this study, two models were built for each rock type (a total of four models). The first model utilized drill cutting stemming and second plaster stemming. In all four models, all parameters were the same except for stemming type, rock type, and explosive. In addition, the accuracy of the model was checked by changing parameters such as the blast pattern, scale of the model, and explosives. Seven different materials – two rock types (limestone and 'Rock II'), plaster, sand, ANFO, TNT, and air – were used in these models. ANFO is widely used in blasting at open pits and quarries. Sand was substituted for drill cuttings since it has similar physical effects in the stemming process. The Lagrange solver is preferred for modelling rock and plaster because it is more suitable for solids (Fairlie, 1998). The Arbitrary Lagrange Euler (ALE) processor can also be used, and is useful to provide automatic rezoning of distorted grids. The Euler solver is used for the blasting process and sand because it is more suitable for fluids and gases. In order to check the accuracy of the Euler solver for sand, the results were compared with those obtained with the Lagrange solver, and were found to be similar. Limestone, Rock II and plaster were defined manually, but sand, ANFO, TNT, and air are specified in Autodyn library and were used as such.

Limestone is defined as reference density 2.69 g/cm$^3$; other parameters defined are linear EOS, Drucker-Prager strength model, principal stress failure model, bulk modulus 65 GPa, shear modulus 27 GPa, yield stress 80 MPa, reference temperature 273 K, specific heat 910 J/kgK, and thermal conductivity 1.3 J/mKs. Plaster is defined as reference density 1 g/cm$^3$, linear EOS, Drucker-Prager strength model, principal stress failure model, bulk modulus 3 GPa, shear modulus 1.1 GPa, yield stress 2 MPa, reference temperature 293 K, specific heat 1000 J/kgK and thermal conductivity 0.3 J/mKs.

Polynomial EOS (Park and Jeon, 2010) and the Riedel, Hiermaier and Thoma (RHT) strength and failure model are used for Rock II, with the parameters listed in Table I (Riedel *et.al.*, 1999; Riedel, 2000).

For models, the initial condition is set and ideal gas EOS is used for air. The internal energy of air is set as 2.0682.10$^5$ J/kg. For modelling high explosive, ANFO and TNT, Euler solver employing Jones-Wilkins-Lee (JWL) EOS for detonation products is preferred. The JWL Equation [1] is implemented in Autodyn as:

$$P = A\left(1 - \frac{W}{R_1 V}\right)e^{-R_1 V} + B\left(1 - \frac{W}{R_2 V}\right)e^{-R_2 V} + \frac{WE}{V} \quad [1]$$

$A$ and $B$ (Pa), the $R_1$ and $R_2$ coefficients, and $W$, the Grüneisen coefficient depend on the composition of the explosive. The variable $V = v/v_o$ is the expansion of the explosive products

*Table I*

**Parameters of the RHT model used in the study**

| Parameter | Value |
|---|---|
| Reference density | 2.75 g/cm$^3$ |
| Bulk modulus, $A_1$ | 35.27 GPa |
| $A_2$ | 39.58 GPa |
| Shear modulus, $G$ | 22.06 GPa |
| Compressive strength, $fc$ | 93.75 MPa |
| Tensile strength/Compressive strength, $f/f_c$ | 0.100 |
| Shear strength/Compressive strength, $f_s/f_c$ | 0.180 |
| Intact failure surface constant, A | 1.600 |
| Intact failure surface exponent, N | 0.610 |
| Tensile/compressive meridian ratio, Q2,0 | 0.6805 |
| Brittle to ductile transition, BQ | 0.001 050 |
| G (elastic)/G (elastic–plastic) | 2.000 |
| Elastic strength per foot | 0.700 |
| $A_3$ | 9.040 MPa |
| $B_0$ | 1.220 |
| $B_1$ | 1.220 |
| $T_1$ | 35.27 GPa |
| $T_2$ | 0.000 MPa |
| Reference temperature | 300 K |
| Specific heat | 654 J/kg K |
| Thermal conductivity | 0.000 J/mKs |
| Elastic strength/ fc | 0.530 |
| Residual strength constant, B | 1.600 |
| Residual strength exponent, M | 0.610 |
| Compressive strain rate exponent, α | 9.090 × 10$^{-3}$ |
| Tensile strain rate exponent, δ | 0.0125 |
| Maximum fracture strength ratio | 1.000 × 1020 |
| Damage constant, $D_1$ | 0.04 |
| Damage constant, $D_2$ | 1.00 |
| Minimum strain to failure, $\varepsilon f^{min}$ | 0.01 |
| Residual shear modulus faction | 0.13 |

and $E$ (J/m$^3$) is detonation energy per unit volume. Various authors such as Dobratz and Crawford (1985), Finger *et al.* (1976), and Souers and Kury (1983) studied the values of JWL coefficients. JWL EOS parameters of ANFO and TNT are as listed in Table II (taken from the library of Autodyn). Euler processor, Compaction EOS, MO Granular strength, Hydro ($P_{min}$) failure are used for sand. The reference density of sand is 2.641 g/cm$^3$.

The mesh size is 10 mm and the same mesh system is applied for both PSM and DCSM. The acceleration due to gravity is set as 9.81 m/s$^2$ through the $x$ direction (according to open pit blasting).

In limestone quarries in Turkey, an average 2.2 m burden and 2.5 m spacing was determined in 89 mm diameter holes and a 10 m bench height by slab blasting tests (Ozkahraman, 1993). Similar geometrical parameters representing the real conditions are chosen for the models. A cylindrical rock specimen is modelled with dimensions of 3000 mm in diameter, 10 000 mm in length, and a 90 mm diameter hole located in the centre (Figure 1). The centre of the drill-hole coordinate at the top of the hole is (0, 0). The length of stemming is 2000 mm in both methods. Gauges are placed in the model as shown in Table III (Figure 1). Gauge 1 is placed 15 mm under the stemming and gauge 2 is 5 mm from the inner surface of hole (50 mm from the hole centre) inside the rock. The main limitation of the gauge is that wherever it is placed, the measurements can be taken only at the middle of the cell.

Initial conditions and boundaries were defined. Interaction and output settings are very important for correct results. The models were built in structured parts that have more than 300 000 nodes and elements. In addition, thousands of cycles were performed.

Detonation was started at the middle of the explosive column (at coordinates 6000, 0). It was assumed in the model that the interface between the plaster stemming and rock was joined, since the plaster plug connects the hole surface. In other words, the plaster plug can move with the main rock mass during blasting (Cevizci, 2013).

## Simulation results

The maximum values of pressure, Y-velocity, Y-force, internal energy, acceleration-Y, and compression from the numerical simulation model are given in Table IV. Compression μ is a ratio (Autodyn, 2013), which is

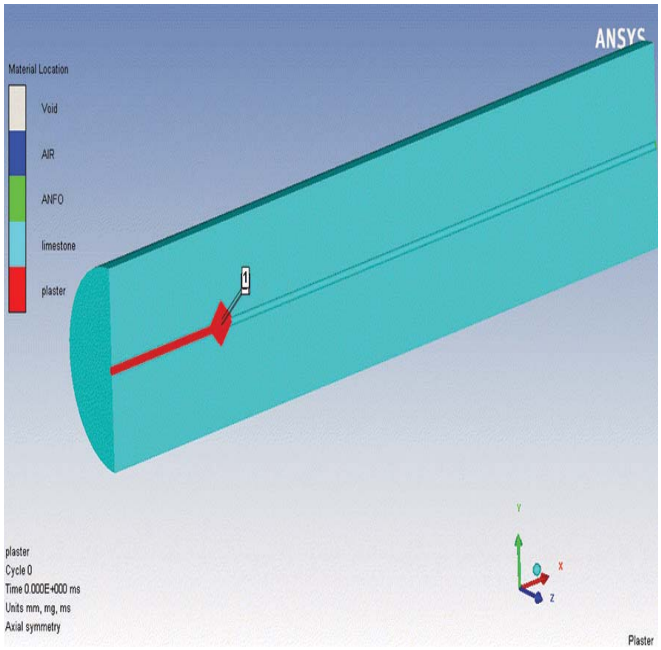


**Figure 1—Simulated cylindrical rock, 180° mirroring model, and gauge points**

*Table III*

**Initial coordinates of the gauges**

| Gauge no. | X (mm) | Y (mm) |
|---|---|---|
| 1 (fixed, in hole) | 2.01500E+03 | 5.00000E+00 |
| 2 (moving, in rock) | 2.03500E+03 | 4.99829E+01 |
| 3 (moving, in rock) | 2.04500E+03 | 4.99829E+01 |
| 4 (moving, in rock) | 2.00500E+03 | 4.99829E+01 |

*Table II*

**Parameters of ANFO and TNT JWL EOS**

| Explosive | Reference density (g/cm$^3$) | Vod (m/s) | *A* (kPa) | *B* (kPa) | $R_1$ | $R_2$ | W | C-J pressure (kPa) | E (kJ/m$^3$) |
|---|---|---|---|---|---|---|---|---|---|
| ANFO | 0.931 | 4160 | 4.946 × 107 | 1.891 × 106 | 3.907 | 1.118 | 0.333 | 5.15 × 106 | 2.484 × 106 |
| TNT | 1.630 | 6930 | 3.73 × 108 | 3.747 × 106 | 4.150 | 0.900 | 0.350 | 2.15 × 107 | 6.000 × 106 |

*Table IV*

**Maximum values**

| Parameter | Gauge | Limestone | | Rock II | |
|---|---|---|---|---|---|
| | | Drill cuttings | Plaster | Drill cuttings | Plaster |
| Pressure (MPa) | 1 | 7 395 | 11 945 | 11 876 | 12 962 |
| Compression | 1 | 0.8327 | 4.4063 | 0.1236 | 0.1565 |
| Y- velocity (m/s) | 1 | 519 | 961 | 473 | 550 |
| Pressure (MPa) | 2 | 3 015 | 3 104 | 4 871 | 5 317 |
| Compression | 2 | $4.638 \times 10^{-2}$ | $4.775 \times 10^{-2}$ | $1.110 \times 10^{-2}$ | $1.193 \times 10^{-2}$ |
| Y-force (N) | 2 | $6.466 \times 10^{5}$ | $7.050 \times 10^{5}$ | $3.213 \times 10^{6}$ | $4.310 \times 10^{6}$ |
| Internal energy (J/kg) | 2 | $2.585 \times 10^{4}$ | $2.722 \times 10^{4}$ | $1.299 \times 10^{5}$ | $1.535 \times 10^{5}$ |
| Acceleration-Y (m/s$^2$) | 2 | $2.194 \times 10^{4}$ | $2.392 \times 10^{4}$ | 1.067 × 105 | $1.431 \times 10^{5}$ |

$$\mu = (\rho/\rho_0) - 1 \quad [2]$$

where ρ is density.

The following nomenclature is used in Figures 2–9:

- Ident 0 - dc : DCSM - limestone – ANFO
- Ident 1 - plaster : PSM - limestone – ANFO
- Ident 2 - dc : DCSM – Rock II – TNT
- Ident 3 – pl : PSM – Rock II – TNT

### *Measurements at gauge 1 (inside hole)*

Figure 2 shows the pressures at gauge 1 location (coordinate 2015, 5) *versus* time. The maximum pressures using DCSM and PSM are 7 395 and 11 945 MPa for limestone, and 11 876 and 12 962 MPa for Rock II. Figure 3 shows the compression at gauge 1 *versus* time. Maximum compression with PSM (4.4063) is higher than that for DCSM (0.8327). Similar results were obtained with Rock II. Figure 4 shows the Y component of velocity at gauge 1 *versus* time. PSM results in higher maximum velocity in both limestone (519 961 $ms^{-1}$) and Rock II (473 550 $ms^{-1}$).

### *Measurements at gauge 2 (inside rock)*

Figure 5 shows pressures at gauge 2 location (coordinate 2035, ~50) *versus* time. The maximum pressures for DCSM and PSM are 3 015 and 3 104 MPa for limestone, and 4 871 and 5 317 MPa for Rock II. Figure 6 shows values of compression at gauge 2 *versus* time. The maximum compression for PSM (4 775 × $10^{-2}$) is higher than that for DCSM (4.638 ×$10^{-2}$). Similar results were obtained with Rock II. Figure 7 shows the Y component of force at gauge 2 *versus* time. PSM results in a higher maximum Y-force in both limestone (6.466 × $10^5$, 7.050 × $10^5$ N) and Rock II (3.213 × $10^6$, 4.310 × $10^6$ N). Figure 8 shows internal energy at gauge 2 *versus* time. Maximum internal energies for DCSM and PSM are 2.585 × $10^4$ and 2.722 × 104 J/kg for limestone and 1.299 × $10^5$ and 1.535 × $10^5$ J/kg for Rock II. Figure 9 shows acceleration-Y at gauge 2 *versus* time. Maximum acceleration-Y

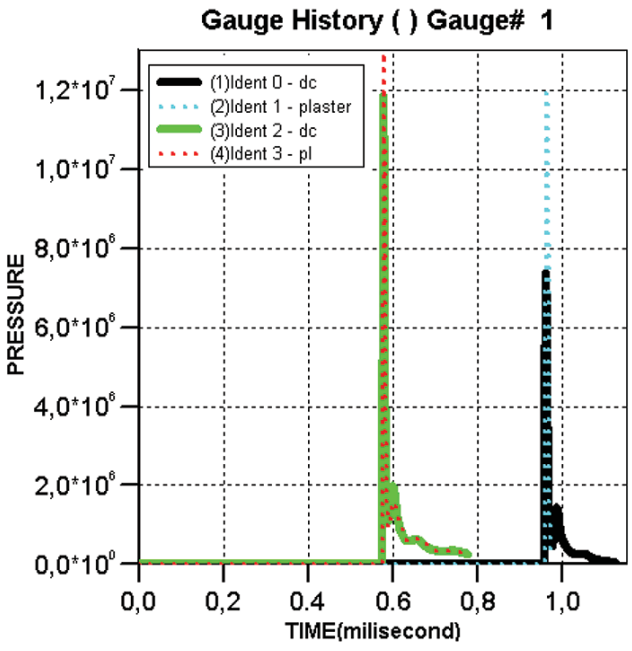


**Figure 2—Pressure (kPa) at gauge 1 *versus* time**

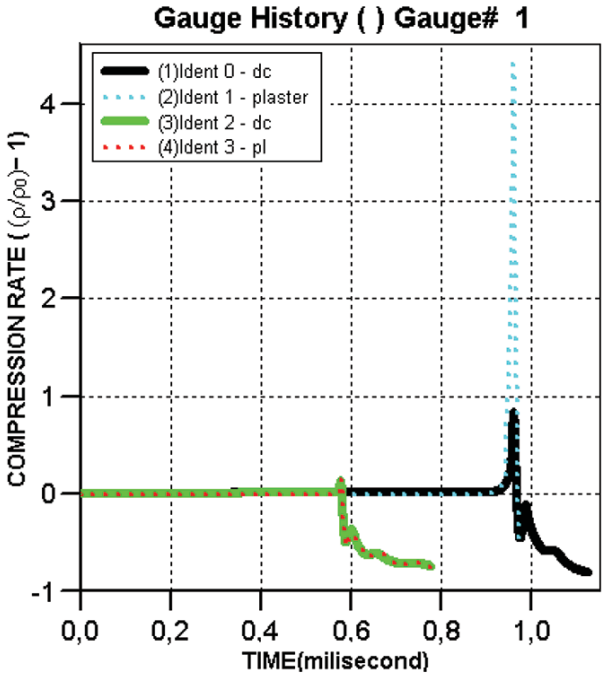


**Figure 3—Compression at gauge 1 *versus* time**

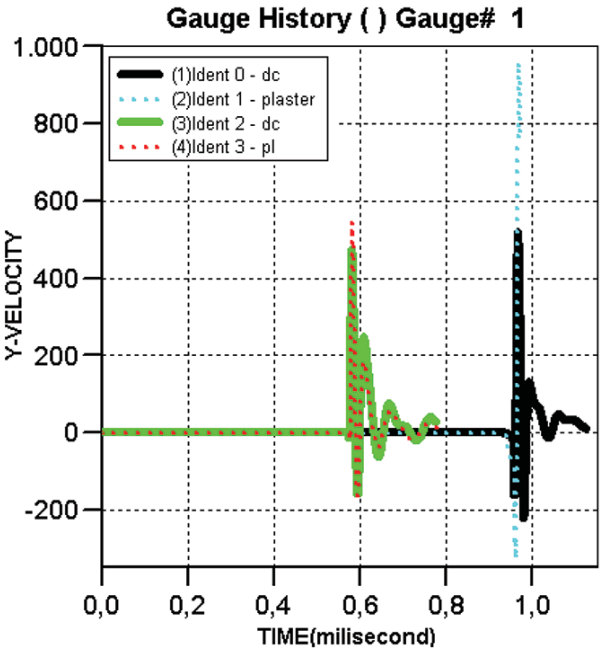


**Figure 4—Y component of velocity ($ms^{-1}$) at gauge 1 *versus* time**

for PSM (2.392 ×$10^4$ $m/s^{-2}$) is higher than that for DCSM (2.194 × 104 $m/s^2$). The Rock II results were similar. The results of gauge 3 and gauge 4 are similar to those of gauge 2.

Moving gauges in the rock were preferred, which is available as a default setting in the software. For the ANFO in limestone rounds, the last locations are shown in Table V for DCSM and in Table VI for PSM. With PSM, the gauges are moved further away from the hole towards the free surface by blasting.

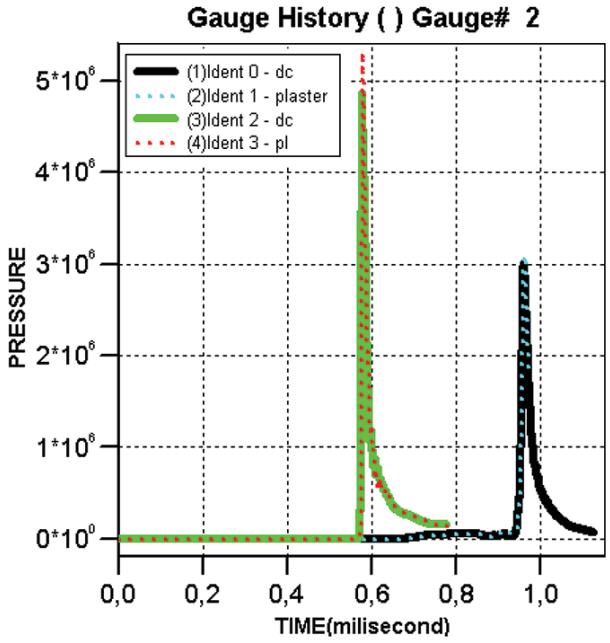


Figure 5—Pressure (kPa) at gauge 2 *versus* time

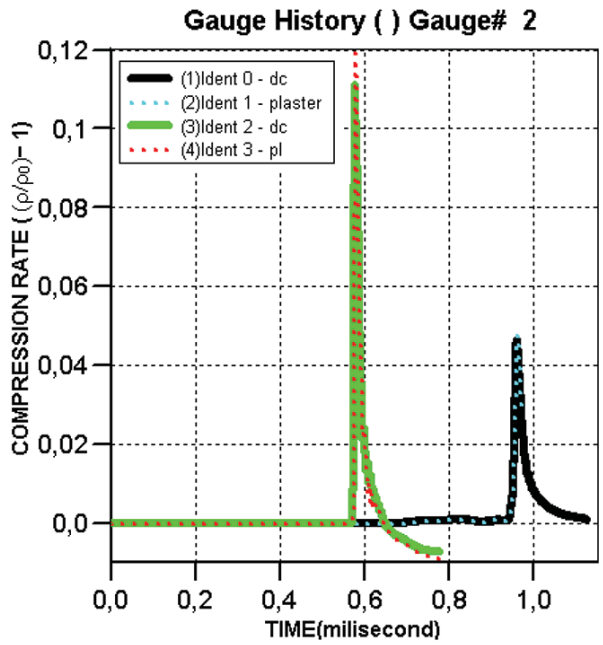


Figure 6—Compression at gauge 2 *versus* time

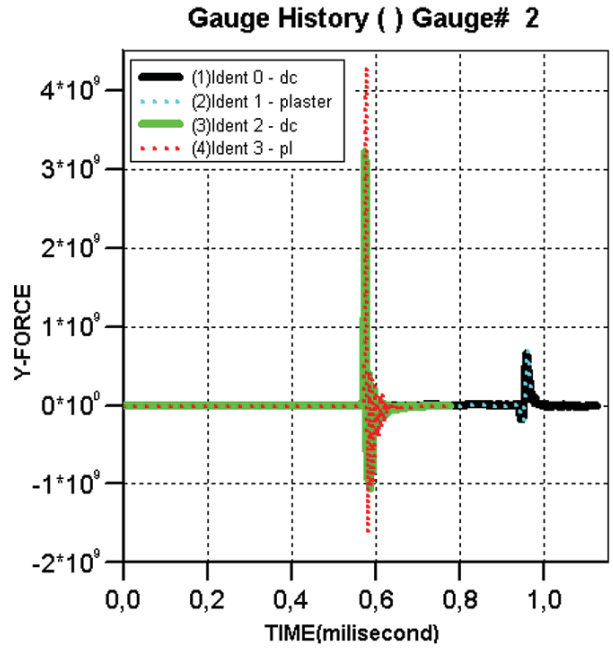


Figure 7—Y component of force (mN) at gauge 2 *versus* time

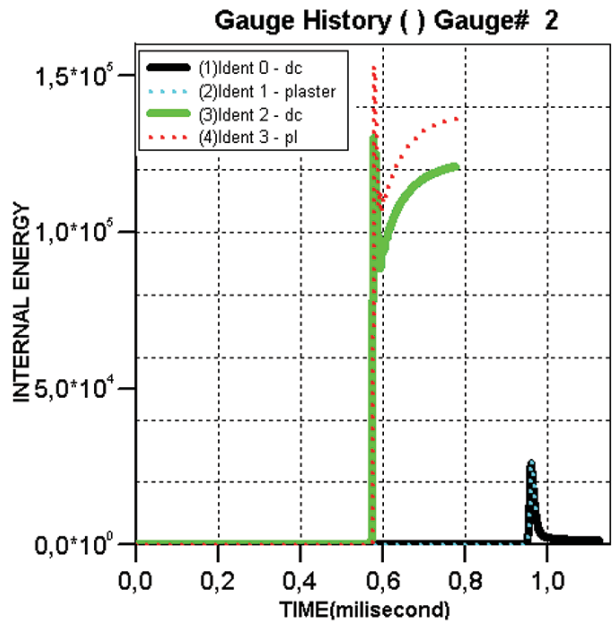


Figure 8—Internal energy (J/kg) at gauge 2 *versus* time

## Conclusion

Numerical simulations of blasting using conventional DCSM and the newly developed PSM were, for the first time, successively compared by using Autodyn software. The simulations clearly revealed that the blasting performance with PSM was better than that with DCSM, as indicated by most of the measured parameters, in both limestone and Rock II.

Plaster stemming results in high stresses due to the more effective confining of gases inside the blast-holes. In the case of drill cuttings stemming, much of the blast energy is wasted by the gases escaped from the hole. Previous work (Cevizci, 2012 2013, 2014) has shown than the measured PPV values are higher with PSM compared to DCSM. For instance, in one blasting test with the same amount of explosive per delay (Cevizci, 2017), the PPV with PSM was approximately twice that measured using DCSM. The initial shock waves due to the better confinement with moulding plaster are responsible for this increased efficiency of the blast energy used in rock breakage.

Site tests support these numerical simulation results. Blast-induced vibration is increased by using plaster stemming instead of drill cuttings stemming. These indicators show that energy is

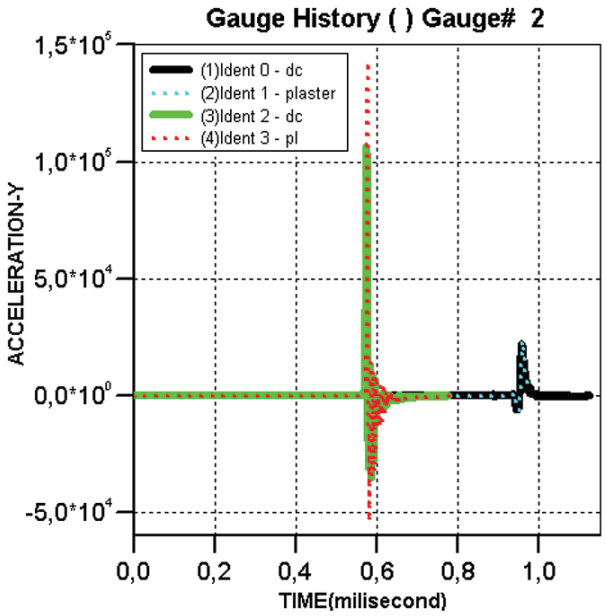


**Figure 9—Acceleration-Y (m/s²) at gauge 2 *versus* time**

*Table V*

**The coordinates of moving gauges after blasting with DCSM**

| Gauge | X (mm) | Y (mm) |
|---|---|---|
| 2 | 2.03425E+03 | 5.08726E+01 |
| 3 | 2.04371E+03 | 5.14698E+01 |
| 4 | 2.00611E+03 | 4.91892E+01 |

*Table VI*

**The coordinates of moving gauges after blasting using PSM**

| Gauge | X (mm) | Y (mm) |
|---|---|---|
| 2 | 2.03430E+03 | 5.09098E+01 |
| 3 | 2.04379E+03 | 5.15781E+01 |
| 4 | 2.00505E+03 | 5.15463E+01 |

transferred to the rock more effectively. *In situ* test results such as better muckpile fragmentation and higher vibration levels with PSM are confirmed by the numerical simulation results. Consequently, because the total drilling and blasting cost with PSM is approximately 20% lower, and the fragmentation is better Cevizci, 2012), PSM should be preferred in blasting operations. Plaster is a cheap material. *In situ* application of the PSM is slightly difficult, but currently a project is under way on the mechanization of PSM. ANFO is water-resistant and the plaster solution can cause problems. However, using a little drill cuttings in conjunction with plaster can solve this problem.

## References


Autodyn. 2013. ANSYS Autodyn User's Manual. Canonsburg, PA.

Benson, D.J. 1992. Computational methods in Lagrangian and Eulerian hydrocodes. *Computer Methods in Applied Mechanics and Engineering*, vol. 99. pp. 235–394.

Cevizci, H. 2012. A newly developed plaster stemming method for blasting. *Journal of the Southern African Institute of Mining and Metallurgy*, vol. 112, no. 12. pp. 1071–1078.

Cevizci, H. 2013. A new stemming application for blasting: a case study. *Rem: Revista Escola de Minas*, vol. 66. pp. 513–519

Cevizci, H. 2014. Fragmentation, cost and environmental effects of plaster stemming method for blasting at a basalt quarry. *Archives of Mining Science*, vol. 59. pp. 837–848.

Cevizci, H. 2015. The environmental and ecological effects of plaster stemming method for blasting: A case study. *Ekoloji*, vol. 24, no. 95. pp. 17–22. doi: 10.5053/ekoloji.2015.11

Cevizci, H. 2017. The effect of plaster stemming for large hole diameter stripping blasting: A case study. *Proceedings of 25th International Mining Congress and Exhibition of Turkey*, Antalya. Chamber of Mining Engineers of Turkey. pp. 333–339.

Cevizci, H. and Özkahraman, H.T. 2012. The effect of blast hole stemming length to rockpile fragmentation at limestone quarries. *International Journal of Rock Mechanics and Mining Sciences*, vol. 53. pp. 32–35.

Dobratz, B.M. and Crawford, P.C. 1985. LLNL explosive handbook: Properties of chemical explosives and explosive simulants. *Technical report* UCRL- 52997-Chg.2. Lawrence Livermore National Laboratory, California.

Fairlie, G.E. 1998. The numerical simulation of high explosives using Autodyn 2D & 3D. *Explo'98: Proceedings of the Institute of Explosive Engineers 4th Biannual Symposium*. http://truegrid.com/paper052f.pdf

Finger, M., Lee, E., Helm, F., Hayes, B., Hornig, H., McGuire, R., Kahara, M., and Guidry, M. 1976. The effect of elemental composition on the detonation behavior of explosives. *Proceedings of the 6th Symposium on Detonation*, San Diego, CA, 24 August 1976. US Department of Energy.

Fiserova, D. 2006. Numerical analyses of buried mine explosions with emphasis on effect of soil properties on loading. PhD thesis, Cranfield University, UK. 239 pp.

Konya, C.J. and Konya, A. 2018. Effect of hole stemming practices on energy efficiency of comminution. *Energy Efficiency in the Mineral Industry*. Awuah-Offei, K. (ed.). Springer, Cham, Switzerland

Oran, E.S. and Boris, J.P. 2001. Numerical Simulation of Reactive Flow. 2nd edn. Cambridge University Press. 529 pp.

Özkahraman, H.T. 1993. Critical evaluation of blast design parameters for discontinuous rocks by slab blasting. PhD thesis, Middle East Technical University, Ankara.

Park, D. and Jeon, S. 2010. Reduction of blast-induced vibration in the direction of tunneling using an air-deck at the bottom of a blasthole. *International Journal of Rock Mechanics and Mining Sciences*, vol. 47. pp. 752–761.

Riedel, W., Thoma, K., Hiermaier, S., and Schmolinske, E. 1999. Penetration of reinforced concrete by BETA-B-500, numerical analysis using a new macroscopic concrete model for hydrocodes. *Proceedings of the Ninth International Symposium on Interaction of the Effects of Munitions with Structures*. Berlin, 3–7 May 1999. Akademie der Bundeswehr für Information und Kommunikation. pp. 315–22.

Riedel, W. 2000. Beton unter dynamischen lasten meso-und makromechanische modelle und ihre parameter. Ernst-Mach-Institut, Freiburg.

Snelling, W. and Hall, C. 1912. The effects of stemming on the efficiency of explosives. US Department of the Interior, Bureau of Mines, Washington, DC.

Souers, P.C. and Kury, J.W. 1993. Comparison of cylinder data and code calculations for homogeneous explosives. *Propellants, Explosives, Pyrotechnics*, vol. 18. pp. 175–183.

Toro, E.F. 1997. Riemann Solvers and Numerical Methods for fluid dynamics: A Practical Introduction. Springer-Verlag. Berlin. 592 pp.

Zukas, J.A.2004. Introduction to Hydrocodes. *Studies in Applied Mechanics*. Elsevier. pp. 175–183. ◆


# An alternative pillar design methodology

**R.W.O. Kersten**[1]

**Affiliation:**
[1]Rock Mechanics Consultant.

**Correspondence to:**
R.W.O. Kersten

**Email:**
rkersten@mweb.co.za

**Dates:**
Received: 25 Jan. 2017
Revised: 16 Sept 2018
Accepted: 6 Nov. 2018
Published: May 2019

**How to cite:**
Kersten, R.W.O.
An alternative pillar design methodology.
The Southern African Insitute of Mining and Metallurgy

DOI ID:
http://dx.doi.org/10.17159/2411-9717/16/388/2019

ORCiD ID:
R.W.O. Kersten
https://orchid.org/0000-0001-6344-7510

## Synopsis

**The aim was to investigate stable pillar design procedures currently in use on chrome and platinum mines, subject them to a critical appraisal, and review some of the alternatives proposed in the literature. It is concluded that these pillar design methodologies suffer from drawbacks that can be detrimental to the mining industry and that an improvement is essential.**

**It was decided that the increased availability of analytical models and failure criteria could be exploited to update the empirical to an analytical/empirical method. The proposed methodology adopted FLAC2D simulations using the Hoek-Brown failure criterion to calculate full stress-deformation curves for typical pillars. The mine stiffness concept was introduced to determine the pillar load, integrating the influence of the pillar and strata stiffness and mining geometry.**

**The proposed methodology was calibrated by comparing experimental and predicted deformations and failure depth of pillars in one hard-rock mine. The conclusion was that the methodology is an improvement over the one currently in use. An improved factor of safety is given by the intersection point of curves for the stiffness of the system and the pillar strength.**

**Keywords**
**stable pillar design, failure criteria, analytical model, stress deformation curve, strata stiffness.**

## Introduction

The paper describes part of the findings of a PhD thesis (Kersten, 2016) on an alternative stable pillar design methodology. This publication contains sufficient information to implement the method for further interpretation and testing. A detailed comparison of measured and predicted data is dealt with in the thesis, and the results show that there is promise in the methodology.

The design of stable pillars in mining is of fundamental importance, not only in the Bushveld Complex mines but throughout the mining industry. Wherever mining occurs, pillars are formed at some stage and it is essential to predict their behaviour, *i.e.* whether they will burst, yield, or remain stable. Although of crucial importance, pillar design still suffers from major shortcomings and weaknesses.

Owing to uncertainty, pillar designs have for the most part been conservative, with the possible result of the loss of millions of tons of ore by being sterilized and unavailable in the future.

The first pillar strength equation was derived empirically by Salamon and Munro (1967) for coal mines, and was subsequently modified empirically by Hedley and Grant (1972) using data from a Canadian uranium mine. This equation for hard rock has been in use in a variety of mining scenarios in South Africa and elsewhere for over 45 years without modification. In the same period a series of codes, such as *FLAC* and *TEXAN*, as well as failure criteria such as the Hoek-Brown criterion, have been developed and updated but are not commonly used in the design of pillars. The majority of pillars in the platinum mines in South Africa are still designed using the modified Hedley-Grant strength equation in conjunction with the tributary area theory.

This paper is an attempt to improve the antiquated empirical system by incorporating analytical methods in the design methodology by:

- Investigating the pillar design method currently in use; its strengths and weaknesses
- Finding alternative methods in use; actual and suggested
- Proposing alternative methods for calculating the pillar strength and the loading system
- Calibrating the proposed method with underground observations.

## Current pillar design method: strengths and weaknesses

The Hedley-Grant pillar strength equation is based on the following relationship:

## An alternative pillar design methodology

$$\sigma_{str} = k\, w^{\gamma}\, h^{\alpha} \quad [1]$$

where $k$ is the strength factor

$w$ and $h$ the width and height of the pillar

$\gamma$ and $\alpha$ variable exponential 'constants', 0.5 and –0.75 for hard rock mines

$\sigma_{str}$ pillar strength.

Except for the width and the height of the pillar, the strength factor is based on back-analysis of failed pillars. In the absence of such data, the strength factor is assumed to be a fraction of the uniaxial compressive strength of the rock mass in the pillar; the value varies from 0.3 to 0.8. This is sometimes increased without sound scientific basis when no pillar failure occurs. This type of approach is not only wasteful but could also lead to regional failures.

The uniaxial compressive strength, on which the strength factor is based, varies significantly in the industry, between mines, and individual mining areas. Numerous samples are required to obtain a statistical significant mean.

The stress imposed on the pillar is determined using the tributary area theory (TAT) based on the percentage extraction over an infinite area, depth below surface, and the rock mass density. The assumption of mining over an infinite area creates a condition of a 'soft' loading system affecting the pre- and post-failure behaviour of pillars.

The above argument presupposes that the values using TAT and the modified Hedley-Grant equation provides the correct answer. From personal observations over 40 years it was found that in the majority of cases the predicted failure does not materialise, suggesting that the input parameters are overly conservative and/or the pillar equation is suspect.

Planes of weakness as well as softer layers cannot be accounted for by using the Hedley-Grant equation.

It is the author's opinion that the major reason for using the Hedley-Grant equation is its simplicity and that it is generally accepted by the industry as well as the authorities.

These shortcomings have been recognized by other authors, and alternative design procedures that cover some of the weaknesses have been developed. These are discussed below.

### Alternative methods, in use and suggested

Esterhuizen (2003) highlighted the degree of uncertainty associated with each design parameter and discussed the influence of the variability of input parameters in the Hedley-Grant equation, specifically the pillar strength factor $k$ and the width, length, and height of a pillar. He ascribed the uncertainty to the inherent variability of the rock material and a lack of understanding of the way in which rock behaves.

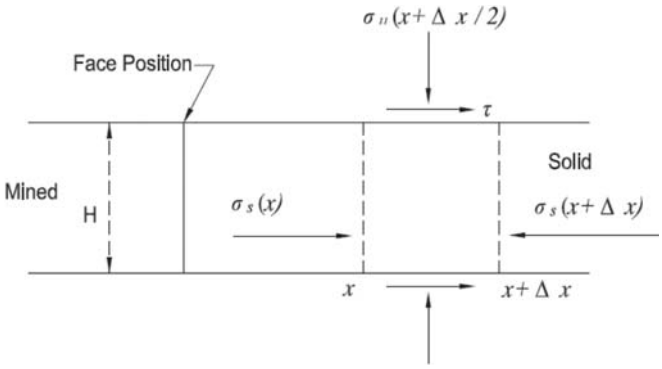


**Figure 1—Analytic finite equilibrium model (Malan and Napier, 2006)**

Determining the mean and standard deviations for the relevant quantities, he used the point estimate method to calculate the mean pillar strength with the standard deviation permutation using the Hedley-Grant equation.

Subjecting the pillars to a uniform stress, using the TAT, he determined the factor of safety as well as the probability of failure (PoF) of the pillars and the reliability of the result as:

$$\text{Reliability} = 100(1 - \text{PoF}) \quad [2]$$

A brief sensitivity study showed that for the specific model the reliability did not increase significantly above a FoS of 2.0. Also, an increase in depth increased the reliability by decreasing the influence of the pillar dimension variation.

The limit equilibrium model proposed by Malan and Napier (2006) simulates the progressive fracturing of the pillar sidewall, illustrated in Figure 1. The progressively created wedges are restrained by the hangingwall and the footwall seam-parallel stress $\sigma_s$, the seam-normal stress $\sigma_n$, and the shear traction, which is proportional to the seam-normal stress $\sigma_n$. The method has the advantage that it proposes a quantifiable failure mechanism, but has not been used in general mine pillar design.

Although the model describes the progressive failure process of a pillar, the pillar strength is obtained by determining the onset of failure as well as the reduction in strength as failure progresses.

Martin and Maybee (2000) studied the brittle failure of pillars in the Canadian Shield hard-rock mines and concluded that the dominant mode of failure was progressive slabbing and spalling. They investigated the commonly used empirical equations listed in Table I, which are based on failed pillars confined to *w/h* ratios less than 2.5.

*Table I*

**List of pillar strength equations summarized by Martin and Maybee (2000)**

| Author | Rock rype | UCS (MPa) | Equation | *k* |
|---|---|---|---|---|
| Hedley and Grant (1972) | Quartzite | 230 | $133^{w^{0.5}/h^{0.75}}$ | 133/230 = 0.58 |
| Von Kimmelman (1984) | Metasediments | 94 | $65^{w^{0.46}/h^{0.66}}$ | 65/94 = 0.69 |
| Krauland (1987) | Limestone | 100 | $35.4(0.778+0.2222\frac{w}{h})$ | 35.4/100 = .35 |
| Potvin (1989) | Canadian Shield | - | $0.42\sigma_{str}(w/h)$ | |
| Sjoberg (1992) | Limestone/skarn | 240 | $74(0.778 + 0.222\frac{w}{h})$ | 74/240 = 0.31 |
| Lunder and Pakalnis (1997) | Hard rocks | - | $0.44\sigma_{str}(0.68 + 0.52)k$ | |

## An alternative pillar design methodology

Martin and Maybee (2000) concluded that:

*'Because at pillar w/h > 2 the confinement at the core of the pillar is increasing significantly, the use of Hoek-Brown brittle parameters will be less appropriate. It should be noted that the pillar-failure database shows that there are only a few pillar failures for pillar w/h > 2, hence, the empirical pillar strength equations should be limited to pillar w/h < 2'.*

Joughin, Swart, and Wesseloo (2000) uses the risk-based approach to incorporate the effect of the variation in rock mass properties as well as pillar dimensions, using the Hoek-Brown failure criterion, to calculate the strength of individual pillars. They also used the point estimate method to evaluate the influence of variable rock mass conditions and pillar geometries.

The following parameters were included:

- The mean and standard deviation of the results from all permutations of the uniaxial compressive strength, geological strength index, and values for pyroxenite and chromitite
- Variation in pillar dimensions
- Span variation of bords
- Composite pillars consisting of chromitite and pyroxenite.

An axisymmetric nonlinear finite element model (PHASE 2) was used to calculate the individual pillar strength for all the abovementioned permutations, with the output given in terms of:

- Factor of safety
- Probability of failure
- Reliability.

The method was applied to an area where the results corresponded reasonably well with the number of collapsed pillars.

Leach (2008) and the author researched the validity of the Hedley-Grant equation on large pyroxenite pillars at Nkomati mine. During discussions it was decided to investigate the influence of mining span on pillar loading. On the basis of these discussions, Leach (2008) prepared a report for Nkomati mine dealing with pillar strength in thick orebodies with limited lateral extent using *FLAC3D* to calculate pillar strength and stress distribution.

The resultant force/closure curves and the calculated load line are shown in Figure 2. In all cases the local mine stiffness line

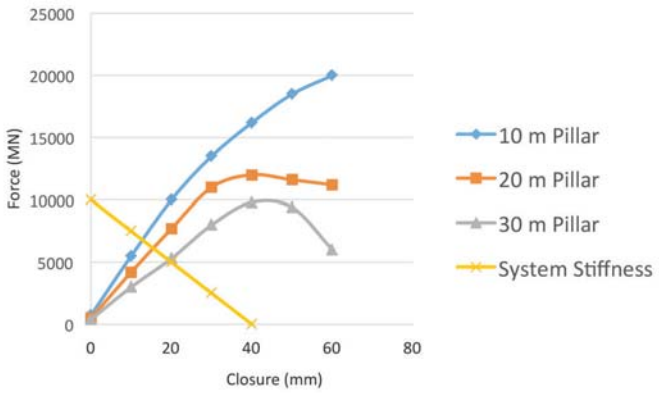


**Figure 2—Force-based comparison of pillar load-deformation characteristics to stope system support requirement (system stiffness) in terms of the 30 x 30 m tributory area associated with pillars in the planned layout (Leach, 2008)**

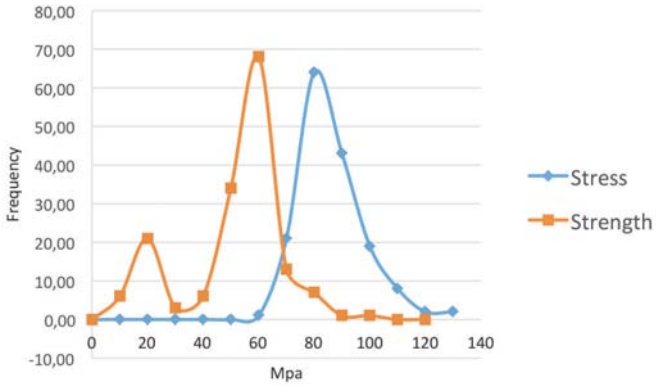


**Figure 3—Frequency distribution of pillar strength and pillar stress (after Kersten, 2009)**

crosses the pillar strength lines in the linearly elastic portion of the pillar curve, well before peak strength is reached.

The procedure included the effect of small spans due to the limited lateral size of the orebody, strata stiffness, full pillar strength curves based on the Hoek-Brown failure criterion, and a comprehensive stress calculation using *FLAC3D*.

The author (Kersten, 2009) proposed a modified TAT for back-analysis of manganese ore pillars at Black Rock mines. The pillar stresses were calculated using the TAT, dividing the entire area by the number of pillars to obtain the tributary area for each pillar assuming a constant pillar centre spacing. The force over the average tributary area was then divided by the area of the individual pillar, giving the resultant individual pillar stresses. Using the Hedley-Grant equation, the strength of each pillar was calculated. The strength and stress values for individual pillars with their varying dimensions are shown in Figure 3 for a specific set of pillars at the mine. The individual FoS values as well as the frequency distribution of the FoS can be interrogated.

Deficiencies that were addressed are the variability of mine dimensions and the use of individual pillar strength values.

The above brief summary shows that bord and pillar layouts can be designed using available analytical procedures, inclusive of variation in pillar and bord dimensions, weaker layers, and the interaction between hanging/footwall and pillar. The use of system stiffness has been reserved for the analysis of the post-failure pillar behaviour (Ryder and Ozbay, 1990), but can be used in the design of stable, elastic pillars.

### Proposed alternative method for calculating pillar strength

The proposed alternative method for calculating the pillar strength is based on a semi-analytical approach using a mathematical model in conjunction with an empirical failure criterion.

- Determining the pillar strength using *FLAC2D*, axial configuration, simulating a circular pillar
- Incorporating the modified Hoek-Brown failure criterion.

It is assumed that the pillar/rock mass remains elastic until pillar failure occurs.

Owing to its versatility, the *FLAC2D* programme can simulate the influence of the hanging- and footwall properties on pillar strength as well as complex interfaces. For the present study it was decided to confine the investigation to simple cases and calibrate these before embarking on more complex structures.

## An alternative pillar design methodology

In the present study, relevant variables included in the *FLAC2D*/Hoek-Brown model were confined to:

- A homogeneous pillar
- Use of known geotechnical parameters
- Development of a simple program for a specific set of conditions
- The $m_i$ value, hence the value $m_r$, was based on the widely used RocLab programme developed by Rocscience.

Details of the program are given in Appendix I.

Using the *FLAC2D*/Hoek-Brown model, the following pillar behaviour was observed:

- The vertical stress is the lowest at the pillar edge after commencement of pillar failure.
- At the average peak pillar stress, $\sigma_{pm}$, the vertical stress at the core of the pillar generally exceeds the uniaxial compressive strength of the rock.
- Pillar failure is a progressive process, moving gradually from the sidewall towards the centre of the pillar.
- Changes in pillar geometry result in the change in the slope of the load-deformation curves as well as the post-failure behaviour. A similar effect has been described by Vogler and Stacey (2016) for different specimen geometries in laboratory studies.
- The *FLAC2D*/Hoek-Brown model is an iterative process incorporating the influence of progressive failure as stepping proceeds.
- The volumetric strain increment could be a possible measure of the depth of fracturing in a pillar.

### Loading system

In the platinum mines geological losses due to faulting and 'potholes' vary between 20% and 30% of the mining area, resulting in limited mining spans between the regional pillars caused by these losses. The influence of the limited span needs to be incorporated in the mine design and can be simulated using the concept of the load line of the system.

Since stable pillar design deals with the pre-failure state of the pillar, the theory of elasticity can be used to the point of pillar failure, allowing accurate calculation of the rock mass deformation and resultant pillar stresses.

To incorporate the influence of limited span geometries it was decided to make use of the load line of a system. Although this concept deals entirely with the post-failure region of pillars it can also be used for the design of stable geometries; stable implying a design with a safety factor in excess of unity.

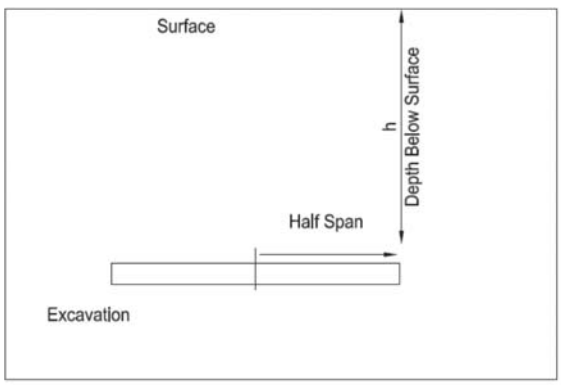


**Figure 4—Schematic drawing of a slot mined at *h* m below surface with a half span of 1 m**

To construct the load line, the force and displacement values need to be calculated.

The closure can be calculated using the theory of elasticity. Figure 4 is a schematic drawing of an infinitely long slot in the third dimension cut at a depth of *h* m below surface having a half span of *l* m. The maximum elastic closure of a tabular excavation is given by equations for infinite as well as finite depth.

The equation for infinite depth is given by Budavari (1983):

$$d_i = 2\frac{[\sigma_y(1-v)l]}{G} \quad [3]$$

where $d_i$ = vertical or y-closure
$l$ = Half span (m)
$\sigma_y$ = Vertical primitive stress component
$v$ = Poisson's ratio
$G$ = Shear modulus of the rock

$$G = E/2(1+v) \quad [4]$$

Mining depth in the Bushveld Complex varies significantly, and for shallow mines Equation [3] needs to be modified to cater for tabular excavation at finite depths:

$$d_i = \left(\frac{2(1-v)\sigma_y l}{G}\right) f(\alpha) \quad [5]$$

$$f(\alpha) = 1 + 0.41\alpha + 0.149\alpha^2 + 0.008\alpha^3$$

where $\alpha = 2l/h$

Equation [5] is attributed to Budavari (1983) as used in his lecture notes. The difference of displacement values between the two equations varies with depth. For 100 m depth, the finite depth equation gives a closure that is 50% higher, while with increasing depth the closure values converge, differing by only 5% at 600 m. For the current investigation, Equation [5] was used.

The above equations deal with a two-dimensional geometry and the half span referred to above is the minimum span in plan of an excavation.

A simplified linear load line for a specific geometry can be determined in the following manner.

To prevent any vertical closure in an excavation, the total reacting force required has to be equal to the negative value of the product of the vertical primitive stress and the mined-out area. Applying this force at the centre of the excavation would have the same effect as a number of distinct units such as pillars,

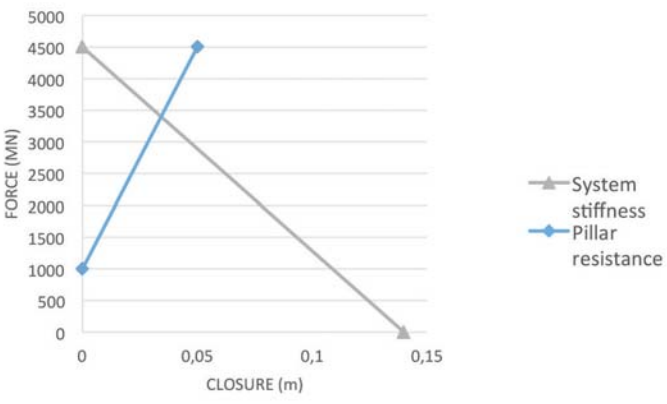


**Figure 5—Pillar resistance and system stiffness curves**

for which the sum of the individual forces is equal to the total required resisting force.

The load line can then be constructed. At zero displacement, the total force required is plotted on the y-axis of the graph shown in Figure 5. For maximum displacement/closure, the force will be zero and is plotted on the x-axis. Connecting the two points gives the linear load line of a system (Figure 5).

The pillar resistance curve is based on the stress and displacement curve obtained using the axisymmetric *FLAC2D* model and the Hoek-Brown failure criterion.

The intersection of the two curves gives the equilibrium condition of a specified two-dimensional geometry.

It must be pointed out that the slope of the *FLAC2D*/Hoek-Brown-determined pillar load deformation curve for individual pillar geometries differs with pillar width as well as pillar height. The span of the excavation also changes the slope of the load line, and in conjunction with the changes in pillar slope affects the value of the equilibrium point significantly and hence the safety factor, especially in limited span, high stope-width excavations such as are generally used in semi-massive ore deposits.

It must be noted that the system stiffness curve can also be determined by incremental load changes, generally resulting in a slightly curved form. For the current proposition, the linear assumption is deemed acceptable; the approach and illustrative portion of the research assumes linearity but the method can be expanded to nonlinear equations.

The pillar/strata system equilibrium point is determined by the intersection point of two equations, assuming the load lines to be linear.

The ground reaction curve is given by:

$$F_g = m_g d_g + c_g \quad [6]$$

The pillar resistance curve for one or more pillars:

$$F_p = m_p d_p + c_p \quad [7]$$

where $F_g$ = System force
$m_g$ = Slope of the ground reaction curve
$d_g$ = System closure
$F_p$ = Force on pillar
$\sigma_{pm}$ = Pillar strength
$m_p$ = Pillar stiffness
$d_p$ = Pillar closure
$c_g$ = Total overburden weight
$c_p$ = Primitive force on pillar

The force at the intersection of the two curves given by Equations [6] and [7] is given by:

$$F = \frac{c_g m_p}{m_p - m_g} \quad [8]$$

Since $c_g$ has been shown to be the overburden total load over the mined-out area $A_m$, it can be expressed as:

$$c_g = \sigma_v A_m \quad [9]$$

The slope of the ground reaction curve, $m_g$, is:

$$m_g = -\frac{c_g}{d_i} \quad [10]$$

where is the maximum deflection of the opening as calculated by Equation [5]. Equation [8] can be extended to:

$$F = (\sigma_v A_m m_p) / \left(m_p + \frac{\sigma_v A_m}{d_i}\right) \quad [11]$$

In practice, there would be a regular layout of approximately equally sized and spaced pillars. If the pillar centre distance is $C$, a strip with width equal to $C$ can be created over a longer distance with span $L$.

The maximum deflection in the absence of pillars is given by Equation [5]. The resistance required to prevent any deflection is the weight of the strip of width $X$ over the panel length $L$.

The system load, $c_g$, is:

$$c_g = XLg\rho H \quad [12]$$

The slope of the ground reaction curve is then:

$$m_g = c_g / d_i \quad [13]$$

The pillars will still have individual closure response. If the maximum pillar stress at failure is $\sigma_{pm}$ the pillar closure at the point of failure is:

$$d_p = \frac{\sigma_{pm}}{E}.h \quad [14]$$

where $h$ is the stoping width.

The pillar load at failure is:

$$F_p = \sigma_{pm}.w^2 \quad [15]$$

where $w$ is the pillar width.

As there is a system of pillars, the total number of pillars across the panel contained in the width $X$ is $\frac{L}{X}$, then the total pillar resistance for the system is:

$$F_{pt} = F_p L / X \quad [16]$$

The slope of the pillar resistance curve is:

$$m_p = F_{pt} / d_p \quad [17]$$

The equilibrium force, $F$, is obtained by substituting the values of $C_g$, $m_g$, and $m_p$ in Equation [8]. The factor of safety is then:

$$\text{FoS} = F_{pt} / F \quad [18]$$

Equations [8] to [18] were incorporated in an Excel spreadsheet to facilitate calculating the average pillar stresses and closures at the equilibrium point as well as the factor of safety.

An alternative formulation of the intersection of the force-displacement suited for incorporation in a spreadsheet model is:

$$d_g = d_p = (c_p - c_p)/(m_g - m_p)$$

$$F_p = F_g = m_p((c_p - c_g)/(m_g - m_p)) + c_p$$

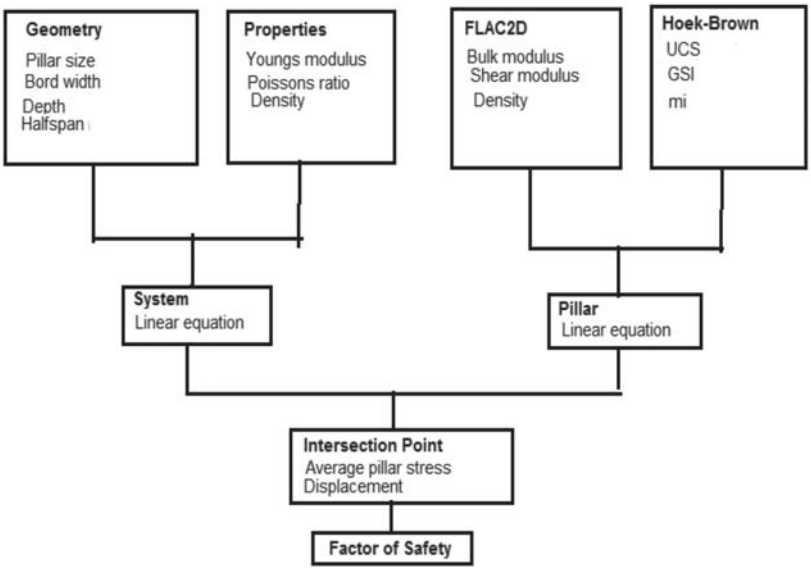


**Figure 6—Schematic presentation of the steps involved in the *FLAC2D*/Hoek-Brown and system pillar equilibrium methodology**

The flow chart in Figure 6 is a schematic presentation of the steps involved in the *FLAC2D*/Hoek-Brown and the system-pillar-equilibrium concept, SPEC.

### Comparison of the proposed method with underground observations

For calibration purposes Impala Platinum Mines was selected because sufficient rock mass property data (Impala Platinum Mines, 2012), as well as experimental observations on pillar fracturing and closure, was available (Piper and Flanagan, 2005).

Data from a six-month monitoring programme at 12 Shaft, Impala Platinum Mine, conducted to quantify the *in-situ* performance of grid pillars by means of rock mass measurements and monitoring, was presented by Piper and Flanagan (2005). The two parameters relevant to the present discussion are the relationship between pillar size and extent of fracturing and closure measurements in individual panels as the span increased.

The pillar geometry was back-analysed as per the sequence illustrated in Figure 6.

A good correlation between the plastic strain component in the strain softening model (*FLAC2D*) and the measured inelastic deformations was found by Kersten and Leach (1996). Roberts (2017) introduced the concept of displacement ratio criteria for accurately predicting borehole breakout. It appears that the use of deformation/strain values offers an alternative approach for prediction of failure zones. In the current study the dimensionless volumetric stain increment (vsi) in the *FLAC2D* model was used.

Figure 7 shows the width of the measured fracture zone and the bracketing vsi values of 1e-2 to 3e-3. The measured reduction in width of the fracture zone with an increase in the pillar width is mirrored by the vsi bracketing the actual values.

Closure measurements by Piper and Flanagan (2005; Figure 8) shows a reduction in closure rate at a span of approximately 30 m. This reduction is due to the effect of the barrier pillars, which are spaced at 60 m intervals on dip, while mining progresses further on strike, limiting the minimum span of the excavation.

Figure 8 is a comparison of the measured closure values with calculated displacements using the proposed pillar system

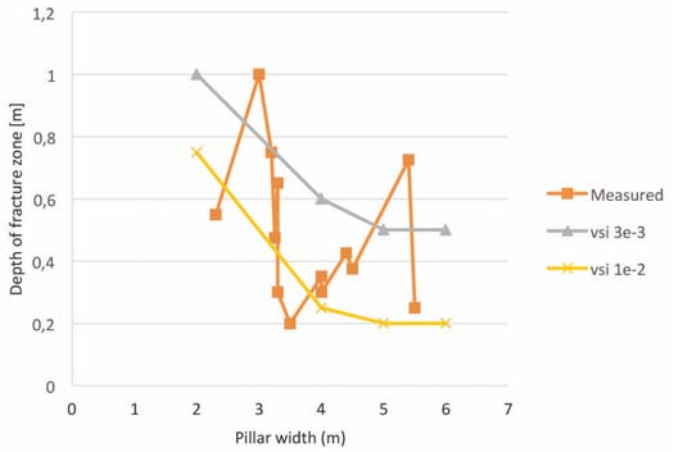


**Figure 7—Width of the measured fracture zone compared to the volumetric strain index values of 3e-3 and 1e-2**

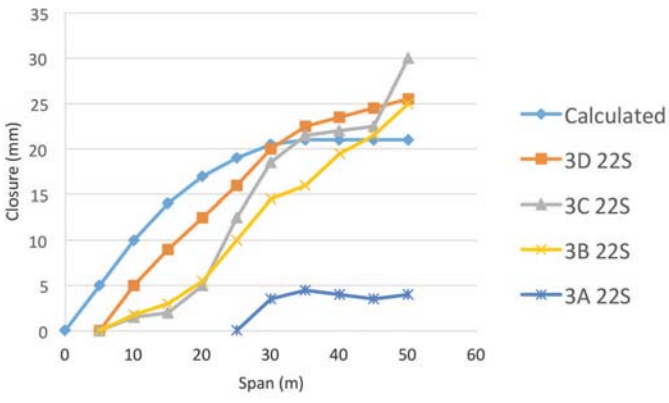


**Figure 8—Closure measurements compared to closure calculated using *FLAC2D*/Hoek-Brown and the system stiffness**

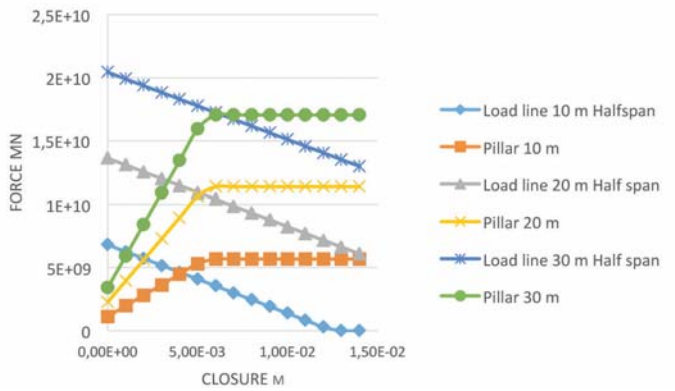


**Figure 9—Force-displacement diagram of the load line and grid pillars for half spans of 10 to 30 m between barrier pillars 60 m apart**

equilibrium concept given above for the different mining spans and specific pillar geometries.

To illustrate the effect of change in span, Figure 9 shows the force-displacement curves for half spans of 10, 20, and 30 m where the intersection points give the FoS of 1.24, 1.05, and 0.98 respectively.

Malan and Napier (2007, 2011) conducted research in the same area as Piper and Flanagan (2005), after further mining had been done, using the *TEXAN* code to calculate the individual pillar stresses. The individual pillar stresses, calculated using the pillar system equilibrium methodology, and with the same elastic constants, compare well with the values obtained by the *TEXAN* code (Table II). As can be expected, the value obtained by the tributary area theory is higher.

In summary:

- The extent of the fracture zone can be predicted reasonably accurately using the volumetric strain increment criterion.
- The amount of closure can be predicted within reasonable accuracy.
- The average pillar stresses agree closely with those obtained using the more elaborate *TEXAN* code.

The combination of the *FLAC2D*/Hoek-Brown model and the system/equilibrium method can be used to obtain realistic values for the average pillar stress, strength, closure, and the factor of safety.

*Table II*

**Comparative pillar stresses. (SPEC - system pillar equilibrium methodology)**

| Geometry | Grid pillar (m) | *APS* (MPa) |
|---|---|---|
| TAT | 12 × 4 | 185 |
| *TEXAN* model | 12 × 4 | 159 |
| SPEC | 12 × 4 | 165 |
| | Barrier pillar (m) | |
| *TEXAN* | 12 × 36 | 63 |
| SPEC | 12 × 36 | 59 |

## Summary and conclusions

It was found that the current bord and pillar design, using the generally accepted empirical Hedley-Grant equation in conjunction with tributary area theory, needs revision. With the availability of analytical methods and failure criteria, it was decided to determine whether it is possible to create an analytical solution to replace the empirical approach.

The proposed methodology uses the load line of the system in conjunction with *FLAC2D* and the Hoek-Brown failure criterion to calculate pillar deformation and failure strength. The intersection point of these two curves gives the equilibrium pillar stress and deformation of the bord and pillar configuration. The pillar edge failure, predicted using a strain-based criterion, as well the elastic deformation, agreed reasonably well with underground measurements.

The stage has been reached where the methodology can be used to predict the influence of rock mass characteristics, most likely failure of pillars at greater depth, and alternative pillar mining methods. The concept deals with intact pillars but can readily be extended to the nonlinear regime.

The results of the investigation dealt with simplified geometries and pillars only, but with the versatility of codes like *FLAC3D/FLAC2D*/Hoek-Brown sets the stage for further investigation and calibration of the interaction between pillars and surrounding country rock using the above or similar available codes and failure criteria.

## Acknowledgments

The author thanks Impala Platinum Mine for making available their rock mass database as well as some unpublished reports, and Professor Nielen van der Merwe for his guidance and patient support.

## Appendix I

The *FLAC2D*/Hoek-Brown model is fundamental to the approach adopted and is, therefore, given in detail in this Appendix. Below is the input file for a simple homogeneous pillar with given dimensions and properties. (This file can be transferred directly into *FLAC2D*).

```
new
ti
Hoek Brown Model for calibration
config axi ; Axial symmetry, simulating a circular geometry
gr 24,20; Grid of 24 by 20
gen 0,0 0,2 2.5,2 2.5,0; Circular pillar 2.5 m high with a radius of 2 m.
mod mo
;Pyroxenite
prop bu=54e9 sh=26.4e9 d=2800 *coh=14e6 ten=1e20 fric=46 ; Shea and, bulk modulus
call hoek2.fis              ;<--(associated rule)
set hb_mmi=12.876 hb_mmr=6.4;. Roclab Modified and residual m, value
set hb_ssi=.1889 hb_ssr=.094 ;0.0010 ; Roclab Modified and residual s values.
set hb_sc=52.1e6 ; Strength value as per Roclab programme
; Circular pillar FISH function for calculating the total force
def load
sum2=yforce(1,jgp)*x(2,jgp)*0.25
loop i (2,igp)
sum2=sum2+yforce(i,jgp)*x(i,jgp)
end_loop
```

```
ftot = 2.*pi*sum2
; (Total area of strip pillar - axi-symmetric mode)
_area = pi*x(igp,jgp)*x(igp,jgp)
load = ftot
aps  = ftot/_area
end
his yd i=1 j=20 ; Histories for selected points
fix x y j=1; Setting boundary conditions
fix x y j=21
fix x i=1
*ini yv 1e-7 j=1; Setting loading rates
ini yv -1e-6 j=21
his aps; Results from FISH functions
his load
his xd i=19 j=10
set nsup=3000 ns=10 ; note, FLAC will cycle nsup*ns times;
Number of steps
supsolve
end
```

Also included is the subroutine hoek2.fis Hoek-Brown failure criterion to be used in all the simulations of homogeneous pillars.

```
FISH routine for Hoek-Brown failure surface
; the dilation angle is specified using hoek_psi
; (hoek_psi = fi for an associated flow rule)
;
def cfi
loop i (1,izones)
loop j (1,jzones)
if state(i,j) > 0 then
h_mm=hb_mmr
h_ss=hb_ssr
else
h_mm=hb_mmi
h_ss=hb_ssi
end_if
effsxx = sxx(i,j) + pp(i,j)
effsyy = syy(i,j) + pp(i,j)
effszz = szz(i,j) + pp(i,j)
tension(i,j)=0.5*hb_sc*(sqrt(h_mm^2+4*h_ss)-h_mm)
temp1=-0.5*(effsxx+effsyy)
temp2=sqrt(sxy(i,j)^2+0.25*(effsxx-effsyy)^2)
s3=min(temp1-temp2,-effszz)
if s3<0.0 then
s3=0. end_if
if s3<0.0 then
s3=0.
end_if
```

## References


Budavari, S. 1983. Stresses and displacements induced by mining. *Rock Mechanics in Mining Practice. Monograph Series* 5. Southern African Institute of Mining and Metallurgy, Johannesburg.

Esterhuizen, G.S. 2003. Variability considerations in hard rock pillar design. *Proceedings of Rock Engineering Problems Related to Hard Rock Mining at Shallow to Intermediate Depth*, Rustenburg. South African National Institute of Rock Engineering. pp. 48–54.

Hedley, D.G.F. and Grant, F. 1972. Stope pillar design for the Elliot Lake uranium mines, *CIM Bulletin,* vol. 65. pp. 37–44.

Impala Platinum Mines. 2012. Composite data bank of rock properties. Personal communication.

Itasca Consulting Group 2011. Fast Lagrangian Analysis of Continua, online manual and user's guide. Minneapolis, MN.

Joughin, W.C., Swart, A.H., and Wesseloo, J. 2000. Risk based chromitite pillar design – Part II. Non-linear modelling. *Proceedings of SANIRE 2000, Keeping it up in the Bushveld and Advances in Support Technology.* South African National Institute of Rock Engineering.

Kersten, R.W.O. 2009. Black Rock Mines; comments on the rock engineering requirements. Internal report. Assmang, Johannesburg.

Kersten, R.W.O. and Leach, A.R. 1996. The calibration of material models in FLAC for deep gold mine problems. *Prediction and Performance in Rock Mechanics & Rock Engineering. Proceedings of the ISRM International Symposium EUROCK '96,* Turin, September 1996. Vol. 2 Barla, G. (ed.). Balkema, Rotterdam. pp. 1179–1084.

Kersten, R.W.O. 2009. Comments on the rock engineering aspects of Black Rock Mining Operations. Contract report to mine management, BRMO operations.

Kersten, R.W.O. 2016. A probabilistic structural design process for bord and pillar workings in chrome and platinum mines in South Africa. PhD thesis, Faculty of Engineering and the Built Environment, University of the Witwatersrand, Johannesburg.

Leach, A R. 2008. Summary Report; Assessment of stability of proposed room and pillar workings for Nkomati Mine. Itasca Africa (Pty) Ltd.

Lougher, D.R and Ozbay M.U. 1995. In-situ measurements of pillars and rock mass behaviour in a moderately deep hard-rock mine. *Journal of the South African Institute of Mining and Metallurgy,* February 1995. pp. 19–24.

Malan, D.F. and Napier, J.A.L. 2006. Practical application of the TEXAN code to solve pillar design problems in tabular excavations. *Proceedings of SANIRE 2006, Facing the Challenges in Rock Mechanics.* South African National Institute of Rock Engineering. pp. 1–20.

Malan, D.F. and Napier, J.A.L. 2007 Numerical modelling of the bord and pillar layout at Impala no 12 Shaft. *Contract report* CR269/0307/IMP021. March 2007.

Mathey, M. 2015. Personal communication.

Martin, C.D. and Maybee, W.G. 2000. The strength of hard rock pillars. *International Journal of Rock Mechanics and Mining Sciences*, vol. 37. pp. 1239–1246.

Piper, P.S. and Flanagan, F.W. 2005. The in-situ performance of yielding pillars at Impala 12 Shaft. *Proceedings of the 3rd Southern African Rock Engineering Symposium*. South African National Institute of Rock Engineering.

Roberts, D. 2017. Calibration of numerical model for bore--and-fill mining. *Journal of the South African Institute of Mining and Metallurgy*, vol, 117, no. 7. pp. 705–718.

Ryder, J.A. and Ozbay, M.U. 1990. A methodology for designing pillar layouts for shallow mining. *Proceedings of the International Symposium on Static and Dynamic Considerations in Rock Engineering,* Swaziland. International Society for Rock Mechanics. pp. 273–286.

Salamon, M.D.G. and Munro, A.H. 1967. A study of the strength of coal pillars. *Journal of the South African Institute of Mining and Metallurgy*, vol. 68. pp 55–67.

Van der Merwe, J.N. and Mathey, M. 2013. Update of coal pillar strength formulae for South African coal using two methods of analysis. *Journal of the Southern African Institute of Mining and Metallurgy,* vol. 113, no. 11. pp. 841–847.

Vogler, W.W.O.L. and Stacey, T.R. 2016. The influence of test specimen geometry on the laboratory-determined Class II characteristics of rocks. *Journal of the Southern African Institute of Mining and Metallurgy,* vol. 116, no. 11. pp. 987–1000.

Watson, B.P., Ryder, J.A., Kataka, M.O., Kuijpers, J.S., and Leteane, F.P. 2008. Merensky pillar strength formulae based on back analysis of pillars at Impala Platinum Mine. *Journal of the Southern African Institute of Mining and Metallurgy,* vol. 108, no. 8. pp. 449–461. ◆

# Mining companies attain relief through deductions on infrastructure relating to Social and Labour Plans: A case of the cart before the horse?

**K. Thambi**[1]

**Affiliation:**
[1]School of Law, University of the Witwatersrand, South Africa.

**Correspondence to:**
K. Thambi

**Email:**
Kiyasha.Thambi@wits.ac.za

**Dates:**
Received: 15 Mar. 2018
Revised: 12 Dec. 2018
Accepted: 15 Jan. 2019
Published: May 2019

**How to cite:**
Thambi, K.
Mining companies attain relief through deductions on infrastructure relating to Social and Labour Plans: A case of the cart before the horse?
The Southern African Insitute of Mining and Metallurgy

DOI ID:
http://dx.doi.org/10.17159/2411-9717/61-132-1/2019

ORCiD ID:
K. Thambi
https://orchid.org/0000-0003-4456-3027

**Synopsis**

**A recent amendment to Section 36(11)(e) of the Income Tax Act, 53 of 1968 (Tax Act) now extends the allowable deduction of 'capital expenditure' incurred by mining companies pursuant to the Mineral and Petroleum Resources Development Act 28 of 2002 (MPRDA). In terms of the Taxation Laws Amendment Bill 2016 (TLAB 2016), the allowable deduction has been extended to include expenditure incurred on infrastructure in terms of Social and Labour Plan (SLP) requirements as per the MPRDA. Interestingly, what necessitated the amendment was the need to recognize SLP requirements and to circumvent administrative difficulties for mining companies and the South African Revenue Services (SARS) in differentiating the use of developmental infrastructure by employees or the community. The successful implementation of such a deduction hinges on a sound SLP system. However, given the challenges within the current SLP system, this amendment could be considered somewhat premature.**

**Keywords**
**Social and Labour Plan, capital expenditure, infrastructure, tax relief.**

## Introduction

Section 36(11) of the Income Tax Act 58 of 1962 (Tax Act) enabled mining companies to deduct certain capital expenditure in lieu of its other sections. In particular, it made provision for mining companies to deduct capital expenditure incurred pursuant to the Mineral and Petroleum Resources Development Act 28 of 2002 (MPRDA), but excluding capital expenditure incurred in respect of infrastructure or environmental rehabilitation. As such, mining companies could only deduct such capital expenditure that related directly to their employees and not to the wider community (Clegg, 2018).

In terms of the Taxation Laws Amendment Bill 2016 (TLAB, 2016) (South Africa, 2016a), the recent amendment to Section 36 extends the relief provided under section 36(11)(e) to include capital expenditure incurred on infrastructure in terms of the Social and Labour Plan (SLP) requirements of the MPRDA. In other words, the capital expenditure incurred by the mining company for the benefit of the people living in mining communities. To qualify for such a deduction, the infrastructure erected or developed by the mining company should reflect what was agreed between the mining company and the Department of Mineral Resources (DMR) as per the SLP requirements of the MPRDA (TLAB 2016).

## The Problem

Considering the current SLP system, there are significant disparities between its various stakeholders as well as limitations, *i.e.* current guidelines on the development of SLPs have proven insufficient, the interpretations of SLP requirements lack standardization and proper guidance, and there is a lack of implementation and active participation by various stakeholders (among others). Therefore, the deduction granted in terms of Section 36(11)(e) is in all likelihood premature, possibly based on insufficiencies in information, leading to premature approvals of SLPs and/ or approval of SLPs that fall short of the requirements as per the MPRDA and the tenets of SLPs.

## Aim

This paper reviews some of the salient disparities that seem to support the notion that the aforementioned amendment may be premature, given the landscape of the current SLP system.

## Background: the mining industry and its socio-economic development impact

The South African mining industry is one of the major building blocks in South Africa's economy. Prior to the new constitutional era, the mining sector was premised on the exploitation of South Africa's mineral

resources, creating only indirect benefits for the majority of South Africans through the infrastructure and the economy it established (Kloppers and du Plessis, 2008). Not only does the mining industry contribute to South Africa's GDP via exports *etc*., but it employs a significant number of the population. Despite being a contributor to exports revenue, employment, and infrastructure, it is responsible for a plethora of negative impacts *i.e.* disputes over land use, pollution, high fatality and injury rates (Finweek Report, 2008), and the impact of mine closure. Yet it has often dismissed its environmentally and socially disruptive business consequences on the basis of cost-benefit analysis; arguing that the monetary benefits outweigh the negative impacts of 'doing business' (Jenkins and Yakovleva, 2006).

As such, the legacy of the mining industry in South Africa has been plagued with controversy given these negative impacts, imbalances between mineworkers, communities, and mining companies. Like a festering wound, this industry has been riddled with the exploitation of a low-wage migrant labour force of black South Africans (Centre for Applied Legal Studies, 2016). Furthermore, the historical tension between mining companies and the communities within which they operate stemmed from the inequity of apartheid, since 'the activities of the mining houses were inextricably linked with colonial, and subsequently apartheid, policies through the migrant labour system' (Hamann, 2003).

In the light of the aforementioned, the South African mining industry, deeply entrenched in the bedrock of South Africa's economy, has faced numerous pressures of varying degrees over the 'extent' of its failure to consider the environment and the communities in which it engages in mining operations. Being a largely capital-intensive industry, with high start-up costs and various regulatory requirements, it is constantly challenged to balance this and regulatory intensive operations with the sustainable integration of some of these pressures *i.e.* Corporate Social Responsibility (CSR) through SLPs, into its core business strategy. Yet it is evident that some mining companies still view this social investment as a means of gaining their social licence to operate (Hamman, 2003).

On average, a mining company incurs a wide range of expenditure in conducting its operations, including current expenditure (deductible in terms of the general deduction formula per the Tax Act) and capital expenditure. The capital expenditure provisions of the Tax Act provide for the immediate deduction of capital expenditure and of expenditure on prospecting and incidental operations. Capital expenditure includes expenditure on shaft sinking, mine equipment, development, general administration, and management. Some assets, such as housing for residential accommodation, motor vehicles for the private use of employees, and some railway lines and pipelines, qualify only for a partial annual redemption (Clegg, 2018). Prior to the aforementioned amendment, Section 36(11) of Tax Act enabled mining companies to deduct certain capital expenditure in lieu of other sections in the Act. In particular, section 36(11)(e) of the Act made provision for mining companies to deduct capital expenditure incurred pursuant to the MPRDA, but excluded capital expenditure incurred in respect of infrastructure or environmental rehabilitation (Explanatory Memorandum on the Draft Taxation Laws Amendment Bill 17B 2016) (South Africa, 2016b). However, the dilemma for mining companies was that they could deduct such capital expenditure only to the extent that it related directly to employees, and not to the wider community.

### The Mineral and Petroleum Resources Development Act 28 of 2002

Against this backdrop, South Africa's economic transition as an emerging market economy 'eclipsed' plans to resuscitate the economy in favour of growth and development. However for the mining industry in particular; even with Constitution of the Republic of South Africa, Act 108 of 1996 (the Constitution) (South Africa, 1996), which recognizes the State's obligation to protect citizens' socio-economic rights such as the right to housing, clean water, and medical assistance, it was not without limitation (Busacca, 2013). Furthermore, the government was challenged by a lack of resources and skilled personnel (Kloppers and du Plessis, 2008). As such, given the political climate in the country, the transformation was inevitable. To circumvent the destabilization of the mining industry, and inculcate transformation in the mining sector, a number of initiatives were established. One such initiative was the MPRDA, administered by the Department of Mineral Resources (DMR) (Cawood, 2004).

The MPRDA was intended to achieve equitable access to, and sustainable development of, South Africa's mineral and petroleum resources. It vests mineral rights in the State as custodian of the mineral wealth (MPRDA, Government Gazette, 2002). Among its multiple purposes, the MPRDA aims to transform the mining and production industries in South Africa. It focuses on the transformation of the minerals and mining industry with specific emphasis on developing black ownership of mines (Munnik, 2010). The MPRDA requires companies to convert their old-order mining rights into new-order rights. To achieve this, companies must meet a number of social and labour targets that overlap with the targets in the Broad-Based Socio-Economic Empowerment Charter for the South African Mining Industry 2003 (Mining Charter) (Cawood, 2004). For CSR, the most important objective of the MPRDA is contained in Section 2(i), which requires that mining companies contribute toward the socio-economic development of the areas in which they operate (Kloppers and du Plessis, 2008) However, it does not explicitly state how this objective should be achieved, and consequently it is left to the industry to adopt the spirit of the Act in a 'meaningful way'. It would, therefore, appear that the mining industry is often left 'unattended' in its adoption of the spirit of the MPRDA in this regard (Centre for Applied Legal Studies, 2016).

The extent to which mining companies subscribe to the MPRDA is voluntary and is visible by the extent of their CSR programmes. In compliance with the MPRDA, when applying for a new mining right, a company must submit a mine works plan, environmental management plan, and a Social and Labour Plan. Mining operations are further required to submit annual compliance reports (Centre for Applied Legal Studies, 2016). As part of its mandate and endeavour toward effective transformation, the MPRDA makes it compulsory for mining companies to submit a Social and Labour Plan (SLP). In terms of the MPRDA, taxpayers seeking to acquire mineral rights are required to submit a SLP in terms of which the mineral right holder is required to assist local communities with infrastructure and other amenities. The challenge with the SLP is that where infrastructure was built for the benefit of non-employees, such expenditure is treated as non-deductible capital expenditure for income tax purposes.

Simultaneously, when applying for a mining license, mining companies are required to conduct a Social Impact Assessment (SIA) to estimate the social consequences that ensue from their mining activities from start to beyond mine closure. SIAs form

part of the Environmental Impact Assessment (EIA) process, attempting to review the social impact of a mining project in consideration of the social environment. However SIAs receive far less focus then they should, given their extent. This is due to the fact that the links between environmental and social impacts are not recognized in the mining sector (Creative Space Media, 2015).

## Insights into the landscape of Social and Labour Plans

SLPs are entered into between the mining company, community, and the DMR. The eligibility for a mining right and renewal thereof is conditional upon the submission by a mining company of a SLP, developed in consultation with affected communities. It contains commitments to the DMR in respect of human resources and local economic development. Upon granting of the mining right, these programmes become binding conditions. In other words, noncompliance with the SLP can lead to the suspension of the mining right. Interestingly, what is not clear in the existing legislation is that each SLP contains commitments over a five-year cycle (Centre for Applied Legal Studies, 2016). The tenets of a SLP are to assist with the development of mining communities. This typically involves a company agreeing to build infrastructure, ranging from roads and drainage systems to crèches, schools, clinics, housing, and recreational facilities – to benefit workers and communities surrounding the mine (South Africa, 2016b). The basis of the SLP system is very much a 'carrot-and-stick approach'. The State's approval (or not) of the right to mine is dependent on mining companies, either directly or indirectly from the resources in their area being mined, creating opportunities for mineworkers and communities to benefit (Centre for Applied Legal Studies, 2016).

Furthermore, mining companies are expected to specifically document their implementation of and compliance with the SLP at various stages in the process. Thereafter they are required to deliver on each undertaking, and to the extent that a SLP falls short of its targets the consent of the Minister of Mineral Resources must be obtained by the mining right holder to amend such SLP. Companies are also required to engage with municipalities and participate in the drafting of Integrated Development Plans (IDPs) which are regulated by the Municipal Systems Act 32 of 2000 (Centre for Applied Legal Studies, 2016). In other words, the Local Economic Development (LED) component of the SLP must be aligned with the municipal IDP. The thinking behind this alignment is that such engagement provides opportunities for investment, economic growth, poverty alleviation, and infrastructural development (Creative Space Media, 2015).

Having considered the landscape of the SLP system (whereupon this amendment is reliant), it is clear that there are four significant stakeholders, *i.e.* mining companies, the DMR, local government, and workers and communities. The disparities between these various stakeholders with regard to responsibilities, expectations, and/or perceptions in the initiation and implementation of SLPs is very evident, as will be seen below. Furthermore, according to the Centre for Applied Legal Studies (2016) 'there is growing evidence that the SLP system does not work and that SLP obligations are not being met'. To support this notion, at the National Council of Provinces (NCOP) the Minister of Mineral Resources stated that as at 31 March 2015, a total of 240 mining right holders failed to comply with their SLPs. An illustration thereof (though this will not be discussed in detail) is evidence per the Marikana Commission of Enquiry which heard submissions regarding Lonmin's compliance with its SLP, following the Marikana massacre.

## SLP stakeholders, the MPRDA and current practices

### *Mining companies*

In practice, mining companies do not consult with communities and workers with regard to SLPs and/or amendments thereto. This leads to a fundamental imbalance of the tenets of the SLP system, and at times a possible derogation from the initial commitments made by mining companies, as per their SLP mandate. Consequently, participation and/or stakeholder engagement through the SLP cycle is compromised, particularly since mining companies fail to identify and understand the affected communities, while they pursue their strategic business objectives (CSI, 2015). This lack of stakeholder engagement creates challenges in informing the process leading up to a viable and sustainable SLP. Hence, under such circumstances, mining companies that fail to implement an SLP in line with the MPRDA and SLP guidelines should not be allowed to rely on a tax deduction in terms of Section 36 of the Tax Act. Hence, a claim for a deduction for capital expenditure on infrastructure in relation to a SLP ought to fail where this requirement has not been fully complied.

### *The DMR*

The DMR has the most significant role of national government departments. It is tasked with managing the mining application process, and the responsibility of monitoring compliance with and enforcement of regulatory requirements, including the approval of SLPs. It is also required to collaborate with various stakeholders to ensure the SLP implementation, which includes the reviewing and approval of applications as well as on-site inspections to verify compliance. Where noncompliance with SLPs is detected, the DMR must use its powers of enforcement, including remedial actions, notices, and (where necessary) suspension or revocation of the mining right (Centre for Applied Legal Studies, 2016). However, the process of SLP evaluation by the DMR is currently inconsistent due to the lack of expertise in evaluating such SLPs. This inconsistency causes undue pressure and weakens the process meant to establish alignment between the strategic objectives of government and mining companies. Fundamentally, the regulatory system does not sufficiently provide clear contextual considerations by which the regulator can evaluate the adequacy and or efficacy of SLPs (Centre for Applied Legal Studies 2016). This will further create a challenge for a mining company claiming a deduction of capital expenditure in relation to infrastructure for a SLP, particularly where reliance is placed on the DMR vetting and approving the claim. To the extent that mining companies are successful in claiming the deductions but have not provided the infrastructure as per SLP requirements, there ought to be misalignment between the SLP and the actual infrastructure built by the mining company. This will create a ripple effect, and an administrative burden for SARS to audit and reconcile deductions granted *versus* the actual SLPs implemented (tangible). Furthermore, it may require some mining companies to refund any deductions granted prematurely.

### *Local government*

Local government is mandated with the implementation of LED in terms of both the Constitution and legislation. Each municipality is tasked with drawing up an IDP, being a strategic plan for the development of the municipality (Centre for Applied Legal Studies, 2016). It has been argued that municipalities are the ideal entities to observe the delivery or lack thereof concerning LED projects. This is due to their local knowledge and historical

relationships with the areas being mined (Creative Space Media, 2015). However, the local government fails in implementing the SLPs due to various factors, *e.g.* lack of technical capacity, resources, and insufficient infrastructure to support the aims of SLPs. This is exacerbated by municipalities' budgetary constraints and poor delivery of basic services to communities (Centre for Applied Legal Studies, 2016). This is yet another challenge to the SLP system. This lack of engagement between mining companies and local government thwarts any possibility of facilitating opportunities for economic growth, infrastructural development, and poverty alleviation. As consequence thereof, mining companies operate in a void when it comes to the implementation of SLPs that are clearly not a core competency of theirs.

### *Mineworkers and communities*

Mineworkers and communities who reside near the mining areas are the beneficiary stakeholders of the SLP system, who are acutely affected by the negative environmental, social, and economic impacts of mining. As stated earlier, a prerequisite of the SLP system is that these stakeholders be consulted and taken into consideration on issues that affect them with regard to SLPs. However, in practice, these stakeholders are not consulted, neither are they involved in the process leading to the compilation of an SLP. In fact, they 'fall through the cracks' of the already compromised SLP system where proper stakeholder engagement from both mining companies and local municipalities has failed (Centre for Applied Legal Studies, 2016). As such, they cannot be considered beneficiaries of any socio-economic development when their fundamental rights are compromised. In the light thereof, any claim for a deduction as per Section 36(11)(e) must at least have passed through this basic requirement, failing which the deduction should not even be considered. The challenge, however, is that failure to comply with and monitor the satisfaction of this particular prerequisite by the DMR may be the very reason for SLPs to be prematurely vetted and approved, resulting in an ensuing 'justifiable' deduction per Section 36(11)(e).

## Putting the cart before the horse

There is no doubt that SLPs have tremendous potential under the optimal regulatory conditions, yet it is clear that some of the aforementioned challenges weaken the SLP system in its current state. Hence, it is argued that the basis upon which the Section 36 amendment is founded is fundamentally flawed, in that it suffers from inactive participation by various stakeholders as well as poor implementation (Creative Space Media, 2015). As stated earlier, the current guidelines on the development of SLPs have proven insufficient. The interpretations of SLP requirements require standardization to ensure proper guidance for all stakeholders when executing these plans. In addressing these issues, consideration ought to be given to the application of governance principles in the implementation cycle of SLPs. Furthermore, the SLP system, which was designed to achieve a social impact through mandating the allocation of resources, can be successful only if the required actions by all stakeholders are fulfilled (Centre for Applied Legal Studies, 2016).

Government's role as a primary social service provider has repeatedly come under scrutiny with regard to the implementation of SLPs. This is because the law does not provide detailed guidance on the role of community participation in SLPs. This is controversial, since the SLPs, and the LED section in particular, should be based on the needs and interests of community members. Furthermore, mining companies do not always view SLPs as core to their business, as further evidenced by their SLPs not being linked to their Social Impact Assessments (SIAs) (Centre for Applied Legal Studies, 2016). Hence, compliance with SLPs requires the State to regard them as binding and not persuasive or discretionary. However, the challenge is that the DMR lacks the critical skilled personnel to intensify enforcement of SLP obligations and sanction noncompliance (Centre for Applied Legal Studies, 2017).

This is further supported by the findings of the Centre for Applied Legal Studies in its latest Social and Labour Plan Series, which indicates the following findings (among others):

- The current guidelines on SLPs have proven to be inadequate, in that although they address the content of SLPs, the guidelines are not hard law and thus cannot function as a prescriptive framework.
- In their design, operation, amendment, and termination, the majority of SLPs showed no support for a plan of community participation.
- SLPs showed limited engagement with social and economic dynamics in mining areas and how these informed the design of SLP projects.
- SLPs were difficult to obtain or access (Centre for Applied Legal Studies, 2017).

## Conclusion

It is said that 'South African government departments; and in this instance the DMR, Water Affairs, and local government have a progressive legislative base for mining, yet due to constraints, the capacity for regulating and monitoring compliance is limited' (Munnik, 2010). Much has changed in how the extractive industry responds to social and community issues, with growing prioritization of community-related issues. This can be attributed partly to pressures on mining companies to take a greater responsibility for the social, economic, and environmental impacts of mining, as well as the risks facing the mining and metals industry, in securing and maintaining the social licence to operate (Coulson, Ledwaba, and McCallum, 2017). Mining companies have more resources and capacity than government, resulting in efficiencies and innovation that surpass regulatory compliance. However, this diminishes government's regulatory responsibilities. To this extent, the mining industry is given powerful incentives for voluntary self-regulation. As such, there is tremendous potential for partnership between direct State intervention and business voluntarism regarding CSR and SLPs (Hamann, 2013).

An amendment such as that of Section 36(11)(e) is duly recognized given the constraints on mining companies to give effect to SLPs. Furthermore, the responsibility placed on mining companies to contribute to local economic development imperatives favours SLPs. Equally, it creates an unreasonable expectation that mining companies solve imbalances of socio-economic development in South Africa but with 'one hand tied behind their back' (Hamann, 2003). Any legislation governing CSR and SLPs demands a greater focus in the long term on governance in social investment, especially since good governance underpins all effective social investment. The DMR will have to consider the inefficiencies during evaluation of SLPs submitted to their provincial offices and SLPs should be accessible to communities, in addition to ensuring monitoring of SLP implementation in their surrounds.

Therefore, the law and regulations pertaining to SLPs need to be clear, enforced, and governable (Creative Space Media, 2015). Put differently, the Centre for Applied Legal Studies (CALS) 2017 report recommended wide-ranging policy and legislative changes to the SLP system, warning that in their absence the system is certain to remain exclusionary and ineffectual. A major problem identified in this process is 'participation'. Pivotal to a meaningful participation process is that notices are sufficient to reach the bulk of affected community members. CALS findings indicate that consultations either take place or are poorly publicized. In the 2017 report CALS indicates that this problem could be addressed if a robust public participation process with clear notice requirements tailored to the circumstances of communities were inserted into the legislative framework. Furthermore, in support of the 'participation' issue, CALS recommends a minimum requirement be set in legislation for consultation meetings between mining companies and communities. A critical facet to this, it is argueed, is for mining companies to be able to identify where in their institutional structure the responsibility for SLPs is located. This becomes important to establish clear lines of accountability and implementation of SLPs. In ensuring this, CALS believes that the DMR should intensify its enforcement of SLP obligations, making sanctions for noncompliance 'real'. The concern with this, however, is the widespread issue of lack of capacity within the DMR to regulate (and monitor) proper implementation of SLPs and therefore the lack of stakeholder engagement. This is a major impediment in the SLP system. A solution suggested by CALS is capacity building within DMR. In addition to this, one cannot ignore the fact that 'SLPs are implemented in the context of a constitutional allocation of powers and functions that includes distinct and overlapping roles by national, provincial and local spheres of government'. In this respect, CALS proposes that a framework be established for the cooperation of all organs of State with a key role in mining-related governance and planning. There has been a shifting of responsibility regarding SLP problems, and legislation ought to be drafted to streamline responsibilities. For example clarity on the role of SLPs in relation to related persons (such as IDPs) pertaining to local economic development. (Centre for Applied Legal Studies, 2017).

Against this backdrop, in spite of these flaws and challenges of the SLP system, the amendment to Section 36(11)(e) of the Tax Act entitles a mining company to allowable deductions of 'capital expenditure' incurred on infrastructure in terms of SLP requirements as per the MPRDA. To this end, an interim solution could be to ensure that such deductions are dependent on concrete evidence provided by the mining companies that the SLPs have in fact been implemented, together with extensive consultation with the respective communities. This should be included in the Mining Charter Scorecard, or at the very least the extent of mine community development should have measurable goals to which mining companies can be held accountable. The Mining Charter 2018 definition of 'Mine Community Development' is a good place to start in establishing these measurable goals. This evidence could be in the form of documentation signed by the respective related parties affirming that SLPS have been implemented and that constructive consultation has taken place (and/or ongoing where necessary). One can only hope that at that stage the DMR has the capacity to verify such evidence. To the extent that there is noncompliance by mining companies in implementation of SLPs, such deduction should not be granted; and furthermore, a negative scoring and/or penalties should be imposed by the DMR on such mining companies for noncompliance.

As it stands, the weaknesses in the system due to regulatory constraints on implementation and enforcement will collapse the very foundation upon which SLPs repose. If pursued within the current SLP system, the deductions in terms of Section 36(11)(e) will have adverse unintended consequences in relation to the governance of the SLP system and the State – whose role as a primary social service provider is already under scrutiny with regard to the implementation of SLPs, especially since the system was designed to redress the historical legacy of inequality by placing binding obligations on companies to ensure that mining benefits workers and communities. However, in its present form, the SLP system is incapable of achieving these objectives (Centre for Applied Legal Studies, 2017), and as such a deduction as per Section 36(11)(e) is clearly 'putting the cart before the horse'.

## References


Busacca, M. 2013. Corporate Social Responsibility in South Africa's Mining Industry: Redressing the legacy of apartheid. Claremont McKenna College. pp. 26-32. http://scholarship.claremont.edu/cgi/viewcontent.cgi?article=1631&context=cmc_theses.

Cawood, F.T. 2004. The Mineral and Petroleum Resources Development Act of 2002: A paradigm shift in mineral policy in South Africa. *Journal of the South African Institute of Mining and Metallurgy*, vol. 104, no. 1. pp. 53–64.

Centre for Applied Legal Studies (CALS). 2017. The Social and Labour Plan Series. Phase 2: Implementation operation analysis report by the Centre of Applied Legal Studies. The University of the Witwatersrand.

Centre for Applied Legal Studies (CALS). 2016. The Social and Labour Plan Series. Phase 1: System design. Trends analysis by Centre of Applied Legal Studies. University of the Witwatersrand.

Clegg, D. 2018. Income Tax in South Africa. par. 20.4

https://www.mylexisnexis.co.za/Index.aspx [accessed 25 November 2016].

Coulson, N., Ledwaba, P., and McCallum, A. 2017. Building resilient company-community relationships: A preliminary observation of the thoughts and experiences of community relations practitioners across Africa. *Journal of the Southern African Institute of Mining and Metallurgy*, vol. 117, no. 1. pp. 7–12.

Creative Space Media. 2015. Tshikululu Research Report: The South African Mining Industry. *CSI: The Human Face of Business*. Lonehill, South Africa. pp. 6-9.

Finweek Report. 2008. Unsafe behaviour is normal behaviour. *Finweek*, 28 February 2008. p. 91.

Hamann, R. 2003. Corporate social responsibility and its implications for governance: The case of mining in South Africa. Oikos Foundation for Economy and Ecology, St. Gallen, Switzerland.

Hamann, R. 2004. Corporate social responsibility, partnerships, and institutional change: The case of mining companies in South Africa. *Natural Resources Forum*, vol. 28, no. 4. pp. 278–290.

Jenkins, H. and Yakovleva, N. 2006. Corporate social responsibility in the mining industry: exploring trends in social and environmental disclosure. *Journal of Cleaner Production*, vol. 14, no. 3-4. pp. 271–84.

Kloppers, H. and du Plessis, W. 2008. Corporate social responsibility, legislative reforms and mining in South Africa. *Journal of Energy and Natural Resources Law*, vol. 26. pp. 91–119.

Koma, S.B. and Kuye, J.O. 2014. The synchronisation of Integrated Development Plan and local economic development policy in South African municipalities- A sine qua non for growth and development. *African Journal of Public Affairs*, vol. 7, no. 1. https://repository.up.ac.za/handle/2263/41526

Munnik, V. 2010.The social and environmental consequences of coal mining in South Africa-A case study. Environmental Monitoring Group, Cape Town, South Africa and Both ENDs, Amsterdam, The Netherlands. January 2010. pp. 8-9.

South Africa. 2016a. Taxation Laws Amendment Bill 17B 2016 (Draft). National Treasury. http://www.treasury.gov.za/public%20comments/TLAB%20and%20TALAB%202016%20Draft/2016%20Draft%20Taxation%20Laws%20Amendment%20Bill.pdf [Accessed 25 November 2016].

South Africa. 2016b. Explanatory Memorandum on the Draft Taxation Laws Amendment Bill 17B 2016. http://www.treasury.gov.za/legislation/bills/2016/EM%20on%20the%20Taxation%20Laws%20Amendment%20Bill%2017B%20of%202016.pdf

South Africa. 2002. Mineral and Petroleum Resources Development Act 2002. Government Gazette, vol. 448. pp. 5-122.

South Africa. 1996. Constitution of the Republic of South Africa, Act 108 of 1996.

South Africa. 1962. Income Tax Act, 58 of 1962.Section 36. ◆

# SAIMM MEMBERSHIP OR UPGRADE

SAIMM
THE SOUTHERN AFRICAN INSTITUTE OF MINING AND METALLURGY

**Website: http://www.saimm.co.za**

## Reasons to join the SAIMM

- Receive the SAIMM Journal which communicates a high standard of technical knowledge to our members
- Access to **OneMine.org** and publications from other international mining and metallurgical societies
- Participation in technical excursions and social events which creates further opportunities for interactive personal and professional association and fellowship
- To make a contribution to the Mining and Metallurgy industries
- The opportunity to network with a wide cross-section of professional people in the mining and metallurgy industry
- Access to the output from international industry-related organizations
- Active participation leads to higher peer recognition of achievements in the minerals industry
- Members of the Institute who are registered with the Engineering Council of SA (ECSA) qualify for a rebate on their ECSA fees
- Opportunity to contribute to the development of young talent through mentoring and participating in schools
- Engagement and involvement in SAIMM structures and networking opportunities allow for additional Continuing Professional Development (CPD) point collection
- Discounted membership prices when attending events hosted by the institute.

Fifth Floor, Minerals Council South Africa
5 Hollard Street, Johannesburg, 2001
P.O. Box 61127, Marshalltown, 2107, South Africa
Tel: 27-11- 834-1273/7 · Fax: 27-11- 838-5923 or 833-8156
E-mail: membership@saimm.co.za

FOLLOW US ON...

www.facebook.com/TheSAIMM/ https://twitter.com/SAIMM1

https://www.linkedin.com/company/saimm--the-southern-african-institute-of-mining-and-metallurgy

# An audit of environmental impact assessments for mining projects in Kenya

**F. Mwaura**[1]

**Affiliation:**
[1]Department of Geography and Environmental Studies, University of Nairobi, Kenya.

**Correspondence to:**
F. Mwaura

**Email:**
mwauraf@uonbi.ac.ke

**Dates:**
Received: 29 May 2018
Revised: 12 Sep. 2018
Accepted: 29 Sep. 2018
Published: May 2019

**How to cite:**
Mwaura, F.
An audit of environmental impact assessments for mining projects in Kenya.
The Southern African Insitute of Mining and Metallurgy

DOI ID:
http://dx.doi.org/10.17159/2411-9717/143/2019

ORCiD ID:
F. Mwaura
https://orchid.org/0000-0002-4054-0218

## Synopsis

**The aim of the audit was to determine whether the mining project environmental impact assessments (EIAs) in Kenya are undertaken according to international best practice. A sample of 50 EIA reports for the 2007–2016 period was evaluated using 18 criteria in the Environmental Law Alliance Worldwide (ELAW) guidelines. The findings showed that only two criteria were considered 'excellent' according to the ELAW guidelines, namely baseline environmental assessment and prediction of physical impacts. Six criteria were found to be 'satisfactory', including prediction of social impacts, analysis of alternative options, and impact mitigation. The reports were quite weak in terms of: consideration of all phases in the mining cycle, environmental regulatory framework, prediction of biological impacts, stakeholder consultation and engagement, integration of human right issues, and integration of climate change and cost-benefit analysis. It is therefore recommended that the Kenyan National Environment Management Authority (NEMA) should consider tightening the EIA terms and conditions in the approval of statutory terms of reference (ToR) for full-scale mining EIAs to ensure improved performance of EIA as a tool for environmental protection.**

**Keywords**
**mining projects; environmental sustainability; EIA reports, best practice.**

## Introduction

The nexus between society and the environment has continued to generate interest because the environment is the source of goods and services that sustain the various needs of human beings as outlined in the UN sustainable development goals (SDGs) (Armstrong and Peart, 2000; Sutton 2004; Chakrabarti 2007; Strange and Bayley 2008). All the five generic categories of societal needs, namely physiological needs (food, water, clothing, medicines, *etc.*), residential and occupational needs (shelter, transport, energy, *etc.*), economic needs (tradeable goods and services), leisure and recreational needs (tourism), and cultural and spiritual needs (*e.g.* sacred resources and ecosystems) (Mwaura *et al.* 2016) are addressed by the environment. Consequently, a wide range of development sectors have been established around the world in order to address the above needs (Lederer, Galtung, and Antal, 1980; Rammelsberg *et al.*, 2006; Noonan, 2014). All these development sectors rely entirely on the environment for their proper functioning, as shown in Table I.

Development activities such as large-scale farming, irrigation, fishing, forestry, mining, manufacturing, tourism, transport, and communication, among many others usually take place within or very close to sensitive environments such as forests, rivers, lakes, wetlands, and wildlife breeding zones. The interface between society, environment, and development always poses a risk of environmental damage to the terrestrial, aquatic, and atmospheric spheres of the world environment. This risk continues to grow as the demands by society on the environment increases due to population growth (Tisdell, 2005; Schaltegger and Wagner 2006). The United Nations estimates the current world population at approximately 7.6 billion, which is expected to increase to 11.2 billion in the year 2100 (UN-DESA 2017).

Most development sectors pose a significant potential risk of negative impact on the environment. However, some economic sectors such as mining pose a higher risk in comparison to other sectors such as pastoralism (Patnaik and Das, 1990; Ripley, Redmann, and Crowder, 1996; Azcue, 1999; Ozkan and Ipekoglu 2002). The mining sector is associated with a wide range of environmental risks due to activities such excavation and earthworks, tailings disposal, and gaseous emissions, which are likely to negatively affect terrestrial, aquatic, and atmospheric environments leading to serious impacts on biodiversity, ecosystems, and society (Dold and Friese 2007; UNDP 2014; Sivi *et al.*, 2015). Generally,

*Table I*

**The linkages between society, development, and environment**

| Society | Development sector | Environmental requirements |
|---|---|---|
| **Physiological needs** – food, water, clothing, medicines *etc.* | Agriculture, irrigation, dam construction, industries | Suitable landscapes, arable soils, rivers, lakes, biodiversity, *etc.* |
| **Residential and occupational needs** – shelter, homes, vehicles, trains, aircraft, ships, energy, *etc.* | Construction, urbanization, transport communication, power stations | Land, forests, rivers, lakes, oceans, airspace, minerals, *etc.* |
| **Economic needs** – goods and services for revenue generation | Agriculture, forestry, mining, fisheries, livestock husbandry, tourism | Terrestrial ecosystems, aquatic ecosystems, biodiversity |
| **Leisure and recreation needs** – human relaxation and entertainment | Tourism | Natural and cultural heritage |
| **Cultural and spiritual needs** – prayer, sacrifice, circumcisions, weddings *etc.* | National heritage | Sacred mountains, rivers, lakes, wetlands, forests, rangelands, sacred species *etc.* |

mining activities lead to extensive vegetation clearing which affects flora and fauna. Mining areas also become vulnerable to degradation through soil erosion and environmental pollution. The management of waste arising from different stages of mining processes is usually a major environmental challenge around the world. Depending on the degree of pollution, this can lead to serious health risks to the public, livestock, and wildlife (Černe *et al.*, 2012). On the social front, the mining sector is also known to cause a wide range of adverse impacts including land acquisitions, displacements, resettlements, as well as illegal engagement of child labour (Jha-Thakur and Fischer, 2008; Salgado 2013).

The environmental risks associated with mining activities therefore demand a very careful interrogation of projects before their commissioning to ensure proper mitigation of potential negative impacts so as to ensure sustainable development. Such projects must also be subjected to regular monitoring to ensure that they are conducted in a sustainable manner. Environmental impact assessment (EIA) has been identified as a suitable management tool that aims at ensuring that all new development projects, including mining, are implemented in a sustainable way, and that their possible negative impacts are identified early and adequately mitigated at the project design stage. Consequently, EIA is considered as a valuable tool for ensuring environmental protection and sustainability (Muttamara, 1996; Zhao, 2009; Morrison-Saunders and Retief, 2012; Safont, Vegas-Vilarrúbia, and Rull, 2012; Arts *et al.*, 2012). Consequently, up to 190 of the 193 member states of the United Nations have adopted and regulated EIA as a systematic process for identifying and mitigating the potential environmental impacts of development projects (Harris, Viliani, and Spickett, 2015). EIA is a useful instrument for ensuring sustainability in the society-environment-development nexus by identifying suitable mitigation strategies for dealing with environmental damages.

The effectiveness of EIA as an environmental protection tool requires the complementary engagement of the processes of strategic environmental assessment (SEA) and environmental audits. A number of studies have considered the linkages between SEA, EIA, and environmental audits (Marshall and Fischer, 2006; Fischer, 2006). EIA is closely related with SEA but the latter is usually undertaken ahead of the former during the development cycle. The SEA interrogates the sustainability of development policies, plans, and programmes from which many types of development projects usually emerge. Projects are usually initially subjected to the EIA process and subsequently undergo environmental audits as shown in Figure 1. Regular environmental audits are necessary to ensure that the EIA recommendations are implemented and fulfilled throughout the project life-cycle. Consequently, SEAs are usually undertaken ahead of EIAs, which makes them capable of informing the implementation of EIAs and environmental audits.

A wide range of studies have been done on the effectiveness of EIA as an instrument for sustainable environmental governance throughout the world (Biswas and Agarwal, 1994; Churie, 1997; Loots, 1997; Staeck and Heinelt 2001; Arts *et al.*, 2012). Numerous EIA evaluation studies on mining projects have been undertaken around the world. Audits of the EIAs for the Ok Tedi mine in Papua New Guinea and Century Mine in northern Australia by Mckillop and Brown (1999), for example, identified a failure to adequately safeguard the biophysical and social environment. The evaluation showed that the EIA process was poorly timed and not well integrated within the early phases of the mining activities because most EIA efforts are concentrated on the mining phase and do not address impacts resulting from the exploration, prospecting, and pre-feasibility phases. Various environmental studies are associated with these phases, after which a decision is made whether to proceed with the project or not. The EIA describes the environmental measures the proponent has committed to and on which the relevant authority approves or disapproves projects. The findings showed that EIA considerations were not integrated in the approval and issuance of mineral exploration and prospecting permits and licenses, and yet these activities also had certain negative impacts on the environment.

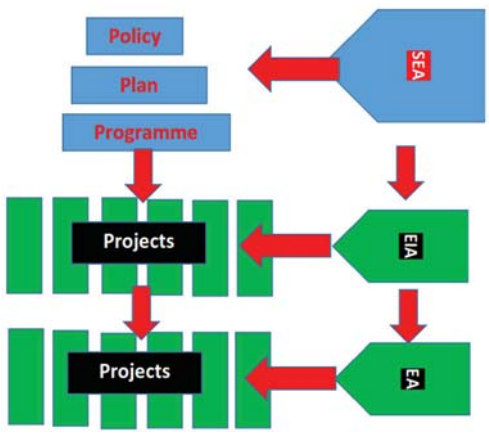


**Figure 1—Linkages between EIA, SEA, and environmental audit (EA)**

Morrison-Saunders *et al.* (2016) evaluated the integration of mine closure and decommissioning in the EIA by comparing the practice in eight African and Australian jurisdictions, including Western Australia, Ghana, Kenya, Nigeria, Mozambique, South Africa, Tanzania, and Zambia. The findings showed that although all eight jurisdictions have appropriate regulatory provisions in place, the implementation capacity is still a challenge which affects the environmental outcomes. Similarly, Kruger *et al.* (1997) noted the inability of the EIA to accurately predict the magnitude of expected impact from mining activities in St Lucia, South Africa. However, Sandham, Hoffmann, and Retief (2008) evaluated the quality of mining EIA reports in South Africa and concluded that 85% were of satisfactory quality. In Ghana, Kuma, Younger, and Bowell (2002) established a weakness in mining EIAs in terms of hydrogeological impact analysis due to inability to clearly determine the pre-mining groundwater status. In Nigeria, Ingelson and Nwapi (2014) evaluated the EIA process for oil and gas projects in the world's twelfth largest producer of crude oil and highlighted a range of reasons why the impacts of such projects are not properly managed despite the application of EIAs.

In 1999, the Republic of Kenya joined the rest of the world as a nation with a clear legal framework on environmental management. The enactment of the Environmental Management and Coordination Act (EMCA, Cap 387) paved the way for EIA and regular environmental audit practice in development activities with a potential for adverse environmental impact. A number of studies have evaluated the effectiveness of EMCA (Cap 387) in environmental protection in Kenya, including the effective application of EIAs and environmental audits. Kibutu and Mwenda (2010), for example, reviewed the provision for EIA in the environmental legislation while Okello *et al.* (2009) and Mwenda *et al.* (2012) evaluated the role of public participation in Kenyan EIAs. Kamau and Mwaura (2013) assessed the level of climate change adaptation and EIA studies in Kenya. To date, there have not been many evaluation studies considering the effectiveness of EIA in mining projects in Kenya.

Kenya is endowed with over 120 different types of mineral deposits, but the exploitation of these assets is yet to reach peak level (Republic of Kenya, 2015). Accordingly, the government of Kenya has recognized the mining sector as a key player for the realization of the UN SDGs as well as the goals for the Africa Mining Vision (2009) and Kenya Vision 2030 (Mutua, 2014; Republic of Kenya, 2015). The government has recently added oil, gas, coal, titanium, and other minerals as priority assets for spurring economic growth through Vision 2030 (Mutua, 2014; Republic of Kenya, 2015). Although the mining industry has an unprecedented opportunity to mobilize significant human, physical, technological, and financial resources to advance the SDGs, its impacts can jeopardize the realization of some environmental SDGs. The development of large-scale mining (LSM) in Kenya will consume vast quantities of land and water resources and is likely to cause land degradation and water pollution which must be mitigated or avoided through good governance with the support of effective application of EIA. The mining sector is also capable of disturbing national biological capital through the loss and degradation of ecosystems such as forests, wetlands, and coastal areas, which can affect the status of the country as a major wildlife tourism destination. It is therefore urgently necessary to evaluate the quality of mining project EIA reports to determine whether the process is undertaken according to international best practice through the approving authorities and financing agencies.

The key research question for the study was – which types of mining EIAs have been undertaken in Kenya during the last decade and do they measure up to the expected standards according to international best practice? The aim of the evaluation of mining projects EIAs in Kenya was therefore to:

(a) Analyse the typology and distribution of mining project EIAs in the country
(b) Determine whether the quality of mining project EIA reports is a reflection of international best practice with regard to the consideration of all the expected issues.

## Study area

Kenya is endowed with over 120 different types of mineral resources, as shown in Figure 2 and Table II. Accordingly, the government of Kenya has recognized the mining sector as a key player in the journey towards Vision 2030, and has recently included oil, gas, and other minerals as the seventh priority economic sector for the country's Vision 2030 (Republic of Kenya, 2015). In the past, both soda ash (trona) and fluorspar contributed significantly to the gross domestic product (GDP). Overall, the country earned more than $232 million from the mining sector in 2015 which was an increase from $203 million in 2014. In 2012, the sector employed approximately 8400 people (Mutua, 2014; Republic of Kenya, 2015). With further exploration and development, it is estimated that Kenya could soon have the capacity to position itself as a regional mining sector hub for East Africa.

The environmental law in Kenya, like most other countries in the world. requires that a full and comprehensive EIA, and not a general project study, be undertaken and an EIA license issued before any mining-related activities, including exploration, prospecting, extraction, and processing, can proceed. However, the final approval may be based on different EIAs carried out for the exploration and prospecting stages in the mining cycle. According to the Environmental Management and Coordination Act (EMCA, Cap 387), all mining projects are listed under the category of 'high-risk projects' that must be screened through

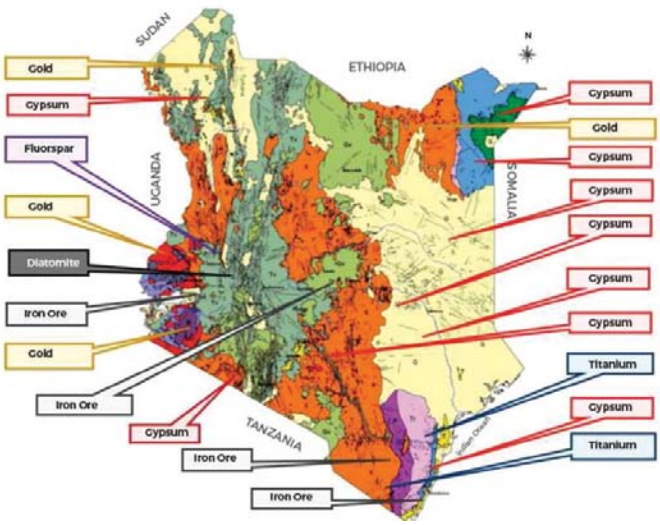


**Figure 2—Distribution of selected minerals in Kenya (Republic of Kenya, 2015)**

*Table II*

**Distribution of mineral in Kenya by county**

| County | | Minerals |
|---|---|---|
| 1. | Kwale | Gemstones, heavy mineral sands (titanium minerals), silica sand, rare earth elements, niobium |
| 2. | Kilifi | Titanium minerals, manganese, barytes, gypsum, gemstones |
| 3. | Taita Taveta | Iron ore, gemstones, manganese, granites |
| 4. | Tana River | Gypsum |
| 5. | Makueni | Vermiculite, gemstones |
| 6. | Kitui | Coal, iron ore, copper, gemstones, limestone, magnetite, alumina clay, marble |
| 7. | Machakos | Gypsum and pozzolana |
| 8. | Kiambu | Carbon dioxide and diatomite |
| 9. | Tharaka Nithi | Iron ore, gemstones, copper |
| 10. | Isiolo | Gemstones |
| 11. | Garissa | Gypsum |
| 12. | Mandera | Gypsum |
| 13. | Isiolo | Gemstones |
| 14. | Marsabit | Gold, manganese, chromite, gemstones |
| 15. | Elgeyo Marakwet | Fluorspar |
| 16. | Baringo | Gemstones (Baringo ruby), diatomite |
| 17. | Nakuru | Diatomite |
| 18. | Kajiado | Soda ash, feldspar, limestone, gypsum, gemstones, marble and granite (dimension stones) |
| 19. | Uasin Gishu | Carbon dioxide gas |
| 20. | Turkana | Gypsum, oil, gold, gemstones |
| 21. | West Pokot | Gold, gemstones, chromite |
| 22. | Samburu | Gold, manganese, chromite, gemstones, and vermiculite |
| 23. | Narok Transmara) | Gold |
| 24. | Nandi (Kibigoni) | Gold |
| 25. | Kakamega | Gold, dimension stone |
| 26. | Siaya | Gold, iron ore |
| 27. | Migori | Gold, copper |
| 28. | Homa Bay | Iron ore and gold |

(Source: Republic of Kenya, 2015)

pre-project EIAs and thereafter through regular environmental audits to ensure environmental sustainability throughout the mining cycle from exploration, through prospecting, extraction, and processing, to mine closure and rehabilitation. The EIA framework in Kenya requires that adequate consultation be undertaken with and among all the relevant stakeholders, especially the mining host communities. EMCA Cap 387 requires the EIA report to be circulated throughout the country by the National Environment Management Authority (NEMA) to allow wider peer review and comprehensive stakeholder consultation, which eventually informs final decision-making regarding the licensing of mining-related projects.

## Methods

The audit was undertaken through an interrogation of a sample of the mining EIA reports in the national database at the NEMA office in Nairobi. The audit was undertaken using standard criteria provided in the Guidebook for Evaluating Mining Project EIAs (Environmental Law Alliance Worldwide, 2010). The approach and methodology for the audit are detailed below.

### *Audit period*

The audit was undertaken for the 2007–2016 period as the decade during which the mining sector was identified as one of the key drivers for economic growth and transformation. The sector is expected to contribute 10% to the GDP by 2030, up from the current 0.9%. Mining activities in the country increased remarkably during this period, hence the need to assess the mining project EIAs during this period.

### *Sampling strategy*

A total of 50 mining project EIA reports were considered in the audit, representing 30.7% of the 163 EIAs undertaken during the study period as shown in Table III.

### *Evaluation criteria*

The audit was undertaken using the standard criteria described in the Guidebook for Evaluating Mining Project EIAs by Environmental Law Alliance Worldwide (ELAW, 2010). Similar standard criteria have been used to evaluate EIAs for proposed mining projects around the world. Each report was evaluated using a standard checklist of 18 parameters used in the evaluation (Table IV). This is an EIA report evaluation checklist and not an EIA implementation checklist as provided in the performance standards for various international agencies such as the World Bank/IFC (World Bank, 2008).

The evaluation was based on four judgements prescribed in the Guidebook (ELAW 2010), namely: (a) 'yes to all' if all the attributes in an evaluation criterion were fully considered in the EIA process, (b) 'yes to most' if 80% of the attributes were considered, (c) 'yes to a few' if less than 50% of the attributes were considered, and (d) 'no to all' if none of the attributed were considered. The overall quality of the EIA process was based on four quality categories as follows: (a) 'excellent' if the 'yes to all' judgment for a given parameter was dominant, (b) satisfactory' if the 'yes to most' grading was dominant, (c) 'poor' if the 'yes to a few' grading was dominant, or (d) 'very poor' if the 'no to all' grading was dominant. Quantification of attributes in percentages was based on the actual counting of the total number of criteria out of the 18 which were considered in an EIA report.

## Results and analysis

The evaluation of the 50 mining project EIA reports in the 2007–2016 period showed that 50% of the EIAs were associated with mining activities, 22% with both prospecting and mining, 18% with exploration and prospecting, 8% with mineral processing, and 2% with both mining and processing. Table V shows the

*Table III*

**Summary of mining project EIAs in 2007–2016**

| Year | Total no. of EIA reports | Audit sample EIA reports |
|---|---|---|
| 2007 | 6 | 2 |
| 2008 | 6 | 2 |
| 2009 | 7 | 3 |
| 2010 | 17 | 5 |
| 2011 | 16 | 4 |
| 2012 | 21 | 6 |
| 2013 | 18 | 6 |
| 2014 | 22 | 7 |
| 2015 | 21 | 6 |
| 2016 | 29 | 9 |
| Total | 163 | 50 |

*Table IV*

**Summary of the parameters used for evaluation of mining project EIAs**

| EIA quality evaluation parameter | Specific attributes |
|---|---|
| 1. Consideration of key EIA stages of the assessment process | Screening, scoping, description of mining project, baseline environmental description, comprehensive environmental regulatory framework, analysis of alternative options, stakeholder engagement, impact analysis, impact mitigation, decommissioning strategy, EMP and environmental monitoring strategy |
| 2. Consideration of all the phases of mining project | Exploration and prospecting, construction of access roads, site preparation and clearing, mining installations, mining activities, disposal of overburden and waste rock, ore extraction, tailings disposal |
| 3. Comprehensive environmental regulatory framework | Policies, laws (Acts of Parliament), regulations, standards, national strategies and action plans, multilateral environmental agreements (MEAs) and other relevant international agreements |
| 4. Consideration of potential physical impacts | Land environment, landscapes, hydrology, groundwater and water resources, water quality, air quality, noise and vibrations, climate change |
| 5. Consideration of potential biological impacts | Flora, fauna, endangered species, sensitive habitats and ecosystems, protected areas, biodiversity hotspots |
| 6. Consideration of potential social impacts | Displacement and resettlement, livelihoods impacts, traffic interruption, solid wastes, public safety and health, employment, CSR, emergency response and contingency plans, conflict resolution |
| 7. Human rights considerations | Right to fair administrative action, right to access public information, right to security and peace, right to proper physical and mental health, prevention of child labour |
| 8. Evidence of actual baseline environmental studies | Characterization of proposed mined materials, soil, water, noise, air quality, flora, fauna, climate, population characteristics, land use, social services |
| 9. Stakeholder engagement and consultation | Stakeholder mapping, identification of stakeholders, directly affected stakeholders (DAS) and indirectly affected stakeholders (IAS), gender balance, youth and vulnerable groups |
| 10. Adequate EIA consultation meetings | Number of meetings, convenient meeting venues, listing of stakeholder consultation meeting (SCM) participants, listing of SCM contacts, stakeholder communication strategy, evidence of full project information disclosure, listing of stakeholder concerns, clear details of project approval or disapproval by stakeholders, adequacy of consideration of stakeholder inputs, identification of issues and concerns and where dealt with in the reports |
| 11. Characterization of potential impacts for all mining stages | Pre-construction, construction, operation, decommissioning, and rehabilitation |
| 12. Climate change considerations | Loss of $CO_2$ uptake through vegetation clearance, $CO_2$ emission by mining machines, $CO_2$ emission through mineral processing, considerations on climate change-proof mining infrastructure, climate change mitigation and adaptation, considerations on climate change-related natural disaster risk reduction in the EMP |
| 13. Consideration of trans-boundary impacts | Inter-village, inter-county, regional, and international |
| 14. Analysis of alternative options | Preferred option, no-action zero option, other options |
| 15. Cost-benefit analysis | Estimated cost of project economic benefits and environmental losses |
| 16. Impact mitigation | Positive impacts, negative impacts, recommendations for mitigation of negative impacts, rehabilitation cost and funding allocation at decommissioning phase, enhancing positive impacts |
| 17. Environmental management and monitoring plan (EMP) | Land environment, soil environment, water resources, air quality, noise and vibration, flora and fauna, public safety and health, decommissioning and rehabilitation, long-term monitoring protocol, responsible persons and agencies, timelines, guidelines |
| 18. Overall quality of EIA report | Comprehensive non-technical summary, illustrative maps, diagrams, and photos, clear conclusion and recommendations, clear and easy to understand |

*Table V*

**Types of minerals covered in the 2006–2016 mining project EIAs**

| Mineral | % of EIA reports in 2006–2016 |
|---|---|
| Gypsum | 32 |
| Gold | 12 |
| Manganese | 12 |
| Copper | 10 |
| Iron ore | 8 |
| Diatomite | 2 |
| Graphite | 2 |
| Barytes | 2 |
| Limestone | 2 |
| Precious and non-precious stones and minerals | 2 |
| Kyanite crystals | 2 |
| Rock material | 2 |
| Copper and non-precious minerals | 2 |
| Carbon dioxide | 2 |
| Pumice | 2 |
| Sodium silicate | 2 |
| Magnetite | 2 |
| Silica sand | 2 |
| **Total** | **100** |

key types of minerals for which mining EIAs were undertaken. These were dominated by gypsum, followed by gold, manganese, copper, and iron ore. Gypsum deposits are common in a number of areas in Kenya such as Kitui, Machakos, Tana River, and Kilifi counties. The mineral is commonly used in the manufacturing of gypsum boards, binders, and plasters for house ceilings and interior partitioning. The demand for gypsum is high as a result of a vibrant construction sector in the urban areas. The geographic distribution of mining project EIAs showed that most of the mining project EIAs were undertaken in Tana River County, followed by Kilifi, Kitui, Migori, and Garissa counties (Table VI). The overall audit showed that 38% of the mining project EIAs were undertaken in the coast region, followed by the Rift Valley (20%), Eastern region (18%), and Nyanza (12.5%).

Table VII shows the findings on the audit of the 50 mining project EIA reports. The 2006–2016 reports were 'excellent' only with regard to prediction of potential physical impacts and baseline environmental assessment. They were satisfactory with regard to the consideration of key EIA stages, prediction of social impacts, analysis of alternative options, impact mitigation, and environmental management and monitoring plan (EMP). The

*Table VI*

**Geographic distribution of mining project EIAs per county**

| County | % of EIA reports in 2006–2016 |
|---|---|
| Tana River | 20.4 |
| Kilifi | 16.3 |
| Kitui | 10.2 |
| Migori | 10.2 |
| Garissa | 6.1 |
| Samburu | 4.1 |
| Machakos | 4.1 |
| Kajiado | 4.1 |
| West Pokot | 4.1 |
| Embu | 2 |
| Baringo | 2 |
| Makueni | 2 |
| Homa Bay | 2 |
| Tharaka Nithi | 2 |
| Kwale | 2 |
| Uasin Gishu | 2 |
| Transmara | 2 |
| Nakuru | 2 |
| Taita Taveta | 2 |
| **Total** | **100** |

findings showed that the quality of the EIA reports was weak in terms of comprehensive consideration of potential impacts across all stages in the mining cycle, adequacy of the environmental regulatory frameworks, prediction of potential biological impacts, and human rights. The quality was very weak in terms of the overall quality of stakeholder engagement and consultations, integration of mining-related climate change, consideration of trans-boundary impacts, and cost-benefit analysis (CBA). The evaluation established that only a mere 7% (3 out of 50 reports) of the approved mining projects in the 2006–2016 period had undertaken third-party post-EIA environmental audits in order to ensure that the EIA recommendations are fulfilled. This means that consistent follow-up of the EIA recommendations, including EMP compliance monitoring by the regulatory authority through environmental audits, is not effectively undertaken.

## Discussion

The high concentration of mining project EIAs in the south-eastern and coastal regions of Kenya is consistent with the geographic distribution of mineral-rich areas in the country. The south-eastern region of Kenya is a source of limestone, gypsum, clays, manganese, and coal plus other (unproven) hydrocarbons. Base metal mineralization, lead-zinc-barite, and copper are also known to occur in the sedimentary basin along the coastal belt. Heavy mineral sands occur along the coast, such as the approximate 3.2 Gt billion tons deposits Kwale County. Exploration around the Mrima Hill in Kwale County have also confirmed up to 105 Mt Inferred Mineral Resource in the area with an average grade of 0.65% niobium pentoxide ($Nb_2O_5$) and up to 12 Mt at 1.21% $Nb_2O_5$.

The findings showed that only two out of the eighteen quality evaluation criteria were considered 'excellent' in the EIA process, namely the baseline environmental assessment and prediction of potential physical impacts, both of which only accounted for 11% of the well-considered issues in the audited reports. On the other hand, six out of the eighteen EIA quality evaluation parameters were considered 'satisfactory' in the EIA process, accounting for 33.3% of the issues in the audited reports. The parameters considered to be satisfactory included (a) consideration of all the key EIA stages, (b) prediction of potential social impacts, (c) analysis of alternative options, (d) impact mitigation, and (e) provision of a reliable environmental management and monitoring plan (EMP). Consequently, only approximately 44% of the environmental sustainability considerations expected in the EIA process were adequately addressed in the audited mining project EIA reports for mining projects undertaken in 2007–2016, while the consideration of 56% of the parameters was below expectation.

The issues that were inadequately considered in the EIAs included (a) consideration of all stages in the mining cycle, (b) description of the environmental regulatory framework, (c) prediction of potential biological impacts, and (d) human rights considerations. Those considered in a very poor and inadequate manner included (a) stakeholder engagement and consultation, (b) integration of climate change considerations, (c) trans-boundary impacts, and (d) application of cost-benefit analysis (CBA). These weaknesses can significantly dilute the impact of EIA in influencing more environmentally sustainable mining project decisions, as has been experienced in other countries (*e.g.* Phylip-Jones and Fischer, 2013). Given that full-scale EIAs cannot be conducted in Kenya unless the Terms of Reference (ToR) are approved by the National Environment Management Authority (NEMA), the above weaknesses in the EIA reports can only be due to negligence and casual regard of critical issues of consideration at the EIA study design and implementation stage. This might signify the inability of the authority to demand and obtain the correct procedure due to certain systemic challenges.

The findings in the audit were found to closely resemble those of similar studies such as the one by Kamijo and Huang (2017), which evaluated the 30-year history of EIA implementation in developing countries. The evaluation identified weak enforcement of EIA obligations and requirements as a common problem in many developing countries, and the lack of serious post-EIA follow-up audits in Kenya could be associated with this challenge. Kamijo and Huang (2017) also recognized the problem of inadequate government capacity to ensure public participation, especially in sub-Saharan Africa, and recommended the use of a standard communications strategy for EIA public consultations. Such a strategy does not exist in most countries, including Kenya, although various financial institutions, including the IFC/World Bank, usually insist on this, which if followed is adequate for most projects. The findings in this study differ from those of Wood (1999), who evaluated the quality of mining project EIA practice in South Africa and considered the practice to be satisfactory. This was echoed by Sandham, Hoffmann, and Retief (2008) who considered up to 85% of the EIA reports in South Africa to be of satisfactory quality but with weaknesses in terms of prediction of impact magnitude and analysis of project alternatives options. The finding by Sandham, Hoffmann, and Retief (2005) on inadequate EIA compliance monitoring in South Africa is in agreement with the findings in the Kenya study.

It is important to note that the above weaknesses in EIA reports are not restricted to the mining sector. Phylip-Jones and Fischer (2013), in an evaluation of EIAs for wind farms in the UK and Germany, for example, established that in the past the process had minor to moderate impact in terms of influencing more environmentally sustainable project decisions.

*Table VII*

**Summary of audit findings for mining project EIA reports in Kenya**

| Audit criteria | | Percentage (%) level of compliance in 50 EIA reports | | | | |
|---|---|---|---|---|---|---|
| | | Yes to all | Yes to most | Yes to a few | No to all | Overall status |
| 1. | **Consideration of key EIA stages** - Description of mining project, screening, scoping, baseline environmental assessment, comprehensive environmental regulatory framework, analysis of alternative options, stakeholder engagement, impact analysis, impact mitigation, decommissioning strategy, ESMP and environmental monitoring strategy | 8 | 80 | 12 | 0 | **Satisfactory** |
| 2. | **Consideration of all the phases of mining project** - Exploration and prospecting, construction of access roads, site preparation and clearing, mining installations, mining activities, disposal of overburden and waste rock, ore extraction, tailings disposal | 2.1 | 29.2 | 37.5 | 31.2 | **Poor** |
| 3. | **Comprehensive environmental regulatory framework** - Policies, laws (Acts of Parliament), regulations, standards, national strategies and action plans, MEAs and other agreements | 2 | 20.4 | 73.5 | 4.1 | **Poor** |
| 4. | **Consideration of potential physical impacts** - Land environment, landscapes, hydrology and water resources, water quality, air quality, noise and vibrations, climate change | 85.4 | 0 | 14.6 | 0 | **Excellent** |
| 5. | **Consideration of potential biological impacts** - Flora, fauna, endangered species, sensitive habitats and ecosystems, protected areas, biodiversity hotspots | 2.1 | 25 | 68.8 | 4.2 | **Poor** |
| 6. | **Consideration of potential social impacts** - Displacement and resettlement, livelihoods impacts, traffic interruption, solid wastes, public safety and health, employment, CSR, emergency response and contingency plans, conflict resolution | 2.1 | 56.2 | 41.7 | 0 | **Satisfactory** |
| 7. | **Human rights considerations** - Right to fair administrative action, right to access public information, right to security and peace, right to proper physical and mental health, prevention of child labour | 16.7 | 0 | 79.2 | 4.2 | **Poor** |
| 8. | **Evidence of actual baseline environmental assessment** - Characterization of proposed mined materials, soil, water, noise, air quality, flora, fauna, climate, population characteristics, land use, social services | 76 | 0 | 20 | 4 | **Excellent** |
| 9. | **Stakeholder engagement and consultation** - Stakeholder mapping, identification of stakeholders, directly affected stakeholders (DAS) and indirectly affected stakeholders (IAS), gender balance, youth and vulnerable groups | 20 | 0 | 32 | 48 | **Very poor** |
| 10. | **Adequate EIA consultation meetings** - Number of meetings, convenient meeting venues, listing of SCM participants, listing of SCM contacts, stakeholder communication strategy, evidence of full project information disclosure, listing of stakeholder concerns, clear details of project approval or disapproval by stakeholders, adequate of consideration of stakeholder inputs | 2 | 24 | 40 | 34 | **Poor** |
| 11. | **Characterization of potential impacts for all mining stages** - Pre-construction, construction, operation, decommissioning and rehabilitation | 24.5 | 26.5 | 26.5 | 22.4 | **Satisfactory** |
| 12. | **Climate change considerations** - Loss of $CO_2$ uptake through vegetation clearance, $CO_2$ emission by mining machines, $CO_2$ emission through mineral processing, considerations on climate change-proof mining infrastructure, climate change mitigation amd adaptation, considerations on climate change related natural disaster risk reduction in the EMP | 2 | 0 | 0 | 98 | **Very poor** |
| 13. | **Consideration of transboundary impacts** - Inter-village, inter-county, regional and international | 8.2 | 0 | 2 | 89.8 | **Very poor** |
| 14. | **Analysis of alternative options** - Preferred option, no-action zero option, other options | 2 | 63.3 | 10.2 | 24.5 | **Satisfactory** |
| 15. | **Cost-benefit analysis** | 4 | 0 | 0 | 96 | **Very poor** |
| 16. | **Impact mitigation** - Positive impacts, negative impacts, recommendations for mitigation of negative impacts, rehabilitation cost and funding allocation at decommissioning phase | 32.7 | 61.2 | 6.1 | 0 | **Satisfactory** |
| 17. | **Environmental management and monitoring plan (EMP)** - Land environment, soil environment, water resources, air quality, noise & vibration, flora and fauna, public safety and health, decommissioning and rehabilitation, long-term monitoring protocol, responsible persons and agencies, timelines, guidelines | 6 | 70 | 16 | 8 | **Satisfactory** |
| 18. | **Overall quality of EIA report** - Comprehensive non-technical summary, illustrative maps, diagrams and photos, clear conclusion and recommendations, clear and easy to understand | 24.4 | 59.2 | 18.4 | 2 | **Satisfactory** |

Mining project EIA practice in Kenya shows major similarities to that in other countries within the East African Community. Kahangirwe (2011) evaluated the EIA process in western Uganda and concluded that poor stakeholder engagement, negative perception of EIA by developers, lack of capacity for post-EIA follow-up, and enforcement as key challenges. Many of these factors were also identified in the Kenya study. Kahangirwe (2011) emphasized the need for stakeholder involvement in the analysis of project alternative options. In Tanzania, an evaluation of general EIA practice by Sosovele (2013) indicated that the country is also grappling with certain challenges, especially with regard to inadequate stakeholder participation.

## Conclusion and recommendations

The overall quality of EIA reports was found to be weak in terms of comprehensive consideration of all the phases of mining projects, adequacy of description of the environmental regulatory framework, prediction of potential biological impacts, quality of stakeholder consultation meetings, and dealing with human right issues. The quality was also quite weak in terms of the overall stakeholder engagement and consultation, mining-related climate change considerations, and cost-benefit analysis. Potential risks that are not adequately mitigated because of poor EIAs practices include:

(a) Violation of environmental laws and regulations leading to frequent court cases, expensive fines and penalties
(b) Inadequate mitigation of biological impacts leading to negative impacts on sensitive biodiversity and ecosystems
(c) Widespread public protests due to inadequate involvement and participation in mining operations
(d) Widespread violation of human rights, including public health problems and child labour
(e) Inadequate mitigation and adaptation for climate change leading to mining-related disasters such as flood-related shaft collapses, mine cave-ins, mine flooding and mine suffocations.

The EIA process is considered to be a useful tool for overcoming a wide range of challenges which can face the mining sector. One of the challenges associated with the expected growth in the mining sector in Kenya is the need to ensure good sectoral governance in order to avoid the problems which other countries, especially in Africa, have encountered, such as:

- Inequitable sharing of mineral resource benefits, which are skewed in favor of those in power
- Neglect of local host communities and economies where such resources are located
- Mineral-related conflicts across inter-county and international boundaries
- Conflicts between existing land uses such as agriculture and livestock husbandry and mining activities
- Environmental degradation due to mining activities
- Violation of human rights by mining activities.

The EIA provides an opportunity for avoiding the paradoxical resource curse in Kenya, which has affected many other mineral-endowed countries in Africa (African Development Bank, 2007; Appiah and Zhang, 2013; Demissie and Naghshpour, 2014). The resource curse (also known as the paradox of plenty) refers to the failure of many resource-rich countries to benefit fully from their natural resource wealth and instead suffer from widespread environmental degradation and social conflicts that stem from such assets.

The African Mining Vision (AMV), adopted in February 2009, recognizes that Africa is the world's top producer of numerous mineral commodities. The continent is a global leader in the production of several key commodities such as gold, diamonds, aluminum, cobalt, platinum, chromium, manganese, vanadium, and phosphate. Consequently, the AMV is a policy tool used to help African governments to better harness their natural resource wealth for socio-economic development. The key goals of the AMV include safeguarding transparency and good governance as well as enforcing internationally acceptable safety and health standards, environmental and material stewardship, and corporate social responsibility. These objectives can be realized through the undertaking of high-quality mining project EIAs which are devoid of the weaknesses identified in the audit.

Based on the above conclusions it is recommended that NEMA should tighten the terms and conditions considered in the approval of the statutory terms of reference (ToR) for full-scale mining project EIAs to ensure the following:

(a) Inclusion of a competent mining engineer or geologist in the EIA team
(b) Comprehensive consideration of all the phases of mining projects
(c) Adequacy of the environmental regulatory framework for the EIAs both in terms of Kenyan and international instruments, including those of the IFC/World Bank
(d) Adequate consideration of potential biological impacts
(e) Adequate consideration of human right issues
(f) Adequate consideration of mining-related climate change implications, especially the minimization of greenhouse gas (GHG) emissions
(g) Convincing and effective stakeholder engagement plans
(h) Adequate strategies for cost-benefit analysis.

## Acknowledgements

The author is grateful to NEMA Director-General Professor Geoffrey Wahungu for authorizing access to the national EIA database for use in this study. Many thanks to Paul Nguru and Reagan Owino for their kind assistance in the EIA information retrieval. The assistance provided by Tiffany Mwake and Sharon Mwende in terms of data analysis is highly appreciated. The comments by two anonymous reviewers as part of the SAIMM editorial process are highly appreciated.

## References

African Development Bank. 2007. African development report 2007: Natural resources for sustainable development in Africa. Oxford University Press, Oxford, UK.

Appiah, M. and Zhang, T. 2013. Escaping the resource curse in sub-Saharan Africa. The Hague Institute for Global Justice, The Hague.

Arts, J., Runhaar, H.A.C., Fischer, T.B., Jha-Thakur, U., Laerhoven, F.S.J. van, Driessen, P.P.J., and Onyango, V. 2012. The effectiveness of EIA as an instrument for environmental governance – a comparison of 25 years of EIA practice in the Netherlands and the UK. Imperial College Press.

Armstrong, W. and Peart, R. 2000. Marrying planning, economics and environment: Is South Africa ahead of the curve? *Development*, vol. 43, no. 4. pp. 75–78.

Azcue, J.M. 1999. Environmental Impacts of Mining Activities: Emphasis on Mitigation and Remedial Measures. Springer, Berlin.

Biswas, A.K. and Agarwala, S.B.C. 1994. Environmental impact assessment for developing countries. Butterworths, Oxford.

Černe, M., Smodiš, B., Štrok, M., and Benedik, L. 2012. Radiation impact assessment on wildlife from a uranium mine area. *Nuclear Engineering and Design*, vol. 246. pp. 203–209.

Chakrabarti, S.B. 2007. Man and environment: Evolving dimensions. *Journal of the Indian Anthropological Society*, vol. 42, no. 2. pp. 103–110.

Churie, A. 1997. An overview for the EIA process in Zimbabwe. *Proceedings of the International Environmental Impact Assessment: European and Comparative Law and Practical Experience Conference*, Milan, October 1996. Environmental Law Network International.

Clark, J. and Scottish Natural Heritage. 1996. Rivers and their catchments: Impacts of opencast coal mining on water quality. Scottish Natural Heritage, Edinburgh.

Demissie, M.Z. 2014. The natural resource curse in Sub-Saharan Africa: Transparency and international initiatives. PhD thesis, University of Southern Mississippi.

Dold, B. and Friese, K. 2007. Biogeochemical studies about the environmental impacts of mining on ground and surface water. *Journal of Geochemical Exploration*, vol. 92, no. 2. pp. v–vi.

Environmental Law Alliance Worldwide. 2010. Guidebook for evaluating mining project EIAs. Eugene, OR.

Fischer, T.B. 2010. Reviewing the quality of strategic environmental assessment reports for English spatial plan core strategies. *Environmental Impact Assessment Review*, vol. 30, no. 1. pp. 62–69.

Fischer, T.B. 2006. SEA and transport planning: towards a generic framework for evaluating practice and developing guidance. *Impact Assessment and Project Appraisal*, vol. 24, no. 3. pp. 183–197.

Freeman, J. 1999. All of Us - Births and Better Life: Population, Development and Environment in a Globalized World. Earth Times Books, New York.

Harris, P., Viliani, F., and Spickett, J. 2015. Assessing health impacts within environmental impact assessments: An opportunity for public health globally which must not remain missed. *International Journal of Environmental Research and Public Health*, vol. 12, no. 1. pp. 1044–1049.

Ingelson, A. and Chilenye, N. 2014. Environmental impact assessment process for oil, gas and mining projects in Nigeria: A critical analysis. *Law, Environment and Development Journal*, vol. 10, no. 1. pp. 35–56.

Jha-Thakur, U. and Fischer, T. 2008. Are open-cast coal mines casting a shadow on the Indian environment? *International Development Planning Review*, vol. 30, no. 4. pp. 441–459.

Kahangirwe, P. 2011. Evaluation of environmental impact assessment (EIA) practice in Western Uganda. *Impact Assessment and Project Appraisal*, vol. 29, no. 1. pp. 79–83.

Kamau, J.W. and Mwaura, F. 2013. Climate change adaptation and EIA studies in Kenya. *International Journal of Climate Change Strategies and Managemen*t, vol. 5, no. 2. pp. 152–165.

Kamijo, T. and Huang, G. 2017. Focusing on the quality of EIS to solve the constraints on EIA systems in developing countries: A literature review. *JICA-RI working paper* no. 144. JICA Research Institute, Tokyo Japan.

Kibutu, T.N. and Mwenda, A.N. 2010. Provision for environmental impact assessment (EIA) in Kenya's legislation: A review of the environmental management and coordination act (EMCA) and environmental (impact assessment and audit) regulations (EIAAR). *Eastern Africa Journal of Humanities and Sciences*, vol. 10, no. 2. pp. 1–13.

Kruger, F.J., Van, W.B.W., Weaver, A.V.B., and Greyling, T. 1997. Sustainable development and the environment: lessons from the St Lucia Environmental Impact Assessment. *South African Journal of Science*, vol. 93, no. 1. pp. 23–33.

Kuma, J.S., Younger, P.L., and Bowell, R.J. 2002. Expanding the hydrogeological base in mining EIA studies: A focus on Ghana. *Environmental Impact Assessment Review*, vol. 22, no. 4. pp. 273–287.

Lederer, K., Galtung, J., and Antal, D. 1980. Human Needs: A Contribution to the Current Debate. Oelgeschlager, Gunn and Hain, Cambridge, MA.

Loots, C. 1997. EIA in South Africa. *Proceedings of the International Conference on International Environmental Impact Assessment: European and Comparative Law and Practical Experience*, Milan, October 1996. Environmental Law Network International.

Marshall, R. and Fischer, T.B. 2006. Regional electricity transmission planning and tiered SEA in the UK – the case of Scottish Power. *Journal of Environmental Planning and Management*, vol. 49, no. 2. pp. 279–299.

McKillop, J. and Brown, A.L. 1999. Linking project appraisal and development: the performance of EIA in large-scale mining projects. *Journal of Environmental Assessment Policy and Management*, vol. 1, no. 4. pp. 407–428.

Morrison-Saunders, A. and Retief, F. 2012. Walking the sustainability assessment talk – Progressing the practice of environmental impact assessment (EIA). *Environmental Impact Assessment Review*, vol. 36. pp. 34–41.

Morrison-Saunders, A., McHenry, M.P., Rita, S.A., Gorey, P., Mtegha, H., and Doepel, D. 2016. Integrating mine closure planning with environmental impact assessment: challenges and opportunities drawn from African and Australian practice. *Impact Assessment and Project Appraisal*, vol. 34, no. 2. pp. 117–128.

Muttamara, S. 1996. Environmental impact assessment (EIA). *Resources, Conservation, and Recycling*, vol. 16. pp. 335–349.

Mwaura, F., Kiringe, J.W., Warinwa, F., and Wandera, P. 2016. Estimation of the economic value for the consumptive water use ecosystem service benefits of the Chyulu Hills watershed, Kenya. *International Journal of Agriculture Forestry and Fisheries,* vol. 4, no. 4. pp. 36–48.

Mwenda, A.N., Bregt, A.K., Ligtenberg, A., and Kibutu, T.N. 2012. Trends in consultation and public participation within environmental impact assessment in Kenya. *Impact Assessment and Project Appraisal*, vol. 30, no. 2. pp. 130–135.

Mutua, E. 2014. Report on the policy, legal and regulatory framework in the extractive industry of Kenya. Law Society of Kenya, Nairobi.

Noonan, J. 2014. Democratic Society and Human Needs. McGill-Queen's University Press, Montreal.

Okello, N., Beevers, L., Douven, W., and Leentvaar, J. 2009. The doing and un-doing of public participation during environmental impact assessments in Kenya. *Impact Assessment and Project Appraisal*, vol. 27, no. 3. pp. 217–226.

Ozkan, S. and Ipekoglu, B. 2002. Investigation of environmental impacts of tailings dams. *Environmental Management and Health*, vol. 13, no. 3. pp. 242–248.

Patnaik, L. N. 1990. Environmental Impacts of Industrial and Mining Activities. Ashish, New Dehli.

Phylip-Jones, J. and Fischer, T.B. 2013. EIA for wind farms in the United Kingdom and Germany. *Journal of Environmental Assessment Policy and Management*, vol. 15, no. 2. pp. 1–30. doi: 10.1142/S1464333213400085

Rammelsberg, L.S., Markus, L., Kerns, S., Richardson, A.V., Howard, B., and Accame, G. 2006. Environment and Society. Schlessinger Media, Wynnewood, PA

Republic of Kenya. 2015. Investment handbook. Ministry of Mining. Government Printer, Nairobi.

Retief, F. 2012. Walking the sustainability assessment talk - Progressing the practice of environmental impact assessment (EIA). *Environmental Impact Assessment Review*. vol. 36. pp, 34–41.

Ripley, A.E., Redmann, E.R., and Crowder, A.A. 1996. Environmental effects of mining. St. Lucie Press, Delray Beach, FL.

Safont, E., Vegas-Vilarrúbia, T., and Rull, V. 2012. Use of Environmental Impact Assessment (EIA) tools to set priorities and optimize strategies in biodiversity conservation. *Biological Conservation*, vol. 149, no. 1. pp. 113–121.

Salgado, I. 2013. The nexus of African growth, environment and conflict: Africa-wide – monitoring economies. *Africa Conflict Monthly Monitor*. February 2013. pp. 20–23.

Sandham, L.A., Hoffmann, A.R., and Retief, F.P. 2008. Reflections on the quality of mining EIA reports in South Africa. *Journal of the Southern African Institute of Mining and Metallurgy*, vol. 108, no. 11. pp. 701–706.

Schaltegger, S. and Wagner, M. 2006. Managing the Business Case for Sustainability: The Integration of Social, Environmental and Economic Performance. Greenleaf Publishing, Sheffield.

Sivi, K., Odari, E., Ataka, V., and Wasunna, M. 2015. Local communities in Kenya's extractive sector: From paternalism to partnership. Norwegian Church Aid (NCA).

Sosovele, H. 2013. Governance challenges in Tanzania's environmental impact assessment practice. *African Journal of Environmental and Waste Management*, vol. 1, no. 5. pp. 81–84.

Staeck, N. and Heinelt, H. 2001. The implementation of EIA in Germany. *European Union Environment Policy and New Forms of Governance: A Study of the Implementation of the Environmental Impact Assessment Directive and the Eco-Management and Audit Scheme Regulation in the Three Member States*. Heinelt, H., Malek, T., Smith, R., and Töller, A.E. (eds). Routledge, Abington, UK. pp. 61–70.

Strange, T. and Bayley, A. 2008. Sustainable development: Linking economy, society, environment. OECD, Paris.

Sutton, P.W. 2004. Nature, Environment, and Society. Palgrave Macmillan, Basingstoke, UK.

Tisdell, C.A. 2005. Economics of Environmental Conservation. Edward Elgar, Cheltenham, UK.

Tuberfield, D. 1994. The quality of environmental impact assessment (EIA) reports. *Industry and Environment*, vol. 17, no. 2. pp. 44–47.

United Nations. Department of Economic and Social Affairs, Population Division. 2017. World Population Prospects: The 2017 Revision, Key Findings and Advance Tables. Working Paper no. ESA/P/WP/248.

United Nations Development Programme (Kenya). 2014. Extractive industries for sustainable development in Kenya: Final assessment report.

Wilson, L. 1998. A practical method for environmental impact assessment audits. *Environmental Impact Assessment Review*, vol. 18, no. 1. pp. 59–72.

World Bank. 2008. Environmental sustainability: An evaluation of World Bank Group support. Washington, DC.

Zhao, Y. 2009. Assessing the environmental impact of projects: A critique of the EIA legal regime in China. *Natural Resources Journal*, vol. 49, no. 2. pp. 485–524. ◆

# SMART MINING SMART ENVIRONMENT SMART SOCIETY

*Implementing change now, for the mine of the future*




## 4-5 July 2019

## Accolades Boutique Venue, Midrand

### BACKGROUND

Society in general, and the economy in particular, is evolving at breakneck speed. Old jobs are being lost and new ones are constantly being created. It is likely that mines developed in the next ten years will have a very different staff complement to those currently in production. It is also clear that we are at tipping points for climate systems and for biodiversity: the challenges facing the extractive sector in the coming decades are likely to be much greater than anything in the past century. What does this mean for environmental management? How should we be planning mines to reduce environmental footprints? What skills do we need to do this? Which energy sources will be available and will they have an impact on production? Can we close mines in a way that ensures that viable post-mining economies can be established? This conference bridges the gap between practitioners and decision-makers and managers in both the public and private sectors. The intention is to transfer knowledge and to debate the big issues facing regulators, mining companies, labour, and communities in a way that identifies solutions. The conference will consist of a number of invited keynote speakers who will focus on strategic issues, with the possibility of a workshop included.

### WHO SHOULD ATTEND

The conference should be of interest to anyone working in or with the mining sector, including government and civil society organizations. It would be of particular relevance to advisors, consultants, practitioners, researchers, organized labour, government officials, and specialists working in the following areas:

- Environmental Management
- Sustainability
- Stakeholder Engagement
- Local and Regional Development Planning
- Mining Legislation.

SAIMM
THE SOUTHERN AFRICAN INSTITUTE OF MINING AND METALLURGY

**FOR FURTHER INFORMATION CONTACT:**
Yolanda Ndimande, Conference Co-ordinator, SAIMM
P O Box 61127, Marshalltown 2107 · Tel: +27 (0) 11 834-1273/7
E-mail: yolanda@saimm.co.za · Website: http://www.saimm.co.za


# Reduction rates of MnO and $SiO_2$ in SiMn slags between 1500 and 1650°C

**P.P. Kim[1], T.A. Larssen[1], and M. Tangstad[1]**

**Affiliation:**
1 Department of Materials Science and Engineering, Norwegian University of Science and Technology, N-7591 Trondheim, Norway.

**Correspondence to:**
P.P. Kim

**Email:**
pyung.h.kim@ntnu.no

**Dates:**
Received: 30 Mar. 2018
Revised: 2 Oct. 2018
Accepted: 29 Oct. 2018
Published: May 2019

**How to cite:**
Kim, P.P., Larssen, T.A., and Tangstad, M.
Reduction rates of MnO and $SiO_2$ in SiMn slags between 1500 and 165O°C
The Southern African Insitute of Mining and Metallurgy

DOI ID:
http://dx.doi.org/10.17159/2411-9717/153/2019

ORCiD ID:
P.P. Kim
https://orchid.org/0000-0001-5449-5385

T.A. Larssen
https://orchid.org/0000-0003-0224-3201

M. Tangstad
https://orchid.org/0000-0001-9751-7716

**Synopsis**

**The kinetics of MnO and $SiO_2$ reduction in SiMn slags based on Assmang/Comilog ore and HCFeMn (high-carbon ferromanganese) slag were investigated between 1500 and 1650°C under a CO atmosphere. The results showed that charges containing HCFeMn slag had relatively faster reduction rates than those without. The difference in the driving force for MnO reduction was insignificant among the SiMn slags at 1500°C, which implies a low contribution of the driving force for reduction rate. The slag viscosities were also rather similar, around 1 poise at 1500°C, which could not explain the different reduction rates. Instead, the different charges containing various sulphur contents are believed to give rise to the varying reduction rates. The estimated activation energies for MnO reduction were around 500–920 kJ/mol for charges containing HCFeMn slag, and between 250–300 kJ/mol for those without. Based on the estimated kinetic parameters, the considered rate models were able to describe the reduction of MnO and $SiO_2$ in SiMn slags between 1500 and 1650°C.**

**Keywords**
SiMn, MnO, $SiO_2$, reduction, kinetics.

## Introduction

Manganese ferroalloys such as ferromanganese (FeMn) and silicomanganese (SiMn) are important ingredients in steel production due to the beneficial effects of manganese on the physical properties of steel. Mn enhances the strength, toughness, and hardness of steel products, and both Mn and Si are used as deoxidizers to prevent the development of porous structures (International Manganese Institute, 2014; Olsen, Tangstad, and Lindstad, 2007; Subramanyam, Swansiger, and Avery, 1990; Tomota *et al.,* 1987).

The thermodynamic background of manganese ferroalloys is well established (Olsen, Tangstad and Lindstad, 2007), but kinetic information is rather scarce, especially for the SiMn process (Tranell *et al.,* 2007; Tore-Andre Skjervheim, 1994). The absence of kinetic information makes it more difficult to understand the reduction mechanisms of MnO and $SiO_2$. It is not clear how different raw materials affect the SiMn process. The main metal-producing reactions in the SiMn process are described by Equations [1] and [2]:

$$MnO_{(1)} + C \rightarrow Mn_{(1)} + CO_{(g)} \quad [1]$$

$$SiO_{2(1)} + 2C \rightarrow Si_{(1)} + 2CO_{(g)} \quad [2]$$

Recent studies have shown that MnO and $SiO_2$ are reduced to Mn and Si significantly above 1500°C (Kim, Holtan, and Tangstad, 2016; Kim *et al.,* 2017). The mass change observed in thermogravimetric experiments was low until 1500°C, but increased significantly at higher temperatures. It was perceived that most of the MnO and $SiO_2$ reduction occurred between 1500 and 1650°C, but the reasons were not fully understood. Therefore, the present study focuses on the kinetic information on MnO and $SiO_2$ reduction in SiMn slags ($MnO\text{-}SiO_2\text{-}CaO\text{-}MgO\text{-}Al_2O_3$) between 1500 and 1650°C using different Mn sources.

## Theoretical considerations

The reduction rate of MnO was studied previously and was described by Equation [1] (Olsen, Tangstad, and Lindstad, 2007; Ostrovski *et al.,* 2002). This equation is based on the FeMn process and implies that

the chemical reaction is the rate-determining step. Since SiMn slags are essentially similar to FeMn slags, Equation [1] can also be used for MnO reduction from SiMn slags. For $SiO_2$, a recent study showed that the dissolution of $SiO_2$ into slag was the rate-determining step (Maroufi *et al.,* 2015). However, contrary results have also been observed where the dissolution of both MnO and $SiO_2$ into slag was completed before significant reduction takes place above 1500°C (Kim and Tangstad, 2018a, 2018b, 2018c; Holtan, 2015). In this study, a similar rate equation for $SiO_2$ reduction was presumed using Equation [2], assuming $SiO_2$ reduction is also mainly controlled by chemical reaction. Both Equations [1] and [2] were considered in this work to estimate the kinetic parameters.

For Equation [1]:

$$r_{MnO} = k_{MnO} \cdot A \cdot (a_{MnO} - a_{MnO,Eqm.}) = k_{o,MnO} \cdot A \cdot e^{-E_{MnO}/RT} \cdot (a_{MnO} - \frac{a_{Mn}}{K_{T,MnO}})$$

For Equation [2]:

$$r_{SiO_2} = k_{SiO_2} \cdot A \cdot (a_{SiO_2} - a_{SiO_2,Eqm.}) = k_{o,SiO_2} \cdot A \cdot e^{-E_{SiO_2}/RT} \cdot (a_{SiO_2} - \frac{a_{Si}}{K_{T,SiO_2}})$$

where $r$ is the reduction rate (g/min), $k$ is the rate constant (g/min·cm$^2$), $k_o$ is the frequency factor, $A$ is the reaction area (cm$^2$), $E$ is the activation energy (kJ/mol), $R$ is the gas constant, $T$ is the temperature, $a_{MnO}$, $a_{SiO_2}$ are the activity values of MnO and $SiO_2$ in the slag phase, $a_{MnO,Eqm.}$, $a_{SiO_2,Eqm.}$ are the activity values of MnO and $SiO_2$ in equilibrium, and $K_T$ is the equilibrium constant at temperature $T$.

The rate models considered for MnO and $SiO_2$ reduction also imply that the driving force, which is the difference between the activity of slag (MnO, $SiO_2$) and the produced metal (Mn, Si), contribute to the reduction rates. The simplified models for activities of slag and metal have been recently studied (Olsen, 2016). These activities were based on FactSage 7.0, database FTOxid and FactPS (CRCT and GTT, 2015), and thermodynamic data from HSC Chemistry 7 (Outotec, n.d.) was used to calculate the driving forces of MnO and $SiO_2$ reduction at different temperatures.

## Experimental procedures

The chemical compositions of the raw materials are shown in Table I and the SiMn charges are described in Table II. Note that manganese is present as MnO and $MnO_2$ in manganese ores. Three different Mn sources, Assmang ore, Comilog ore, and HCFeMn slag, were used to study different SiMn charges in this work. The sizes of the raw materials were between 0.6 and 1.6 mm. Each raw material was weighed to aim at approximately 40 wt% $SiO_2$ in slag and 18 wt% Si in the metal phase, which is close to the thermodynamic equilibrium at 1600°C (Olsen, Tangstad, and Lindstad, 2007). The charge materials were added into graphite crucibles (36 mm outer diameter, 30 mm inner diameter, 70 mm height, and 61 mm depth).

A TGA furnace, which is schematically depicted in Figure 1, was used to conduct the experiments. The furnace can reach temperatures up to 1700°C and the maximum heating rate is 25°C/min. A mass balance is installed at the top and a molybdenum (Mo) wire was used to suspend the graphite crucible inside the chamber. The temperature schedule of the experiment was considered to simulate an industrial furnace operation and is described in Figure 2. Initially, the furnace was rapidly heated up

*Table I*

**Chemical composition of raw materials (wt%)**

| Material | MnO | $MnO_2$ | $SiO_2$ | $Fe_2O_3$ | CaO | MgO | $Al_2O_3$ | S | C | $CO_2$ | $H_2O$ | Total |
|---|---|---|---|---|---|---|---|---|---|---|---|---|
| Assmang | 32.7 | 33.2 | 5.8 | 15.1 | 6.3 | 1.1 | 0.3 | 0.16 | 0.3 | 3.5 | 1.6 | 100.6 |
| Comilog | 3.0 | 72.4 | 4.6 | 6.7 | 0.1 | 0.1 | 5.6 | - | - | 0.1 | 5.0 | 97.6 |
| Quartz | 0.1 | - | 93.9 | - | 0.1 | 0.1 | 1.2 | - | - | - | - | 95.4 |
| HCS* | 35.2 | - | 25.5 | - | 18.5 | 7.5 | 12.3 | 0.46 | 0.4 | - | 2.2 | 102.1 |
| Coke | - | - | 5.6 | 0.86 | 0.4 | 0.2 | 2.8 | 0.4 | 87.7 | - | 15.5 | 113.5 |

* HCS: high-carbon FeMn slag

*Table II*

**Composition of SiMn charges used in the experiments (g)**

| Charge | Assmang* | Comilog* | Quartz | HCS* | Coke | Total |
|---|---|---|---|---|---|---|
| As | 7 | - | 1.9 | - | 2.2 | 11.1 |
| As/HCS | 4 | - | 1.7 | 4 | 2.5 | 12.2 |
| Com | - | 6 | 1.4 | - | 2.0 | 9.4 |
| Com/HCS | - | 4 | 1.6 | 4 | 2.3 | 11.9 |
| HCS | - | - | 1.5 | 10 | 3.0 | 14.5 |

* Mn-bearing materials

# Reduction rates of MnO and $SiO_2$ in SiMn slags between 1500 and 1650°C

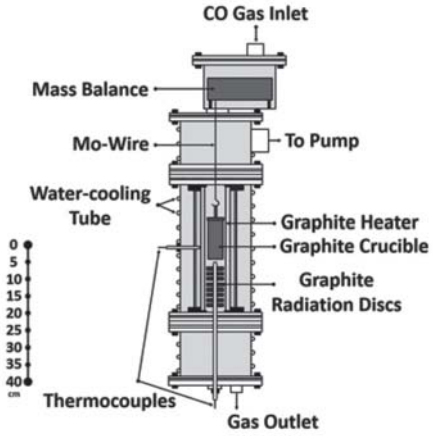


Figure 1—Schematic of the TGA furnace

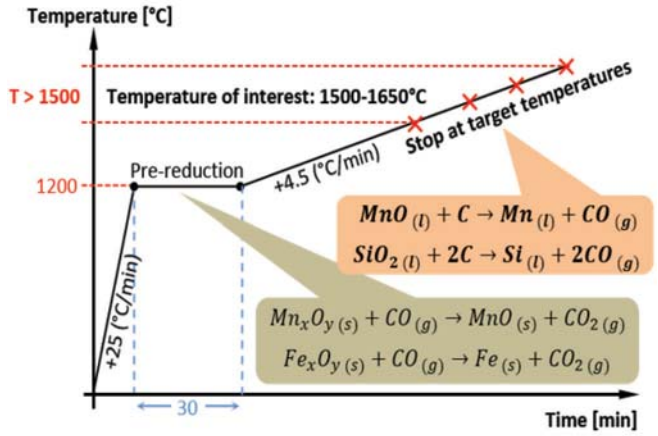


Figure 2—The temperature schedule

to 1200°C at a rate of 25°C/min and held for 30 minutes to secure complete prereduction (Olsen, Tangstad, and Lindstad, 2007). Then, further heating at a rate of 4.5°C/min was done and stopped at targeted temperatures between 1500 and 1650°C, followed by cooling. All experiments were conducted in CO at atmospheric pressure.

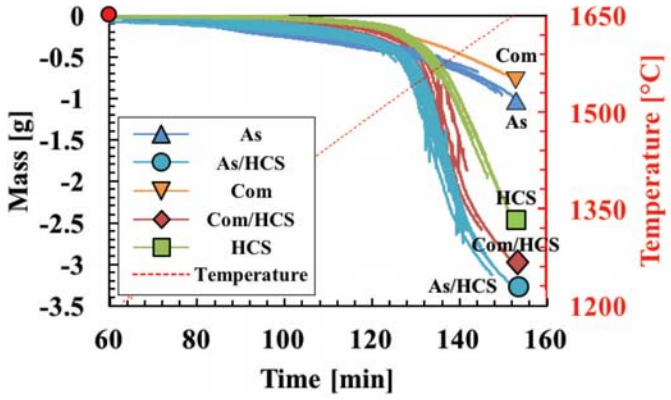


Figure 3 – TGA results for several experiments for each charge between 1500 and 1650°C, with respect to the new reference point (red circle) at 1200°C

The weight loss of each charge sample was recorded and the data was logged every 5 seconds during the experiment. Lastly, a portion from each charge sample was prepared by mounting it in epoxy for electron probe microanalysis (EPMA) using a JEOL JXA-8500F instrument. The average slag composition from more than five analysed points was used to calculate the metal composition (as the metal analyses are more uncertain than the slag analyses).

## Results and discussion

The mass changes recorded during the TGA runs were the main information used. Figure 3 describes the TGA results from different SiMn charges between 1200 and 1650°C. Note that complete prereduction was assumed at 1200°C and used as a new reference point for further reduction of MnO and $SiO_2$. The mass changes for all SiMn charges were insignificant below 1500°C, which indicated a low degree of MnO and $SiO_2$ reduction. The reduction rate increased above 1500°C, which is in accordance with previous studies (Kim, Holtan, and Tangstad, 2016; Kim *et al.,* 2017), but the degree of reduction differed with different SiMn charges. It was observed that charges containing HCFeMn slag were reduced faster and attained higher degrees of reduction. Although the apparent accelerated reduction can be thought to result from the use of HCFeMn slag, the TGA results

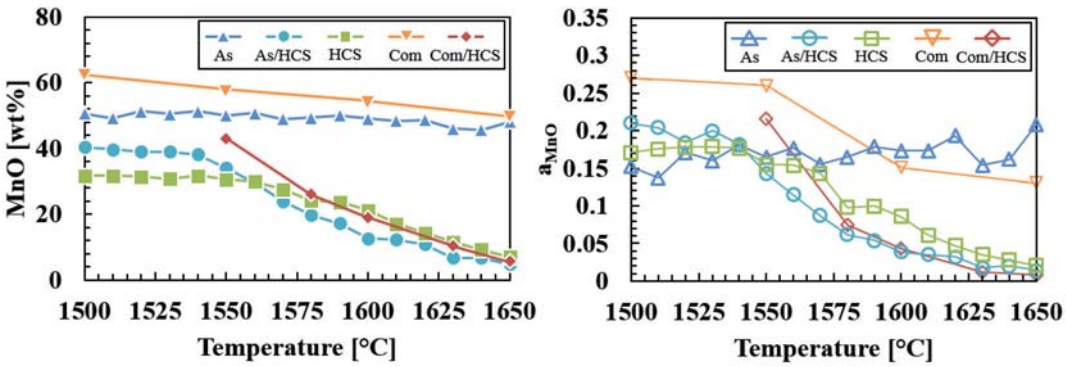


Figure 4 – Comparison of MnO (left) and $a_{MnO}$ (right) between 1500 and 1650°C

# Reduction rates of MnO and $SiO_2$ in SiMn slags between 1500 and 1650°C

**Table III**

**Slag analyses (EPMA) and calculated metal compositions with the respective activities between 1500 and 1650°C**

| Charge temp. | Slag (wt%) | | | | | | | | Metal (calculated, wt%) | | | | | |
|---|---|---|---|---|---|---|---|---|---|---|---|---|---|---|
| | MnO | $SiO_2$ | CaO | MgO | $Al_2O_3$ | $a_{MnO}$ | $aSiO_2$ | C+M/A | Mn | Si | Fe | C | $a_{Mn}$/KT | $a_{Si}$/KT |
| As-1500 | 50.6 | 39.1 | 7.6 | 1.2 | 0.5 | 0.152 | 0.285 | 17.2 | 54.6 | 4.3 | 35.9 | 5.2 | 0.0037 | 0.1280 |
| 1510 | 49.3 | 40.5 | 7.7 | 1.3 | 0.7 | 0.137 | 0.339 | 13.7 | 55.9 | 2.0 | 35.9 | 6.2 | 0.0035 | 0.0378 |
| 1520 | 51.3 | 37.9 | 7.2 | 1.3 | 0.5 | 0.171 | 0.237 | 16.0 | 54.4 | 7.4 | 34.0 | 4.2 | 0.0030 | 0.1914 |
| 1530 | 50.5 | 38.8 | 7.7 | 1.2 | 0.5 | 0.160 | 0.269 | 16.4 | 55.2 | 5.8 | 34.3 | 4.6 | 0.0029 | 0.0994 |
| 1540 | 51.4 | 37.4 | 8.4 | 0.7 | 0.7 | 0.181 | 0.218 | 13.3 | 55.0 | 8.8 | 32.6 | 3.5 | 0.0026 | 0.1598 |
| 1550 | 50.1 | 38.7 | 8.3 | 0.8 | 0.7 | 0.165 | 0.258 | 12.7 | 56.4 | 7.4 | 32.2 | 4.1 | 0.0025 | 0.0915 |
| 1560 | 50.8 | 37.9 | 7.5 | 1.4 | 0.5 | 0.177 | 0.229 | 16.3 | 55.8 | 8.7 | 31.7 | 3.8 | 0.0021 | 0.1026 |
| 1570 | 49.0 | 39.7 | 7.7 | 1.3 | 0.5 | 0.155 | 0.289 | 16.6 | 57.6 | 6.7 | 31.3 | 4.5 | 0.0021 | 0.0504 |
| 1580 | 49.4 | 39.0 | 8.6 | 0.7 | 0.8 | 0.165 | 0.261 | 11.7 | 57.5 | 8.1 | 30.6 | 3.9 | 0.0019 | 0.0543 |
| 1590 | 50.1 | 38.2 | 8.9 | 0.8 | 0.7 | 0.179 | 0.230 | 13.4 | 57.1 | 9.4 | 30.1 | 3.4 | 0.0017 | 0.0587 |
| 1600 | 49.1 | 38.7 | 8.9 | 0.7 | 0.9 | 0.173 | 0.243 | 11.1 | 58.3 | 9.7 | 28.6 | 3.5 | 0.0016 | 0.0511 |
| 1610 | 48.4 | 38.8 | 9.1 | 0.7 | 0.8 | 0.173 | 0.240 | 12.5 | 59.1 | 10.4 | 27.3 | 3.2 | 0.0015 | 0.0479 |
| 1620 | 48.7 | 37.7 | 9.4 | 0.7 | 0.9 | 0.193 | 0.198 | 11.0 | 59.2 | 12.3 | 25.8 | 2.7 | 0.0013 | 0.0581 |
| 1630 | 46.1 | 40.5 | 8.0 | 1.4 | 0.8 | 0.154 | 0.289 | 11.6 | 60.8 | 9.9 | 25.6 | 3.6 | 0.0013 | 0.0311 |
| 1640 | 45.7 | 40.1 | 9.3 | 1.4 | 0.8 | 0.162 | 0.263 | 13.3 | 61.1 | 11.3 | 24.3 | 3.3 | 0.0011 | 0.0339 |
| 1650 | 48.1 | 37.3 | 7.5 | 1.3 | 0.7 | 0.208 | 0.175 | 12.0 | 59.6 | 13.5 | 24.2 | 2.8 | 0.0009 | 0.0443 |
| As/HCS-1500 | 40.5 | 35.1 | 12.3 | 3.8 | 5.2 | 0.210 | 0.107 | 3.1 | 50.0 | 10.7 | 36.5 | 2.9 | 0.0031 | |
| 1510 | 39.8 | 35.4 | 12.2 | 3.5 | 5.8 | 0.204 | 0.111 | 2.7 | 52.7 | 10.6 | 33.8 | 3.0 | 0.0030 | 0.4818 |
| 1520 | 39.1 | 36.6 | 12.0 | 3.9 | 5.6 | 0.184 | 0.135 | 2.9 | 54.5 | 5.2 | 35.6 | 4.7 | 0.0032 | 0.1010 |
| 1530 | 39.1 | 35.7 | 12.1 | 3.7 | 4.9 | 0.200 | 0.113 | 3.3 | 54.6 | 10.5 | 31.8 | 3.1 | 0.0026 | 0.2934 |
| 1540 | 38.3 | 36.8 | 12.2 | 3.9 | 5.0 | 0.182 | 0.135 | 3.2 | 56.8 | 6.4 | 32.4 | 4.4 | 0.0028 | 0.0904 |
| 1550 | 34.1 | 39.0 | 13.2 | 3.7 | 6.3 | 0.143 | 0.168 | 2.7 | 64.8 | 6.5 | 24.1 | 4.6 | 0.0029 | 0.0734 |
| 1560 | 29.5 | 40.4 | 14.4 | 4.0 | 6.7 | 0.115 | 0.182 | 2.7 | 68.4 | 8.9 | 18.7 | 3.9 | 0.0027 | 0.1021 |
| 1570 | 24.0 | 41.8 | 16.2 | 4.3 | 8.0 | 0.087 | 0.187 | 2.6 | 70.2 | 11.1 | 15.3 | 3.4 | 0.0024 | 0.1244 |
| 1580 | 19.7 | 44.1 | 18.3 | 5.2 | 8.8 | 0.062 | 0.227 | 2.7 | 72.0 | 10.3 | 14.1 | 3.7 | 0.0023 | 0.0838 |
| 1590 | 17.2 | 44.2 | 19.2 | 5.2 | 9.2 | 0.054 | 0.212 | 2.7 | 71.8 | 11.6 | 13.2 | 3.4 | 0.0020 | 0.0882 |
| 1600 | 12.7 | 43.8 | 21.6 | 6.2 | 10.4 | 0.039 | 0.174 | 2.7 | 71.3 | 13.9 | 12.0 | 2.9 | 0.0016 | 0.1094 |
| 1610 | 12.3 | 45.4 | 21.2 | 6.0 | 10.7 | 0.035 | 0.213 | 2.6 | 72.2 | 12.4 | 12.1 | 3.2 | 0.0016 | 0.0682 |
| 1620 | 10.9 | 44.6 | 22.5 | 6.4 | 11.5 | 0.032 | 0.183 | 2.5 | 71.6 | 13.7 | 11.7 | 3.0 | 0.0014 | 0.0710 |
| 1630 | 6.8 | 45.5 | 24.2 | 6.7 | 12.4 | 0.018 | 0.181 | 2.5 | 71.8 | 14.1 | 11.1 | 2.9 | 0.0013 | 0.0637 |
| 1640 | 6.8 | 44.0 | 24.9 | 7.2 | 12.8 | 0.020 | 0.147 | 2.5 | 71.0 | 15.2 | 11.0 | 2.8 | 0.0011 | 0.0651 |
| 1650 | 4.9 | 43.9 | 26.5 | 7.1 | 13.8 | 0.014 | 0.136 | 2.4 | 70.9 | 15.7 | 10.7 | 2.8 | 0.0010 | 0.0591 |
| HCS-1500 | 31.7 | 34.5 | 15.4 | 4.9 | 9.4 | 0.171 | 0.076 | 2.2 | 27.3 | 30.1 | 36.2 | 6.4 | 0.0005 | - |
| 1510 | 31.7 | 34.2 | 15.8 | 5.0 | 9.7 | 0.176 | 0.072 | 2.2 | 29.7 | 32.4 | 27.2 | 10.7 | 0.0002 | - |
| 1520 | 31.5 | 34.1 | 15.9 | 5.1 | 9.7 | 0.178 | 0.069 | 2.2 | 35.5 | 32.1 | 22.2 | 10.2 | 0.0002 | - |
| 1530 | 30.8 | 33.8 | 15.8 | 5.2 | 10.0 | 0.179 | 0.064 | 2.1 | 43.8 | 31.5 | 15.0 | 9.6 | 0.0001 | - |
| 1540 | 31.7 | 34.4 | 15.8 | 5.5 | 9.2 | 0.177 | 0.074 | 2.3 | 28.6 | 30.7 | 33.2 | 7.6 | 0.0002 | - |
| 1550 | 30.6 | 35.8 | 16.1 | 5.6 | 9.5 | 0.155 | 0.092 | 2.3 | 58.6 | 0.1 | 34.5 | 6.9 | 0.0027 | - |
| 1560 | 30.0 | 35.7 | 16.3 | 5.8 | 9.7 | 0.154 | 0.090 | 2.3 | 63.9 | 8.8 | 23.5 | 3.9 | 0.0025 | 0.1012 |
| 1570 | 27.6 | 35.6 | 16.9 | 5.8 | 10.0 | 0.143 | 0.080 | 2.3 | 68.5 | 18.9 | 10.1 | 2.5 | 0.0013 | 0.5175 |
| 1580 | 24.1 | 38.8 | 17.3 | 5.5 | 11.3 | 0.098 | 0.124 | 2.0 | 82.1 | 3.4 | 8.2 | 6.3 | 0.0028 | 0.0126 |
| 1590 | 23.7 | 38.4 | 17.5 | 5.8 | 11.4 | 0.100 | 0.116 | 2.1 | 80.5 | 7.0 | 7.6 | 5.0 | 0.0025 | 0.0302 |
| 1600 | 21.2 | 38.8 | 18.5 | 6.2 | 11.5 | 0.086 | 0.114 | 2.2 | 79.9 | 10.4 | 5.9 | 3.9 | 0.0021 | 0.0507 |
| 1610 | 17.1 | 40.1 | 19.4 | 6.3 | 12.9 | 0.061 | 0.124 | 2.0 | 80.8 | 10.8 | 4.6 | 3.8 | 0.0019 | 0.0444 |
| 1620 | 14.3 | 40.8 | 21.3 | 6.8 | 13.3 | 0.047 | 0.127 | 2.1 | 80.8 | 11.6 | 4.0 | 3.7 | 0.0017 | 0.0423 |
| 1630 | 11.6 | 41.5 | 22.9 | 7.1 | 13.9 | 0.035 | 0.130 | 2.2 | 80.8 | 12.1 | 3.6 | 3.6 | 0.0016 | 0.0385 |
| 1640 | 9.2 | 40.2 | 23.6 | 7.8 | 15.3 | 0.028 | 0.097 | 2.0 | 77.7 | 16.4 | 3.2 | 2.9 | 0.0010 | 0.0694 |
| 1650 | 7.1 | 40.2 | 25.5 | 7.8 | 15.9 | 0.021 | 0.092 | 2.1 | 77.3 | 17.0 | 3.0 | 2.8 | 0.0009 | 0.0657 |
| Com-1500 | 62.4 | 28.8 | 0.1 | 0.2 | 2.5 | 0.306 | 0.106 | 0.1 | 51.8 | 14.3 | 31.7 | 2.2 | 0.0028 | 1.2916 |
| 1550 | 57.9 | 30.4 | 0.3 | 0.2 | 4.4 | 0.264 | 0.136 | 0.1 | 66.3 | 15.0 | 16.2 | 2.5 | 0.0022 | 0.4250 |
| 1600 | 54.7 | 30.0 | 0.4 | 0.2 | 5.3 | 0.242 | 0.138 | 0.1 | 68.8 | 16.5 | 12.2 | 2.5 | 0.0013 | 0.1802 |
| 1650 | 49.7 | 35.5 | 0.3 | 0.2 | 5.6 | 0.161 | 0.261 | 0.1 | 71.8 | 12.9 | 12.1 | 3.2 | 0.0012 | 0.0359 |
| Com/HCS-1550 | 43.1 | 33.9 | 9.0 | 3.6 | 7.4 | 0.220 | 0.113 | 1.7 | 61.7 | 9.8 | 25.0 | 3.5 | 0.0026 | 0.1588 |
| 1580 | 26.2 | 41.3 | 13.0 | 4.4 | 11.8 | 0.077 | 0.225 | 1.5 | 78.4 | 9.9 | 7.8 | 4.0 | 0.0025 | 0.0714 |
| 1600 | 19.0 | 43.0 | 14.7 | 5.1 | 14.2 | 0.045 | 0.234 | 1.4 | 78.3 | 11.9 | 6.4 | 3.5 | 0.0020 | 0.0694 |
| 1630 | 10.4 | 43.3 | 19.0 | 6.5 | 17.7 | 0.019 | 0.200 | 1.4 | 77.0 | 14.6 | 5.4 | 3.0 | 0.0013 | 0.0638 |
| 1650 | 5.7 | 40.9 | 22.2 | 7.6 | 20.6 | 0.009 | 0.134 | 1.5 | 75.1 | 17.1 | 5.0 | 2.8 | 0.0026 | 0.1588 |

## Reduction rates of MnO and $SiO_2$ in SiMn slags between 1500 and 1650°C

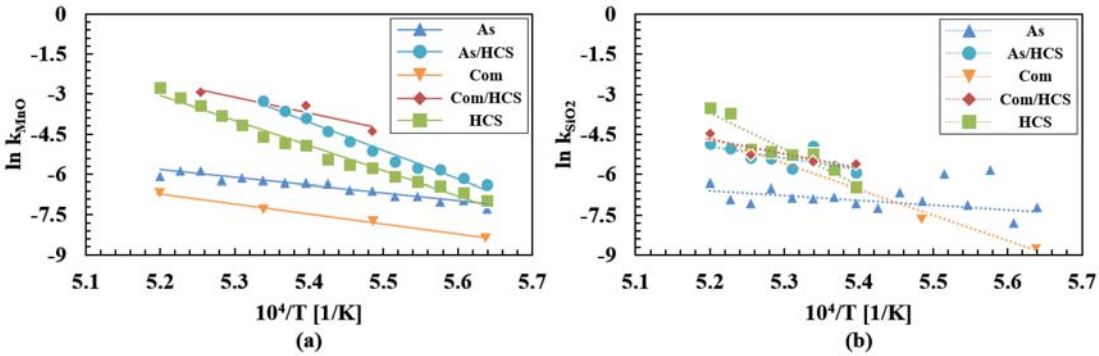


Figure 5—Arrhenius plots of (a) MnO reduction and (b) $SiO_2$ reduction between 1500 and 1650°C

do not adequately describes the reduction degrees of MnO and $SiO_2$ separately. Quantitative slag and metal analyses are required to provide further information.

The average slag and metal compositions of the different charges, with their respective activities (slag: $a_{MnO}$ and $a_{SiO_2}$, metal: $a_{Mn}/K_T$ and $a_{Si}/K_T$), between 1500 and 1650°C are shown in Table III. Significant reduction of MnO was clearly observed with charges containing HCFeMn slag. The MnO content in slag between 1500 and 1650°C for charges 'As/HCS' and 'HCS' decreased from approximately 40 and 31 wt% to 5 and 7 wt%, respectively. Similar degrees of reduction were also observed from charge 'Com/HCS', where the decrease of MnO was from approximately 43 to 6 wt% between 1500 and 1650°C. On the other hand, for charges without HCFeMn slag ('As' and 'Com') the MnO contents were still relatively high compared to the charges containing HCFeMn slag. This shows good accordance with the TGA results in Figure 3, which imply that most of the mass change was due to MnO reduction between 1500 and 1650°C.

*Table IV*

**Summary of the estimated activation energies for MnO and $SiO_2$ reduction between 1500 and 1650°C**

| Charge | MnO reduction (kJ/mol) | $SiO_2$ reduction (kJ/mol) |
|---|---|---|
| As | 250 | 160 |
| As/HCS | 920 | 870 |
| Com | 305 | 450 |
| Com/HCS | 500 | 790 |
| HCS | 780 | 1130 |

The $a_{MnO}$ also represents the reduction of MnO for all charges. Figure 4 compares the $a_{MnO}$ for all charges between 1500 and 1650°C. Note that each point represents an experimental run. The $a_{MnO}$ for all the charges was similar at 1500°C: approximately 0.2 (1550°C for 'Com/HCS'). Only for charges containing HCFeMn slag have the $a_{MnO}$ values dropped down near to zero at 1650°C, which also indicates a higher degree of MnO reduction. This implies that the driving force for MnO reduction ($a_{MnO} - a_{Mn} \approx a_{MnO}$) will have insignificant impact on the reduction rate according to Equations [1] and [2] at the start of reduction Hence it is not the driving force, but the rate constant, that differs more between the reactions occurring with different charges.

The rate constants in this study are expressed as the Arrhenius equation according to Equations [1] and [2]. The Arrhenius plots of MnO and $SiO_2$ reduction for all charges are described in Figure 5, and the estimated activation energies are shown in Table IV. The Arrhenius plot for MnO reduction shows that charges containing HCFeMn slag have higher rate constants

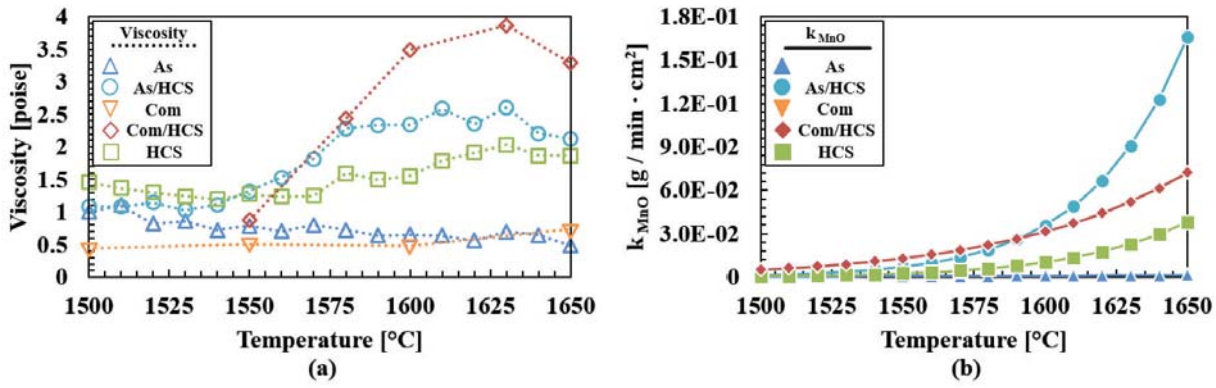


Figure 6—Comparison of (a) slag viscosity and (b) rate constants (MnO reduction) between 1500 and 1650°C

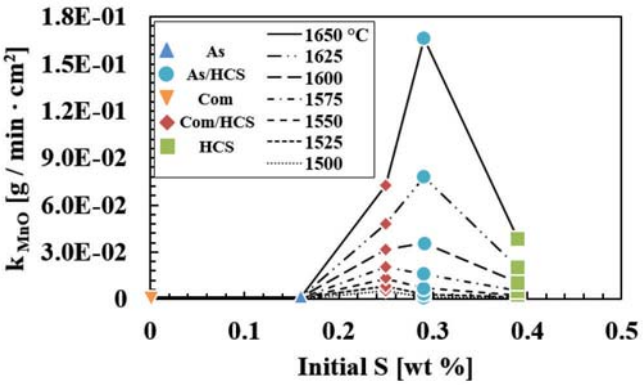


**Figure 7 – Comparison of initial amount of sulphur in charge and rate constants (MnO reduction) between 1500 and 1650°C**

with increasing temperature. Also, the temperature dependency (activation energy) seems to be similar with different charges types: charges including HCFeMn slag ('As/HCS', 'Com/HCS', and 'HCS') were approximately between 500 and 920 kJ/mol and charges without HCFeMn slag ('As' and 'Com') were between 250 and 300 kJ/mol. The Arrhenius plot for $SiO_2$ reduction was difficult to estimate due to small amount of Si produced. However, the temperature dependencies for $SiO_2$ reduction were somewhat similar within the range of experimental conditions.

As the main difference between the different charges is the rate constant, the rate constants for MnO reduction were compared with the viscosity of the slag (Figure 6). If the assumption of chemical reaction being rate-determining is not valid, the viscosity could affect the rate. The viscosities were calculated by using FactSage 7.0 (CRCT and GTT, 2015). No correlation between the viscosity of the slag in the initial phase of the reduction was found at 1500°C, and the rate constant is hence not affected by the viscosity in the slag and probably neither the diffusion, which can be correlated with viscosity.

Sulphur is known to behave as a strong surface-active species for most metals (Stølen and Grande, 2004). The comparison of the initial amount of sulphur in the charge and the rate constants (MnO reduction) between 1500 and 1650°C is shown in Figure 7. Note that the amount of sulphur was calculated from the raw materials (excluding coke). It is seen that the rate constant initially increases with the sulphur content and then decreases again. This is in accordance with previous observations where the sulphur content was studied separately (Kim and Tangstad, 2018a, 2018b, 2018c; Kawamoto, 2016; Larrsen, 2016).

By applying the estimated kinetic parameters in Figure 5, the changing amounts of MnO and $SiO_2$ in SiMn slags can be described by using the rate models (Equations [1] and [2]). The comparisons between the rate models and the measured amount of MnO and $SiO_2$ between 1500 and 1650°C are described in Figure 8. Note that the parameters which describe the optimal fit were applied to the rate models (approximately 2% error in the raw materials analyses). The comparison showed that the rate models considered in this study are applicable to describe the amounts of MnO and $SiO_2$ for SiMn slags. The symbols, which indicate the measured amounts of MnO and $SiO_2$ from the experiments, show a good match with the calculated amounts (solid and dotted lines) between 1500 and 1650°C. The considered rate models were successfully used to describe the changing amounts of MnO and $SiO_2$ regardless of the charge type and degree of reduction.

## Conclusions

The objective of this study was to estimate the kinetics of MnO and $SiO_2$ reduction in SiMn slags and to observe the reduction rate between 1500 and 1650°C. The results showed that SiMn charges containing HCFeMn slag as raw material are reduced faster than those without. The measured amount of MnO in slag at 1650°C was low for charges containing HCFeMn slag, and the $a_{MnO}$ showed good accordance: The $a_{MnO}$ was around 0.2 at 1500°C but decreased to near zero at 1650°C. Also, the $a_{MnO}$ at 1500°C was approximately 0.2 for all charges, which implies a low contribution to the driving force for reduction rate. From the kinetic estimations, the activation energies differed for the two types of charge: for MnO reduction, the values for charges containing HCFeMn slag were approximately 500–920 kJ/mol, and for those without, approximately 250–300 kJ/mol. The comparison of slag viscosity with rate constants showed that slag viscosity does not significantly influence the reduction rate of MnO. Instead, small amounts of sulphur impurity in the charge showed significant impact on the reduction rates. At more than 0.15 wt% of initial sulphur, the rate constants increased drastically with increasing temperature. In addition, the

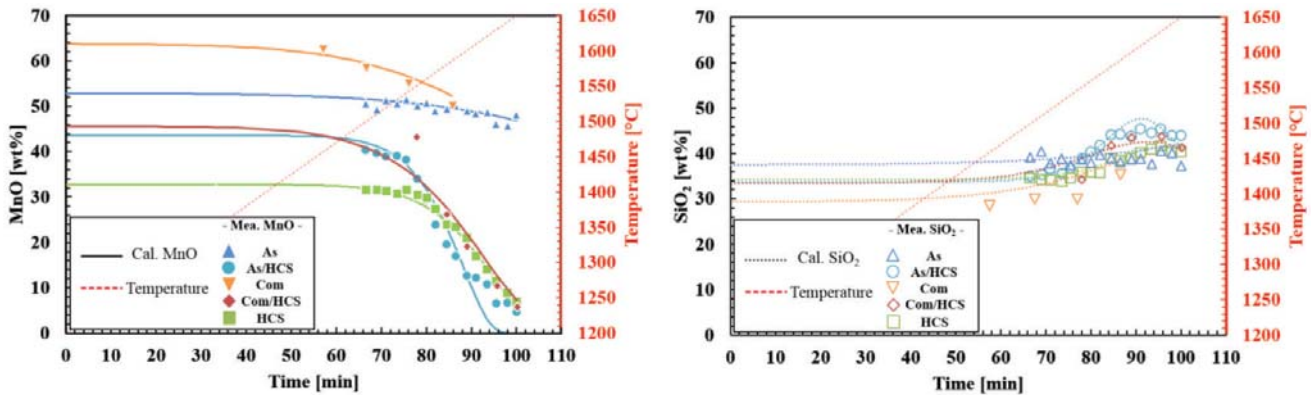


**Figure 8 – Comparison of calculated (solid and dotted lines) and measured (symbols) amounts of MnO and $SiO_2$ in SiMn slags between 1200 and 1650°C**

considered rate models for MnO and $SiO_2$ reduction were able to describe the changing amounts of MnO and $SiO_2$ in SiMn slags. The results are applicable for estimating the production rate during SiMn smelting.


## Acknowledgments

This publication has been partly funded by the SFI Metal Production (Centre for Research-based Innovation, 237738). The authors gratefully acknowledge the financial support from the Research Council of Norway and the partners of the SFI Metal Production.


## References


CRCT: Canada, GTT: Germany. FactSage 7.0 http://www.factsage.com

Holtan, J. 2015. Phase composition in Comilog charges during heating and reduction. Internal report: TMT 4500 Materials Technology, Specialization Project, Norwegian University of Science and Technology.

International Manganese Institute. 2014. http://www.manganese.org

Kawamoto, R. 2016. Effect of sulfur addition on reduction mechanism of synthetic ore. Internal report: TMT 4500 Materials Technology, Specialization Project, Norwegian University of Science and Technology.

Kim P., Holtan J., and Tangstad M. 2016. Reduction behavior of Assmang and Comilog ore in the SiMn process. *Proceedings of the 10th International Conference on Molten Slags, Fluxes and Salts (MOLTEN 16),* Seattle, Washington, 22–25 May 2016. Wiley. pp. 1285–1292.

Kim P., Larrsen T., Tangstad M., and Kawamoto R. 2017. Empirical activation energies of MnO and $SiO_2$ reduction in SiMn slags between 1500 and 1650°C. *Applications of Process Engineering Principles in Materials Processing, Energy and Environmental Technologies.* Wang, S., Free, M., Alam, S., Zhang, M., and Taylor. P. (eds). The Minerals, Metals & Materials Series. Springer. pp. 475–483.

Kim P. and Tangstad M. 2018a. The effect of sulfur content on the reduction rate in SiMn slags. *Metallurgical. Transactions. B* (in press).

Kim P. and Tangstad M. 2018b. The effect of sulfur for MnO and $SiO_2$ reduction in synthetic SiMn slag. *Metallurgical. Transactions. B* (in press).

Kim P. and Tangstad M. 2018c. Melting behavior of Assmang ore and quartz in the SiMn process. *Metallurgical. Transactions. B* (in press).

Larrsen T. 2016. Reduction of MnO and $SiO_2$ from Comilog-based charges. Internal report: TMT 4500 Materials Technology, Specialization Project, Norwegian University of Science and Technology (NTNU).

Maroufi S., Ciezki G., Jahanshahi S., Shouyi S., and Ostrovski O. 2015. Dissolution of silica in slag in SiMn production. *Infacon XIV - Proceedings of the Fourteenth International Ferro-Alloys Congress,* Kyiv, Ukraine, 1-4 June 2015. pp. 479–487. https://www.pyrometallurgy.co.za/InfaconXIV/479-Maroufi.pdf

Olsen, H. 2016. A theoretical study on the reaction rates in the SiMn production process. Master's thesis, Department of Materials Science and Engineering, Norwegian University of Science and Technology (NTNU).

Olsen, S.E., Tangstad, M. and Lindstad, T. 2007. Production of manganese ferroalloys. Tapir Academic Press, Trondheim, Norway.

Ostrovski. O., Olsen. S.E., Tangstad. M., and Yastreboff. M. 2002. Kinetic modelling of MnO reduction from manganese ore. *Canadian Metallurgical Quarterly,* vol. 41, no. 3. pp. 309–318.

Outotec. Not dated. HSC Chemistry 7. www.hsc-chemistry.com

Skjervheim, T. 1994. Kinetics and mechanisms for transfer of manganese and silicon from molten oxides to liquid manganese metal. PhD thesis, Department of Metallurgy, Norwegian Institute of Technology (NTNU) .

Støylen, S. and Grande, T. 2004. Chemical thermodynamics of materials. Wiley, Chichester, UK.

Subramanyam, D K., Swansiger, A.E., and Avery, H.S. 1990. Austenitic manganese steels. *ASM Handbook Volume 1, Properties and Selection: Irons, Steels, and High-Performance Alloys.* ASM International. Materials Park, OH.

Tomota, Y., Strum, M., and Morris, Jr. J. 1987. The relationship between toughness and microstructure in Fe-high Mn binary alloys. *Metallurgical Transactions* A, vol. 18A. pp. 1073–1081.

Tranell, G., Gaal, S., Lu, D., Tangstad, M., and Safarian, J. 2007. Reduction kinetics of manganese oxide from HCFeMn slags. *Infacon 11, Proceedings of the Eleventh International Ferro-Alloys Congress.* New Delhi, India, 18-21 February 2007. Indian Ferro Alloy Producers Association. pp. 231–240. https://www.pyrometallurgy.co.za/InfaconXI/231-Tranell.pdf ◆


## Erratum - June 2018

It has come to our attention that some text in the Summary and Conclusions and the Acknowledgment in the paper entitled: '**Reduction of Kemi chromite with methane'**, by M. Leikola*, P. Taskinen*, and R.H. Eric*†' was omitted. The paper was published in the SAIMM *Journal* vol. 118, no. 6, pp. 575–580.

The complete wording for paragraph 4 should read as follows:

'Metallization was observed to start immediately after the chromite was exposed to $CH_4$-$H_2$ mixtures, as chromite reduction to metal was observable after only 10 minutes of reduction time. At temperatures of 1300°C and 1350°C, metallization was completed within the duration of the experiments, as only very small amounts of iron and chromium remained in the unreacted zones. Therefore, reduction of Kemi chromite with a $CH_4$-$H_2$ mixture can be regarded as highly efficient compared to reduction with only solid carbon as the reductant. Similar levels of almost complete reduction of chromite spinels by ordinary carbothermic reduction require temperatures over 1500°C. This can be attributed to the high thermodynamic activity of carbon when it is provided by cracking of methane into carbon and hydrogen'.

**Acknowledgements**

The authors are grateful to Tekes and Finland Academy for providing the part-time Finland Distinguished Professor position to R.H. Eric and funds for this research project. The CMEco project and the Technology Industries of Finland Centennial Foundation are acknowledged for their collaboration and support.

The appropriate correction has been made to the copy of the June 2018 *Journal* on the SAIMM website.

SAIMM
THE SOUTHERN AFRICAN INSTITUTE OF MINING AND METALLURGY

# Surface Mining Masterclass 2019

## 4–5 September 2019

Birchwood Hotel & OR Tambo Conference Centre, Johannesburg

## BACKGROUND

As the mining industry is rapidly pursuing Artificial Intelligence and Machine Learning - definitely the right thing to do – there is still a need to keep the miner grounded in leading practices in the field of surface mining. For example, poor drilling or the incorrect selection of the blast hole diameter can lead to poor blasts which impacts on the whole mining process such as highwall stability, fragmentation, loading and hauling, dilution, mining loss and increased comminution costs - just to name a few. Incorrect equipment selection or matching of equipment results in unoptimized cycle times and higher operating costs.

## OBJECTIVES

The objective of the masterclass is to reinforce learning around the surface mining cycle. The mining cycle is an interrelated process whereby drill-blast-load-haul impacts on each other as well as other aspects to surface mining e.g. safety, highwall design and stability, environment and economic sustainability. The symposium's objective is to review specifics aspects of the mining cycle so as to inform the attendee of leading practices in the area of surface mining.

## Preliminary Programme

### Day 1 – 4 September 2019

| | |
|---|---|
| 08:00–09:00 | **Scene Setting** |
| 09:00–10:00 | **Drilling Session 1** |
| 10:00–10:15 | **Mid-Morning Refreshments** |
| 10:15–10:45 | **Drilling Best Practice** |
| 10:45–12:30 | **Blasting** |
| 12:30–13:30 | **Lunch** |
| 13:30– 15:00 | **Equipment Selection** |
| 15:00–15:15 | **Afternoon Refreshments** |
| 15:15–6:00 | **Equipment Costing** |

### Day 2 – 5 September 2019

| | |
|---|---|
| 08:00–10:00 | **Haul Road** |
| | • Design |
| | • Construction |
| | • Maintenance |
| 10:00–10:30 | **Mid-Morning Refreshments** |
| 10:30–11:00 | **Dustaside** |
| 11:00–12:30 | **Geotech** |
| | • Guidelines |
| | • High Wall Stability |
| | • Monitoring |
| 12:30–13:30 | **Lunch** |
| 13:30–14:00 | **Contract Mining** |
| 14:00–15:30 | **Augmentation Reality** |

**SPONSORSHIP**
Sponsorship opportunities are available. Companies wishing to sponsor or exhibit should contact the Conference Coordinator.


**FOR FURTHER INFORMATION CONTACT:**
Camielah Jardine, Head of Conferencing, SAIMM
Tel: (011) 834-1273/7 · Fax: (011) 833-8156 or (011) 838-5923
E-mail: camielah@saimm.co.za · Website: www.saimm.co.za

# Characterization of hot deformation behaviour of Nb-Ti microalloyed high-strength steel

**G-L. Wu[1], Y-J. Zhang[1], and S-W. Wu[1]**

**Affiliation:**
[1]School of Minerals Processing and Bioengineering, Central South University, China.

**Correspondence to:**
Y-J. Zhang

**Email:**
zhangyongji_csu@163.com

**Dates:**
Received: 23 Aug. 2017
Revised: 20 Oct. 2018
Accepted: 14 Nov. 2018
Published: May 2019

**How to cite:**
Zhang, Y-J.
Characterization of hot deformation behaviour of Nb-Ti microalloyed high-strength steel.
The Southern African Insitute of Mining and Metallurgy

DOI ID:
http://dx.doi.org/10.17159/2411-9717/17/380/2019

ORCiD ID:
Y-J. Zhang
https://orchid.org/0000-0002-8216-2091

## Synopsis

**The hot deformation behaviour of Nb-Ti microalloyed high-strength steel was investigated. Hot compression tests were conducted in the temperature range 900 to 1100°C under strain rates of 0.1, 1, and 5 $s^{-1}$. Dynamic recrystallization (DRX) occurs as the main flow softening mechanism at high temperature and low strain rate. The hot deformation activation energy was calculated to be about 404 699 J/mol. The constitutive equation was developed to describe the relationship between peak stress, strain rate, and deformation temperature. The characteristics of DRX at different deformation conditions were extracted from the stress-strain curves using the work hardening parameter. The Cingara-McQueen equation was developed to predict the flow curves up to the peak strain. The processing maps were obtained on the basis of a dynamic materials model. The results predict an instability region in the temperature range 1010 to 1100°C when the strain rate exceeds 0.78 $s^{-1}$.**

**Keywords**
**flow stress; high-strength steel; constitutive model; material constants; processing map.**

## Introduction

The 700 MPa grade HSLA steel is widely used in engineering machinery, automotive beams, carriages, and axle tubes, *etc.* (Pan *et al.*, 2017 ). Generally, such grades contain a moderately high amount of Mn (approx. 1.4% and above), and microalloying elements like Nb, Ti, V, and Mo to impart the desired strength and toughness through solid-solution strengthening, precipitation hardening, and grain refinement dislocation strengthening (Chen and Yu, 2012; Opiela, 2014). However, the production costs can be greatly reduced by replacing part of the Nb, V, or Mo with inexpensive Ti and adopting the compact strip production CSP process (Opiela, 2014; Chen *et al.*, 2015). Furthermore, the microalloying technology coupled with new-generation thermomechanical control processing (NG-TMCP) has proved efficient for achieving the proper balance between strength, toughness, ductility, and formability by means of a suitable combination of chemical composition and thermomechanical treatment parameters (Shukla *et al.*, 2012; Wu, Zhou, and Liu, 2017).

In hot forming processes, the complex microstructural evolutions are often induced by multiplicative hot deformation mechanisms, such as work hardening (WH), dynamic recovery (DRV), and dynamic recrystallization (DRX) (Zhang *et al.*, 2014; Liang *et al.*, 2015). Dynamic softening behaviour during hot processing has generated considerable interest because component properties are influenced significantly by its corresponding microstructural evolution (Wu *et al.*, 2010). During deformation in the DRX process, deformed grains are replaced with substructures and newly formed fine and uniformly distributed grains. This occurs only when a critical strain for the onset of DRX is reached, and at the same time, the minimum rate of energy dissipating is reached (Ferdowsi *et al.*, 2014). DRV occurs at a high strain rate and low temperature, reducing the stored energy greatly and making DRX difficult (Liang *et al.*, 2015). The microstructural changes during DRX are sensitive to the processing parameters, such as strain rate, deformation temperature, and strain (Zhang *et al.*, 2014; Ferdowsi *et al.*, 2014). Therefore, in order to optimize the hot processing parameters, it is important to understand the behaviour of hot deformation *vis-à-vis* control of microstructural evolution.

Constitutive equations are widely used to reveal the relationship between stress and strain at different strain rates or temperatures, providing microstructural information related to the mechanisms of hot deformation. The modelling of the hot flow stress and the prediction of flow curves are employed in rolling and forging processes from the mechanical and metallurgical standpoints (Cabrera *et al.*, 1997; Mirzadeh, Cabrera, and Najafizadeh, 2012). Since DRX is an important metallurgical phenomenon for controlling

microstructural evolution during hot working, the prediction of the critical stress for initiation of DRX is of significant importance in modeling hot working processes. However, the concomitant occurrence of different metallurgical mechanisms during hot working makes it difficult to exactly predict the critical stress for onset of DRX from the true stress–true strain curve. Earlier studies (Poliak and Jonas, 2003; Mirzadeh and Najafizadeh, 2010) showed that the critical conditions for DRX initiation can be obtained by using the relationship between WH rate and stress. Hence predicting peak stress characteristics during hot deformation using appropriate constitutive models is essential in order to understand the microstructural evolution mechanisms.

The dynamic materials model (DMM) was developed for studying the workability parameter, based on principles of continuum mechanics of large plastic flow using the concepts of physical systems modelling and extremum principles of irreversible thermodynamics (Banerjee, Robi, and Srinivasan, 2012). A processing map based on the DMM and consisting of the efficiency map and the instability map is a valuable approach for coupling the processing conditions such as deformation rate and temperature with desired microstructure to optimize the deformation process (Lou *et al.*, 2014). For optimizing hot workability and controlling the microstructure, DRX is a chosen domain. On the one hand, the damage processes are sometimes very efficient in dissipating power for the generation of new surfaces. On the other hand, the safe processes may become less efficient, because power dissipates through the annihilation of dislocations (Banerjee, Robi, and Srinivasan, 2012). In recent investigations, the constitutive equation and processing map have been proposed for steel (Churyumov *et al.*, 2015; Guo *et al.*, 2012), Al-based alloys (Li *et al.*, 2015), Ni-based alloys (Chen *et al.*, 2015), Ti-based alloys (Quan *et al.*, 2015), composite materials (Momeni, Dehghanib, and Poletti, 2013; Rajamuthamilselvan and Ramanathans, 2012) and other materials (Wang *et al.*, 2015).

In order to control the production cost of 700 MPa grade HSLA steel, the composition design and process optimization were investigated. The Mn and Nb contents of the steel were reduced without adding Mo, while the Ti content was increased. A comprehensive understanding of hot deformation characteristics can elucidate the best design of a processing route such as hot rolling or thermomechanical processing. Therefore, the hot deformation behaviour of Nb-Ti HSLA steel was studied in this work. The experimental results have a certain practical significance for the high-temperature deformation of Nb-Ti HSLA steel.

## Experimental

The chemical composition of the investigated steel is shown in Table I. Cylindrical hot compression specimens 12 in mm height and 8 mm in diameter of were machined. In order to minimize the friction between the specimens and die during hot deformation, the flat ends of the specimen were recessed to a depth of 0.1 mm to entrap the lubricant of graphite mixed with machine oil.

*Table I*

**Chemical composition of the experiment material (mass %)**

| C | Si | Mn | P | S | Al | Nb | Ti |
|---|---|---|---|---|---|---|---|
| 0.04 | 0.01 | 0.78 | 0.015 | 0.007 | 0.023 | 0.048 | 0.11 |

The hot compression tests were performed on a Gleeble 3500 thermomechanical simulation machine in the temperature range 900 to 1100°C at 50°C intervals under constant strain rates of 0.1, 1, and 5 $s^{-1}$ up to a true strain of 0.7. Each specimen was heated to 1200°C at a rate of 10°$Cs^{-1}$ and held for 180 seconds, and then cooled to the deformed temperature at a cooling rate of 5°$Cs^{-1}$ and held for 30 seconds before deformation for temperature equalization. After deformation, the specimens were immediately quenched in tap water. Throughout each test, high-purity argon was used as protective gas.

## Results and discussion

### *Flow curves analysis*

The typical true stress–true strain curves of the steel obtained at various deformation temperatures and strain rates are presented in Figure 1. Based on these curves, the flow stress is sensitive to the deformation temperature and strain rate. In the initial stages of deformation, the flow stress increases rapidly until a peak stress, which indicates that work hardening plays a dominant role. After the rapid flow stress increase, the flow stress decreases slowly as the deformation proceeds until a relatively stable stress appears, indicating a dynamic flow softening. DRX begins to play a dominant role when the strain exceeds peak strain. As the strain increases continually, it enters a steady-state region. Finally, the curves show the equilibrium between work hardening and work softening

Before the stress reaches the peak stress, the work hardening and dislocation density increase, which will lead to a critical microstructural condition. Therefore, the flow stress increases up to a maximum value but the rate of increase steadily decreases until the softening mechanism prevails over work hardening (Solhjoo, 2010). The typical form of the DRX flow curve is observed at high temperatures and low strain rates. At high strain rates, deformation decelerates the rate of work softening (Momeni *et al.*, 2012). Other researchers (Ferdowsi *et al.*, 2014; Mirzadeh, Cabrera, and Najafizadeh, 2012) also point out that higher temperatures and lower strain rates promote the softening process by increasing the mobility of grain boundaries and providing a longer time for dislocation annihilation and the occurrence of DRX.

### *Establishment of constitutive equations*

Hot working can be considered as a thermally activated process, and it can be described by strain rate equations. The relationship between flow stress, strain rate, and temperature can be

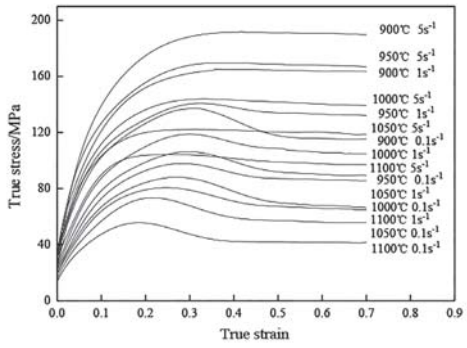


**Figure 1—Stress-strain curves of Nb-Ti microalloyed high-strength steel at different deformation temperatures and strain rates**

expressed by the hyperbolic sine law (Equation [1]), exponential law (Equation [2]), and power law (Equation [3]) (Ferdowsi *et al.*, 2014, Mirzadeh, Cabrera, and Najafizadeh, 2012):

$$\dot{\varepsilon} = A[\sinh(\alpha\sigma_p)]^n \exp(-\frac{Q}{RT}) \quad [1]$$

$$\dot{\varepsilon} = A_2 \exp(\beta\sigma_p) \quad [2]$$

$$\dot{\varepsilon} = A_1\sigma_p^{n_1} \quad [3]$$

where $\dot{\varepsilon}$ is the strain rate ($s^{-1}$), $\sigma_p$ is the peak stress (MPa), and $Q$ is the activation energy for deformation (J/mol). $A$, $A_1$ $A_2$, $\beta$, $\alpha$, $n$, and $n_1$ are material constants, and $R$ is the universal gas constant (8.314 J/mol/K).

Taking natural logarithms of both sides of Equations [2] and [3] at a constant temperature yields:

$$\sigma_p = \frac{1}{\beta}\ln\dot{\varepsilon} - \frac{1}{\beta}\ln A_2 \quad [4]$$

$$\ln\sigma_p = \frac{1}{n_1}\ln\dot{\varepsilon} - \frac{1}{n_1}\ln A_1 \quad [5]$$

Substituting the values of the flow stress and corresponding strain rate into Equations [4] and [5] gives the relationship between the flow stress and strain rate, as shown in Figure 2. The values of $\beta$ and $n_1$ obtained are 0.073 and 8.31 respectively. The value of the constant $\alpha$ is derived by the division of $\beta$ by $n_1$ (Ferdowsi *et al.*,2014; Mirzadeh, Cabrera, and Najafizadeh, 2012), which yields 0.0087.

Taking natural logarithms of both sides of Equation [1] and rearranging, the following equation is derived:

$$\ln[\sinh(\alpha\sigma_p)] = \frac{\ln\dot{\varepsilon}}{n} + \frac{Q}{nRT} - \frac{\ln A}{n} \quad [6]$$

Partially differentiating Equation [6] at constant temperature and strain rate respectively yields:

$$n = \frac{\partial\ln\dot{\varepsilon}}{\partial\ln[\sinh(\alpha\sigma_p)]} \quad [7]$$

$$Q = Rn\frac{\partial\ln[\sinh(\alpha\sigma_p)]}{\partial\frac{1}{T}} \quad [8]$$

The value of $n$ can be derived from the average slope of the lines in $\ln[\sinh(\alpha\sigma_p)]$ *versus* $\ln\dot{\varepsilon}$, shown in Figure 3a. The value of $n$ is calculated to be 6.2. Similarly, the value of $Q$ is determined from the slope of $\ln[\sinh(\alpha\sigma_p)]$ *versus* $1/T$ through averaging the slope values at different strain rates shown in Figure 3b; the Q value is obtained as 404 699 J/mol. The value of lnA can be derived by substituting the obtained values into Equation 6. Thus lnA is calculated to be 37.03.

Substituting all the obtained values into Equation [1], the constitutive equation can be expressed as

$$\dot{\varepsilon} = 1.20\times10^{16}\times [\sinh(0.0087\sigma_p)]^{6.20}\exp(-\frac{404699}{RT}) \quad [9]$$

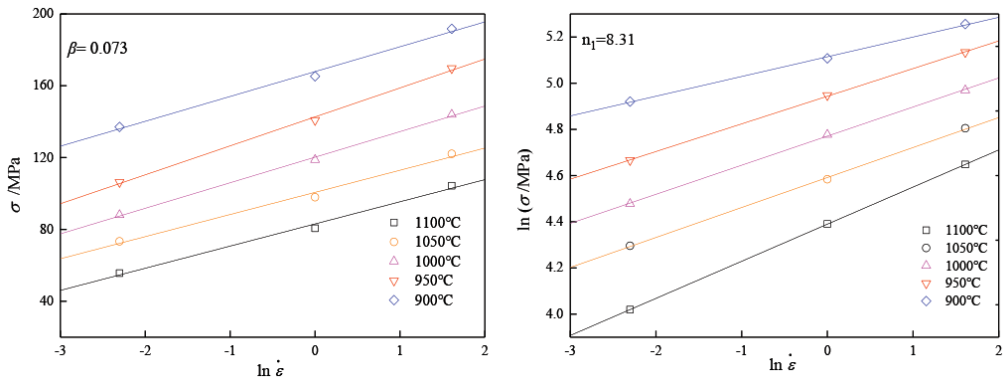


**Figure 2—The relationship between flow stress and strain rate according to (a) the exponential law and (b) the power law**

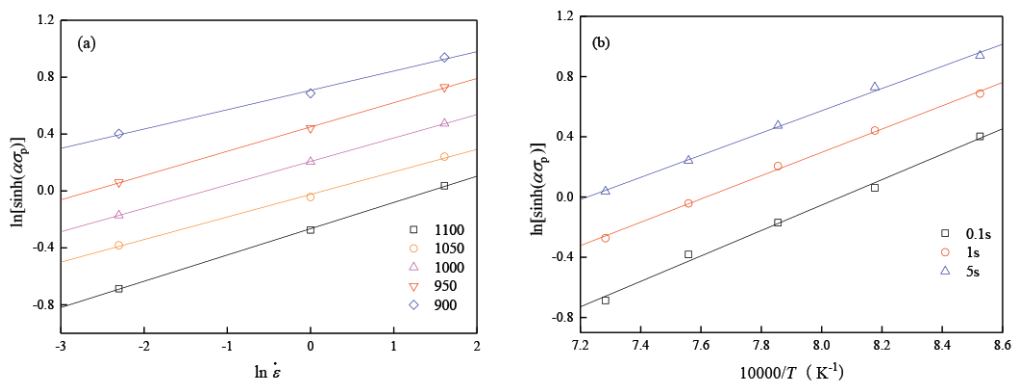


**Figure 3—Linear relationship between (a) $\ln[\sinh(\alpha\sigma_p)]$ and $\ln\dot{\varepsilon}$, (b) $\ln[\sinh(\alpha\sigma_p)]$ and $1/T$ for Nb-Ti microalloyed high-strength steel**

Equation [9] describes the quantitative relationship between peak stress and the parameters, which reflects the influence of deformation temperature and strain rate on the hot deformation flow stress.

### Determination and modelling of critical strain

Generally speaking, DRX can be initiated at a critical level of stress accumulation during hot deformation. However, DRX actually starts at a critical strain ($\varepsilon_c$) which is lower than the strain at peak stress. Only when the strain exceeds $\varepsilon_c$ does DRX occur during hot deformation. Therefore it is important to accurately confirm the value of $\varepsilon_c$ in the research of hot deformation parameters.

On the flow curve, the point at which the strain hardening rate equals zero represents the peak stress ($\sigma_p$) and the inflection point indicates the critical stress ($\sigma_c$) for the initiation of DRX. The critical strains can be determined from the inflection points of the $\ln\theta$-$\varepsilon$ plots, and the critical stresses can be subsequently obtained either from the $\theta$-$\sigma$ plots or from the initial flow curves (Poliak and Jonas, 2003).

$$\ln\theta = A_1\varepsilon^3 + A_2\varepsilon^2 + A_3\varepsilon + A_4 \quad [10]$$

where $A_1$, $A_2$, $A_3$, and $A_4$ are constant parameters for each deformation condition. The second derivative of Equation [10] with respect to $\varepsilon$ can be expressed as:

$$\frac{d^2\ln\theta}{d\varepsilon^2} = 6A_1\varepsilon + 2A_2 \quad [11]$$

At the critical stress for initiation of DRX, the second derivative becomes zero. Therefore

$$\varepsilon_c = -A_2/(3A_1) \quad [12]$$

The peak and critical stresses and strains for temperatures of 900, 950, 1000, 1050, and 1100°C at strain rates of 0.1, 1, and 5 $s^{-1}$ are summarized in Table II, and the data is linear fitted as shown in Figure 4. The normalized critical strain ($\varepsilon_c/\varepsilon_p$) can be presented as:

$$\varepsilon_c/\varepsilon_p = 0.41 \quad [13]$$

### *The relationship between characteristics of DRX and hot deformation parameters*

The critical strain varies with strain rate and deformation temperature. The relationship can be described by the Sellars model (Yang *et al.*, 2014):

$$\varepsilon = AZ^n \quad [14]$$

where $A$ and $n$ are material constants, $Z$ is the Zener-Hollomon parameter, and $Q$ is the deformation activation energy (J/mol). Taking the natural logarithm on both sides of Equation [14]:

$$\ln\varepsilon = \ln A + n\ln Z \quad [16]$$

The relationship between $\ln\varepsilon$ and $\ln Z$ is depicted in Figure 5.

Figure 5 exhibits the linear regression results of critical and peak strain versus the Zener-Hollomon parameter. It can be seen that the critical characteristics of DRX increase with increasing Z parameter. The relationship between these parameters and deformation conditions is expressed by a power law. According to the linear regression results, the following relationships hold for the investigated steel:

$$\varepsilon_c = 0.0064Z^{0.077} \quad [17]$$

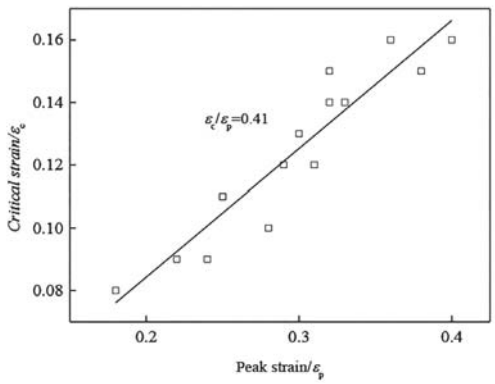


Figure 4—Critical strain *versus* peak strain

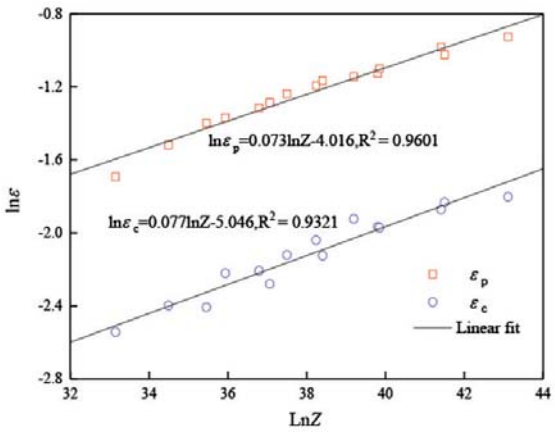


Figure 5—The relationship between $\varepsilon_c$, $\varepsilon_p$, and the *Z* parameter

*Table II*

**Critical strain and peak strain at different deformation conditions**

| Temperature (°C) | 0.1 $s^{-1}$ | | | 1 $s^{-1}$ | | | 5 $s^{-1}$ | | |
|---|---|---|---|---|---|---|---|---|---|
| | $\varepsilon_c$ | $\varepsilon_p$ | $\varepsilon_c/\varepsilon_p$ | $\varepsilon_c$ | $\varepsilon_p$ | $\varepsilon_c/\varepsilon_p$ | $\varepsilon_c$ | $\varepsilon_p$ | $\varepsilon_c/\varepsilon_p$ |
| 900 | 0.15 | 0.32 | 0.45 | 0.16 | 0.36 | 0.44 | 0.16 | 0.40 | 0.42 |
| 950 | 0.12 | 0.29 | 0.41 | 0.14 | 0.32 | 0.43 | 0.15 | 0.38 | 0.41 |
| 1000 | 0.11 | 0.25 | 0.43 | 0.13 | 0.30 | 0.43 | 0.14 | 0.33 | 0.42 |
| 1050 | 0.09 | 0.22 | 0.41 | 0.11 | 0.25 | 0.42 | 0.12 | 0.31 | 0.38 |
| 1100 | 0.08 | 0.18 | 0.43 | 0.09 | 0.24 | 0.38 | 0.10 | 0.28 | 0.37 |

$$\varepsilon_p = 0.018Z^{0.073} \quad [18]$$

The quantitative relationship between these critical conditions of dynamic recrystallization and Zener-Hollomon parameter indicates that the hot deformation behaviour is a thermally activated process.

### Flow curve modelling up to peak stress

The flow curve up to peak stress is the region of interest for determination of critical conditions for the initiation of DRX by means of work hardening. Thus, it is becoming increasingly important to be able to calculate the flow stress for specific values of strain, strain rate, and temperature. To model the flow curve up to the peak stress, the flow curve model proposed by Cingara and McQueen can be used (Momeni *et al.*, 2012):

$$\frac{\sigma}{\sigma_p} = [(\frac{\varepsilon}{\varepsilon_p})\exp(1-\frac{\varepsilon}{\varepsilon_p})]^C \quad [19]$$

where σ is stress (MPa), $\sigma_p$ is the peak stress (MPa), ε is strain, $\varepsilon_p$ is the peak strain, and *C* is the material constant.

Taking the natural logarithm of this equation yields the following expression:

$$\ln\frac{\sigma}{\sigma_p} = C[1-\frac{\varepsilon}{\varepsilon_p}+\ln\frac{\varepsilon}{\varepsilon_p}] \quad [20]$$

The experimental data on a logarithmic-scale plot can be used to determine the value of *C*. The plot of $\ln\frac{\sigma}{\sigma_p}$ *vs.* $1-\frac{\varepsilon}{\varepsilon_p}+\ln\frac{\varepsilon}{\varepsilon_p}$ at a strain rate of 5 $s^{-1}$ is shown in Figure 6, and the average value of *C* at all deformation conditions was calculated to be 0.519.

By using the average value of *C*, the predicted flow curves up to the peak strain are shown in Figure 7, which indicate that the models give a better approximation of the flow curve up to the peak.

### Processing map

The processing maps not only describes the energy consumption by microstructure evolution during hot deformation, but also visually shows the instability flow regions that should be avoided during the forming process.

The power dissipation through microstructural evolution is represented by a dimensionless efficiency index η as a function of strain rate sensitivity *m*. The efficiency index η can be defined as (Liang *et al.*, 2015; Lou *et al.*, 2014):

$$\eta = \frac{2m}{m+1} \quad [21]$$

where *m* is the strain rate sensitivity exponent, which when the deformation temperature is fixed is a function of the strain rate. The variation of η with deformation temperature and strain rate constitutes a power dissipation map, which represents the power dissipated by the material through microstructural evolution.

The instability criterion parameter ξ(ε̇) is defined as (Liang *et al.*, 2015; Lou *et al.*, 2014)

$$\xi(\dot{\varepsilon}) = \frac{\partial n(\frac{m}{m+1})}{\partial n\dot{\varepsilon}} + m \quad [22]$$

The variation of the instability parameter ξ(ε̇) with ε̇ and *T* at constant strain constitutes an instability map, and flow instability is estimated to occur when ξ(ε̇) becomes negative.

Figure 8 shows the typical processing maps of Nb-Ti microalloyed high-strength steel during hot working at strains of 0.4 and 0.6. The information obtained from the processing map can be used to guide industrial production. First, the temperature and strain rate corresponding to high η represent the optimum working area for the investigated steel, because a high η means that the evolution of microstructure consumes a greater proportion of energy. Secondly, the deformation conditions for

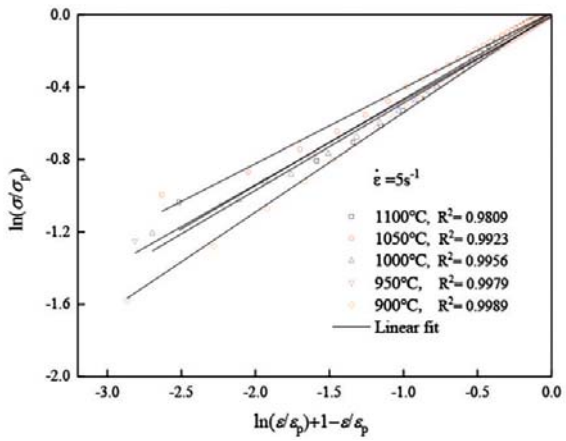


**Figure 6—Regression analysis of experimental data at a strain rate of 5 $s^{-1}$ according to the Cingara-McQueen equation**

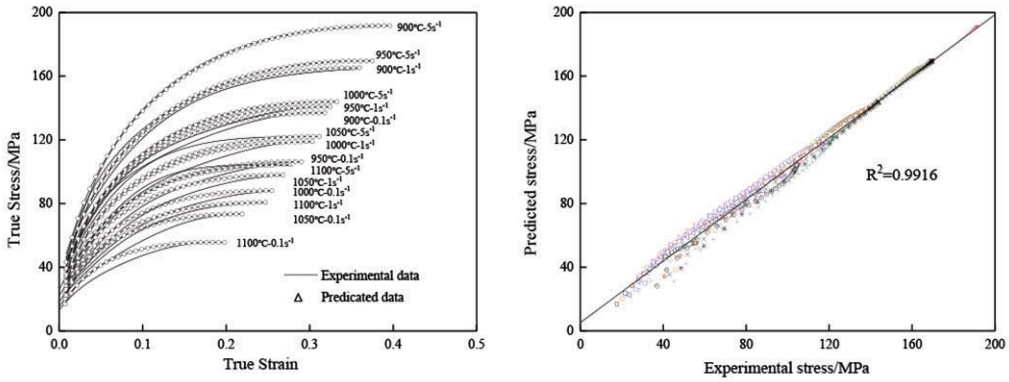


**Figure 7—Prediction of flow curves at different deformation conditions**

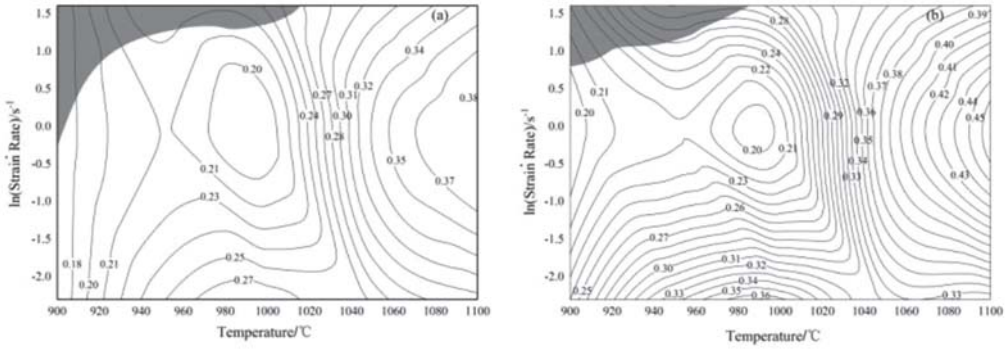


**Figure 8—The processing map at strains of (a) 0.4 and (b) 0.6, showing regions of instability**

avoiding flow instability can be obtained from the processing map. As shown in Figure 8, the flow instability region appears at deformation temperature between 1010 and 1100°C when the strain rate exceeds 0.78 $s^{-1}$.

## Conclusions

(1) The flow stress is strongly dependent on deformation temperature and strain rate. DRX occurs at a high temperature and low strain rate, which is found to be the main flow softening mechanism in almost all deformation conditions.

(2) The calculated deformation activation energy of the Nb-Ti HSLA steel is about 404 699 J/mol. The constitutive equation is derived as:

$$\dot{\varepsilon} = 1.20\times10^{16} \times [\sinh(0.0087\sigma_p)]^{6.20} \exp(-\frac{404699}{RT}) \quad [23]$$

(3) The characteristics of DRX at different deformation conditions are extracted from the stress-strain curves. Using the work hardening parameter, the value of $\varepsilon_c/\varepsilon_p$ is found to be 0.41. The critical and peak strain can be expressed as $\varepsilon_c = 0.0064Z^{0.077}$, $\varepsilon_p = 0.018Z^{0.073}$. The Cingara-MuQueen equation can model the flow stress accurately up to peak stress for the investigated steel.

(4) Processing map for strains of 0.4 and 0.6 were constructed, and the results show that an instability region exists at a temperature range between 1010 and 1100°C when the strain rate exceeds 0.78 $s^{-1}$.

## References


Banerjee, S., Robi, P.S., and Srinivasan, A. 2012. Deformation processing maps for control of microstructure in Al-Cu-Mg alloys microalloyed with Sn. *Metallurgical and Materials Transactions A*, vol. 43, no.10. pp. 3834–3849.

Cabrera, J.M., Omar, A.A., Prado, J.M., and Jonas, J.J. 1997. Modeling the flow behavior of a medium carbon microalloyed steel under hot working conditions. *Metallurgical and Materials Transactions A*, vol. 28, no. 11. pp. 2233–2244.

Chen, B.H. and Yu, H. 2012. Hot ductility behavior of V-N and V-Nb microalloyed steels. *International Journal of Minerals, Metallurgy and Materials*, vol. 19, no. 6. pp. 525–529.

Chen, X.M., Lin, Y.C., Chen, M.S., Li, H.B., Wen, D.X., Zhang, J.L., and He, M. 2015. Microstructural evolution of a nickel-based superalloy during hot deformation. *Materials and Design*, vol. 77. pp. 41–49.

Churyumov, A.Y., Khomutov, M.G., Solonin, A.N., Pozdniakov, A. V., Churyumova, T.A., and Minyaylo, B.F. 2015. Hot deformation behaviour and fracture of 10CrMoWNb ferritic-martensitic steel. *Materials and Design*, vol. 74, no. 5. pp. 44–54.

Ferdowsi, M.R.G., Nakhaie, D., Benhangi, P.H., and Ebrahimi, G.R. 2014. Modeling the high temperature flow behavior and dynamic recrystallization kinetics of a medium carbon microalloyed steel. *Journal of Materials Engineering and Performance*, vol. 23, no. 3. pp. 1077–1087.

Guo, B.F., Ji, H.P., Liu, X.G., Gao, L., Dong, R.M., Jin, M., and Zhang, Q.H. 2012. Research on flow stress during hot deformation process and processing map for 316LN austenitic stainless steel. *Journal of Materials Engineering and Performance*, vol. 21, no. 7. pp.1455–1461.

Liang, H.Q., Nan, Y., Ning, Y.Q., Li, H., Zhang, J.L., Shi, Z.F., and Guo, H.Z. 2015. Correlation between strain-rate sensitivity and dynamic softening behavior during hot processing. *Journal of Alloys and Compounds*, vol. 632. pp. 478–485.

Lou, Y., Chen, H., Ke, C.X., and Long, M. 2014. Hot tensile deformation characteristics and processing map of extruded AZ80 Mg alloys. *Journal of Materials Engineering and Performance*, vol. 23, no.5. pp. 1904–1914.

Li, L., Li, H.Z, Liang, X.P., Huang, L., and Hong, T. 2015. Flow stress behavior of high-purity Al-Cu-Mg alloy and microstructure evolution. *Journal of Central South University*, vol. 22, no. 3. pp. 815–820.

Mirzadeh, H. and Najafizadeh, A. 2010. Prediction of the critical conditions for initiation of dynamic recrystallization. *Materials and Design*, vol. 31, no. 3. pp. 1174–1179.

Mirzadeh, H., Cabrera, J.M., and Najafizadeh, A. 2012. Modeling and prediction of hot deformation flow curves. *Metallurgical and Materials Transactions A*, vol. 43, no. 1. pp. 108–123.

Momeni, A., Dehghani, K., Heidari, M., and Vaseghi, M. 2012. Modeling the flow curve of AISI 410 martensitic stainless steel. *Journal of Materials Engineering and Performance*, vol. 21, no. 11. pp. 2238–2243.

Momeni, A., Dehghanib, K., and Poletti, M.C. 2013. Law of mixture used to model the flow behavior of a duplex stainless steel at high temperatures. *Materials Chemistry and Physics*, vol. 139. no. 2-3. pp. 747–755.

Opiela, M. 2014. Effect of thermomechanical processing on the microstructure and mechanical properties of Nb-Ti-V microalloyed steel. *Journal of Materials Engineering and Performance*, vol. 23, no. 9. pp. 3379–3388.

Pan, H., Wang, Z.D., Zhou, N., Hui, Y.J., Wu, K.M., and Deng, X.T. 2017. Research on the performance uniformity of 700 MPa grade Ti-microalloying high strength steel. *Steel Rolling*, vol. 34, no. 2. pp.7–13.

Poliak, E.I. and Jonas, J.J. 2003. Initiation of dynamic recrystallization in constant strain rate hot deformation. *ISIJ International*, vol. 43, no. 5. pp. 684–691.

Quan, G.Z., Lv, W.Q., Liang, J.T., Pu, S.A., Luo, G.C., and Liu, Q. 2015. Evaluation of the hot workability corresponding to complex deformation mechanism evolution for Ti–10V–2Fe–3Al alloy in a wide condition range. *Journal of Materials Processing Technology*, vol. 221. pp. 66–79.

Rajamuthamilselvan, M. and Ramanathan, S. 2012. Development of processing map for 7075Al/20% SiCp composite. *Journal of Materials Engineering and Performance*, vol. 21, no. 2 pp. 191–196.

Solhjoo, S. 2010. Determination of critical strain for initiation of dynamic recrystallization. *Materials and Design*, vol. 31, no. 3. pp. 1360–1364.

Shukla, R., Das, S.K., Ravikumar, B., Ghosh, S.K., Kundu, S., and Chatterjee, S. 2012. An ultra-low carbon, thermomechanically controlled processed microalloyed steel: microstructure and mechanical properties. *Metallurgical and Materials Transactions A*, vol. 43, no. 12. pp. 4835–4845.

Wu, L.Z., Li, X.S., Chen, J., Zhang, H.B., and Cui, Z.S. 2010. Dynamic recrystallization behavior and microstructural evolution in SPHC steel. *Journal of Shanghai Jiaotong University (Science)*, vol. 15, no. 3. pp. 301–306.

Wang, M.H., Huang, L., Chen, M.L., and Wang, Y.L. 2015. Processing map and hot working mechanisms of Cu-Ag alloy in hot compression process. *Journal of Central South University*, vol. 22, no. 3. pp. 821–828.

Wu, G.L., Zhou, C.Y., and Liu, X.B. 2017. Static recrystallization behavior of Ti-Nb microalloyed high strength steel. *Journal of the Southern African Institute of Mining and Metallurgy*, vol. 117, no. 5. pp. 451–456.

Yang, Z.Q., Liu, Y., Tian, B.H., and Zhang, Y. 2014. Model of critical strain for dynamic recrystallization in 10%TiC/Cu–$Al_2O_3$ composite. *Journal of Central South University*, vol. 21, no. 11. pp. 4059–4065.

Zhang, W.F., Sha, W., Yan, W., Wang, W., Shan, Y.J., and Ke, Y. 2014. Constitutive modeling, microstructure evolution, and processing map for a nitride-strengthened heat-resistant steel. *Journal of Materials Engineering and Performance*, vol. 23, no. 8. pp. 3042–3050. ◆


# Performance optimization of an industrial gamma activation assay system for analysing gold and rare metal ores

**A. Sokolov[1], V. Gostilo[1], M. Demsky[2], and E. Hasikova[1]**

**Affiliation:**
[1]Baltic Scientific Instruments, Latvia.
[2]CORAD, Russia.

**Correspondence to:**
A. Sokolov

**Email:**
a.sokolov@bsi.lv

**Dates:**
Received: 26 Jun. 2018
Revised: 30 Jan. 2019
Accepted: 15 Feb. 2019
Published: May 2019

**How to cite:**
Sokolov, A., Gostilo, V., Demsky, M., and Hasikova, E. Performance optimization of an industrial gamma activation assay system for analysing gold and rare metal ores.
The Southern African Insitute of Mining and Metallurgy

DOI ID:
http://dx.doi.org/10.17159/2411-9717/194/2019

ORCiD ID:
V. Gostilo
https://orchid.org/0000-0003-0411-1309

## Synopsis

**Previously, we upgraded and implemented two gamma activation assay (GAA) systems designed to analyse the gold content in raw ores at Zarafshan laboratory, Uzbekistan, and achieved a detection limit of less than 0.05 g/t under actual industrial conditions. Having started to design a fully modern, industrial GAA system for mining companies, this paper analyses the advantages, disadvantages, and special features of all major system components that can influence the sensitivity and accuracy of the analysis. The results of a study to optimize the detector geometry and sample size are presented and the performances of the linear electron accelerator, detector array, and sample transportation system of a modern, industrial GAA system for analysing gold, silver, and rare earth elements are considered.**

**Keywords**
**gamma activation analysis; gold ore; mining.**

## Introduction

Gamma activation analysis (GAA) has considerable potential as a future replacement for traditional fire assay analysis in gold mining (Hoffman, Clark, and Yeager, 1998; Morse, 1977; Bourmistenko, 1986, 1981; Sammut, 2016; Tickner *et al.*, 2017). The essence of GAA is to irradiate ore samples with high-energy gamma quanta generated by an electron linear accelerator (LINAC) and then to use a gamma spectrometer to detect the induced activity of the excited gold nuclei. The advantages of this method are discussed in detail elsewhere (Hoffman, Clark, and Yeager, 1998; Morse, 1977; Bourmistenko, 1986, 1981; Sammut, 2016; Tickner *et al.*, 2017), where it is shown that GAA is uniquely suited to analysing ore samples when mining for gold, other precious metals, and accompanying elements.

These advantages were realized in three industrial GAA laboratories that were commissioned in Zarafshan, Uzbekistan in 1977, in Magadan, Russia in 1979, and in Batagay, Russia in 1986 (Bourmistenko, 1986; Nii Tekhnicheskoy Fiziki I Avtomatiki, n.d). In 1989, a fourth industrial GAA laboratory was commissioned at a gold mine in Tommot, Russia. However, the project was subsequently halted due to economic reasons (Moshkov and Tjamisov, 2017). Currently, only the laboratory of the Muruntau mine in Zarafshan, Uzbekistan is in operation. The gamma activation method for gold determination is widely applicable at this mine owing to its high productivity and low cost of analysis. An outstanding aspect is the performance of more than one million analyses per year.

We have previously reported the progress in developing the GAA method for industrial gold analysis at this mine (Sokolov *et al.*, 2018a, 2017). It involves a precision two-channel gamma spectrometer based on high-purity germanium (HPGe) three-crystal detector assemblies, providing highly efficient gamma radiation detection and high-energy resolution. The system for packaging and transporting the sample containers from the loading drum, via the irradiation and detection zones to the output drum, was not altered.

Despite the fact that in both assay systems the components from the previous system manufactured in the 1970s were used, they could be updated and modified to achieve appropriate detection limits for gold. The first commissioned gamma activation assay system provided a detection limit of 0.08–0.20 g/t gold with a 15-second measurement time, depending on the barium and hafnium contents (Sokolov *et al.*, 2018a). With the same measurement time, the second assay system had a detection limit of less than 0.05 g/t gold (Sokolov *et al.*, 2017. Furthermore, there is the possibility to analyse silver and rare earth elements too (Sokolov *et al.*, 2018a, 2017). Nevertheless, the error in gold determination between the two

GAA systems has remained constant at 10% (Bourmistenko, 1986). This is defined by the accuracy of the provided calibration samples and the performance of the obsolescent parts that we had to use without improvement.

Gold and rare earth elements are now mined on every continent. This has led to growing interest from mining enterprises in using GAA, as well as alternative methods (Robertson and Feather, 2004)to determine the elemental concentrations in those ores. Optimizing the GAA method further will involve developing a completely modern gamma activation assay system that incorporates up-to-date technological solutions, advanced methodical support, and contemporary computer engineering. All together, this should provide a GAA that is highly sensitive, accurate, and with increased productively.

All factors that limit both the sensitivity and accuracy of the method for determining the gold concentration in ores have been published in detail in previous studies (Tickner *et al.*, 2017). A three-standard-deviations detection limit between 60–75 parts per billion (ppb) has been demonstrated under laboratory conditions, with an accuracy of around 2.5% relative to a gold concentration of 3 ppm (parts per million).

Our present work involves analysing the performance of the modern components of the gamma activation system. Our aim is to identify the best design and technological solutions to optimize the process of analysing gold, other precious metals, and rare earth elements. As shown previously (Sokolov *et al.*, 2018b), the obvious disadvantage of GAA is the high initial financial investment; commissioning a GAA laboratory (including construction) will cost between US$4–5 million. Although that cost should be recouped relatively quickly (1–2 years) (Sokolov *et al.*, 2018b), considerable attention should be given to the economic aspects of developing and designing a GAA laboratory to provide the best technical performance for a reasonable financial investment. From a practical perspective, our goal is to develop and implement a third industrial GAA system for gold and accompanying elements for the mining industry based on modern elements, technological methods, and methodological concepts.

## LINAC performance optimization

Analysing the characteristics of commercially available LINACs indicates that several companies are producing models that meet the energy and power requirements of GAA; that is MEVEX (Canada), L3 Communications (USA), Wuxi El Pont (China), Nuctech (China), and CORAD (Russia) (Mevex, n.d.; L3 Communications, n.d.; Wuxi El Pont, n.d.; Nuctech, n.d.; Corad, n.d.). However, the technical specifications of commercially available LINACs do not contain sufficient information about the temporal stabilities of the energy spectrum and beam power. These stabilities are very important in providing high accuracy in elemental analysis (Tickner *et al.*, 2017).

For our GAA system, we provided a LINAC that, in our opinion, meets all the application requirements. It generates an electron beam with a maximum power of 10 kW and electron energy of 7–9 MeV, with the option of adjusting the electron energy in that range. The ability to adjust the electron energy during gold ore analysis affords ample possibility to optimize the sample irradiation conditions in order to suppress the lines of the associated elements that can overlap with gold in the GAA spectrum. This, in turn, affords higher accuracy at a lower detection limit.

To provide high operational stability, an additional circuit for electron beam stabilization was added to decrease the intensity spread to 2%. Constant inspection of the beam current and electron energy was introduced by displaying the parameters in the operator's software window. The safety and control of all the LINAC components were improved and the actual power consumed was decreased to 70 kW.

## System for transporting samples

The ground ore samples for analysis should be packed in transportation containers and then brought to the GAA system. The sample will then be subjected to the gamma radiation and measurement process before being stocked. For a highly productive GAA system, the technological process should be automated. That will require an automatic system for sample/container transportation.

At the GAA laboratory at the Muruntau mine, the ground ore samples are packed in plastic cylinders (100 mm diameter by 40 mm height; sample weight approx. 500 g) and placed in a loading drum which is loaded automatically into the system's transportation channel (Bourmistenko, 1986). The filled containers are moved on a transportation tray from the loading point to the irradiation site and then by gravity to the measurement zone. After leaving the transportation tray, the containers are loaded automatically into another drum.

The movement of the sample containers in the transportation channel is adjusted with a system of dampers that close or open the further movement in the channel. Such a simple gravity transportation system makes the entire system highly efficient. However, a three-storey building had to be constructed to separate the packaging and loading zones (third floor), irradiation zone (second floor), and the measurement and storage zones (first floor), which certainly increased the project cost.

The GAA laboratories constructed at mines in Magadan (1979) and Batagay (1986) in Russia rely on a single-storey variant, using pneumatic posts. Moreover, by using a linear transport channel, Batagay mine has implemented multiple irradiation of the samples to increase sensitivity. A horizontal sample-transportation system was used also by Tickner *et al.* (2017). To date, feeding the samples pneumatically in a horizontal single-storey transportation system has proved sufficiently simple and safe in a GAA system.

To transport samples in the current project, a linear motion system was selected. These highly automated systems appeared in industry over the past few decades. They represent a complex solution incorporating hardware and software for tasks that involve fast and precise motion and positioning (THK, n.d.; Thomson, n.d.; Bosch Rexroth, n.d.). Linear motion systems available in the market have a wide range of characteristics. For example, the step length can be specified from centimetres to tens of metres and the payload from grams to tons. The maximum carriage rate is 10 m/s, which in the GAA system minimizes the sample cooling time to between 1–2 seconds. A positioning accuracy of up to 10 µm is acceptable if requested, but this has no practical impact on the measurement accuracy due to the precise mutual positioning of the detectors and the sample container. Another advantage of linear motion systems is the durability of the equipment in operation under the high loads associated with industrial applications, something that is very important for continuous operation of the GAA system. Additionally, it is easy to incorporate the linear motion systems into the automated sample measurement process.

### Protective bunker

In the GAA system, the LINAC and irradiation area should be isolated from other premises by a concrete layer of biological shielding. Using a horizontal system to transport samples with linear motion systems allows us to construct a rather simple single-storey protective bunker, thereby reducing the construction cost considerably. The entire GAA system can be accommodated in this relatively small and inexpensive concrete building (see Figure 1). The protective bunker (height approx. 2.3 m) containing the 3 MeV LINAC is built directly in an existing production hangar. The bunker for the LINAC with energy of 8 MeV and a power of 10 kW will have a footprint of 7.5 × 8 m and a height between 3–4 m, depending on the materials used.

### Detection system

The characteristics of the detection system largely determine both the minimum detectable concentration and the accuracy for the measured elements. The background count rate $B(\varepsilon)$, together with other basic parameters of the detector (*i.e.* the relative registration efficiency $E(\varepsilon)$ and the energy resolution $R(\varepsilon)$), forms a complex spectrometer parameter called the figure of merit (FoM) (Gilmore, 2008). This parameter is inversely proportional to the minimum detectable isomeric concentration at a given energy and is expressed as

$$FoM = \frac{E(\varepsilon)}{R(\varepsilon)} \times \sqrt{\frac{t}{B(\varepsilon)}} \quad [1]$$

where $t$ is the live measurement time.

Equation [1] shows that the better the detector resolution and the higher the registration efficiency, the lower the minimum detectable concentration. In the spectrometer set for GAA, these two detector parameters, being in contradiction, should be optimized. The need for background reduction is especially crucial in scientific experiments (*e.g.* double beta decay, searching for dark matter). However, in GAA, reducing the background level in the registered spectrum decreases the minimum detectable concentration of elements and makes the measurements more accurate. The background level in the registered GAA spectrum could also be lowered by the obligatory use of passive and (sometimes) active detector shielding; however, the technical and commercial expediency of such use should be evaluated in each case.

As specified by Equation [1], the detector efficiency and energy resolution have a significant effect on the detection limit and the measurement accuracy. Over the past decades, the most precise instruments for detecting nuclear radiation in nuclear and elementary particle physics have been PGe spectrometers (Gilmore, 2008). The technology for manufacturing HPGe single- and multi-crystal detectors is mature and highly flexible, enabling detectors to be manufactured with specific energy resolutions and various registration efficiencies, thereby offering a range of registered energies (Baltic Scientific Instruments, n.d. (a)). In any configuration of HPGe detector assemblies, the crystal sizes and quantity should be defined by the optimum compromise between (i) the energy resolution, (ii) the registration sum efficiency, and (iii) the instrumental background level. This is why the design and sizes of the detector multi-crystal assemblies in GAA spectrometers should always be optimized under the sizes and shape of the sample container.

### Simulation of mutual geometry of detector and sample

In previous work (Sokolov *et al.*, (2018a, 2017) we analysed 500-g gold ore samples that were packed in plastic cylinders (100 mm diameter × 40 mm height). The mutual geometry of the detectors and the plastic sample container is simulated in Figure 2a. To provide the maximum registration efficiency of the gamma radiation from the sample, a two-channel spectrometer was used and each of the two detector assemblies comprised three HPGe crystals of size 80 mm diameter × 30 mm height. Despite the effective overlapping of the sample area by the two three-crystal assemblies (six crystals from both sides of the container; the total sensitive area is 6 × 21.90 cm² = 131.4 cm²), the redundant sizes of the crystals themselves provides the surplus capacity of the detector assembly and therefore the energy resolution is poorer than what could ideally be achieved.

To optimize the mutual geometry of the samples and detector assemblies in the developed GAA system, we use rectangular plastic containers of size 170 × 90 × 40 mm (Figure 2b). This enables us to increase the mass of the sample from 500 g to 1000 g. That provides a larger flux of exciting gamma radiation and in turn makes the analysis more representative. Besides, to overlap the area of that sample, it is more effective to use the

Figure 1—Protective bunker with a height of 2.3 m for the LINAC with an energy of 3 MeV

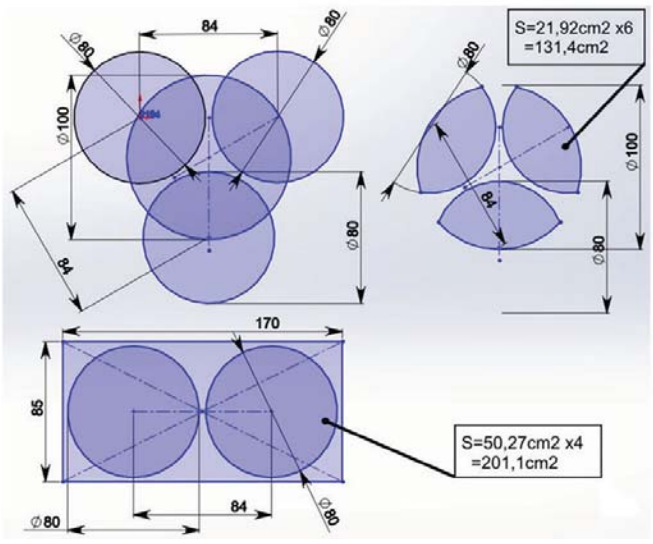


Figure 2—Simulation of mutual geometry of sample and detector assemblies

two-crystal detector assembly with crystals of the former size. The total sensitive area from both sides is now 4 × 50.265 $cm^2$ = 201.1 $cm^2$, *i.e.* an increase of 1.5 times. Using a two-crystal detector assembly instead of a three-crystal has reduced the price of the registration system by about 30%.

### Ore analysis technique development in laboratory conditions

Experience gained in manufacturing and applying online XRF conveyor-belt analysers for the mining industry (Baltic Scientific Instruments, n.d. (b)) confirms the need to develop a specific technique that can provide low detection limits with high accuracy for analysis in industrial conditions. To develop the method for analysing different elements in various ores using GAA, we conducted research to simulate analysis conditions for ores from different mines. The research is based on an accelerator with energy of 8 MeV and power of 2 kW. Ore samples were crushed and packed manually in the laboratory in rectangular containers 170 × 80 × 35 mm in size. The operator fixes the sample manually on the carriage of the linear motion system against the accelerator target. The operator exits the radiation zone and starts the accelerator beam for the specified irradiation time (10–20 seconds). Immediately after irradiation, the sample is relocated to the detectors to register the isomeric radiation. Then, if required, the sample can again be moved to the accelerator target for multiple irradiations. The distance between the radiation and detection zones is 4 m. After the required number of irradiation measurement cycles, the operator replaces the sample manually. The time required for replacement is 5 minutes, and the total time to analyse one sample is 10 minutes. That means that during an eight-hour working shift, 48 samples can be measured.

The gold calibration samples (Sokolov *et al.*, (2018a, 2017) were prepared in the 1970s with a certified accuracy of approximately 10%. This defined the accuracy of gold analysis under industrial conditions. Currently, calibration samples with a certified accuracy of 1% in the ppm concentration range can be prepared (Fluxana, n.d.; Scott Automation., n.d.). These calibration standards improved the accuracy considerably, and in turn the total accuracy of the developed GAA system. The measurement accuracy was evaluated on a calibration sample with a certified gold concentration of 1.08 ppm and a certified accuracy of 1% (Scott Automation, n.d.), measuring 12 spectra for that sample. The irradiation time was 10 seconds, the measurement time 15 seconds, and the time between the end of irradiation and the beginning of measurement 2.7 seconds. The region of the spectrum containing the gold line at 279 keV is shown in Figure. 3. All measurements were made using local GAA software, details of which are presented in Sokolov *et al.* (2018b). All calculations were performed using the measured spectral parameters in accordance to methodology (Iskroline, n.d.). The calculations provided a minimum detectable concentration of 42 ppb and an accuracy of measurement of 3.9% for 1.08 ppm gold concentration.

### Conclusions

The results obtained using industrial samples show that GAA systems can provide a detection limit of less than 0.05 g/t gold with an analysis accuracy of approximately 10% and a maximum production rate of one million analyses per year (Sokolov *et al.*, 2018a, 2017). The investigation of various modern technological solutions and the characteristics of various components of a GAA system presented here demonstrates that the sensitivity and accuracy of the GAA method could be improved further while maintaining high productivity. Errors introduced by the excitation, transportation, and registration systems, as well as the accuracy of the certified reference material, provide an overall GAA accuracy of 3.9%. By using a linear motion system and modern software, a fully automated GAA system for analysing precious metals and rare-earth elements was developed. The return on investment is within 1–2 years (Sokolov *et al.*, (2018b).

### Acknowledgements

The authors are extremely grateful to V. A. Moshkov (Atomredmetzoloto) for discussions regarding the practicalities of implementing the GAA method for ores in mining and other useful practical information.

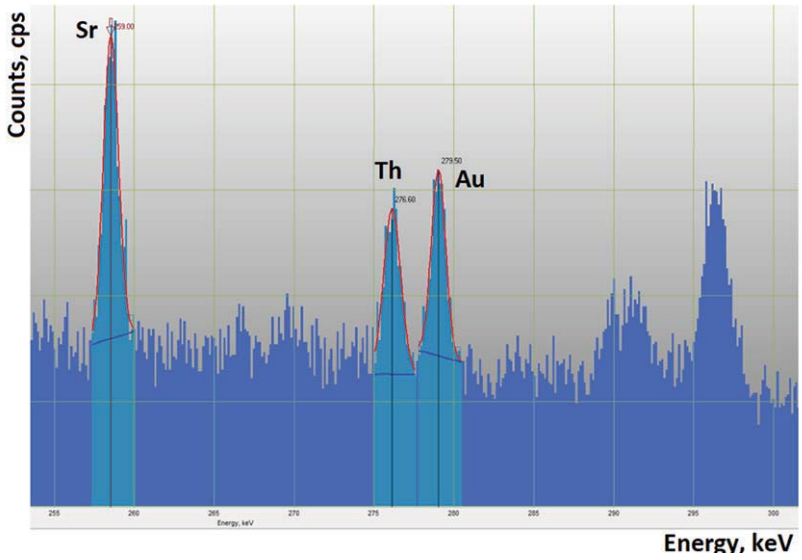


**Figure 3—Spectral region containing gold line at 279 keV. The gold concentration is 1.08 ppm**

## References


Baltic Scientific Instruments. Not dated (a). http://bsi.lv/en/products/hpge-detectors-spectrometers/ [accessed 25 June 2018].

Baltic Scientific Instruments. Not dated (b). http://bsi.lv/en/products/xrf-analyzers/-line-xrf-conveyor-analyzer-con-x/ [accessed 25 June 2018].

Bosch Rexroth. Not dated. https://www.boschrexroth.com [accessed 25 June 2018].

Bourmistenko, Y.N. 1981. Gamma activation installation for fast determination of gold and its accompanying elements in ore sample. *Izotopenpraxis,* vol. 17, no. 6. pp.2 41-243.

Bourmistenko, Y.N. 1986. Photonuclear analysis of materials composition. Energoatomizdat, Moscow. 200 pp. [in Russian].

Corad Ltd. Not dated. Linear electron accelerator (LINAC) for radiation sterilization, food irradiation, shrinkable tubes irradiation and other radiation processing. http://www.corad.pro/linacs.aspx [accessed 25 June 2018].

Fluxana GmbH. Not dated. https://www.fluxana.com/ [accessed 25 June 2018].

Gilmore, G. 2008. Practical Gamma-Ray Spectrometry. 2nd edition. Wiley.

Hoffman, E.L., Clark, J.R., and Yeager, J.R. 1998. Gold analysis - fire assaying and alternative methods. *Exploration and Mining Geology*, vol. 7, no 1-2. pp.155–160.

Iskroline Inc. Not dated. https://iskroline.com/ [accessed 25 June 2018].

L3 Communications (USA). Not dated. https://www.l3t.com/ [accessed 25 June 2018].

Mevex (Canada). Not dated. 10 MeV system. http://mevex.com/products/10mev-system/ [accessed 25 June 2018].

Morse, J.G. 1977. Nuclear Methods in Mineral Exploration and Production. Elsevier.

Moshkov V.A. and Tjamisov N.E. 2017. Gamma-activation analysis for gold and silver – an effective development of Soviet physicists. *Zolotodobicha* (Gold Mining), no. 225, August.

Nii Tekhnicheskoy Fiziki I Avtomatiki. Not dated. http://www.niitfa.ru [accessed 25 June 2018].

Nuctech (China). Not dated. http://www.nuctech.com/en [accessed 25 June 2018].

Robertson M.E.A and Feather C.E. 2004. Determination of gold, platinum and uranium in South African ores by high energy XRF spectrometry. *X-ray Spectrometry,* vol. 33. pp. 164–173.

Sammut, D. 2016. Gamma activation analysis. A new gold standard? *Chemistry in Australia*, February. pp.18–21.

Scott Automation. Not dated. https://www.scottautomation.com/rocklabs/products/reference-materials [accessed 25 June 2018].

Sokolov, A.D., Burmistenko, Y.N., Gostilo, V.V., and Titov, V.L. 2018a. Industrial gamma-activation assay system for gold ore analysis. *Minerals Engineering*, vol.117, 15 January. pp 179–181.

Sokolov, A., Gostilo, V., Demsky, M., and Hasikova, E. 2018b. Optimization of industrial gamma-activation assay system for analysis of gold and rare metals ores. *Proceedings of ALTA Gold 2018*. ALTA Metallurgical Services, Perth. pp. 61–71.

Sokolov A.D., Demsky M.I., Gostilo V.V., Hasikova E.I., and Titov V.L. 2017. Gold ore analysis using industrial gamma-activation assay system. *Proceedings of ALTA Au 2017*, Perth, WA, 20-27 May. ALTA Metallurgical Services, Perth. pp.146–153.

THK. Not dated. http://www.thk.com [accessed 25 June 2018]..

Thomson. Not dated. http://www.thomsonlinear.com [accessed 25 June 2018].

Tickner, J., Ganly, B. Lovric, B., and O'Dwyer, J. 2017. Improving the sensitivity and accuracy of gamma activation analysis for the rapid determination of gold in mineral ores. *Applied Radiation and Isotopes: Including Data, Instrumentation and Methods for use in Agriculture, Industry and Medicine*, vol. 122. pp. 28–36.

Wuxi El Pont (China). Not dated. http://www.elpont.net/en/ [accessed 25 June 2018]. ◆


## 31 July – 1 August 2019

**The Canvas Riversands, Fourways**
**Johannesburg, South Africa**

YOUNG PROFESSIONALS COUNCIL

SAIMM
THE SOUTHERN AFRICAN INSTITUTE
OF MINING AND METALLURGY

## ENTREPRENEURSHIP IN THE MINERALS INDUSTRY CONFERENCE 2019

BRINGING IDEAS TO LIFE

# TAILING STORAGE CONFERENCE 2019

Investing in a Sustainable Future

**16–17 October 2019**
**Birchwood Hotel & OR Tambo**
**Conference Centre**
**Johannesburg, South Africa**

*In collaboration with the MMMA*

SAIMM
THE SOUTHERN AFRICAN INSTITUTE
OF MINING AND METALLURGY

# NATIONAL & INTERNATIONAL ACTIVITIES

## 2019

18–25 May 2019 — **ALTA 2019 Nickel-Cobalt-Copper**
Uranium-REE, Gold-PM, In Situ Recovery, Lithium Processing Conference & Exhibition, Perth, Australia
Contact: Allison Taylor
Tel: +61 411 692 442, E-mail: allisontaylor@altamet.com.au
Website: https://www.altamet.com.au/conferences/alta-2019/

22–23 May 2019 — **SA Mining Supply Chain Conference and Strategy Workshop**
Bateleur Conference Venue, Nasrec, Johannesburg
Contact: Yolanda Ndimande
Tel: +27 11 834-1273/7, Fax: +27 11 838-5923/833-8156
E-mail: yolanda@saimm.co.za, Website: http://www.saimm.co.za

22–23 May 2019 — **Mine Planner's Colloquium 2019**
*'Skills for the future – yours and your mine's'*
Glenhove Conference Centre, Melrose Estate, Johannesburg
Contact: Camielah Jardine
Tel: +27 11 834-1273/7, Fax: +27 11 838-5923/833-8156
E-mail: camielah@saimm.co.za, Website: http://www.saimm.co.za

27–29 May 2019 — **The 9th International Conference on Sustainable Development in the Minerals Industry**
Park Royal Darling Harbour, Sydney , Australia
Contact: Georgios Barakos
Tel: +49(0)3731 39 3602, Fax: +49(0)3731 39 2087
E-mail: Georgios.Barakos@mabb.tu-freiberg.de
Website: http://sdimi.ausimm.com/

5–6 June 2019 — **New Technology Conference and Trade Show**
'*Embracing the Fourth Industrial Revolution in the Minerals Industry*'
The Canvas Riversands, Fourways, Johannesburg, South Africa
Contact: Yolanda Ndimande
Tel: +27 11 834-1273/7, Fax: +27 11 838-5923/833-8156
E-mail: yolanda@saimm.co.za, Website: http://www.saimm.co.za

24–27 June 2019 — **Ninth International Conference on Deep and High Stress Mining 2019**
Misty Hills Country Hotel & Conference Centre, Muldersdrift, Johannesburg
Contact: Camielah Jardine
Tel: +27 11 834-1273/7, Fax: +27 11 838-5923/833-8156
E-mail: camielah@saimm.co.za, Website: http://www.saimm.co.za

4–5 July 2019 — **Smart Mining, Smart Environment, Smart Society**
*'Implementing change now, for the mine of the future'*
Accolades Boutique Venue, Midrand
Contact: Yolanda Ndimande
Tel: +27 11 834-1273/7, Fax: +27 11 838-5923/833-8156
E-mail: yolanda@saimm.co.za, Website: http://www.saimm.co.za

10–11 July 2019 — **Revitalising exploration activity in southern Africa**
Misty Hills Country Hotel & Conference Centre, Muldersdrift, Johannesburg
Contact: Camielah Jardine
Tel: +27 11 834-1273/7, Fax: +27 11 838-5923/833-8156
E-mail: camielah@saimm.co.za, Website: http://www.saimm.co.za

31 July–1 August 2019 — **Entrepreneurship in the Minerals Industry Conference 2019**
*'Bringing ideas to life'*
The Canvas Riversands, Fourways, Johannesburg, South Africa
Contact: Camielah Jardine
Tel: +27 11 834-1273/7, Fax: +27 11 838-5923/833-8156
E-mail: camielah@saimm.co.za, Website: http://www.saimm.co.za

5–7 August 2019 — **The Southern African Institute of Mining and Metallurgy in collaboration with the Zululand Branch is organising The Eleventh International Heavy Minerals Conference**
*'Renewed focus on Process and Optimization'*
The Vineyard, Cape Town, South Africa
Contact: Yolanda Ndimande
Tel: +27 11 834-1273/7, Fax: +27 11 838-5923/833-8156
E-mail: yolanda@saimm.co.za, Website: http://www.saimm.co.za

18–21 August 2019 — **Copper 2019**
Vancouver Convention Centre, Canada
Contact: Brigitte Farah
Tel: +1 514-939-2710 (ext. 1329), E-mail: metsoc@cim.org
Website: http://com.metsoc.org

19–22 Augusts 2019 — **Southern African Coal Processing Society 2019 Conference and Networking Opportunity**
Graceland Hotel Casino and Country Club, Secunda
Contact: Johan de Korte
Tel: 079 872-6403
E-mail: dekorte.johan@gmail.com
Website: http://www.sacoalprep.co.za

28–30 August 2019 — **IFAC MMM 2019 Symposium**
Stellenbosch Institute for Advanced Studies Conference Centre, Stellenbosch, Cape Town, South Africa
Email: info@ifacmmm2019.org
Website: https://www.ifacmmm2019.org

4–5 September 2019 — **Surface Mining Masterclass 2019**
Birchwood Hotel & OR Tambo Conference Centre, Johannesburg
Contact: Camielah Jardine
Tel: +27 11 834-1273/7, Fax: +27 11 838-5923/833-8156
E-mail: camielah@saimm.co.za, Website: http://www.saimm.co.za

17–18 September 2019 — **Hydrometallurgy Colloquium 2019**
*'Impurity removal in hydrometallurgy'*
Glenhove Conference Centre, Melrose Estate, Johannesburg
Contact: Yolanda Ndimande
Tel: +27 11 834-1273/7, Fax: +27 11 838-5923/833-8156
E-mail: yolanda@saimm.co.za, Website: http://www.saimm.co.za

16–17 October 2019 — **Tailing Storage Conference 2019**
*'Investing in a Sustainable Future'*
Birchwood Hotel & OR Tambo Conference Centre, Johannesburg
Contact: Camielah Jardine
Tel: +27 11 834-1273/7, Fax: +27 11 838-5923/833-8156
E-mail: camielah@saimm.co.za, Website: http://www.saimm.co.za

31 October–1 November 2019 — **International Mine Health and SafetyConference 2019**
Misty Hills Country Hotel & Conference Centre, Muldersdrift, Johannesburg
Contact: Camielah Jardine
Tel: +27 11 834-1273/7, Fax: +27 11 838-5923/833-8156
E-mail: camielah@saimm.co.za, Website: http://www.saimm.co.za

13–15 November 2019 — **XIX International Coal Preparation Congress & Expo 2019**
New Delhi, India
Contact: Coal Preparation Society of India
Tel/Fax: +91-11-26136416, 4166 1820
E-mail: cpsidelhi. india@gmail.com, president@cpsi.org. inrksachdev01@gmail.com, hi.sapru@monnetgroup.com

## 2020

25–29 May 2020 — **The 11th International Conference on Molten Slags, Fluxes and Salts**
The Westin Chosun Seoul Hotel, Seoul, Korea
Tel: +82-2-565-3571, Email: secretary@molten2020.org
http://www.molten2020.org

# Company affiliates

**The following organizations have been admitted to the Institute as Company Affiliates**

3M South Africa (Pty) Limited
AECOM SA (Pty) Ltd
AEL Mining Services Limited
Air Liquide (Pty) Ltd
Alexander Proudfoot Africa (Pty) Ltd
AMEC Foster Wheeler
AMIRA International Africa (Pty) Ltd
ANDRITZ Delkor (Pty) Ltd
ANGLO Operations Proprietary Limited
Anglogold Ashanti Ltd
Arcus Gibb (Pty) Ltd
ASPASA
Atlas Copco Holdings South Africa (Pty) Limited
Aurecon South Africa (Pty) Ltd
Aveng Engineering
Aveng Mining Shafts and Underground
Axis House Pty Ltd
Bafokeng Rasimone Platinum Mine
Barloworld Equipment -Mining
BASF Holdings SA (Pty) Ltd
BCL Limited
Becker Mining (Pty) Ltd
BedRock Mining Support Pty Ltd
BHP Billiton Energy Coal SA Ltd
Blue Cube Systems (Pty) Ltd
Bluhm Burton Engineering Pty Ltd
Bouygues Travaux Publics
CDM Group
CGG Services SA
Coalmin Process Technologies CC
Concor Opencast Mining
Concor Technicrete
Council for Geoscience Library
CRONIMET Mining Processing SA Pty Ltd
CSIR Natural Resources and the Environment
Data Mine SA
Digby Wells and Associates
DRA Mineral Projects (Pty) Ltd
DTP Mining - Bouygues Construction
Duraset
Elbroc Mining Products (Pty) Ltd
eThekwini Municipality
Expectra 2004 (Pty) Ltd
Exxaro Coal (Pty) Ltd
Exxaro Resources Limited
Filtaquip (Pty) Ltd
FLSmidth Minerals (Pty) Ltd
Fluor Daniel SA ( Pty) Ltd
Franki Africa (Pty) Ltd-JHB
Fraser Alexander (Pty) Ltd
G H H Mining Machines (Pty) Ltd
Geobrugg Southern Africa (Pty) Ltd
Glencore
Hall Core Drilling (Pty) Ltd
Hatch (Pty) Ltd
Herrenknecht AG
HPE Hydro Power Equipment (Pty) Ltd
Immersive Technologies
IMS Engineering (Pty) Ltd
Ingwenya Mineral Processing
Ivanhoe Mines SA
Joy Global Inc.(Africa)
Kudumane Manganese Resources
Leco Africa (Pty) Limited
Longyear South Africa (Pty) Ltd
Lonmin Plc
Lull Storm Trading (Pty) Ltd
Maccaferri SA (Pty) Ltd
Magnetech (Pty) Ltd
MAGOTTEAUX (Pty) Ltd
Maptek (Pty) Ltd
MBE Minerals SA Pty Ltd
MCC Contracts (Pty) Ltd
MD Mineral Technologies SA (Pty) Ltd
MDM Technical Africa (Pty) Ltd
Metalock Engineering RSA (Pty)Ltd
Metorex Limited
Metso Minerals (South Africa) Pty Ltd
Micromine Africa (Pty) Ltd
Minerals Council of South Africa
Minerals Operations Executive (Pty) Ltd
MineRP Holding (Pty) Ltd
Mintek
MIP Process Technologies (Pty) Limited
Modular Mining Systems Africa (Pty) Ltd
MSA Group (Pty) Ltd
Multotec (Pty) Ltd
Murray and Roberts Cementation
Nalco Africa (Pty) Ltd
Namakwa Sands(Pty) Ltd
Ncamiso Trading (Pty) Ltd
New Concept Mining (Pty) Limited
Northam Platinum Ltd - Zondereinde
Opermin Operational Excellence
OPTRON (Pty) Ltd
PANalytical (Pty) Ltd
Paterson & Cooke Consulting Engineers (Pty) Ltd
Perkinelmer
Polysius A Division Of Thyssenkrupp Industrial Sol
Precious Metals Refiners
Rand Refinery Limited
Redpath Mining (South Africa) (Pty) Ltd
Rocbolt Technologies
Rosond (Pty) Ltd
Royal Bafokeng Platinum
Roytec Global (Pty) Ltd
RungePincockMinarco Limited
Rustenburg Platinum Mines Limited
Salene Mining (Pty) Ltd
Sandvik Mining and Construction Delmas (Pty) Ltd
Sandvik Mining and Construction RSA(Pty) Ltd
SANIRE
Schauenburg (Pty) Ltd
Sebilo Resources (Pty) Ltd
SENET (Pty) Ltd
Senmin International (Pty) Ltd
Smec South Africa
Sound Mining Solution (Pty) Ltd
Speciality Construction Products (Pty) Ltd
SRK Consulting SA (Pty) Ltd
Time Mining and Processing (Pty) Ltd
Timrite Pty Ltd
Tomra (Pty) Ltd
Ukwazi Mining Solutions (Pty) Ltd
Umgeni Water
Webber Wentzel
Weir Minerals Africa
Worley Parsons RSA (Pty) Ltd

# INTERNATIONAL MINE HEALTH AND SAFETY CONFERENCE 2019

## 31 OCT - 1 NOV

**Misty Hills Country Hotel & Conference Centre, Muldersdrift, Johannesburg**

## OBJECTIVES

The conference will focus on improvement in health and safety, as well as the environmental impact the mining and metallurgy industries have on the local communities they serve while highlighting actions to be taken.

It will be a learning platform, allowing people to share ideas on health and safety, the environmental aspects which local communities' need to be aware of, concerning the industry and its relationships with them.

This conference aims to bring together management, DMR, Minerals Council South Africa, Unions, Health and Safety practitioners at all levels from the industry.
Sharing best practice and successful strategies for zero harm and a value-based approach to health and safety. With the purpose of addressing the main challenges in the mining industry such as logistics, energy, employee safety, contractors and the communities at large.

## WHO SHOULD ATTEND

The conference should be of value to:

- Safety practitioners
- Mine management
- Mine health and safety officials
- Engineering managers
- Underground production supervisors
- Surface production supervisors
- Environmental scientists
- Minimizing of waste
- Operations manager
- Processing manager
- Contractors (mining)
- Including mining consultants, suppliers & manufacturers
- Education and training
- Energy solving projects
- Water solving projects
- Unions
- Academics and students
- DMR.

## SPONSORSHIP

Sponsorship opportunities are available. Companies wishing to sponsor or exhibit should contact the Conference Coordinator.


**For further information contact:**
Head of Conferencing
Camielah Jardine, SAIMM
Tel: +27 11 834-1273/7
Fax: +27 11 833-8156 or +27 11 838-5923
E-mail: camielah@saimm.co.za
Website: http://www.saimm.co.za



SAIMM
THE SOUTHERN AFRICAN INSTITUTE OF MINING AND METALLURGY

HMC 2019
HEAVY MINERALS 2019

The Southern African Institute of Mining and Metallurgy

in collaboration with the Zululand Branch is organising

The Eleventh International

# HEAVY MINERALS CONFERENCE

*'Renewed focus on Process and Optimization'*

## 5–6 August 2019—Conference

## The Vineyard, Cape Town, South Africa

## ABOUT THE VENUE

The Vineyard is nestled on an eco-award-winning riverside estate, overlooking the eastern slopes of Table Mountain and conveniently located on the edge of the city. A short distance from the hotel in any direction allows you to easily explore some of the world's top tourist destinations.

August and September in the Western Cape is flower season. Explore the Cape's unique 'fynbos' floral kingdom at the world-famous Kirstenbosch Botanical Gardens, where one of the many attractions is the staggering aerial tree-canopy walkway.

A short distance from the hotel is the Constantia Winelands, which affords guests the opportunity to discover classic vintages and Cape Dutch homesteads, and within a five-minute walk is the well-known retail centre, the upmarket shopping precinct of Cavendish, with exclusive local and global outlets, travel agencies, foreign exchange outlets, and more.

## CONFERENCE THEME

This series of heavy minerals conferences has traditionally focused on the industries associated with ilmenite, rutile and zircon. There are many other economic minerals which have specific gravities such that they may also be classed as 'heavy minerals'. The physical and chemical properties of these other minerals result in them being processed by similar technologies and sharing similar markets with the more traditional heavy minerals. In this conference we focus on optimization of mining, processing, and recovery.

## CONFERENCE OBJECTIVE

This series of conferences was started in 1997 and has run since that date. The Conference alternates between South Africa and other heavy mineral producing countries. It provides a forum for an exchange of knowledge in all aspects of heavy minerals, from exploration through processing and product applications.

This is a strictly technical conference, and efforts by the Organizing Committee are aimed at preserving its technical nature. The benefit of this focus is that it allows the operators of businesses within this sector to discuss topics not normally covered in such forums. The focus on heavy minerals includes the more obvious minerals such as ilmenite, rutile and zircon; and also other heavy minerals such as garnet, andalusite, and sillimanite.

## WHO SHOULD ATTEND

- Academics
- Business development managers
- Concentrator managers
- Consultants
- Engineers
- Exploration managers
- Geologists
- Hydrogeologists
- Innovation managers
- Mechanical engineers
- Metallurgical managers
- Metallurgical consultants
- Metallurgists
- Mine managers
- Mining engineers
- New business development managers
- Planning managers
- Process engineers
- Product developers
- Production managers
- Project managers
- Pyrometallurgists
- Researchers
- Scientists

SPONSORS DERRICK FLSmidth Mineral Technologies A Downer Company

**Contact: Yolanda Ndimande, Conference Co-ordinator · Tel: +27 11 834-1273/7**
**Fax: +27 11 833-8156 or +27 11 838-5923 · E-mail: yolanda@saimm.co.za · Website: http://www.saimm.co.za**

SAIMM
THE SOUTHERN AFRICAN INSTITUTE OF MINING AND METALLURGY